MEASUREMENTS AND APPLICATIONS OF THE EXCITATION FUNCTIONS FOR FAST NEUTRON INDUCED REACTIONS

BY

RAIK A. JARJIS

A thesis submitted to the
University of Aston in Birmingham
for the degree of
Doctor of Philosophy in Physics

December 1976

ABSTRACT

The concentric ring technique has been devised for the measurement of fast neutron fluxes and energies by using different standard materials and their measured excitation functions. It has been shown experimentally that for the determination of flux and energy in the 14 MeV region, this novel technique can yield accuracy values of the order of 1.0% and 1.2% respectively. An experimental cross-section ratio curve for the (n,2n) reaction on ^{63}Cu and the (n,p) reaction on ^{27}Al has been established as a standard reference for fast neutron energy measurement.

The technique has been applied to the measurement of the excitation functions for the following nuclear reactions:-

a) The 12.9 to 15.9 MeV neutron energy region

(1) $^{27}Al(n,p)^{27}Mg$ (2) $^{56}Fe(n,p)^{56}Mn$ (3) $^{59}Co(n,\alpha)^{56}Mn$

(4) $^{64}Zn(n,2n)^{63}Zn$ (5) $^{63}Cu(n,2n)^{62}Cu$ (6) $^{121}Sb(n,2n)^{120g}Sb$

b) The 13.4 to 14.9 MeV neutron energy region

(7) $^{28}Si(n,p)^{28}Al$ (8) $^{27}Al(n,\alpha)^{24}Na$ (9) $^{64}Zn(n,p)^{64}Cu$

(10) $^{65}Cu(n,2n)^{64}Cu$

The cross-section data obtained by using an 0.5 MeV Van de Graaff and 3.0 MeV Dynamitron accelerators are consistent and are in good general agreement with the published data. This investigation includes also detailed studies of fast neutron production by the $T(d,n)^{4}He$ reaction, fast neutron monitoring, activation analysis and cross-section data systematics.

Some of the recommedations proposed include flux monitoring by

the $^{121}Sb(n,2n)^{120g}Sb$ reaction, further possible applications of the concentric ring technique, and a possible system for the standardization of neutron cross-section data.

CONTENTS

I N T R O D U C T I O N

The measurement of fast neutron induced reaction cross-sections and their variations with neutron energy specially around 14 MeV is an important field in nuclear science and technology. The cross section data are applied to nuclear theories to yield information about the relevant nuclear models and nuclear interaction theories, such as in testing the validity of the statistical theory and in determining the contribution of direct interaction mechanism. More practically, the measured data are extensively used in neutron spectroscopy, reactor physics, activation analysis, nuclear medicine, and in the design of D-T plasma type nuclear fusion devices.

In spite of the frequent measurements of the excitation functions for neutron induced reactions, a considerable number of the published results reveal large discrepancies on even the reactions which are used as standards. Discrepancies in the data can be mainly attributed to the undetected sources of systematic errors, inaccuracies in the values of the standard cross-sections, and also in the experimental techniques used to carry out the experiments. Furthermore, the early measurements

with the activation method include also additional errors due to β-counting, and poor gamma resolution when complex spectra are involved.

The limited yield of neutron sources plays an important role in causing the scarcity of the data for reactions of relatively small cross section. Finally, for reactions in which the cross-sections exhibit strong variations with energy, failure to estimate the incident neutron beam energies accurately is a further source of error.

CHAPTER ONE

SYSTEMATIC STUDIES OF FAST NEUTRON CROSS-SECTIONS

The fact that the neutron is electrically neutral and interacts strongly with the nucleus enables us to study nuclear structure with fast neutrons and to investigate with considerable efficiency the excited states of nuclei at energies between 10 and 20 MeV, where the Coulomb barrier complicates the use of charged particles. Several types of neutron reactions are energetically possible in the 14 MeV region and these reactions compete with each other to give variable degrees of relative contributions to the total cross-sections as shown in Fig. (1.1) [1]. Such contributions therefore determine the general shapes of the excitation functions; but more accurately, the threshold energies are determined by the negative Q-values of the various reactions and the yield curves are also controlled by the Coulomb barriers for (n, charged particle) reactions, and the positions of maximum yields are determined by the threshold of the competing reactions.

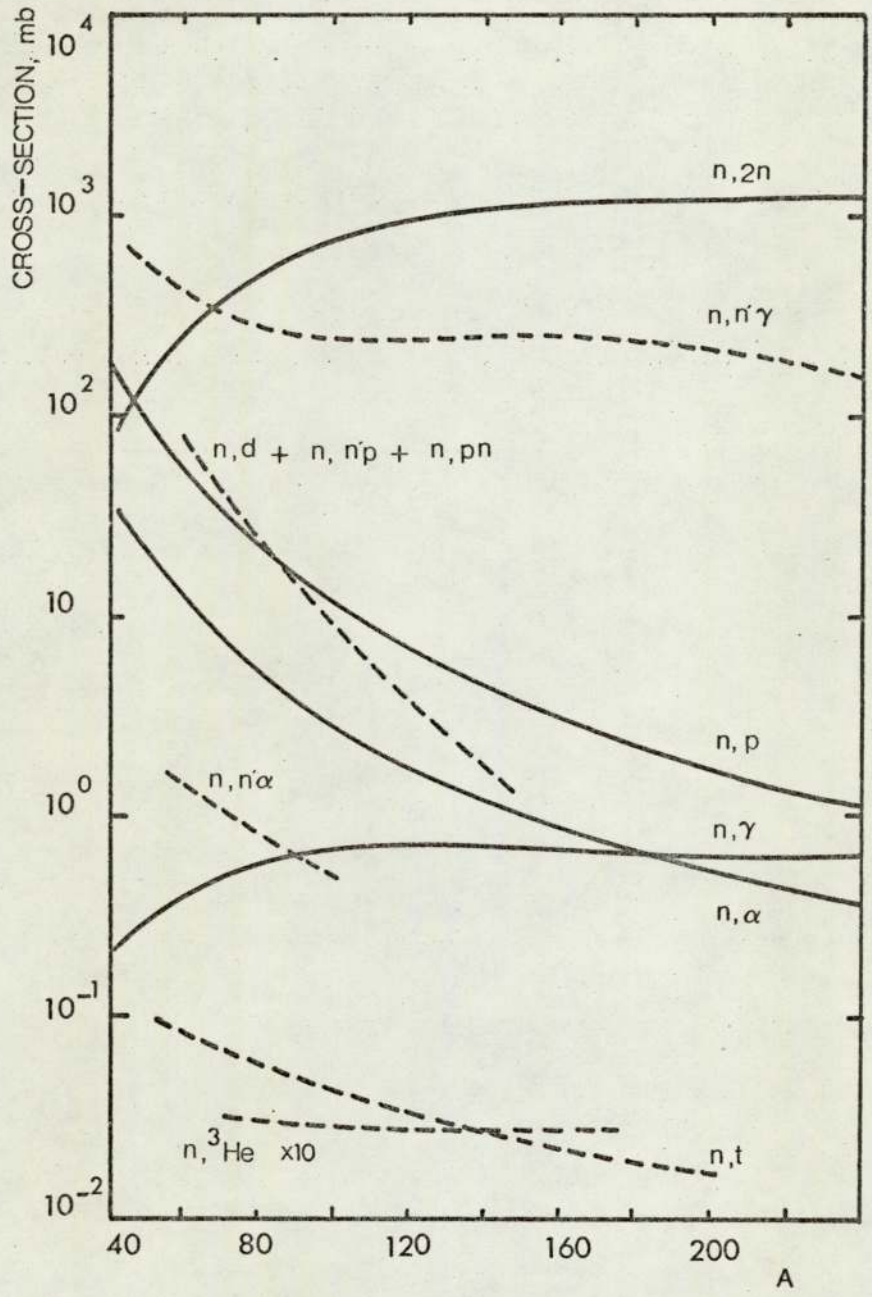

Fig. 1.1

Relative Contributions of Nuclear Reactions Produced by 14 MeV Neutrons on Medium and Heavy Mass Nuclei

1.1 Methods of Neutron Cross-Section Determination

Since the subject of neutron cross-section determination methods is very wide indeed, and its full review is beyond the scope of this thesis, we have therefore settled to only a limited discussion.

1.1.1 Activation and direct detection methods

Neutron cross-section data in the 14 MeV region are most commonly determined by using the activation method which follows the production of radioactive residual nuclei. This method has the advantage that the yields of constituent isotopes of an element can be well separated by gamma spectroscopy. Also, it is possible to irradiate large amounts of material, therefore eliminating most of the difficulties presented by the relatively low neutron cross-sections in the 14 MeV region and the limited incident neutron flux, self absorption corrections are required specially for β-counting. The progress in gamma ray spectroscopy and radiochemical separation methods have increased the reliability of this method even in the determination of rare reaction cross-sections.

The cross-sections values obtained by the activation method represent the integral values which include the sums of differential cross-sections, and the method offers no discrimination between the cross-sections for the formation of daughter nuclei in ground and very short-lived excitation states. Good separation between the induced activities on the basis of the differences in decay rates is possible and it can provide cross-section data for ground and isomeric states.

The other method of cross-section measurement is by the direct on-line detection of the emitted particles, and this method can usually yield information about the differential cross-sections and angular

distributions to study reaction mechanisms. By comparing the theoretical and experimental excitation functions, emitted particles and angular distributions, a sensitive check on the predictions of the statistical model can be made and data for the level densities and compound nucleus formation cross-sections could be obtained. If the angular distribution of the emitted particles is not symmetric about 90^{o} and the observed correlations between the particles can not be explained within the limitations of the statistical theory, direct process effect is usually introduced.

It is clear therefore, that the direct detection method can provide vast amounts of information, but if only the determination of excitation functions is required the activation method without doubt will be the right choice. The limitations presented by the direct detection method which restrict its use for the determination of neutron excitation functions can be explained as follows:

1) The measurements have to be carried out in high background environment due to the interaction of neutrons with the T-target and its backing, detector, and reaction chamber.

2) For the detection of emitted charged particles, the experiments are usually carried out under vacuum on thin targets containing small amounts of the studied materials, and accordingly small count rates are produced which limit the accuracy.

3) For reactions of small cross-sections such as the (n,α) reaction on heavy nuclei, an attempt to increase the count rate by using thicker targets would mean the complete loss of the α-spectrum.

1.1.2 The reciprocity method

The excitation functions of fast neutron induced charged particle reactions can be estimated with reasonable accuracy by using the reciprocity theorem [2] which employs the excitation functions of neutron emitting reactions. According to the theorem, the cross-section $\sigma(a,b)$ for the reaction A(a,b)B can be expressed in terms of the cross-section $\sigma(b,a)$ for the B(b,a)A reaction according to the relationship [3].

$$\frac{\sigma(a,b)(2I_A+1)(2I_a+1)}{\lambda\!\!\!^{-2}_a} = \frac{\sigma(b,a)(2I_B+1)(2I_b+1)}{\lambda\!\!\!^{-2}_b}$$

where I_A, I_B, I_a, I_b = spins of nuclei A, B, a, b and $\lambda\!\!\!^{-}_a$, $\lambda\!\!\!^{-}_b$ = $1/2\pi$ x the De Broglie wave length of the particle a, b in the centre-of-mass system.

The excitation functions for neutron producing reactions are usually known precisely due to the high resolution of the incident charged particle beams which are mainly obtained by using ripple free Van de Graaff accelerators. Thus, by using the reciprocity theorem one would expect to be able to study even the structure in fast neutron excitation functions, when they exist, where the inaccuracies due to the energy spreads of incident neutron beams are difficult to eliminate. So far, this method has been used only on a small scale for bombardment energies lower than 6.5 MeV, such as in determining the $^{16}O(n,\alpha)^{13}C$ cross-section from $^{13}C(\alpha,n)^{16}O$ cross-section [3] and the $^{3}He(n,p)T$ cross-section from $T(p,n)^{3}He$ cross-section [4].

1.2 Shell Closure Effect

The studies of shell closure effects on the systematic trends of the most common (n,2n), (n,P) and (n,α) cross-sections have been the

subject of interesting investigations in the 14 MeV region. The contradictory results obtained by the researchers so far, specially for the (n,2n) cross-sections, leaves the understanding of the subject in a rather uncertain state and indicates the necessity for further explorations in this field. Therefore, it is not possible at this stage to state whether the shell effects exist or not, but a brief review of the important results might be worthwhile, as follows.

1) By plotting (n,α) and (n,p) cross-sections against Z_R, the charge of the residual nucleus, depressions in the cross-sections are observed at just these values of Z_R corresponding to proton magic numbers [5,6], with an odd-even effect for (n,p) cross-sections between Z_R = 10 to 20.

2) By introducing the isotope effect of Gardner [7], both shell and odd-even effects become obscure, which indicates that the previous results of Chatterjee [5,6] were obtained by using the cross-sections of the most abundant isotopes. According to Gardner, for a given nuclear charge (n,p) cross-sections should differ by a factor of two between neighbouring isotopes with the isotope of higher mass number having the lower cross-section. The same considerations may well apply to the (n,α) reaction cross-section.

3) Distinctive minima and maxima in the mass dependence of (n,2n) cross-sections in the region of closed neutron and proton shells were observed by Bormann [8] when the cross-sections were plotted against the target mass number A. More recently, similar effects were confirmed by Mohindra and Gupta [9] who showed definite shell effects at N = 20, 28 and 50 when the (n,2n) cross-sections are plotted against N and (N-Z)/A for magic number nuclei in comparison with the neighbouring nuclei of same N-Z and pairing effects.

4) On the other hand, Qaim [10] plotted also the (n,2n) cross-sections versus the relative neutron excess (N-Z)/A as an asymmetry parameter and showed a complete lack of evidence for shell effects. His explanation for the formerly observed minima was attributed to the use of partial (n,2n) cross-sections in those cases in which the corresponding total cross-sections were not experimentally known. Kondaiah [11] also confirms this conclusion by observing no tangible evidence of shell effects when the weighted averages of the experimental cross-sections are compared with the theoretical predictions of the statistical model.

In view of the important role of the Q-value effect on (n,2n) cross-sections at a given incident energy, Holub and Cindro [12] lately looked at the dependence of (n,2n) cross-sections on the asymmetry parameter (N-Z) at a given maximum residual excitation energy, $U_R = E_n + Q_{n,2n}$ as suggested by Csikai and Peto [13]. The investigation indicated that the total (n,2n) cross-sections against the (N-Z)/A or $(N-Z)_R$ at a constant value of U_R follow smooth, structureless curves. Also the systematic difference of the total (n,2n) cross-sections compared with the statistical estimates would be interpreted in terms of the presence of pre-equilibrium processes, which harden the spectra of first neutrons and diminish the probability for the emission of second neutrons.

1.3 The Effect of Overlapping Excited Levels

For the standardization of 14 MeV neutron cross-section data for fast neutron flux monitoring, a smooth cross-section variation with energy is usually assumed. This procedure is valid due to the large neutron energy spreads of the incident beams and to the formation of highly excited compound nuclei with energies around 20 MeV in the continuum

regions. Even at such high excitation energies fluctuations in the cross-sections variations with energy have been observed for charged particle induced reactions, and several attempts to examine the existence of such fluctuations in neutron induced reactions have been carried out with good beam energy resolutions. The statistical fluctuations in cross-section for total and partial (n,p), (n,α) and (n,2n) reactions have to be compared, if they exist, with the relevant theory which was developed originally by Ericson [14], and this can be stated briefly as follows.

At energies where several or many channels can be contributed to a nuclear reaction cross-section, the total width of compound nucleus levels can be greater than their average spacing i.e. $\Gamma/D \gg 1$. Accordingly, in this overlapping resonance region partial cross-sections are not smooth functions of energies but fluctuate violently with amplitudes which are inversely proportional to the square roots of the numbers of the final states.

$$\overline{\{(\sigma - \bar{\sigma})^2/\sigma^2\}}^{\frac{1}{2}} = (2/n)^{\frac{1}{2}} \qquad (1.1)$$

where $\bar{\sigma}$ being the mean value of the cross-section on a large energy interval, $\overline{\{(\sigma - \bar{\sigma})^2\}}^{\frac{1}{2}}$ is the root mean square deviation of the cross-section and n the number of the final states.

Ericson's theory states also that in spite of the random nature of the overlapping of the resonances in the continuum region of the compound nucleus, the structure should reflect the average nucleus level width. The correlation width of the fluctuations Γ is related to the lifet-time τ of the compound nucleus by an uncertainty type of relation

$$\Gamma\tau \sim h \qquad (1.2)$$

The selection of the energy steps and required neutron beam resolution is very critical indeed for such measurements, and the uncertain existence of Ericson fluctuations in 14 MeV excitation functions can be attributed to incident neutron beam energy spreads. Fine structure studies require small neutron energy spreads such that $\Delta E < \Gamma$, and one has to keep in mind that the energy spread is further enhanced by the small-angle multiple scattering of deuterons in the tritium target [15] and by neutron scatter in the vicinity of the target [16]. It is worthwhile mentioning here that for studying the angular distributions symmetry or asymmetry the neutron beam energy spread should be much larger than the compound nucleus level width Γ i.e. $\Delta E >> \Gamma$ to discriminate between compound nucleus processes and direct reaction processes. According to Ericson, the $\Delta E >> \Gamma$ here is needed to average to zero the interference between compound nucleus levels and therefore eliminate any possible effect on the symmetry of the angular distribution about 90^{o}.

Both the activation and direct detection methods are being employed for the investigation of Ericson fluctuations in 14 MeV neutron cross-sections, and two examples for the (n,α) reaction are given here.

1) Whereas researchers such as Cindro et al [17], Strohal et al [18] and Csikai [19] have reported the existence of large fluctuations in $^{19}F(n,2n)^{18}F$ and $^{27}A\ell(n,\alpha)^{24}Mg$ cross-sections and even in those for heavier nuclei [19], others like Ferguson et al [20] disagree with that. Vonach et al [16] support Bormann and Riehle's conclusions [21] that the large fluctuations do not exist, and are probably due to systematic errors. The most recent publication [22] on this subject, however, confirms the existence of Ericson fluctuations in $^{27}A\ell(n,\alpha)^{24}Na$ total cross-section with the aid of a carefully evaluated neutron energy

resolution. The experiment of Gardner and Gardner[22] was done by using a high intensity insulated core transformer neutron facility operating at 4.5 kW of beam power. The neutron resolution obtained was 360 keV at 30^{o}, 10 keV at 98^{o} and 220 keV at 150^{o} for a tritium loading factor of 1.0 on an 0.05 mg / cm^2 thick titanium layer. By making the measurements in steps of 15 keV the excitation function obtained revealed distinct fluctuations of about 1.5% in magnitude on the average with a width of under 65 keV between the neutron energies of 13.7 and 14.2 MeV. Fig. 1.2 shows Gardner and Gardner's data for the total $^{27}A\ell(n,\alpha)^{24}Na$ reaction cross-section on a relative scale together with few previously determined detailed excitation functions for comparison. The general trends of the excitation functions seem to be similar to each other, but the only conclusion we can draw from the reported fluctuations is the need for further high resolution investigations at extended energy ranges. The excitation function of Strohal et al [18], for example, covers a narrow range of about 700 keV only.

2) For an excitation energy of about 23 MeV for 14 MeV bombardment energy, the ^{29}Si compound nucleus represents a very interesting subject for studying the evaporation mechanism and Ericson fluctuations in the complete level mixing region. The direct detection method here employs silicon semiconductor detectors as both targets and detectors, and the resulting pulse height spectra contain well separated peaks which are mainly due to the proton and alpha groups from the (n,p) and (n,α) reactions on ^{28}Si. The appropriate selection of the thickness of the depletion layer provides an accurate facility for determining the $^{28}Si(n,\alpha)^{25}Mg$ excitation functions for the formation of ^{25}Mg nucleus in its various energy levels. The fluctuating excitation functions which were first measured by Collie et al [23,24,25]

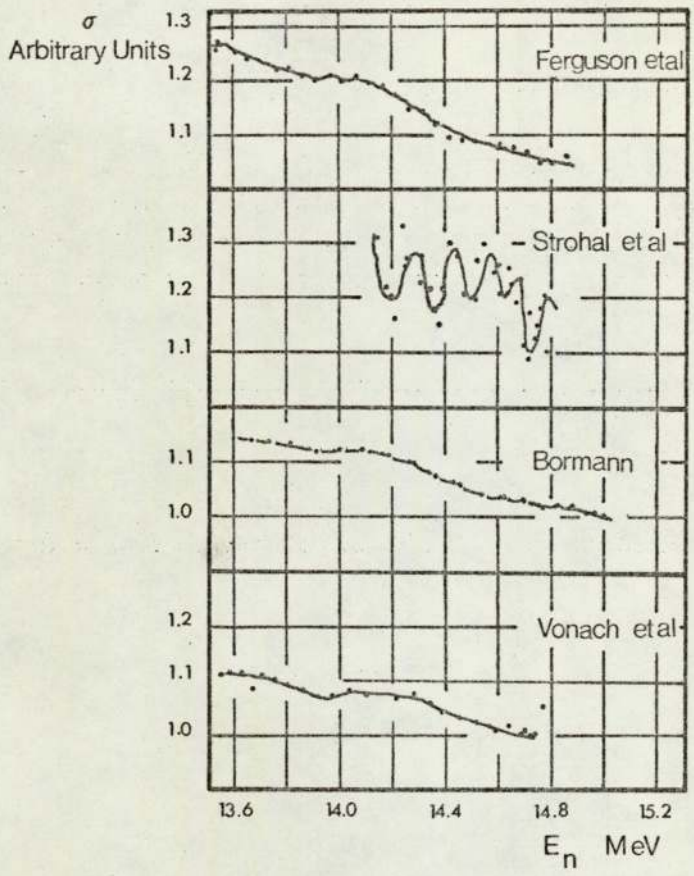

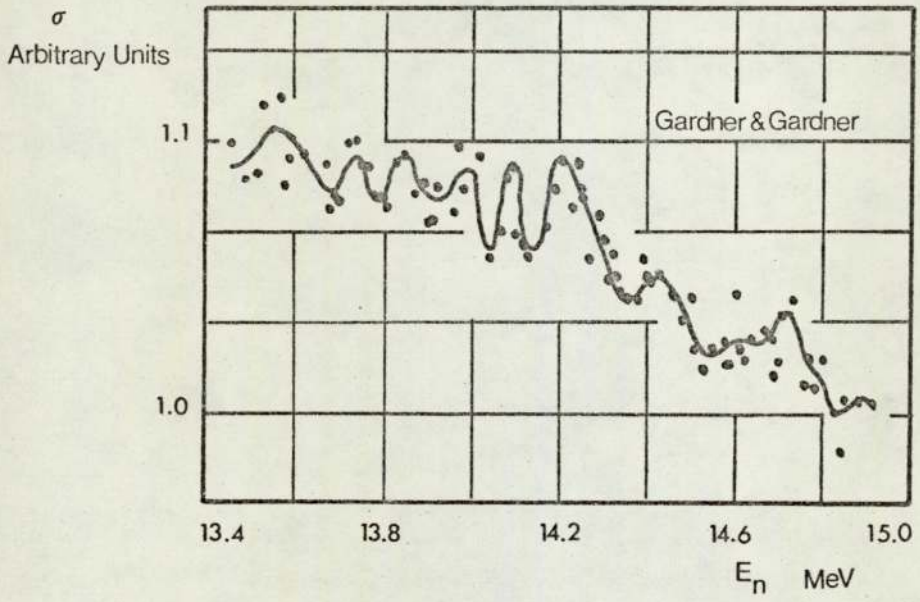

Fig. 1.2
Excitation Function for the $^{27}Al(n,\alpha)^{24}Na$ Reaction

are completely uncorrelated, showing that they are not characteristic of compound nucleus excitation energy but arise from a direct interaction interference effect. Recently, Siddiq et al [25] made similar measurements for the 12 - 18 MeV region again but with better energy resolution of values between 20 and 25 keV. Siddiq et al's excitation functions for ground, second, third and fourth excited states show strong fluctuations with amplitudes that lead to a factor of 2 agreement with Ericson predictions by using eq. 1.1. The mean lifetime of the compound nucleus as determined from the average width of the fluctuations according to eq. 1.2, is about four times smaller than that from Ericson's hypothesis, and one and a half times smaller than that of Colli et al.

1.4 Coulomb Barrier Effect

In the excitation functions for (n, charged particle) reactions a wide (8 to 10 MeV) maximum can be observed. The position of the maximum apart from several light nucleides is located between 10 and 20 MeV, and the accurate knowledge of these positions is of great practical importance.

According to the statistical theory for compound nucleus reactions, the cross-section for a given reaction depends strongly on the decay probabilities of the compound nucleus by other possible channels. At sufficient high excitation energies, the emission of a single particle may leave the nucleus still in a sufficiently high state of excitation to "boil off" a second particle. Therefore, one would expect the probability of single-particle emission to drop because of the competition of the two particle emissions. Since the neutron emission

process is relatively simple due to the lack of Coulomb barrier effect, therefore the opening of the (pn) and (αn) channels are the most competitive processes to the decay through the (p) and (α) channels. So, we should expect that the (n,p) and (n,α) reactions will reach their cross-section maxima at about the energies where the (n,pn) and (n,αn) reactions start to have noticeable yields. Bormann et al [27] have developed a simple method based on these principles to estimate the positions of (n,p) and (n,α) cross-section maxima for cases where the statistical reaction mechanism dominates, and their procedures are explained as follows.

Let us start with the reaction (n,xn), where x stands for a proton or alpha particle. Therefore the total reaction energy required to produce this reaction should be at least equal to the Coulomb barrier height $E_c(x)$ of the product nucleus for charged particle x.

$$E_n + Q_{n,xn} = E_c(x) \qquad (1.3)$$

Since the consequence of the (n,xn) reaction becoming possible is the occurrence of the maximum cross section for the (n,x) reaction, therefore the total (n,xn) reaction energy should be equal to maximum cross section.

Therefore $(E_{max})_{n,x} = E_n \simeq E_c(x) - Q_{n,xn}$

$$(E_{max})_{n,x} + Q_{n,xn} = E_c(x) \qquad (1.4)$$

If the relation (1.4) is valid, therefore the ratio $[(E_{max})_{n,x} + Q_{n,xn}]/E_c(x)$ should be unity. Fig. 1.3 shows plots of the quantities $[(E_{max})_{n,p} + Q_{n,pn}]/E_c(p)$ and $[(E_{max})_{n,\alpha} + Q_{n,\alpha n}]/E_c(\alpha)$ against the mass number A, in the mass region A = 20 to 90 as obtained from Bormann et al [27] results and the excitation function compilations of

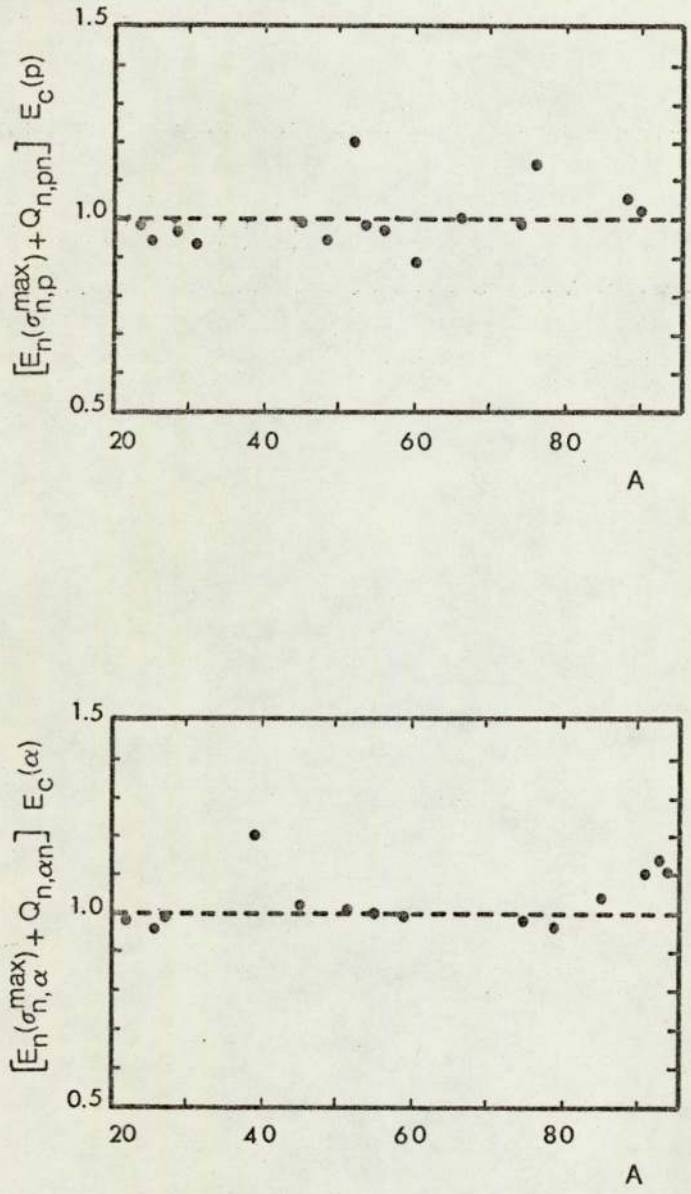

Fig. 1.3

Neutron Energy For the Maximum (n,p) and (n,α) Cross-Sections as a Function of the Target Mass Number A

Jessen et al [28]. As it can be observed from the figure, the quantities have values near to unity which proves that eq. 1.4 holds very well, and therefore can be used for the rough estimation of $(E_{max})_{n,p}$ and $(E_{max})_{n,\alpha}$.

1.5 Prediction of Fast Neutron Excitation Functions

Whereas the discrepancies in 13 - 15 MeV neutron cross-section data have already been indicated in the introduction of this thesis, the discrepancies in the excitation functions for a wider energy range of up to 20 MeV in width are even more pronounced and for many reactions no experimental data exist. Therefore, an attempt to use a neutron source of a wide continuous energy spectrum for activation purposes is limited by the lack of suitable cross-section data. Since the theoretical predictions of neutron excitation functions are not fully developed yet, empirically based estimations are therefore needed.

By using an empirical method, which was designed originally for the estimation of excitation functions for charged particle induced reactions, Krivan and Munzel [28-31] developed a rather interesting method for estimating the excitation functions for (n,p), (n,α) and (n,2n) reactions. The method is useful for predicting unknown excitation functions and extrapolating those for which data for only a narrow energy range are known. The approach of the method is interesting, but one could not expect it to be very accurate because it depends entirely on the published experimental data which is in considerable disagreement as we have explained already. Therefore, we hope that improving the accuracy of fast neutron excitation function

measurements will have a direct impact on the accuracy of this method.

According to Krivan and Munzel, the general form of the excitation functions for fast neutron induced reactions can be characterised by means of the following parameters, which are also shown in Fig. 1.4.

1) The reaction threshold energy E_{th}.

2) The maximum cross-section σ_{max}.

3) The position of maximum cross-section with respect to the Q-value of the reaction (E_{max} + Q).

4) The full and half widths at half maximum height (FWHM, HWHM) and if possible the full and half widths at tenth maximum height (FWTM,HWTM).

$$FWHM = HWHM_L + HWHM_R$$

$$FWTM = HWTM_L + HWTM_R$$

5) The asymmetry factors $F_{0.5}$ and $F_{0.1}$ at FWHM and FWTM respectively.

$$F_{0.5} = HWHM_R/HWHM_L$$

$$F_{0.1} = HWTM_R/HWTM_L$$

The analysis of the systematic trends of (n,p), (n,α) and (n,2n) reactions, as evaluated from the reported excitation functions, are shown in Fig. 1.5. This includes the three parameters (σ_{max}), (E_{max}+Q) and (FWHM), which are plotted versus the atomic number of the target nucleus. The systematic curves clearly reflect the basic differences between the reactions and are used for excitation function estimation. Finally, we would like to summarize the effects of the experimental data scatter on this method by the following points.

1) (FWHM) Curves contain relatively large standard deviations, and the determination of the trends for (FWTM), ($F_{0.5}$) and ($F_{0.1}$) is just

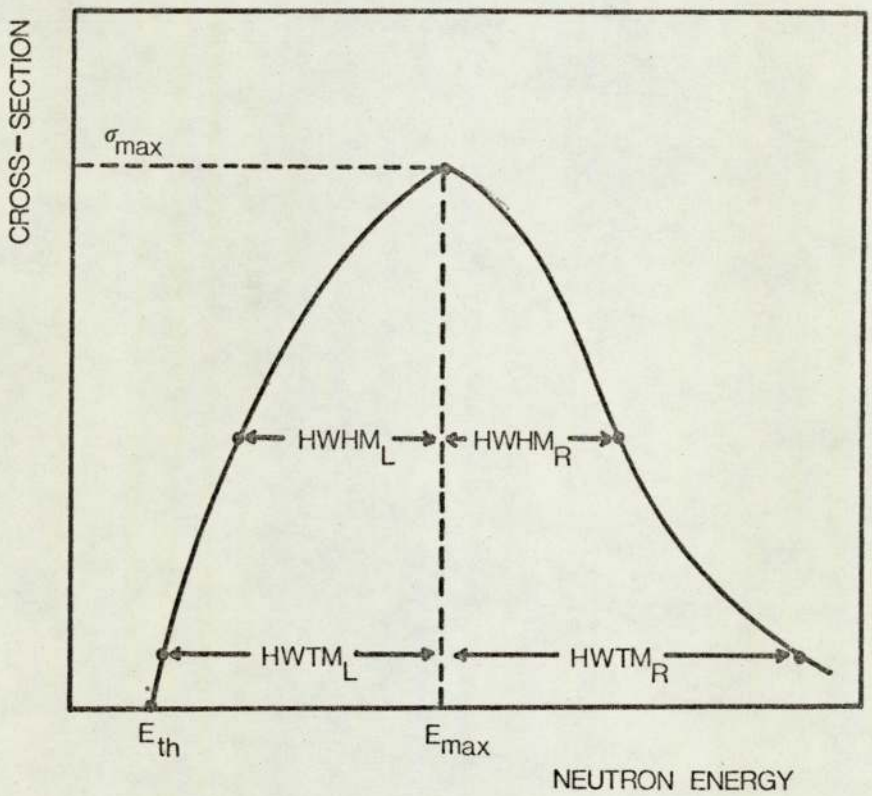

Fig. 1.4
Parameters Used to Characterize an Excitation Function

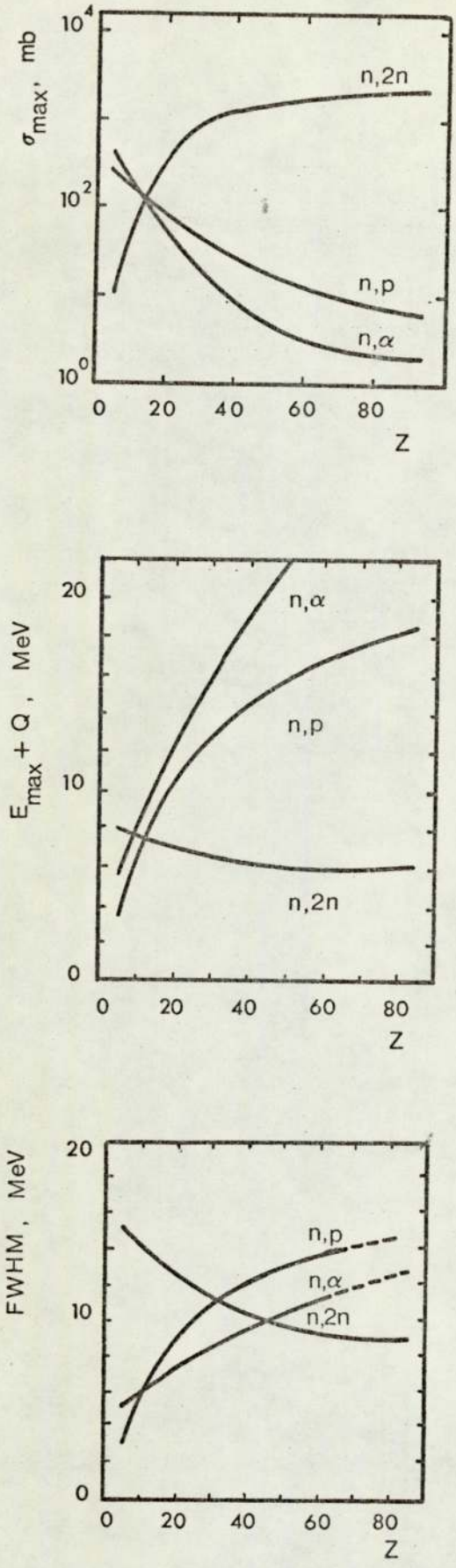

Fig. 1.5

Systematics of Excitation Functions for (n,p), (n,α) and (n,2n) Reactions

not possible. Therefore Krivan and Munzel have constructed their excitation functions by estimating the following values for ($F_{0.5}$) and ($F_{0.1}$).

Asymmetry Factor	Z = 13 - 45 (n,p)	(n,α)	Z = 27 - 69 (n,2n)
$F_{0.5}$	1.30	1.22	1.60
$F_{0.1}$	1.66	1.42	2.00

2) To a first approximation, it was assumed that the characteristics of the excitation functions depend only on the proton number Z of the target nucleus. But it is expected that the systematics will be improved if the influence of the neutron number N is taken into account by adding a correction term which depends on the neutron to proton ratio relative to that of the stability line [30]. Due to the scatter of data from published excitation functions such an approach can not be established and therefore only the target nucleus charge dependence is taken into account.

CHAPTER TWO

ACTIVATION ANALYSIS

2.1 Nuclear Analytical Techniques

An outstanding contribution to the analytical studies is being made by the non destructive nuclear techniques which are now routinely used in a wide range of disciplines in science and technology. Basically, nuclear analytical techniques require irradiating stable nuclei by a beam of photons, charged particles, or neutrons; and observing the radiation promptly emitted by the compound nuclei, or of delayed radiation from the decaying daughter nuclei. As a by-product of the nuclear power programme, activation analysis specially with neutrons advanced remarkably to a powerful analytical method for measuring the concentration of trace elements, often in amounts less than a billionth of a gram. The appropriate selection of the most efficient activation analysis method for any specific case is possibly by choosing the suitable irradiation beam and the energy of its particles or photons.

2.2 Non-Neutron Activation

2.2.1 Photon activation analysis

Activation analysis of light elements is possible by the use of photons from the heavy targets of electron accelerators. The shape of the incident gamma ray spectrum is usually a continuous bremsstrahlung spectrum of an anisotropic angular distribution, with a maximum energy value equal to the incident electron energy. The photons are emitted preferentially in the forward direction, and at low electron bombardment energies the analysis is restricted to the use of the (γ,γ') reaction which gives rise to isomeric states that decay by gamma emission. To make use of the (gamma, particle) reactions for activation analysis, the incident electron bombardment energies should be in excess of the reaction thresholds and this means that energetic electron beams from linear electron accelerators, betatrons, and electron synchrotrons are required. As in the case of neutrons, photon activation analysis leads to information about the bulk of the sample, but precise gamma absorption corrections are required. The limitations of this method are mainly the required chemical separation, and the relatively high irradiation costs when high sensitivites by using the (gamma, particle) reactions are needed.

2.2.2 Charged particle activation analysis

The relatively low operating costs and high ion beam energy resolution of Van de Graaff accelerators, make these machines very attractive tools for charged particle activation analysis. In the MeV region, analysis of light nuclei by nuclear reactions is very attractive specially when use is made of reactions which exhibit very strong resonances, typically about 1 keV wide and several keV apart. Access

to heavier elements requires higher ion bombardment energies, and this can be provided by using tandem van de graaffs with rather low beam current or cyclotrons; but increasing the bombardment energies is restricted by giving rise to spallation [32] which introduces complicated interferences. Also, information about heavy elements can be obtained even at low ion bombardment energies if backscattered ions and ion induced x-rays are observed.

Due to the short range of the incident particles, penetration depth is usually very limited, and this makes the technique very good for surface layer analysis when the ion beam energy variation with depth is taken into account. On the other hand, the technique is limited by its need of considerable care compared with neutron activation analysis and by its vacuum requirements. Also, the accuracy of charged particle activation analysis is affected by surface contamination, sample inhomogeneities, and sample overheating for large ion beam currents.

2.3 Neutron Activation Analysis

As with the other nuclear analytical techniques, activation analysis by neutrons is associated usually with high sensitivity and simplicity which puts it in a class of its own for material analysis. The transparency of samples to neutrons makes the accurate analysis of large samples quite possible, and accordingly neutron activation analysis is accepted as a standard technique for many industrial, medical and geological applications.

2.3.1 Reactor neutron source

This is the most important source of thermal neutrons for activation

analysis and other applications. Neutron thermalisation is essential to sustain the chain reaction, and the process yields thermal neutron fluxes of the order of 10^{13} - 10^{15} n/cm^2. S by fission neutron elastic collision with the moderator atoms. Fission neutrons are usually emitted in a broad spectrum which ranges approximately between 0 and 25 MeV for ^{235}U fission, but by neutron slowing down this wide energy range factor is eliminated, and the activation yields enhanced by orders of magnitude due to the large thermal neutron cross-section values. Reactors are used efficiently for long irradiation times as steady neutron sources; but with special arrangements they can also be used for pulsed activation analysis. As described by Yule and Guinn [33], a rapid removal of the main control rod causes a sudden increase in the reactivity and releases neutron fluxes of the order of 10^{16} n/cm^2 S for a few milliseconds. The sharpness of the reactor pulse duration for this special type of reactor is here determined by the temperature increase due to the reactivity build up, which makes the reactor go sub-critical automatically and shuts itself off. But, in spite of this interesting method, we can generally emphasise that the use of reactors is more reliable for activation analysis processes involving long lived isotopes. Thermal neutron activation analysis by using nuclear reactors requires a high degree of care specially to eliminate the level of interferences which affect the sensitivity of the technique. The homogeneity of the thermal neutron flux is needed of course to ensure that samples and monitors are exposed to similar neutron fluxes. Also to accomplish the activation analysis mainly by thermal neutrons, irradiations have to be carried out in the thermal column since in-core irradiations will generally yield an appreciable fission neutron contribution. Attempts to use the reactor fast neutrons for activation analysis is even more difficult, since the presence of thermal neutrons whose neutron

cross-sections may be several orders of magnitude more than fast neutrons presents a serious problem. It is obvious, therefore, that the exothermic capture reactions may very well completely overshadow the (n,p), (n,α) or (n,2n) reactions. To increase the sensitivity for the investigation of certain elements, resonance neutrons may be used by surrounding the sample with ^{10}B to absorb thermal neutrons and allow neutrons with higher energies to activate the sample [34]. But this method is limited since it requires the ratio between the resonance cross-sections of the trace element and those of the matrix to be high. On a small scale 14 MeV neutrons can be produced on the reactor site if necessary using a special arrangement. Thermal neutrons are converted to 14 MeV neutrons with an efficiency of 2.1 x 10^{-4} by using a ^{6}Li D converter [35]. The reaction sequence is as follows:

1) Tritons are produced by the $^{6}Li(n,\alpha)T$ reaction in the lithium converter which is made infinitely thick for thermal neutrons, followed by

2) Production of 14 MeV neutrons by the reaction $D(t,n)^{4}He$, the tritons from reaction (1) having an energy of 2.8 MeV.

In conclusion, if we are thinking in terms of activation analysis facilities for small laboratories, nuclear reactors do not seem to fit the requirements on the basis of complicated operating procedures. This point of view is further confirmed by taking the costs also into account, since the purchase and operation costs for a modest 100 - kW facility are well above $500,000. We can add to this other disadvantages such as heavy shielding requirements to reduce the relatively high radiation levels, handling highly radioactive spent fuel elements, and release of radioactive substances in case of an accident.

2.3.2 Isotopic neutron sources

Isotopic neutron sources are formed by using the (α,n) or (γ,n) reaction on isotopes of light elements, whose (α,n) or (γ,n) threshold is low compared with gamma or alpha energy. For example, a portable low intensity ~~zero power~~ neutron source can be produced by mixing ^{241}Am, which is an alpha emitter, with beryllium. Since the emitted alphas and gammas are not monenergetic, the emitted neutrons are not monoenergetic either; and an additional neutron energy spread occurs for (α,n) sources because alpha energies get degraded by the source materials before interacting with the beryllium. Mixing of the radio-active isotope and converter in a powder form is not essential for (γ,n) sources, e.g. $^{24}Na/Be$ or $^{24}Na/D_2O$.

The neutron output from this type of neutron source is rather low and is of the order of 10^6 n/s. c_i, but the stability of neutron production is very good specially for $^{241}Am/Be$ sources due to the long half life of ^{241}Au (248 years). The thermalization efficiencies for isotopic neutron sources are good due to their low mean neutron energies, but their reliability for accurate thermal neutron activation analysis is again affected by the low neutron output. An alternative source to provide about 4.4×10^9 n/s c_i is the ^{252}Cf which undergoes spontaneous fission and can be designed in small sizes for better geometry. But the limited commercial production of ^{252}Cf at the present time, and its short half life which is effectively 2.6 years make this source extremely expensive. The gamma ray background from ^{252}Cf source is slightly high, and it varies appreciably for (α,n) sources, where $^{241}Am/Be$ is one of the very low gamma background sources.

2.3.3 Accelerator neutron sources

2.3.3.1 14 MeV neutron generator

In spite of the important role of nuclear reactors in the activation analysis field, the development of smaller and easily operated neutron sources is extremely useful in establishing activation analysis as a more widespread analytical tool. The limitations of the isotopic neutron source that have been outlined, leaves without any doubt the so called "neutron generator" as the most promising answer.

The subject of neutron producing reactions using ion beam accelerators is well established in nuclear physics. By using low energy accelerators, occurrence of (p,n) and (d,n) reactions on several light nuclei is energetically possible, and the emitted neutrons differ in both yield and spectrum due to the difference in cross-sections, reaction Q-values and nuclear energy levels.

An ideal accelerator neutron source for activation analysis is a reaction with large positive Q-value to allow the use of low ion bombardment energies, large cross sections for good neutron yield, and also with a single neutron group emission. It is not surprising, therefore, that the $^{3}H(d,n)^{4}He$ reaction has been accepted as an excellent neutron source for activation analysis due to its unique properties. The D-T reaction has a positive Q-value of 17.59 MeV and a cross-section of 5 barns at deuteron energy of about 110 keV only. It has also the advantage of producing monoenergetic neutrons at relatively high energy (14 MeV), which is due to the high threshold for break-up of ^{4}He and the absence of excited states in this nucleus.

In neutron generators, deuterons are usually extracted from RF or PIG ion source and accelerated by using a small voltage generator such as a Van de Graaff, Cockroft-Walton, Electrostatic Rotor machine (SAMES),

or Insulating Coil Transformer to energies of the order of 120 - 200 keV. The ion beam is then allowed to strike targets in which tritium has been diffused in a thermally stable material such as titanium. By using such a simple and economical set up, intense fast neutron ~~fluxes~~ sources of 10^{11} n/mA.S are produced with a total neutron energy variation with angle of emission of about 2 MeV. The neutron beam so produced can be obtained in a continuous mode or in a pulsed mode to enhance the yield of short lived radio-isotopes. The beam pulsing can be carried out by using a common pulsing technique such as ion beam electrostatic deflection, or as suggested recently by Tazanowski [36] by using the storage ring concept to multiply the beam intensity.

Neutron generators can also be used for thermal neutron activation analysis by using an appropriate moderator surrounding the tritiated target. But, due to the steep fast neutron flux variation with distance and the low thermalization efficiency for 14 MeV neutrons, low thermal neutron flux is produced at the sample position. Monoenergetic neutrons with energies around 2.8 MeV can also be produced by using the exothermic $^{2}H(d,n)^{3}He$ reaction on deuterium targets. The D-D reaction is a better source for thermal neutrons, but for bombardment energies lower than 1.0 MeV the D-D reaction yield is much lower than that for the D-T reaction, for example for E_d = 150 keV it is 300 times lower, Fig. 3.1.

Both the variety of nuclear reactions produced by 14 MeV neutrons and the simplicity of sealed tubes for neutron generation, make the analysis by 14 MeV neutrons widely accepted specially for on-line analysis. In the steel industry, for example, the most common application of 14 MeV neutron activation analysis is the determination of oxygen [37] with a sensitivity of 5 ppm in about 1.0 minutes of analysis time. The analysis is performed by using the $^{16}O(n,p)^{16}N$ reaction and detecting

the 6.13 and 7.11 MeV gammas emitted by ^{16}N with a half-life of 7.35 S. For analysis involving very short lived radio-isotopes, cyclic activation analysis can be used to reveal their contributions. This can be achieved by accumulating in the detector the radiation induced by a number of consecutive short irradiations.

The accuracy of 14 MeV neutron activation analysis is dependent to a large extent on the accuracy of the cross-section data used in the analysis [38], and this dependence can be clearly explained as follows. 1) Neutron cross-section data are needed for determining the absolute concentrations of trace elements and also in estimating the contribution of interfering reactions. 2) For an ideal programme in activation analysis, one would also need to know the cross-section variations over an appropriate energy range to account for the neutron energy variation with angle. 3) Also positions and values of maximum energies for better reaction yields, and therefore better sensitivities. 4) The neutron flux determination for activation analysis is dependent on the excitation functions for standard reactions to whom relative measurements can be made. The use of a comparator with a known impurity concentration can avoid the requirement for precise cross-sections, but has other disadvantages. This subject will be further discussed later in this thesis.

2.3.3.2 Other accelerator neutron sources

The variety of nuclear reactions that occur under 14 MeV neutron irradiation have the disadvantage of possible creation of interferences from the matrix elements. Also, they may lead to the most serious limitation of fast neutron activation analysis which is the production of the same radio-nucleides from more than one element. By an appropriate

choice of neutron bombardment energies one can reduce the contribution made by an interfering reaction; but such requirements can not be met by using a neutron generator since the available neutron energy range is about 2 MeV only for the $T(d,n)^4He$ reaction.

By having a more powerful machine one can produce neutrons with widely varying energies using different ion beams and targets. Variable-energy cyclotrons operating at energies of about 10 MeV per nucleon can provide good selectivity for neutron activation analysis [39]. For the determination of small amounts of iron in the presence of large amounts of cobalt, 14 MeV neutrons produce the radioisotope ^{56}Mn via the $^{56}Fe(n,p)^{56}Mn$ and $^{59}Co(n,\alpha)^{56}Mn$ reactions which make the analysis impossible. The method used by Steele et al [39] to solve this problem is to use the small cyclotron and take into consideration both the reaction thresholds and the coulombic barriers. The reaction thresholds for iron and cobalt are 2.9 and zero MeV and their coulombic barriers are 4.6 and 8.3 MeV respectively. Therefore by irradiating Fe - Co samples with neutrons having energy appreciably less than 8.3 MeV, but above 2.9 MeV, ^{56}Mn activity will be produced essentially from the iron present in the samples.

By bombarding a beryllium target with deuterons of energies lower than 10 MeV stable and intense source of few MeV neutrons is produced, the $^9Be(d,n)^{10}B$ neutrons under these conditions have limited applications in fast neutron activation analysis but they offer a good source for thermal neutrons. At higher deuteron bombardment energies stripping and break-up neutrons are produced preferentially in the forward direction with a neutron flux increasing steadily by increasing the deuteron energy. The fast neutrons so produced, at deuteron energies above 10 MeV on thick beryllium targets, have energy distributions with

broad asymmetric peaks occuring at neutron energies approximately equal to 0.4 times the incident deuteron energies. By using deuteron energies varying between 16 and 53 MeV Krivan and Munzel [31] have carried out systematic studies for the detection limits of cyclotron neutrons compared with 14 MeV neutrons for (n,p), (n,α) and (n,2n) reactions. For their given experimental conditions, it was estimated that for 53 MeV deuterons the limits of detection for cyclotron-produced neutrons are lower than those for 14 MeV neutrons by a factor of 20 to 100.

By using Harwell 280 cm. synchrocylclotron, Jarvis et al [40] performed thermal neutron activation analysis on large samples by prompt and delayed gamma detection. The particle beam extracted from the synchrocyclotron was transported into the experimental area and directed towards a cylinder of natural uranium, and the neutrons were readily thermalized in a large polythene cylinder surrounding the uranium source. It is interesting to note that the proton beam intensity actually used (0.08 μA for 160 MeV) provides a neutron flux density comparable with that obtainable from a few milligrams ^{252}Cf. In spite of the prolific neutron yields produced by high energy beams, their use of course is limited; the required accelerators are expensive to install and operate and therefore they are not justified for the sole use of activation analysis.

CHAPTER THREE

THE D-T NEUTRON SOURCE

3.1 Nuclear Data for the D-T Reaction

The experimental information on absolute cross sections and angular distributions of the D-T reaction are well documented for deuteron energies up to 10 MeV [41], and with the recent measurements on Hamburg isochronous cyclotron the limit was moved to 15 MeV [42]. As shown in Fig. 3.1a [43], the average neutron energy available from the $T(d,n)^4He$ reaction is appreciably higher than those from the $D(d,n)^3He$ and $^9Be(d,n)^{10}B$ reactions throughout most of the deuteron energy range. Following a steady increase in the average neutron energy for the D-T reaction, a drop around 4 MeV is observed. This drop is explained according to the three-body system as due to the appearance of the other neutron groups above the deuteron break-up threshold. The existence of break-up neutrons presents no problem if neutron energies are below the thresholds of the neutron reactions studied. Also the energy discrimination between the two neutron groups is possible due

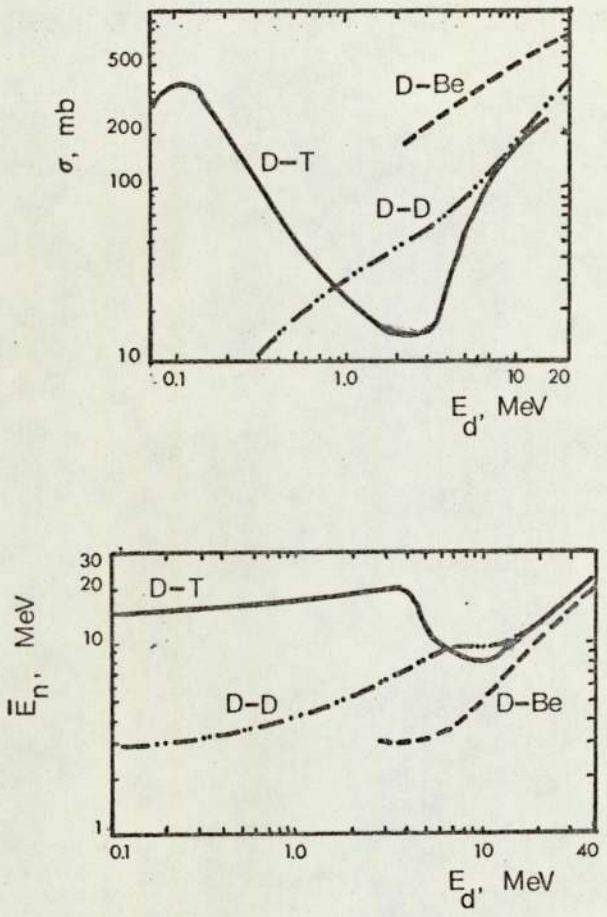

Fig. 3.1a
$D(d,n)^3He$, $T(d,n)^4He$ and $^9Be(d,n)^{10}B$ Reactions.
The Variation of Reaction Cross-Section and Average Neutron Energy with Incident Deuteron Energy.

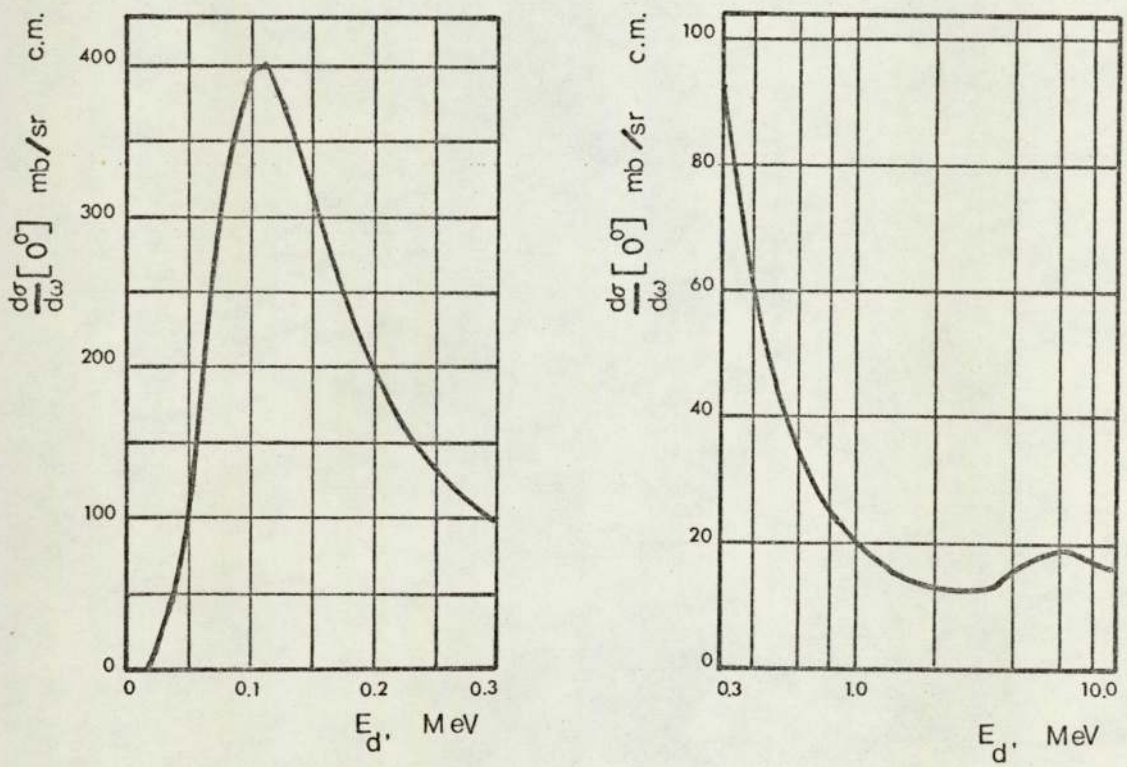

Fig. 3.1b
0^{o} Differential Cross-Section for the $T(d,n)^{4}He$ Reaction

to their large energy gap.

At low deuteron bombardment energies, the maximum neutron yield is obtained at a bombardment energy of 0.11 MeV for a thin target stopping only about 1.0 keV deuterons. This corresponds to the broad resonance peak at 0.11 MeV which has a cross section value of about 5 barns, as shown in Fig. 3.1b[41]. In practice however, thick targets are used in order to stop the whole deuteron beam, and so in this case the maximum neutron production occurs for deuteron energies higher than 0.11 MeV, Fig. 3.6.

3.2 Particle Accelerators

3.2.1 The Van de Graaff accelerator

To produce neutrons with energies ranging between 13 and 15 MeV which is the region that has the most extensive applications, low energy particle accelerators are needed. For this project, the 0.5 MeV Van de Graaff accelerator at the University of Aston in Birmingham was therefore used for the production of neutrons.

Fig. 3.2 illustrates one of the basic design features of this machine, which is the separation of the belt from the acceleration tube. The operation of this machine is similar to more modern single ended machines in which the belt and the acceleration tube are housed inside a single stack. The charging system in Astons Van de Graaff is also standard i.e. by corona discharge from a set of corona points close to the belt and situated near to the ground potential pulley. The belt charging system is dependent on the uniformity of the charge distribution which is a function of the insulation properties of the belt, (note here that this is not the case for pelletron charging system).

Fig. 3.2

The 0.5 MeV Van de Graaff Accelerator

Therefore, care in maintaining the belt was always needed; during the period in which this project was running a new belt was installed.

The neutron producing target was situated at the end of a short beam tube which was positioned directly below the acceleration tube. When beam alignment was required, a fine adjustment system was used to minimize the current readings on four slits placed at the entrance of the beam tube. The deuteron beam currents delivered by the RF source were stable and at an operating voltage of 0.3 MeV for our neutron experiments the machine conditions were satisfactory.

3.2.2 Wide neutron energy region requirements

Although much work has been done in the 13 - 15 MeV energy range because of the availability of small accelerators, excitation function measurements for neutrons having energies within a region larger than the standard 13 - 15 MeV region have certain advantages for the following reasons:-

1) Revealing the shapes of the excitation functions more clearly.

2) The possibility of making cross section measurements around σ_{max} is useful for more sensitive activation analysis work.

3) Accurate investigation of E_{max} might also lead to information about the thresholds for competing reactions.

4) By increasing the incident neutron energy above 15 MeV rare reaction investigations become much easier.

5) A good check for our own neutron monitoring technique can be obtained by working with an extended energy range and under different experimental conditions.

3.2.3 The Dynamitron accelerator

In addition to our experiments on the Van de Graaff, we have made further measurements in a wider neutron energy region. This was possible by using higher deuteron bombardment energy and a tritium target that does not stop the beam entirely. For these experiments we used a 1.4 MeV deuteron molecular beam D_2^+ which is equivalent in energy to an atomic beam D^+ of 0.7 MeV. The molecular beam was used to create a higher D^+ particle flux by breaking the molecular ions up on the tritium target. The vertical 3.0 MeV Dynamitron at Birmingham Radiation Centre was used as a source for the molecular beam and the experiments were carried out in a low scatter room.

The pressurised accelerator was manufactured by Radiation Dynamics Inc. of New York which is responsible for the development of the Dynamitron which can be considered as an R/F parallel fed Cockroft-Walton machine [44]. Basically, the accelerator design includes a resonant pressure tank circuit consisting of a toroidal coil and two electrodes. The two electrodes are C shaped and act as two capacitors, producing R.F. field between them. The induced R.F. voltages on the corona grading hoops of the acceleration stack are then transferred to the high-voltage terminal by an R.F. choke. On the Dynamitron, increase in the frequency of the driving voltage is achieved by using thermionic hard-vacuum rectifier tubes instead of the conventional rectifiers to reduce the diode shunt capacity. The required power for the thermionic rectifier at a given stage is supplied by the ripple R.F. voltage at that stage. A schematic representation of a Dynamitron accelerator is shown in Fig. 3.3 [45]. Positive ions and electron beams can be supplied with currents of the order of mA with a ripple voltage less than 3 kV peak-to-peak and a short term voltage stability of the order of 1%.

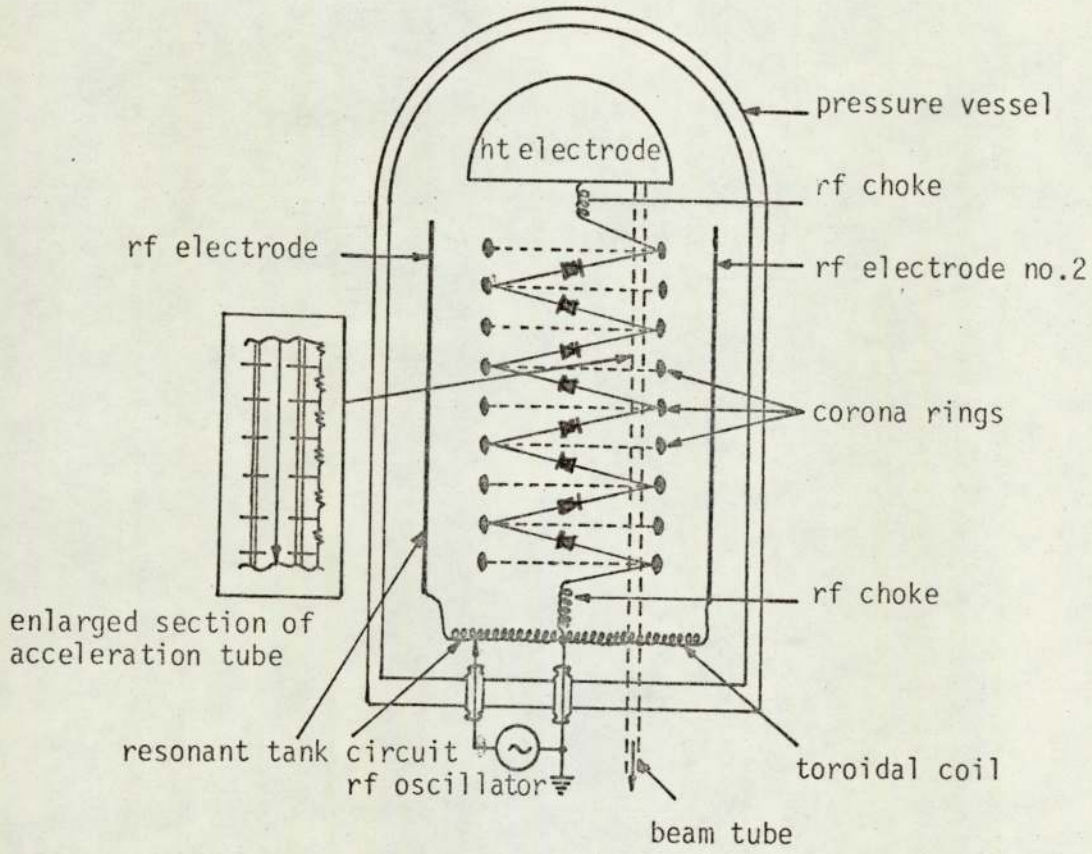

Fig. 3.3

Schematic Representation of a Vertical Section Through a Vertical Dynamitron Accelerator

The required vacuum conditions were reached by using a large diffusion pump with a cold trap for the machine and ion pumps for the beam lines. The ion beam leaving the duoplasmatron ion source is usually magnetically analysed before entering the accelerator tube. The accelerated beam then is directed towards the appropriate beam line using magnetic analysers and for our experiments a 90^{o} analyser was used.

3.3 The Tritiated Target and Target Assembly

The tritiated titanium targets used in our experiments are of the type TRT.51 and are supplied by the Radiochemical Centre at Amersham. According to the manufacturers specifications [46], these targets are made of 0.25 mm thickness and 28.17 mm diameter copper backing on which a thin titanium layer of 1.08 mg/cm^2 thickness and 2.54 cm diameter is deposited. The tritium is absorbed in the titanium layer by heating the targets to a temperature of about $400^{o}C$ and cooling them in an atmosphere of tritium. The absorbed tritium layer in our targets has a thickness of 0.77 $curies/cm^2$. The use of thick tritium targets is important for producing high neutron yields and in reducing the rate of reduction in yield. On the other hand such targets degrade the energy of incident deuteron beam and generate some spread in energies of the emitted neutrons. The TRT.51 targets are thick enough to stop the whole 0.3 MeV deuteron beam, but they present partial stopping for the 0.7 MeV beam (1.4 MeV D_2^+) which is required to expand the neutron energy range. Our measurements show that for an 0.3 MeV deuteron beam the TRT.51 target produces a neutron yield of about 10^8 n/s μA depending on the age of the target.

3.3.1 Behaviour of the neutron output from T-T_i targets

It is important to recognise that the neutron flux from gas-in-metal targets decreases with usage, and this is less pronounced for short irradiations than for longer ones. The half-life of a target is influenced by mainly deuteron bombardment time and beam current and it can be defined as the time at which the yield falls to half of the original neutron output at constant beam current. For a 2 curies target the half-life is of the order of 0.5 mA. hour, for irradiations of 5 sec at 300 μA [47]. By measuring the yield curves for a new target of uniform tritium distribution, Broerse et al [48] concluded that the curves measured after 17 and 30 hours of irradiation show that more tritium has disappeared from the front layers of the target than from the deeper layers.

It has been reported that the target deterioration with time falls in a manner defined by two exponential decays, one having a half-life of the order of 150 minutes and the other a half-life of the order of 1100 minutes [49]. These data were obtained by using 0.1 to 0.14 MeV deuteron beams with target currents of 0.25 mA to 1.0 mA, and with tritium content of 6.5 to 13.7 curies. The initial rapid fall of neutron output is explained mainly by outgassing due to local heating and positive ion bombardment, together with a limited amount of sputtering [49]. By improving the target cooling, increase of the initial half-life by 50 to 100% can be obtained [50]. The longer half-life, which takes place after about 500 min. of operating time, can be explained by the diffusion of tritium from the lower layers of the target to the region where the D-T reaction is occuring. The same mechanism applies also to a short lived increase in the neutron yield observed at the beginning of the irradiation time [51,52]. In this case

the yield proceeds by reaching a maximum after a few minutes and then follows the usual neutron yield decline ~~fasion~~ pattern in about 15 minutes. This short time interval behaviour was observed using 0.2 and 0.12 MeV deuteron beams with effective diameters of 4 and 6 mm and beam intensities of 200 and 100 μA. (51,52)

In a recent experiment by Stengle et al (53) using an analysed deuteron beam, the measured short half-lives of T-Ti targets were found to be more than an order of magnitude longer than those observed using unanalysed beams. It appeared, therefore, that the short-lives observed with unanalysed beams are mainly due to sputtering and radiation damage caused by heavy ion contaminants always present in unanalysed beams. The other improvement approach is by Bibby et al (54) who have demonstrated the effect of thermal treatment on the neutron output of used T-Ti targets. By redistributing the residual tritium a remarkable neutron output enhancement was obtained, which shows that thicker targets may be used giving a saving in running costs of a generator.

Our experience with T-Ti targets show that improved neutron outputs can be obtained by allowing the targets to rest after use for some time, this is in support of the work by Cossutta (55). To account for the neutron yield variation with irradiation time, the neutron rate of production was monitored continuously by using a BF_3 counter surrounded by a moderator. The amplified detector output was fed to a rate meter and a plotter and the cross section data were then corrected for the neutron flux variation with time.

To reduce the effect of ion beam heating on neutron production, various methods of target cooling are usually employed. Better results can be obtained if rotating targets are used, since they are capable of dissipating 600 W of power and have half-lives of up to 200 hours for

normal operation [56]. The other major development in this subject is the acceleration of a mixed deuteron-triton beam towards a metal plate and allow the ions to diffuse and reach a stage where the rate of ion loss from target is equal to the rate of ion loading. Since the acceleration of tritons is usually not desirable, hence "sealed" tubes are required to replace the pumped accelerators [57], and these are commercially available. A significant development in activation analysis can be achieved by increasing the yield of the portable sealed tubes; and a good step in this direction would be of course by increasing the beam current on self regenerating targets by using for example, a modified Duoplasmatron type ion source [58].

3.3.2 The target assembly

Various methods can be used for target cooling by water or gas, but our water cooled target assemblies were designed specially for neutron excitation function measurements. In the Van de Graaff target assembly, the T-Ti target is clamped, to ensure good thermal conductivity, on the top of a heat sink which has a cross sectional geometry of half a circle. This design was adopted so that neutrons emitted between 0^{o} and 90^{o} pass through the same thickness of material. To compensate for the neutron attenuation at angles larger than 90^{o}, calculations of the percentage of neutrons likely to interact in the backing and in the compensator were made to estimate the size of a converter which was then placed on the outside wall of the chamber. The chamber diameter was made small so that positioning the samples at short distances from the neutron source will become possible if necessary. The water cooling system was designed in a special way such that the water path does not coincide with the "direct line" of target to specimen.

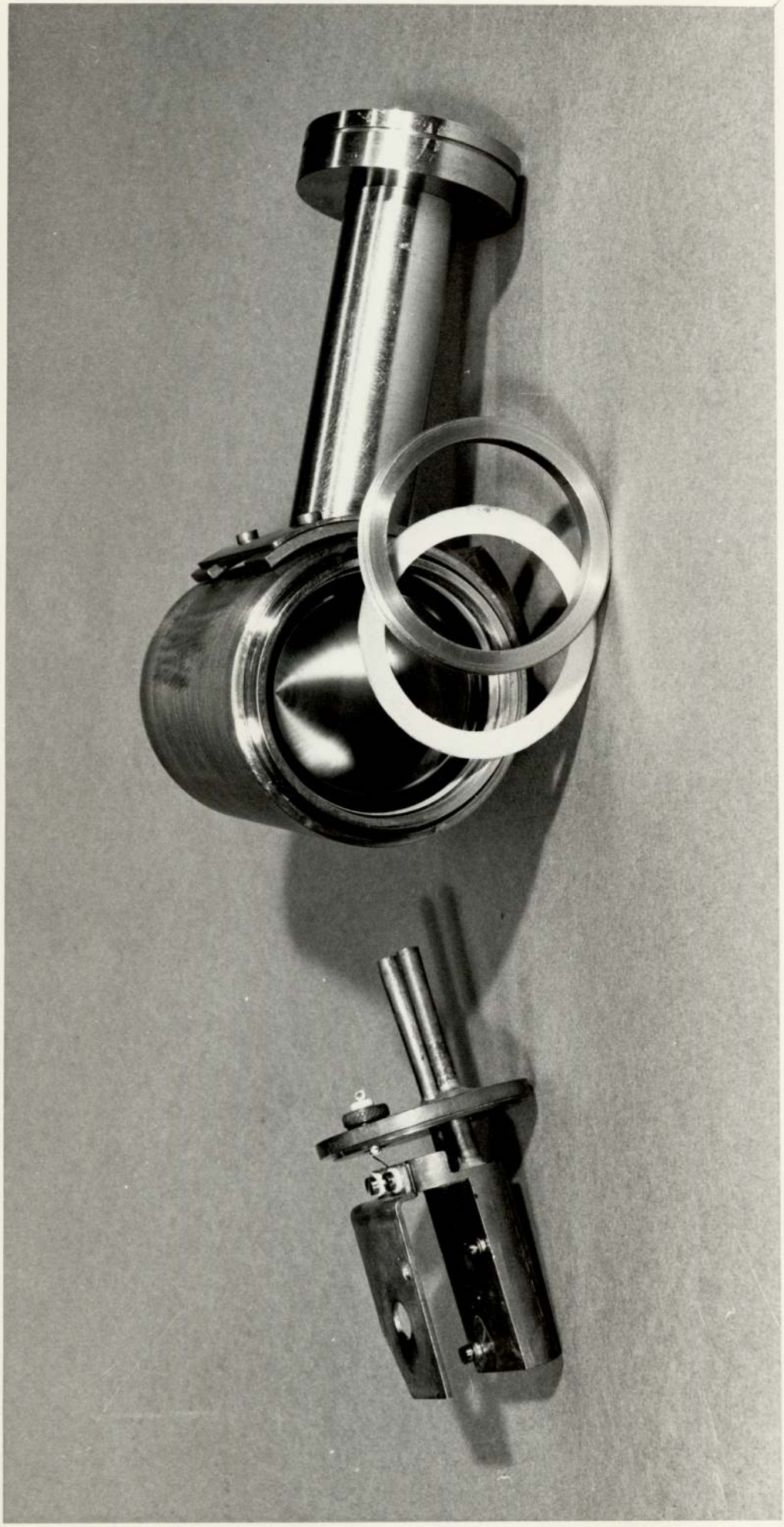

Fig. 3.4 The Water Cooled Target Assembly

A collimator of 1.2 cm diameter was used to limit the size of the deuteron beam spot on target, and by monitoring the current on this collimator efficient accelerator operation is obtained. Target current was also measured continuously on a micrometer by taking the readings from the heat sink. The heat sink is supported through the cooling water inlet and outlet on a flange which is in good electrical insulation from the rest of the chamber. The procedure used for improving the neutron yield is that another spot on the target is brought into the beam, when the former impact is exhausted.

The target assembly shown in Fig. 3.4 was used for the Dynamitron experiments. This has design features similar to the Van de Graaff target assembly, except the use of stainless steel instead of brass to satisfy the vacuum requirements on the Dynamitron. The heat sink is made of copper to obtain good thermal conductivity.

3.4 Evaluation of the D-T Source Parameters

3.4.1 Deuteron beam energy loss and straggling

Energy losses of deuteron beam in tritiated titanium targets are calculated under the assumption that Bragg's law holds, i.e. the energy loss in a compound is the sum of the energy losses in its separate constituents. Benveniste and Zenger [59] used this law and produced the following formula for T-Ti targets:

$$\left(\frac{dE}{dx}\right)_{T\text{-}Ti} = \frac{48}{48+3n}\left(\frac{dE}{dx}\right)_{Ti} + \frac{3n}{48+3n}\left(\frac{dE}{dx}\right)_{T} \qquad (3.1)$$

where (n) represents the loading factor i.e. the number of tritium atoms per titanium atom.

Due to the lack of experimental data on the energy loss of deuterons in titanium, $(\frac{dE}{dx})_{Ti}$ data for deuterons were evaluated by Benveniste and Zeneger [59], Saker and Wood [60], Gunnersen and James [61] using energy loss results of protons on different materials. Warshaw [62] has carried out experiments for the determination of $(\frac{dE}{dx})$ in aluminium, copper, silver and gold for protons in the energy region 0.05 to 0.35 MeV. By transferring Warshaw's data on aluminium and copper using an $A^{-\frac{1}{2}}$ relationship the rate of energy loss for protons in titanium was obtained. Values of $(\frac{dE}{dx})_{Ti}$ for deuterons are derived from the proton data according to the assumption that the rate of energy loss is a function only of the velocity of the particle

$$(\frac{dE}{dx})_{\text{protons}} (E) = (\frac{dE}{dx})_{\text{deuterons}} (2E) \qquad (3.2)$$

Since no results on the rate of energy loss for deuterons in tritium are available, it is therefore necessary to make a transformation from the proton energy loss data in hydrogen. The following formula is therefore valid since tritium and hydrogen have the same nuclear charge and tritium has an atomic weight equal to 3:

$$(\frac{dE}{dx})_{\text{tritium}} (\text{keV/mg/cm}^2) = \frac{1}{3} (\frac{dE}{dx})_{\text{hydrogen}} (\text{keV/mg/cm}^2) \qquad (3.3)$$

Calculations of $(\frac{dE}{dx})_{T\text{-}Ti}$ is one of the functions of the computer program which we have developed for D-T neutron production ('NEUTRED', Appendix 1). It is assumed that the energy degradation of the incident beam takes place in stages of 50 keV in the region from the incident energy to 200 keV, 10 keV in the region from 200 keV to 50 keV, and 5 keV in the region from 50 keV to 10 keV. These small steps ensure that average values for the functions $(\frac{dE}{dx})_{T}$ and $(\frac{dE}{dx})_{Ti}$ may be assumed

between energy steps. To calculate the deuteron rate of energy loss for 0.3 MeV and 0.7 MeV beams in TRT.51 T-Ti target, a loading factor of 1.2 was used. These evaluations were made by assuming a uniform tritium distribution throughout the target thickness, and the results are shown in Fig. 3.5. The accuracy of $(\frac{dE}{dx})_{T\text{-}Ti}$ results depends strongly on the accuracy of the data for its separate constituents. The uncertainties associated with each of these constituents vary with deuteron energy, but generally they are about $\pm$5% in the high energy region and rise to about $\pm$ 10% in the low energy region due to the extrapolation involved.

Deuteron beam energy spread is rather small and less than 0.1% for Van de Graaff machines. But due to the statistical nature of the energy loss processes, a deuteron experiences an energy straggling as it penetrates the target. If $f(E_d)$ denotes the energy distribution function at some depth of an initially monoenergetic beam, then energy straggling is defined as the standard deviation of $f(E_d)$ with respect to the average. If we consider the distribution to be Gaussian function of energy, therefore as the beam penetrates the distribution gets wider due to straggling.

The simplest theoretical approach to straggling is due to Bohr [63] who described the energy straggling for a given projectile as a dependent on the square root of $(Z_2 N \Delta R)$, where (Z_2) is the target atomic number, (N) is the number of target atoms per unit volume, and (R) is the thickness of the target. Bohr's theory is based on the assumptions that target atoms are randomly distributed, energy loss during single interaction is very much less than the total energy loss over the entire path, and the projectile velocity is much greater than the orbital electron velocity of the target atoms. Unfortunately, at low and medium energies the

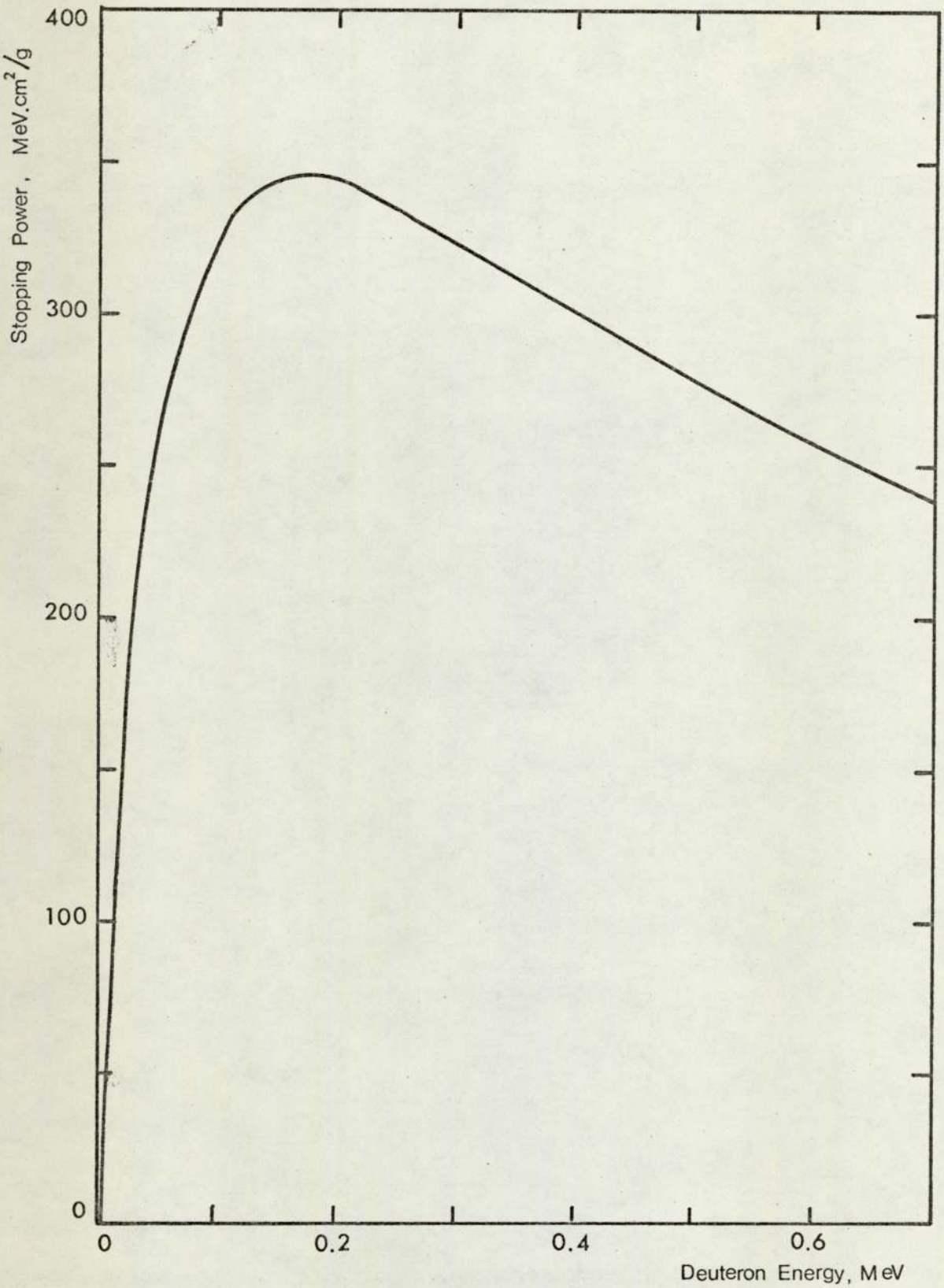

Fig. 3.5

Deuteron Rate of Energy Loss in Tritiated Titanium Target with a Loading Factor of 1.2

third assumption breaks down and the energy dependence correction of Lindhard and Scharff [64] should be considered. In addition to this it is difficult to estimate the accuracy of the theoretical calculations esepcially if a (Z_2) structure in energy straggling is present at low energies. There are no empirical values at the present time for the energy straggling in tritium or titanium to be used for the calculations. Therefore it was not possible to take the straggling factor into account.

3.4.2 Tritium target yield

Before selecting the operating conditions for neutron production it is useful to calculate the values of total neutron yield per incident deuteron of energy (E_d). The calculated values are important for choosing sample to target geometry, prediction of the magnitude of the induced activity per unit weight of the sample material, and also they are important in accelerator shielding design. The probability (P) of a deuteron undergoing a D-T reaction while travelling a distance (dx) in a T-Ti target material containing N_t tritium atoms/cm^3 is given by:

$$P = N_t \cdot \sigma \cdot dx \qquad (3.4)$$

where σ is the cross section of the D-T reaction.

Since (σ) is a strong function of deuteron energy, the following relation is used to take into account this variation effect of (σ) on (P).

$$\sigma dx = \frac{\sigma dE}{(dE/dx)_{T\text{-}Ti}} \qquad (3.5)$$

Therefore equation 3.4 will take the form

$$P = \frac{N_t \cdot \sigma \cdot dE}{(dE/dx)_{T\text{-}Ti}} \qquad (3.6)$$

For complete stopping of the deuteron beam in the target material, each deuteron will have a finite probability of reacting throughout the range of energy from zero to the accelerating energy (E_d). Thus the total probability of a deuteron reacting in the target will represent the total neutron yield per incident deuteron, (Y), and is obtained by the integration of (P) over the whole energy range.

$$Y \leq \int_0^{E_d} P.\, dE = N_t \int_0^{E_d} \frac{\sigma.\ dE}{(dE/dx)_{T-Ti}}$$

Therefore

$$Y = 4\pi N_t \int_0^{E_d} \frac{\sigma(\Omega)}{(dE/dx)_{T-Ti}}.\, dE \qquad (3.7)$$

where $\sigma(\Omega)$ represents the differential cross section for the D-T reaction given in units of barn/steradian i.e. $\sigma(\Omega) = \frac{\sigma}{4\pi}$.

The solution of eq. 3.7 produces absolute neutron yield results for thick tritium targets using the appropriate value of tritium number of atoms. The equation can also be used to calculate the depth distribution of the reactions as they occur in the target.

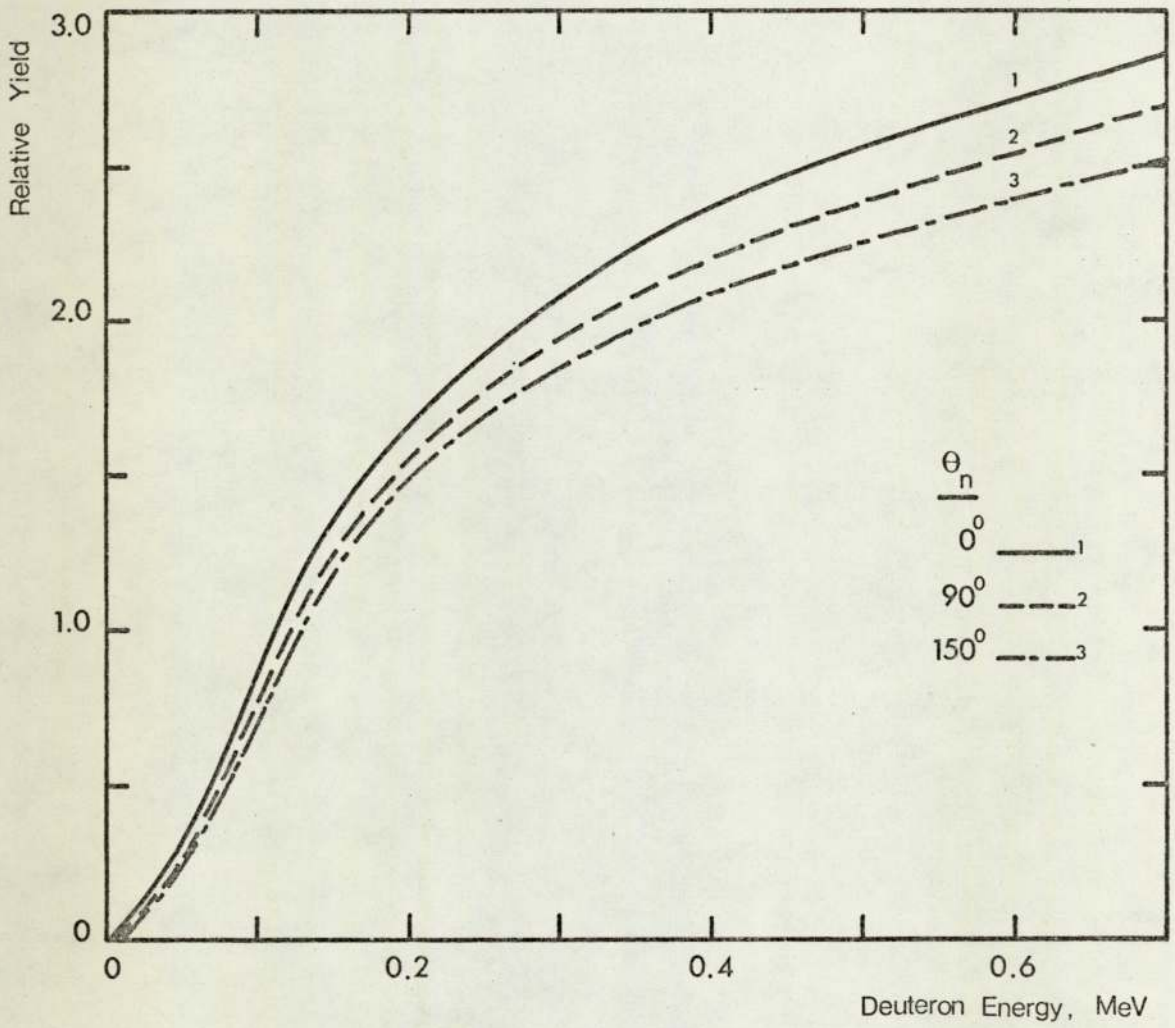

Fig. 3.6

The Variation of D-T Neutron Yield With Incident Deuteron Energy and Emission Angle for Thick T-Ti Target

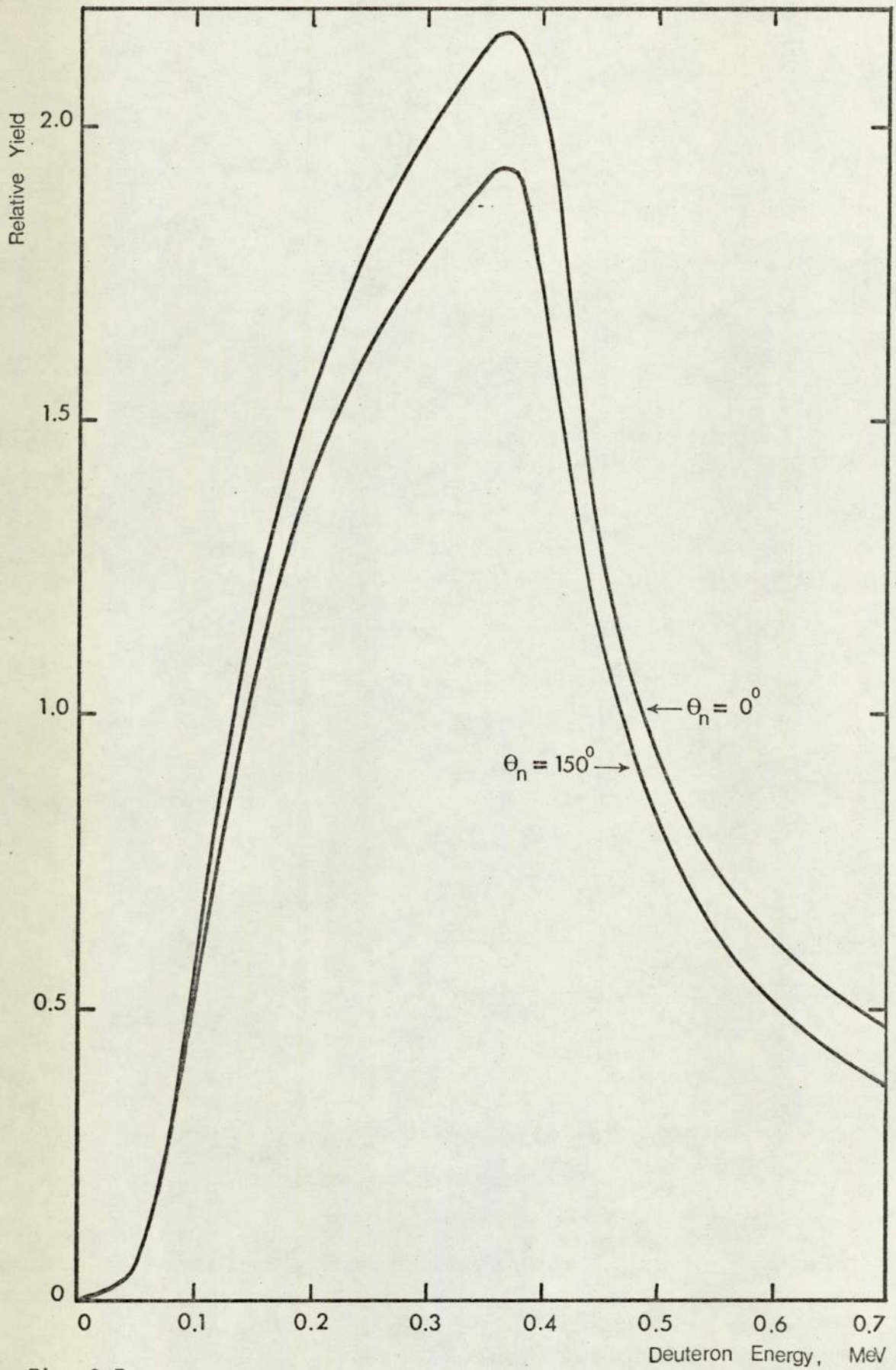

Fig. 3.7

Calculated D-T Neutron Yield Curves For a 1.08 mg/cm^2 T-Ti Target

In the present work, the absolute neutron yield curves are not required, although estimation of the neutron yield curves on a relative scale is worthwhile for calculating the neutron mean energies. This can be achieved by the integration of neutron spectra, which are evaluated on a relative scale using equation(3.15).

The yield curves for thick targets are shown in Fig.3.6 These were determined for deuteron energies up to 0.7 MeV and for different emission angles. For TRT.51 T-Ti target, the titanium layer (1.08 mg/cm^2) is not sufficiently thick to stop completely the deuteron beam above 0.37 MeV. Therefore a fall in the neutron yield is observed at higher energies as is shown in Fig.3.7.

3.4.3 Neutron anisotropy

Although in the centre of mass system of co-ordinates, the angular distribution of the reaction products from the T(d,n)^{4}He reaction is isotropic up to about 0.4 MeV; the case is different in the laboratory system. In the laboratory system the angular distribution of the reaction products is anisotropic even at lower energies, and the anisotropy increases with increasing the incident deuteron energy. Since we are dealing with the laboratory systems, a suitable transformation procedure from the centre of mass system to the laboratory system is required.

Neutron anisotropy is the ratio of neutron flux in the forward to backward directions, but since the neutron flux is isotropic in the centre of mass system, the anisotropy in the laboratory system is equal to the ratio of neutron flux in the lab. system (ϕ_ℓ) to that in the c.m. system ($\phi_{c.m.}$) over the angular range.

Let the angles made by the emitted neutron directions in the lab. and c.m. systems to be θ_ℓ and $\theta_{c.m.}$ respectively. Therefore the neutron anisotropy which equals the ratio between the solid angles in c.m. and lab. system is given by[59]:

$$\frac{dW_{c.m.}}{dW_\ell} = \frac{\phi_\ell}{\phi_{c.m.}} = \frac{\sin\theta_{c.m.}\, d\theta_{c.m.}}{\sin\theta_\ell\, d\theta_\ell} \qquad (3.11)$$

Now, if $$\gamma = \frac{V_{\ell(c.m.)}}{V_{c.m.(n)}} \qquad (3.12)$$

where $V_{\ell(c.m.)}$ = velocity of the c.m. in the lab. system,

and $V_{c.m.(n)}$ = velocity of the neutron in the c.m. system;

Therefore,

$$\cos\theta_{c.m.} = -\gamma \sin^2\theta_\ell \pm \cos\theta_\ell \sqrt{1 - \gamma^2\sin^2\theta_\ell} \qquad (3.13)$$

By differentiating eq. (3.13) we can get

$$\sin\theta_{c.m.}\, d\theta_{c.m.} = \left(2\gamma \sin\theta_\ell + \sin\theta_\ell \sqrt{1 - \gamma^2\sin^2\theta_\ell} + \frac{\gamma^2\cos^2\theta_\ell \sin\theta_\ell}{\sqrt{1 - \gamma^2\sin^2\theta_\ell}}\right) d\theta_\ell \qquad (3.14)$$

Therefore,

$$\frac{dW_{c.m.}}{dW_\ell} = \frac{\gamma(\cos\theta_\ell + 1/\gamma^2 - \sin^2\theta_\ell)^2}{\sqrt{\gamma^2 - \sin^2\theta_\ell}} \qquad (3.15)$$

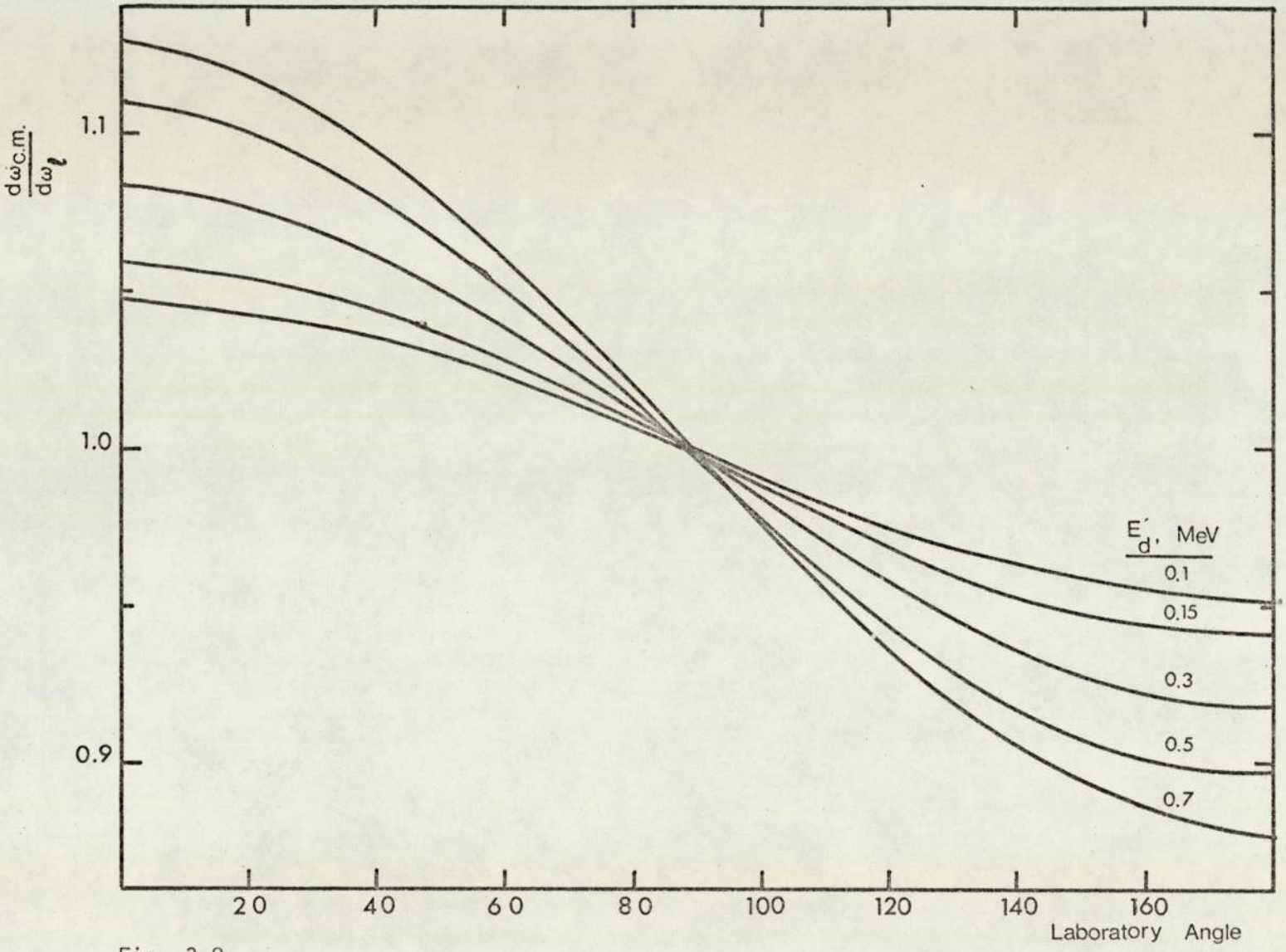

Fig. 3.8

The Ratio of the Solid Angles in the Centre of Mass and Laboratory Systems into which the Neutron is Produced as a Function of the Neutron Laboratory Angle

To evaluate the neutron anisotropy as a function of deuteron energy and lab. angle, the function $\gamma(E_d)$ has to be calculated. According to the kinematics of the reaction and according to eq. ~~3.19~~ 3.9, the following relation is obtained:

$$\frac{1}{\gamma^2} = \frac{M_\alpha}{M_n} \cdot \frac{(M_d + M_t)}{M_d} \cdot \left(\frac{M_t}{M_d+M_t} + \frac{Q}{E_d}\right) \qquad (3.18)$$

Here M_d, M_t, M_n and M_α represent the masses of incident deuteron, tritium nucleus, and the emitted neutron and alpha particles respectively. Q and E_d respresent D-T reaction Q-value and deuteron energy respectively. Fig. 3.8 shows the anisotropy plotted as a function of laboratory angle for different deuteron bombardment energies. These curves were obtained by using the computer programme 'NEUTRED'.

3.4.4 Neutron energies

For very thin targets, it is assumed that the energy spread introduced by target effects is negligible and neutron energies can be calculated from the kinematics of the two-body reaction

i.e.

$$\sqrt{E_n} = \frac{\sqrt{M_d M_n}}{(M_\alpha+M_n)} \cdot E_d \cdot \cos\theta_n \pm \sqrt{\frac{M_d M_n}{(M_\alpha+M_n)^2} \cdot E_d \cos^2\theta_n + \frac{M_\alpha - M_d}{M_\alpha+M_n} E_d + \frac{M_\alpha \cdot Q}{M_\alpha+M_n}} \qquad (3.17)$$

This consideration is not valid once thick targets are used, because of the slowing down of deuterons in the target. Fast neutrons from thick targets are produced by deuterons of energies ranging from the initial incidence energy to zero energy. Therefore the emitted neutrons at a given angle exhibit an energy distribution due to

variation in effective incident deuteron energy. Once the neutron spectra are calculated, mean neutron energies and their energy spreads can be obtained. These calculations are of great importance for the measurement of neutron cross sections where data at specific neutron energies are measured.

Neutron spectra were calculated by using 'NEUTRED' on a relative yield scale by taking into consideration anisotropy, deuteron energy loss, and D-T reaction cross section. The recommended cross section data made by Liskein and Paulsen [41] were used.

If RN = Relative number of neutrons,

ANISO = Neutron anisotropy,

DEL = Deuteron energy loss in T-Ti target,

and DTCRS = D-T reaction cross section

$$\text{Therefore, } RN(E_d,E_n,\theta_n) \alpha \frac{ANISO(E_d,\theta_n)}{DEL\ (E_d)} \cdot DTCRS(E_d,\theta_n) \qquad (3.18)$$

Neutron spectra calculations made by using this relation were obtained in deuteron energy steps similar to those used for energy loss calculations. Laboratory angle was varied in steps of 10^o from 0^o to 180^o. The angle 98^o was also taken into account because neutrons emitted at this angle have the minimum energy spread. Neutrons emitted at 98^o have the nearest mean energy value to 14 MeV which is important as a reference at which absolute cross section results are preferably obtained.

It is clear from Fig. 3.9 that neutron spectra do not show symmetry around the peaks, but as a whole they show a symmetry around 98^o spectrum, with a decreasing peak height as we increase the neutron emission angle. The spectra peaks correspond to neutrons produced by

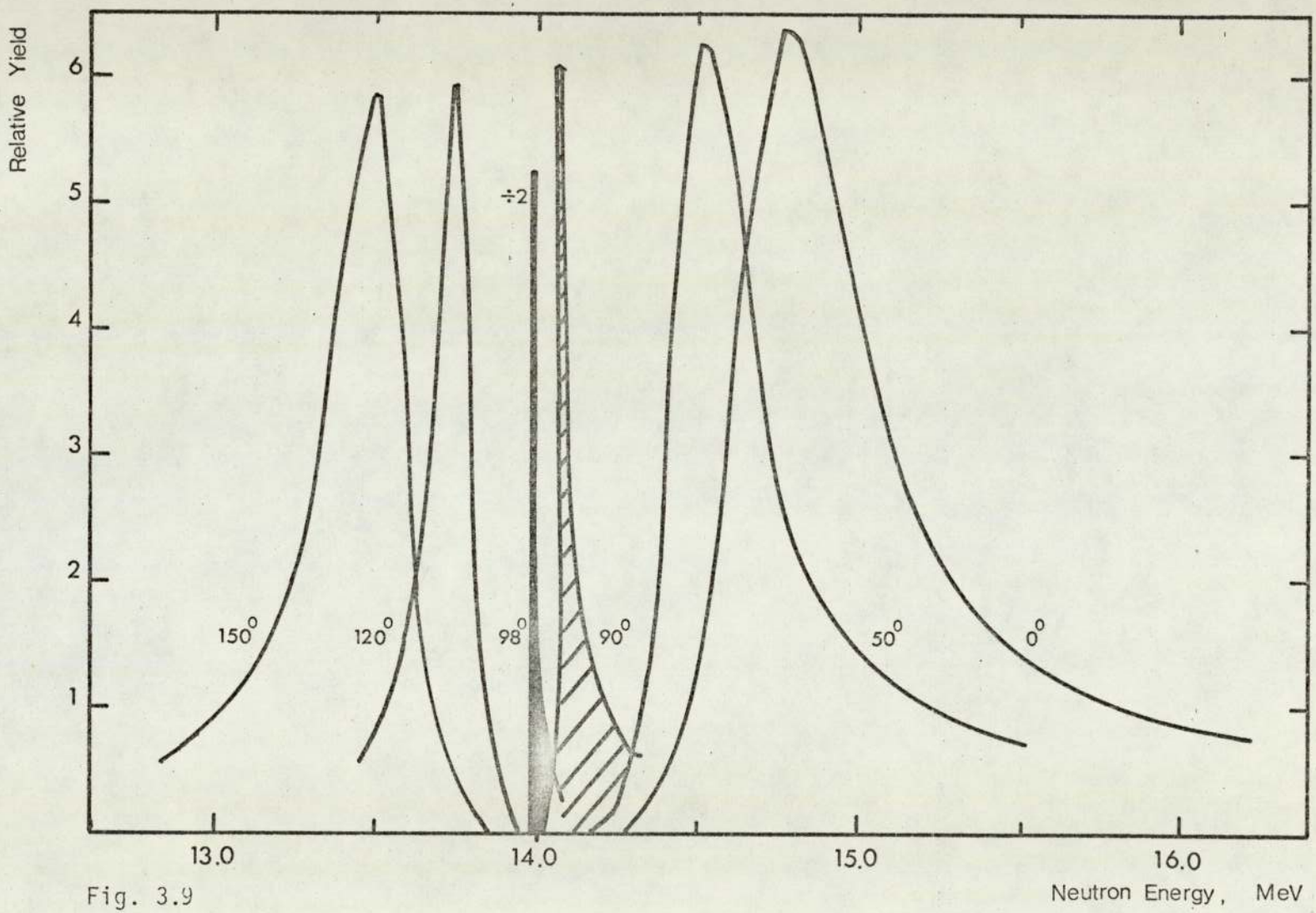

Fig. 3.9

The Energy Distributions for D-T Neutrons at Different Angles of Observation for a Thick Tritiated Titanium Target. E_d = 0.7 MeV

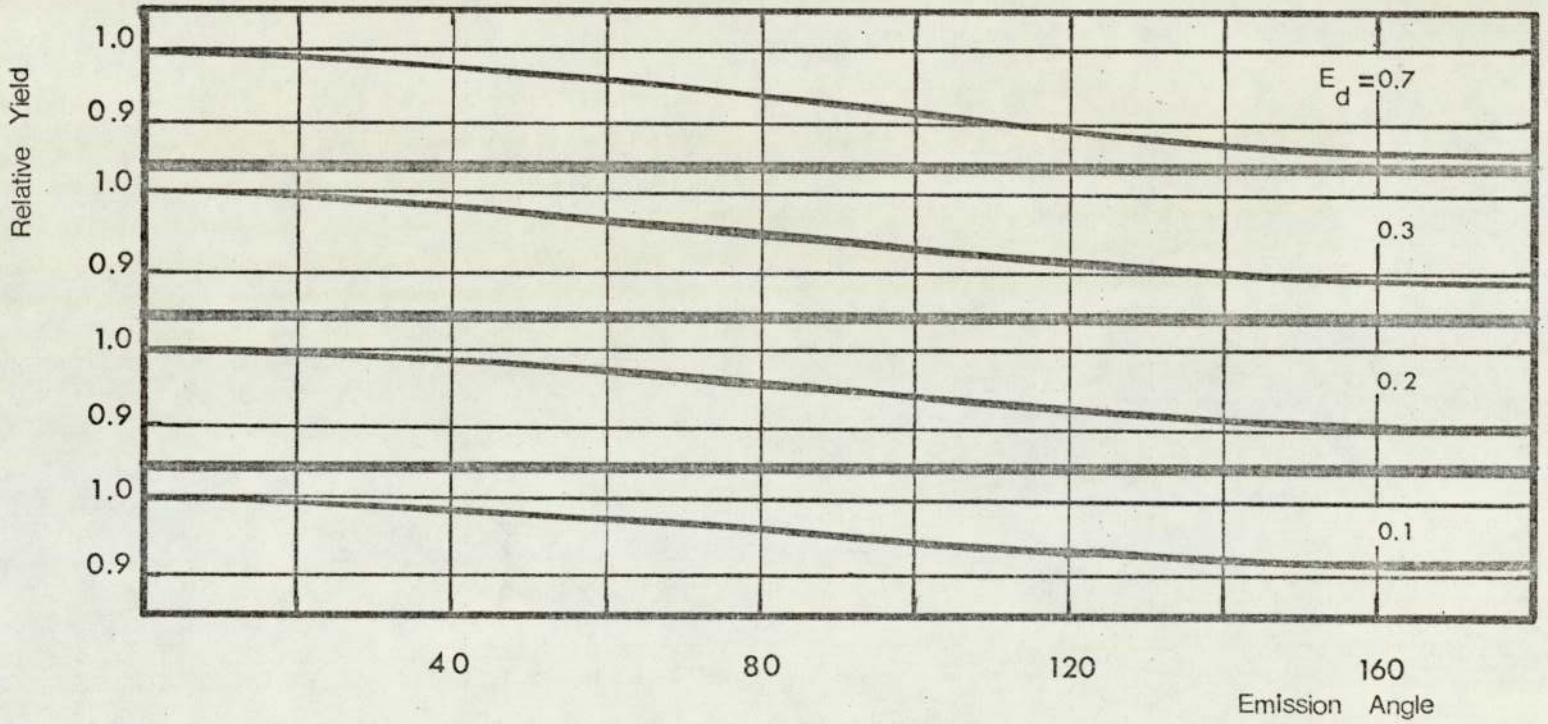

Fig. 3.10

The Relative Angular Distributions of Neutron Intensity for the (d,n) Reaction on Thick Tritiated Titanium Target

0.11 MeV deuterons; the increase in peak height by decreasing θ_n indicates that slightly more neutrons are produced by E_d = 0.11 MeV in the forward direction than in the backward direction, and the same effect ~~phenomena~~ applies to other deuteron energies. This can be demonstrated by determining the neutron angular distribution, Fig. 3.10, which is very important in making the appropriate correction for fast neutron flux slight variation with emission angle.

Neutron spectra were used to calculate the mean neutron energies numerically by using the following relationships for different angles of neutron emission.

$$\bar{E}\ (\theta_n) = \int_0^{E_d} \frac{RN(E)\ .\ E_n(E)}{TRN\ (\theta_n)}\ .\ dE \qquad (3.16)$$

where TRN is the total relative number of neutrons.

The mean neutron energy results are shown in Fig. 3.11, and here the neutron energy spreads due to deuteron energy degradation in the target are determined by the widths at half maxima for neutron spectra. The mean neutron energy range for 0.7 MeV deuteron beam on TRT.51 T-Ti target is wider than that for thicker targets. This is due to the target thickness which corresponds to an energy loss of 0.26 MeV at E_d = 0.7 MeV. Hence, for this case only the neutron groups which are due to the contributions of deuterons with energies between 0.7 and 0.44 MeV are taken into account.

In our case, the additional fractional increase in neutron energy spread due to deuteron multiple scattering has not been taken into account. This is justified because we have been interested in determining the general trends of fast neutron excitation functions. Multiple deuteron scattering effect has to be taken into account if an

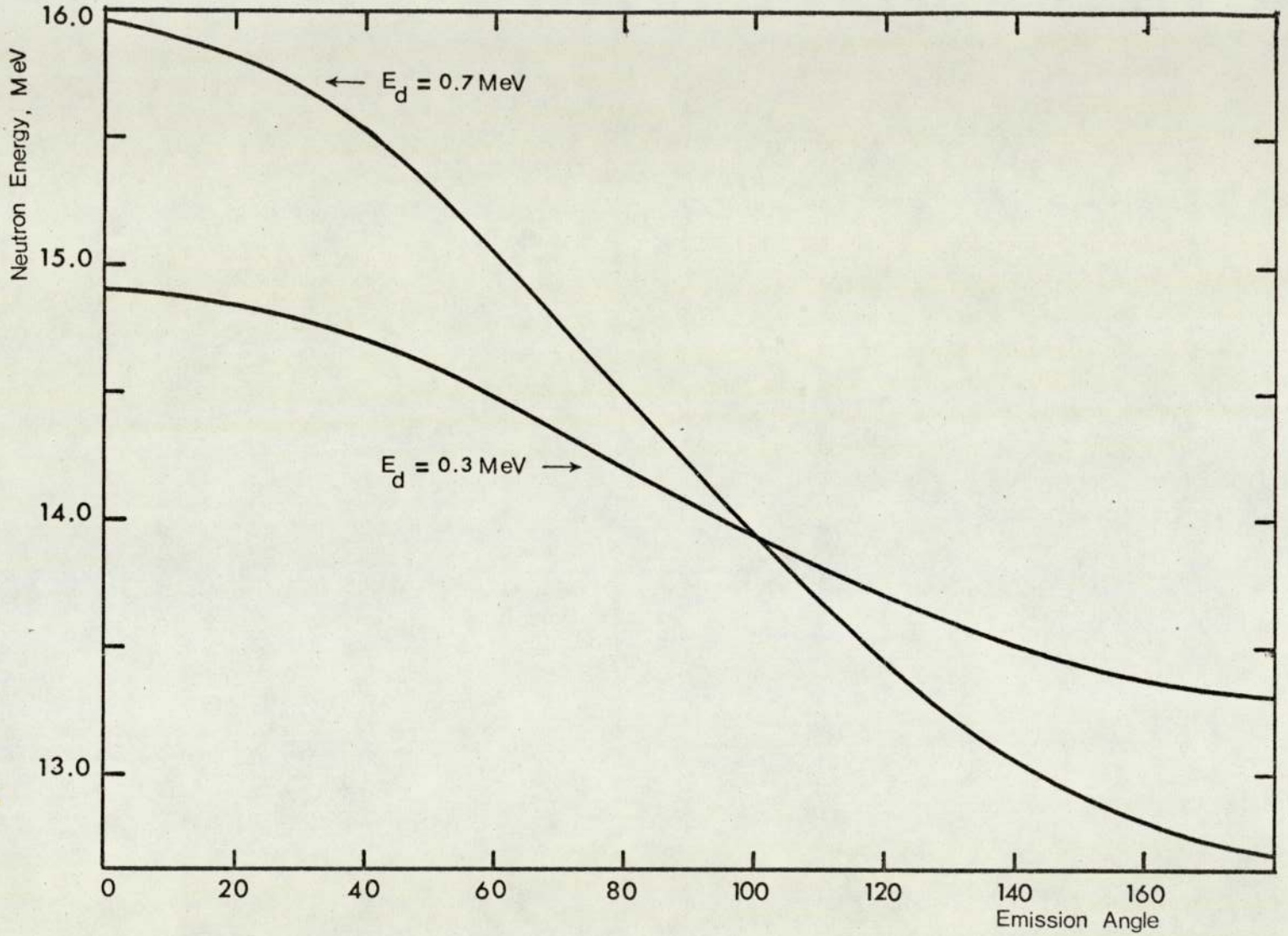

Fig. 3.11

Mean Neutron Energy as a Function of Observation Angle for a 1.08 mg/cm^2 T-Ti Target With a Loading Factor = 1.2

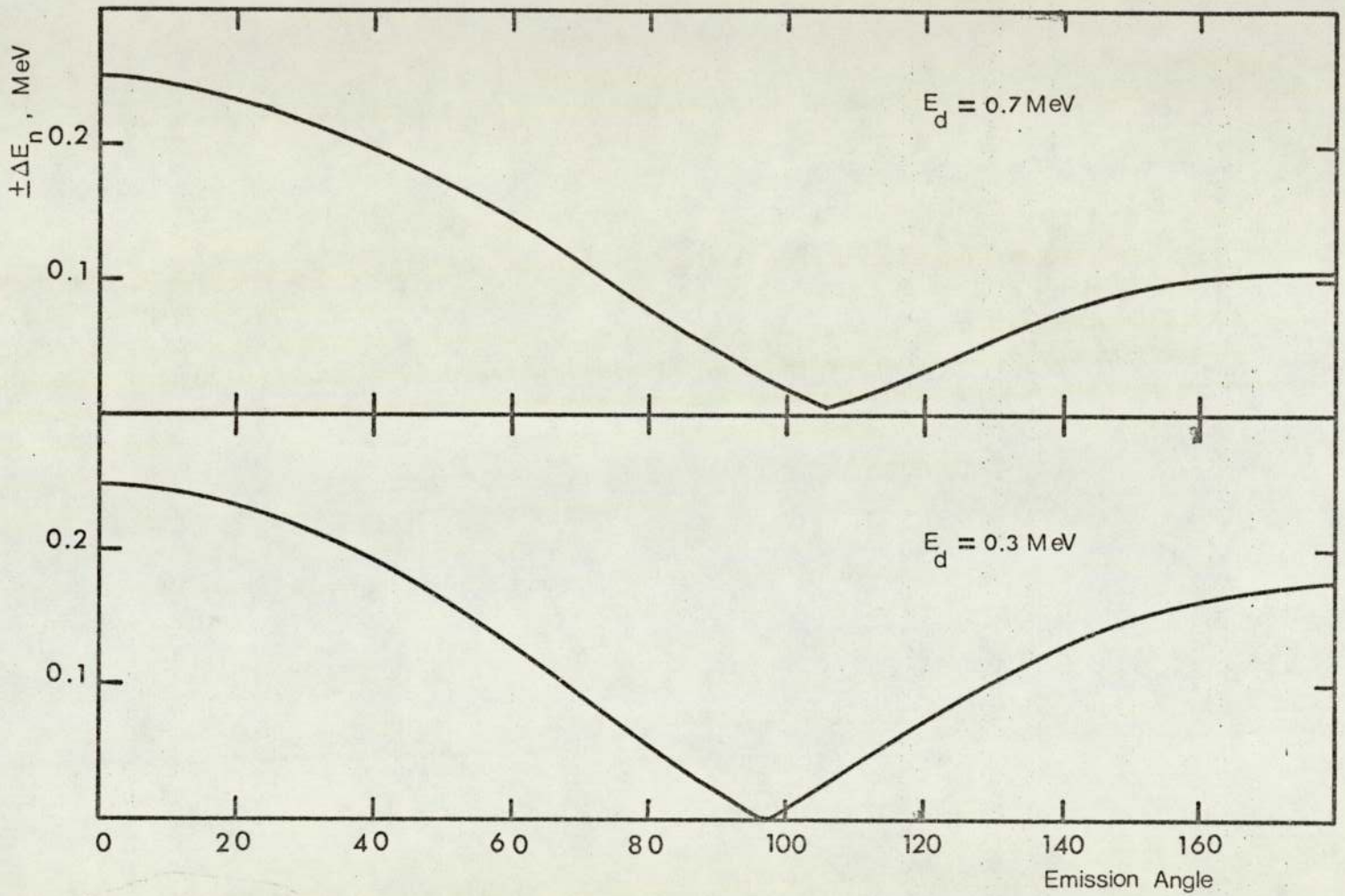

Fig. 3.12

Neutron Beam Energy Spread Due to Deuteron Energy Loss in a 1.08 mg/cm^2 T-Ti Target

attempt to investigate the fine structure in neutron excitation functions is required.

CHAPTER 4

DETERMINATION OF FAST NEUTRON BEAM PARAMETERS

4.1 Fast Neutron Detection

In neutron spectroscopy, the progress in improving neutron detection efficiencies and resolution has direct applications in studying the properties and locations of nuclear energy levels, and this information is required in nuclear terminology where accurate spectroscopic data are very important in reactor design, radiotherapy and activation analysis. Much more work is required for fast neutrons with energies up in the 14 MeV region due to the increasing interest which is being given to the controlled fusion programmes.

Generally, two principles are employed in neutron spectroscopy. The first depends on the (n,p) elastic scattering, by detecting the recoil protons produced. The second method depends on specific neutron reactions and involves determining the energies of the charged particles

produced.

The majority of fast neutron time-of-flight facilities use organic scintillators for the detection of neutrons; these scintillators have high hydrogen content and fast rise and decay times of the fluorescence output. The faster time of the scintillation pulse, with the corresponding better time resolution is an important feature of modern plastic and liquid scintillators which are excellent for coincidence measurements. The use of organic scintillators for fast neutron detection is hampered by the interferences from the gamma-ray background. The separation between neutron and gamma ray contributions is obtained by using pulse shape discrimination techniques which utilize the difference between the pulse shape of light produced by electrons and that produced by protons.

Below about 8 MeV, the (n,p) scattering is sufficiently isotropic in the centre of mass system [65], but above this energy the anisotropy begins to appear and it increases by increasing neutron energy. The lack of accurate 0^{o} differential scattering data of neutrons from protons above 8 MeV leads to uncertainties of more than 2% above 14 MeV, which is a significant contribution to the overall error in a flux measurement by recoiled protons. Therefore, the determination of detection efficiencies for such neutron spectrometers is essential. For example, Cookson et al [66] have carried out recently liquid scintillator experimental efficiency measurements below 30 MeV relative to the associated particle technique.

Generally, the use of neutron induced exoergic reactions, e.g. $^{6}Li(n,\alpha)T$, $^{10}B(n,\alpha)^{7}Li$ is primarily restricted to slow neutron detection by detecting the emitted energetic charged particles. By using neutron moderators, neutron detectors based on such reactions can also be used

for fast neutron detection, e.g. the use of BF_3 counter as a flat response Long Counter. Alternatively, fast neutron detection is more commonly carried out by using fast fission and threshold reactions in which the emitted particles are more difficult to detect. In this case the radiation emitted by the residual nuclei are detected, i.e. the activation method.

4.2 Some Activation Methods for the Measurement of Accelerator Fast Neutron Source Properties

4.2.1 Neutron spectra

Although fast neutron spectra measurements can be done by the known measuring techniques such as scintillators, solid state detectors, and proton recoil telescopes; the threshold detectors technique has been considered more reliable. The threshold detectors method, which was developed originally for reactor physics studies [67], requires a rather small amount of effort. It has also the advantages of being insensitive to non-neutron radiations and presenting negligible perturbing effects on neutron flux distributions. The technique's basic requirements are knowing the threshold energies and having sufficient accurate information about the absolute neutron cross-sections as functions of neutron energy. By covering the entire neutron energy range which is under investigation with the threshold detectros, with suitably spread thresholds, one can obtain accurate and detailed information about fast neutron yield, spectrum and angular distribution.

A proposal was made by Heertje [68] to use the threshold detectors for measuring the properties of neutrons produced by irradiating Be, Al, Co, Ag and Ta targets by 26 MeV deuterons fron a cyclotron. Although the use of threshold detectors in the early works was affected by the

limited availability of accurate data on neutron excitation functions, valuable information concerning the effect of target atomic weight and deuteron beam energy on the neutron flux and spectra were obtained. It was concluded by Heertje [68] and Heertje et al [69] that the accelerator fast neutron spectra can be described by an expression similar to that used for fission spectrum.

Also using this assumption, Bruninx and Crobeen [70] were able to study the neutron spectra of a thick beryllium target under the bombardment by 20 MeV helium-3 ions, 14 MeV protons and 7.5 MeV deuterons using the threshold detector method. Foils of carbon, aluminium, copper, silicon and indium (the reaction thresholds of which range between 0.5 MeV and 20 MeV) were irradiated as a compact sandwich at a given distance from the neutron source and in the forward direction. Following the irradiation, the corrected disintegration rate of each foil was fitted to the activation equation. The neutron flux at the sandwich position was then found by substituting the average cross-section value in the activation equation and making the appropriate corrections.

$$\phi = \frac{A}{M.\bar{\sigma}} \qquad (4.1)$$

Measurements of neutron angular distributions for each charged particle reaction were made on aluminium foils placed at different angles with respect to the incident charged particle beam direction. The activity at each angle as formed by the $^{27}Al(n,\alpha)^{24}Na$ reaction was related to the activity at (0^o) to determine the corresponding fluxes (n/sec. μA. cm^2) from the relation

$$\phi(\theta) = \frac{A(\theta^o)}{A(0^o)}. \ \phi(0^o) \qquad (4.2)$$

It should be noted here that no corrections for the $^{27}Al(n,\alpha)^{24}Na$ reaction cross-section variation with energy are given, therefore, when (r) is the distance from the neutron producing target, the total neutron yield will be given by:

$$N(n/sec.\ \mu A.\ 4\pi) = 2\pi r^2 \int_0^{\pi} \phi(\theta).\ \sin\theta\ .\ d\theta \qquad (4.3)$$

For a sealed tube D - T neutron generator, Lawson et al [71,72] established a simple activation method for measuring neutron production rate and scattered neutron fraction. The authors proposed the use of a set of threshold detectors taking into account the reaction excitation function of each detector from the threshold energies to about 15 MeV and normalizing the excitation curves to unity at 14.75 MeV. The 14.75 MeV flux densities at a given distance from the neutron source were plotted against the threshold energies and the variation trend with threshold energy indicated the presence of degraded neutrons. Also a peak centred in the region 13.5 - 15 MeV was found during spectra measurements when the response of each detector was represented by the equation:

$$\phi_{exp} = \sum_{i=1}^{n} \frac{\bar{\sigma}_i}{\sigma_{14.75}}\ \phi_i \qquad (4.4)$$

where

ϕ_{exp} = The experimental flux density deduced using the 14.75 MeV sensitivity factor,

$\bar{\sigma}_i$ = The average cross-section in the ith energy interval

n = The number of detectors used,

and ϕ_i = The mean flux density in the ith interval.

The variation of neutron flux and energy along a neutron generator axis with and without the presence of a moderating material (polythene) was the subject of an investigation by Oldham and Darrall [73]. A set

of threshold reactions with threshold energies varying between 6.3 and 15.6 MeV was used, and the method was based on suppressing the activities produced on the materials of higher threshold energies by using the moderating material. By selecting the appropriate polythene thickness the incident neutron energy was reduced by an adequate amount. The results are useful for 14 MeV activation analysis of elements which give radioactive nuclei having the same principle γ-energies and similar half-lives.

4.2.2 Neutron yields

By using the continuous flow manganese bath, which was originally produced for yield measurements of radio isotopic neutron sources, Scott [74] measured the yield of Li, Be, Co and Cu targets under the bombardment by 5 to 10 MeV protons. The neutron source was placed at the centre of an 85 cm. diameter sphere containing a solution of manganese, and the irradiation solution was then pumped continuously to a remote counting chamber containing a NaI detector. Due to the shorter half-life of ^{52}V compared with ^{56}Mn, the proposal to use vanadium as the activated element was made by De Valpi and Porges [75] for isotopic neutron sources, and later adopted for the accelerator measurements by Atta and Scott [76]. The continuous flow bath has limited applications and compared with threshold detectors it is more complicated. It provides information about neutron yields only.

To measure the neutron yield of a thick beryllium target, Bruninx [77,78,79] has used a cadmium shielded paraffin-indium detector as proposed by Stephens and Smith [80]. The method employs the activation of indium via the reaction $^{115}In(n,\gamma)^{116m}In$ by thermal neutrons resulting from the moderation of fast neutrons in a paraffin-wax sphere

shielded by cadmium foil. The detector has to be calibrated by a neutron source of known yield, and again it does not give any indication of the neutron energy spectrum. As reported by Bruninx, this detector gives higher neutron yield results compared with the threshold detectors due to the different shape of the angular distributions of neutrons with lower energies. The effect of lower energy neutrons is here more pronounced because the paraffin box is essentially an integrating device. Therefore care has to be taken to minimize the effect of lower energy neutrons in different irradiation environments.

4.3 14 MeV Neutron Flux Monitoring

4.3.1 Integral flux monitoring methods

On-line neutron integral output monitoring is useful for estimating the fast neutron flux and its changes for subsequent irradiations. It can also be utilized as the sensor for a servo-mechanism to control the neutron flux. Such flux monitoring can be achieved by using a neutron detector such as a proton recoil based detector or moderated BF_3 counter. For a good discrimination against lower energy neutrons, ZnS scintillator can be used to detect alpha particles produced by the $^{12}C(n,n')3^4He$ reaction on carbon foil, good stability and accuracy of 1% compared with standard copper foil[81] were reported. Alternatively, fast neutron flux monitoring can be done by counting the ^{16}N activity induced in the tritium target cooling water [82], although a rather poor precision is obtained due to the fluctuation in water flow rate [83].

By using the associated particle method, neutron flux determination with accuracies better than 2% is obtainable for the $T(d,n)^4He$ reaction. The α-particles produced by the reaction are counted in a well defined geometry and with very high efficiency by using an appropriate detector. At low deuteron bombardment energies the reaction angular distribution is expected to be isotropic, and therefore α-counting can serve to determine directly the neutron flux in any cone at any laboratory angle. The good energy separation between the emitted α-particles and the high yield scattered deuterons is advantageous specially for eliminating the pile-up which is introduced by the amplification system even with very short time constants. For using the associated particle method one has to take into account the interferences due to deuterium and carbon build ups which lead to the formation of new products via the (d,p) and (d,n) reactions. Furthermore, for old tritium targets α-backgrounds are produced by the (d,p) reaction on ^3He which is formed by tritium β-decay. At deuteron bombardment energies below the $^3He(d,p)^4He$ resonance at 0.44 MeV, the contribution of this interfering effect is negligible [84]. Non-uniformity of tritium loading in the target is usually considered as the most serious limitations of this method [85], and according to Fieldhouse et al [86] this effect has to be estimated by a coincidence method. In this case the tritium density distribution is determined by observing the coincidences between the emitted 14 MeV neutrons and associated alpha particles, and defining the deuteron reaction energy and hence the reaction depth according to the lab. angles of neutron and alpha detectors.

For experiments involving neutron cross-section measurements or activation analysis, the integral flux monitoring systems share generally

similar major disadvantages. As has been indicated, the D-T neutron flux changes with time during irradiation, and practically such changes are irregular and irreproducible. Therefore, magnitudes of the induced activites, specially for short-lived isotopes will be highly dependent on such changes.

4.3.2 Flux monitoring by standard materials

By monitoring the neutron flux with a standard containing an element yielding activity of a half-life approximately equal to that of the element to be analysed, the instantaneous fluctuations due to neutron production rise and fall are followed and corrected for. The standardisation of flux monitoring reactions is essential to establish interlaboratory comparison of fluxes, and establish a common basis for the determination of fast neutron fluxes for cross section measurements and activation analysis. The following set of critera is presented here to summarise the requirements for the precise selection of 14 MeV neutron flux monitoring standards.

1. The monitor material must be simple to handle, obtainable in high purity, and preferably contain predominantly one stable isotope.

2. The residual nucleus should be radioactive and must emit a γ-ray. It is very much advantageous if no chemical separation is required to count the product activity.

3. The emitted gamma rays should have a simple γ-ray spectrum and preferably it would emit only a single gamma line.

4. The γ-rays from the residual nucleus must be in the proper energy range for detection by standard gamma detectors.

5. The half-life of the residual nucleus should be of a convenient length and of a value close to that of the sample.

6. The monitor reaction cross-section variation with energy is very small or similar to that of the sample.

7. Matching the reaction thresholds for monitor and sample is beneficial to eliminate the effect of neutrons with degraded energies.

8. The excitation function of the monitor should be accurately known to take into account the neutron energy spread specially when monitor is placed close to the neutron source. This is also applied to the sample, and in both cases the incident neutron energy should be well known.

The "Texas Convention" was proposed at the 1965 Conference on Modern Trends in Activation Analysis [87], and it has stated normalized conditions for fast neutron flux measurements by a standard. A 99.9% copper disc of 1 cm or 2.5 cm diameter and 0.25 mm thick should be irradiated for 1 min. by 14 MeV neutrons. The induced β^+ activity formed by the $^{63}Cu(n,2n)^{62}Cu$ reaction, is then measured by sandwiching the monitor between two lg/cm^2 thick plastic beta absorbers for complete β^+ annihilation. After a minimum cooling time of 1 min, the sandwich is positioned along the central axis and 3 cms apart from the surface of 3" x 3" NaI(Tl) crystal. The measured flux will be then given in terms of the corrected number of disintegrations per min. per gram of Cu. Standard procedure for calculating the corrected disintegration rate for the copper standard is given by Heath [88].

Recommending the $^{63}Cu(n,2n)^{62}Cu$ reaction offers only single cross-section response with energy and single half-life. To form common basis for 14 MeV cross-section measurements and activation

analysis one has to establish a collection of standard reactions offering a wide range of excitation functions trends and half-lives. Flux monitoring by using copper standard is restricted to irradiations of less than 30 min. [$^{63}Cu(n,2n)^{62}Cu$, $T_{\frac{1}{2}}$ = 9.5 min] or for irradiations lasting more than several hours [$^{65}Cu(n,2n)^{64}Cu$, $T_{\frac{1}{2}}$=12.8h]. Accordingly, Shiokawa et al [89] have investigated the $^{19}F(n,2n)^{18}F$ excitation function on Teflon [$(CF_2)_n$] as an alternative standard. The $^{19}F(n,2n)^{18}F$ is suitable for irradiations of intermediate time ($T_{\frac{1}{2}}$ = 1.87h), but on the other hand the cross-section in the 14 MeV region is nearly one order of magnitude lower than that of the $^{63}Cu(n,2n)^{62}Cu$ reaction.

On the basis of excitation function slope, the $^{63}Cu(n,2n)^{62}Cu$ reaction does not seem to be ideal since its cross-section is a very steep function of energy. Alternatively, the use of $^{27}Al(n,p)^{27}Mg$ reaction has been suggested by Partington et al [90] due to its nearly flat response in the 14 MeV region. Actually, $^{27}Al(n,p)^{27}Mg$ cross-section is relatively low, and therefore a much more powerful standard is proposed in this thesis, i.e. $^{121}Sb(n,2n)^{120g}Sb$, and this is explained in Chapter 8.

CHAPTER 5

GEOMETRIC FACTORS AFFECTING THE D-T NEUTRON FLUX AND ITS MONITORING

5.1 The Non-Uniformity of 14 MeV Neutron Irradiation

Of more importance than time stability are D-T flux variations as a function of irradiation position. Several experimental [91-94] and theoretical [95-99] studies have been reported on the neutron flux distributions around tritium targets. Sample/target irradiation geometrical factors are also important, and these also have been the subject of several publications [100-104].

The fast neutrons produced by the D-T reaction for irradiation purposes have variable energies and fluxes due to such factors as 1) the variations in sample to target geometry, 2) neutron scattering and absorption [16,105], 3) non-uniform loading of tritium in the target [85], 4) deuteron beam diameter and conditions, 5) build-up of deuterium and depletion of tritium in target [106] and 6) scattering

from neighbouring materials. Therefore, each accelerator installation has its own neutron flux distribution patterns which are sensitive functions of several perturbing effects. This means that the use of a "universal standard" for flux estimation such as the $^{63}Cu(n,2n)^{62}Cu$ reaction can lead to inaccuracies due to anisotropy and inhomogeneity of the neutron flux. In fact the measured integrated activity on a sample must be related to a calculated average energy of the neutron flux through appropriate scattering calculations such as those proposed by Ricci [105].

5.1.1 Production of lower energy neutrons

For standard target/sample forward geometry using water cooled targets, Ricci used probability calculations to estimate the fractions of unscattered and scattered neutrons that are reaching the sample. In his particular geometry the results indicate that 58.4% of the neutrons are of the direct and unscattered type, while 27.4%, 7.6% and 6.8% are those due to scattering in target assembly aluminium and cooling water jacket hydrogen and oxygen respectively. The neutron energy ranges for the scattered neutrons are determined by taking into account first-order single scattering and using the non-relativistic scattering equation [107].

$$E_n' = E_n \cdot \frac{A^2 + 2A\,\mathrm{Cos}\theta + 1}{(A+1)^2} \qquad (5.1)$$

where A is the mass number of scattering nucleus, and θ is the scattering angle in the centre-of-mass system or the laboratory system for $A > 10$.

The neutron spectrum is formed by the direct and scattered components. While the direct component and the scattering component

from hydrogen are assumed to be rectangular within their corresponding energy ranges, the scattering components of aluminium and oxygen are assumed to be triangular. The triangular shapes with positive slope hypothenuses, are here determined by the forward peaking of the scattered neutrons angular distributions for Al and O [108] which enhance the high energy parts.

Due to the high neutron energy loss per collision with hydrogen nuclei, the presence of water in the vicinity of the neutron source will lead to the formation of a tail in the energy spectrum extending down to very low energies. Therefore 14 MeV nuetron flux measurement by $^{27}Al(n,\alpha)^{24}Na$ reaction will ~~und~~over estimate the flux by 14%, double that obtained by $^{63}Cu(n,2n)^{62}Cu$ reaction for the geometrical set-up of Ricci. This can be attributed to the threshold energy of the aluminium reaction which is much lower than that of the copper reaction. For an experimental set-up that produces 14 MeV neutrons within much narrower energy spectrum, less pronounced deviation of the results is expected due to the elimination of the threshold energy difference effect.

In most of the neutron generator facilities, the neutron producing target is housed in a limited space. In the majority of cases this is due to neutron shielding problems, and as an example we refer here to the "hole in the ground" geometry for sealed tube generators. Therefore additional low energy neutron background is expected to exist in the vicinity of the target due to neutron scattering by walls and nearby equipment. This effect is more pronounced if samples are placed far away from the target.

Interference effects due to deuterium build-up in the tritium target can be corrected for by using the corresponding element response

data for 3 MeV neutrons. It is possible to estimate the D-D neutron flux build-up which is a function of deuteron energy, integrated beam current, and target thickness.

At this point, we would like to emphasis that cross-section measurements for reactions with low thresholds should be carried out under improved irradiation conditions. This includes eliminating the effect of hydrogenous materials and the use of new tritium targets. Even then it is necessary to apply the appropriate corrections. For example, the use of the $^{27}Al(n,p)^{27}Mg$ reaction for 14 MeV flux monitoring would require full details concerning the experimental arrangements and in particular those about the cooling water and deuterium build-up. The effect of energy degraded neutrons discussed previously should also be taken into account.

The failure to fulfill such requirements will impose some doubts on the proposed use of Partington et al,[90] aluminium excitation function as a standard. Perhaps neutron scattering can also explain the rather low slope of their excitation function in the 14 MeV region.

5.1.2 Neutron flux patterns

For uniform target assemblies, like those used in this work, one would expect the fast neutron flux patterns to be nearly uniform around the neutron source, with slight anisotropy which is a basic property of the $T(d,n)^4He$ reaction in the lab. system. But, for other target assemblies larger flux pattern non-uniformities can be observed. Mapping the neutron flux distribution is useful for excitation function measurements and should materially aid the activation analyst in ensuring that the best irradiation configuration is being utilized for

the particular sample configuration being used. Simple techniques based on the use of photographic films and standard copper and teflon samples, have been studied by Priest et al. [93] to carry out such measurements. The measurements by Priest et al. [93] and Oldham and Bibby [94] indicate clearly the presence of flux angular anisotropies around the target due to angle-dependent neutron attenuation. The equiflux lines determined by Oldham and Bibby [94] reveal a "waist" effect due to neutron attenuation in the thick cooling jacket rim and target edges. As an example, by using the appropriate macroscopic cross-section it can be estimated that 1 cm of copper can be found to produce a 12% attenuation to 14 MeV neutron flux.

The neutron flux pattern properties are dependent on neutron absorption and scattering, therefore existence of enhanced scattered neutron yields can be expected at those angles which correspond to the "waist" effect. This can be estimated mathematically by means of numerical integration over the contribution of all volume elements of the target assembly and backing to the intensity for a particular angle. The scattering correction factor used by Vorach et al. [16] is based on such calculations and is given by

$$\frac{1}{(1 + \phi_{sc}(\theta)/\phi_{direct}(\theta))}$$

and for their particular experimental set-up the required corrections were up to 2.9%. For a uniform target assembly the correction factor should be nearly constant for all irradiation angles. In general, neutron flux pattern symmetry about the generator axis can be maintained if uniformity of the tritium distribution in the target is kept by using a uniform deuteron beam under good ion source operating conditions.

In fact, target deterioration leads to significant flux asymmetry of up to 30 per cent at short distances from the target [91], but the asymmetry decreases by increasing the distance. Practically, irradiation at large distances is not feasible because of the deterioration in the sensitivity due to the reduction of neutron flux with distance.

Systematic errors due to secondary neutron production by multiple reactions, i.e. (n,2n), (n,n) and (n,pn), in the target assemblies are negligible for the measurement of threshold reaction cross-sections. The situation is different for the measurement of 14 MeV neutron capture cross-sections [109], and in this case target assembly material, sample dimensions, and sample/target separation are very critical factors. Therefore, accurate relevant corrections are required for (n,γ) measurements [110,111].

5.1.3 General properties

It is obvious from the characters that we have discussed in this section that the optimization of neutron irradiation is dependent on the specific installation used. But, it will be worthwhile stressing here that neutron generating facilities share some common characters, such as neutron flux gradients. This fact has therefore prompted theoretical treatment of this general problem to the stage where its effect can be estimated with reasonable accuracy.

It is known that for a point radioactive source, the radiation intensity drop-off with distance can be well expressed by $1/R^2$ function. For 14 MeV neutron source, the $1/R^2$ relationship seems to hold at large distances but is not valid within very short distances from the tritiated metal target [92]. At such distances, a $1/R$

relation is a better approximation. This is of course due to the fact that the target is not a true point source. Thus the neutrons must travel one or two target diameters before approaching the $1/R^2$ relation. Along the deuteron beam direction, the axial neutron flux distribution (ϕ_r) can be expressed in terms of the flux at target surface (ϕ), target radius (d), and distance from target (r) in the following form [95]:

$$\phi_r = 0.58\ \phi \log_{10} \frac{d^2 + r^2}{r^2} \qquad (5.2)$$

Although enhancement and time stability of neutron production are expected to take place by increasing the deuteron beam diameter, the relevant calculations by Op de Beeck [96] have shown that this increases in axial flux gradients and to a lesser extent reductions in the laterial flux gradients. To account for the effect of variation in target radius and distances from target axis and its plane, Price [112] has carried out comprehensive calculations to estimate the neutron flux.

5.1.4 Improvement of fast neutron irradiation homogenity

To establish the conditions of maximum analytical accuracy for activation analysis with 14 MeV neutrons, the effects of spatial and time fluctuation of irradiating flux on random errors have to be determined. According to the recent calculations by Vass et al. [113], random fluctuations in detected counts of an irradiated sample are related by a simple formula to the small changes in parameters describing the sample position and irradiating flux. Experimentally, effects of the changes in these parameters can be reduced by spinning the sample. In this case two major systems have been reported for reproducible routine neutron activation purposes, and have demonstrated

reasonable levels of reliability. At close separations form the target where the flux gradients are high, the concept developed by Anders and Bricken [114] depends on rotating the cylindrical sample perpendicularly to the beam axis and along its longitudinal axis. A similar system was also produced by Vogt and Ehman [115], and the rotation can be performed either mechanically or by means of an air jet.

To irradiate sample and standard simultaneously, a dual biaxial rotor system was proposed by Guinn and Wagner [116], Mott and Orange[117], and Wood et al. [118]. The suggested systems are based on rotating sample and standard simultaneously around their longitudinal axes and around the deuteron beam axis. The dual biaxial rotation systems require positioning at large distances from the target, and therefore smaller neutron fluxes are obtained. On the other hand, the longitudinal axis rotation systems do not eliminate the effect of transverse neutron flux gradients.

5.2 The Limitations of Fast Neutron Flux Monitoring Techniques

5.2.1 The separate monitoring foil technique

In this technique, fast neutron flux is measured in terms of the induced activity on a standard material placed at a laboratory angle different from that of the sample. Due to neutron anisotropy, the monitor foil will be exposed to neutrons of different energies and flux; therefore appropriate corrections should be made. Changes in deuteron beam conditions could cause the variation of neutron flux to occur in different manners at monitor and sample positions.

More accurately, the absolute neutron flux at sample position can

be estimated by averaging the activities produced in two monitor foils placed on both sides of the sample. Let us consider a sample and two monitors of identical diameters ~ 1 cm, at about 10 cm distance from the neutron source. In such geometry each of them will be subtending an angle of about 12^{o} on the target. At a mean angle of 90^{o}, Fig. 5.1, the corresponding energy spread across the triple system will be approximately $\pm$ 0.25 MeV for 0.3 MeV deuterons on the tritium target. The flux averaging procedure will be then dependent on the linear variation of neutron flux and monitor cross-section within an 0.5 MeV interval.

$$\text{i.e.} \qquad \frac{\phi_{m_1} + \phi_{m_2}}{2} \sim \phi_s \tag{5.3}$$

where ϕ_s, ϕ_{m_1} abd ϕ_{m_2} are neutron fluxes at the positions of sample, monitor no. 1 and monitor no. 2.

This assumption is not very accurate for close separation from the neutron source due to the enhanced neutron energy spread, but short distance irradiation is desirable for better sensitivity.

In the forward direction, the conditions for flux averaging at close separation from the tritium target are more complicated, see Fig. 5.1.

$$\text{Although } \phi_{m_1} \sim \phi_{m_2}, \tag{5.4}$$

$$\frac{\phi_{m_1} + \phi_{m_2}}{2} < \phi_s \tag{5.5}$$

which is due to neutron flux anisotropy.

It is advisable to replace the sample by a third monitor and compare its induced activity with the activities of the other two monitors. This is necessary for estimating the accuracy of the determined

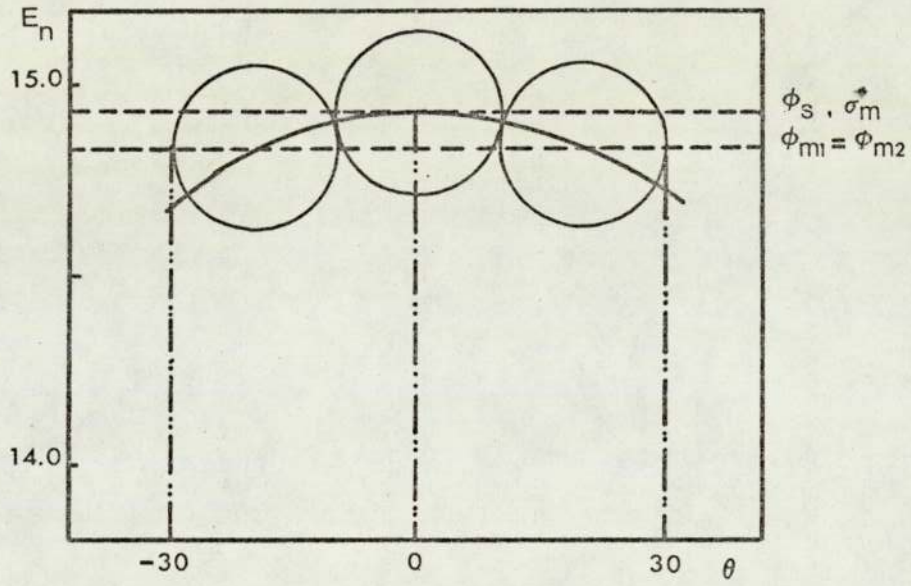

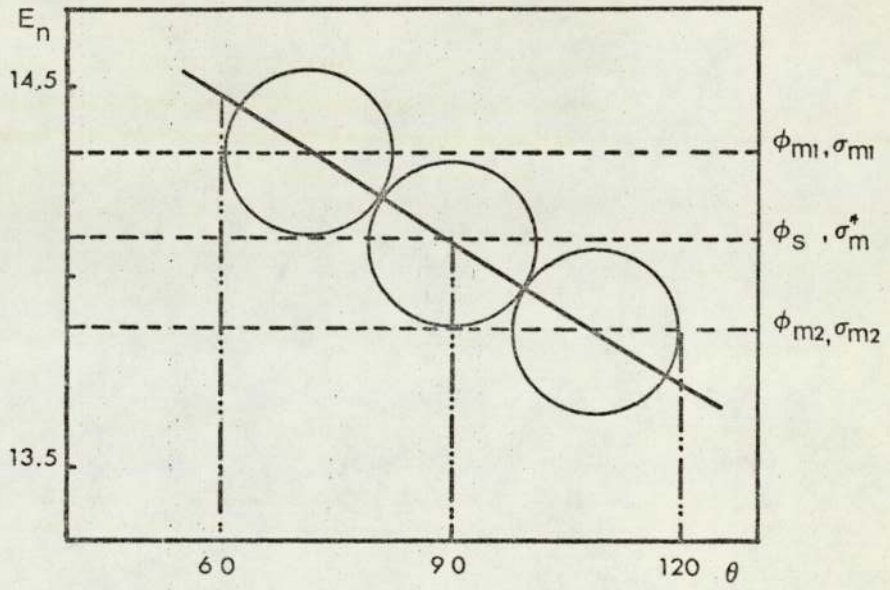

Fig. 5.1
Limitations of Neutron Flux Averaging By the Separate Foil Technique

neutron flux at sample position. The difference in the measured activities between the three monitors will be in this case due to the monitor cross-section variation with energy and due to neutron flux variations.

$$\frac{\sigma_{m_1} + \sigma_{m_2}}{2} \sim \sigma^*_m \quad \text{at } 90^o \tag{5.6}$$

$$\sigma_m = \sigma_m \neq \sigma^*_m \quad \text{at } 0^o \tag{5.7}$$

where σ_{m_1}, σ_{m_2} and σ^*_m are monitor cross-sections at the corresponding monitor 1 and 2 positions and at sample position.

This method will therefore yield information about the estimated flux at sample position, and it is dependent on the accuracy of the monitor excitation function and its slope.

Perhaps the best approach to the separate foil system is to place the two monitors on the circumference of the angle at which the sample is positioned. This method will ensure that monitors and sample are exposed to neutrons of similar mean energies. The advantages of this method will not be fully exploited unless a constant neutron attentuation is provided over the whole angular range of neutron emission by a specially designed target assembly.

By monitoring the neutron flux with a standard material, errors are usually introduced due to the uncertainties in the cross-section data of the standard. Fast neutron flux monitoring is best performed with the sample element if accurate standard cross-section data are not available, although this is no longer possible for multielemental determinations. The relative activities of comparator and sample will be then proportional to the relative concentrations by assuming the

exposure to a constant neutron flux. Although the absolute neutron cross-sections are not required in this case, the variation trends of neutron cross-sections with energy are needed.

5.2.2 The sandwich foil technique

Fast neutron flux can also be estimated by sandwiching the sample between two foils of the standard flux monitoring material. In this technique, which is widely used for cross-section measurements, corrections for the monitor reaction cross-section variation with energy are not required. This is due to the fact that the three components of the sandwich are being placed at the same mean laboratory angle. The situation for incident neutron flux measurement is rather more complicated since it is affected by the readial flux gradient and neutron screening as described below.

1. Due to the finite thickness of the sample and monitors, they will be effectively situated at different distances from the neutron source. Therefore they will be exposed to a neutron flux of negative gradient. This effect is more pronounced for short distances due to the 1/R flux dependence. The magnitude of the introduced systematic errors will be then determined by the components' thickness, and by their positions with respect to the target. From the results of Op de Beeck [95], it appears that at R = 1 cm and R = 1.8 cm, an axial displacement of 0.1 cm will correspond to a flux variation of 14% and 8.5% respectively.

2. By irradiating the sample and monitors in a sandwich geometry, a neutron screening effect will be experienced by the sample and back monitor. This is determined by the thickness (d_m) and macroscopic cross-section (Σ_m) of the front monitor in the case of the sample. Similarly, the back monitor will be screened by the front monitor plus the sample which has its own thickness (d_s) and macroscopic cross-

section (Σ_s). The estimated flux as determined by averaging those measured on the monitor foils should then be corrected for neutron screening in the sandwich. This is of course in addition to the radial flux gradient. For such calculations, removal macroscopic cross-section data are used [119,120,121]. The concept of removed cross-sections, as used in reactor shielding design, was found experimentally to yield better results for 14 MeV neutron attenuation than the use of total cross-sections [122,123].

Basically, two identical flux monitoring standards can be irradiated behind each other yielding at the end of irradiation similar activities, but with a screening effect factor due to front monitor upon back monitor, i.e. exp ($-\Sigma_m d_m$). If the monitor is now irradiated behind the sample, the screening factor will be changed to exp ($-\Sigma_s d_s$). Such experiments will therefore provide essential information for cross-section measurements by the sandwich technique, and also for activation analysis.

Several systems have been described for oxygen analysis in metals by the simultaneous irradiation of sample and standard behind each other [47,122,124]. In these cases a single comparator containing a known concentration of oxygen is irradiation behind the sample. Gijbels et al [122] have reported detailed study of this method for industrial routine analysis, and explained the necessary comparator calibration procedure to determine oxygen concentration in the sample.

5.2.3 The mixed powder technique

To eliminate the errors obtained by using the sandwich foil technique, the mixed powder technique was suggested by Rao and Fink [125] as an alternative for fast neutron cross-section measurements. In their publication, Rao and Fink applied this method for the measurement

of $^{74}Se(n,2n)^{73g}Se$ and $^{77}Se(n,2n)^{76}Se$ cross-sections at 14.4 MeV. Flux monitoring was performed internally by mixing a powder of the material under investigation with powder of the flux monitoring material. For measuring the (n,2n) reaction cross-section on ^{74}Se and ^{77}Se, the $^{56}Fe(n,p)^{56}Mn$ cross-section was used as the primary standard, and in addition $^{27}Al(n,\alpha)^{24}Na$ as the secondary standard on the other set of samples. To detect the gamma activities produced by the (n,2n), (n,p) and (n,α) reactions, it was necessary to use a Ge(Li) detector, and the known ratio of iron and aluminium cross-sections was used for checking the results. The limitations associated with this method for general applications are indicated below.

1. Materials in powder form are required, and they should have the same grain size; but even so the problems of incomplete mixing can be comparatively high. The attenuation of 14 MeV neutron beam is described by an exponential absorption law.

$$\frac{\phi}{\phi_o} = \exp(-\Sigma d) \qquad (5.8)$$

where ϕ = neutron flux after traversing the sample,

ϕ_o = neutron flux without the sample present,

d = the sample thickness,

and Σ = macroscopic cross-section for 14 MeV neutrons

Therefore attenuation of neutron flux by the sample will make the inner parts less active than the outside. In such conditions the incomplete mixing of powders will lead to the formation of variable concentration distributions of the monitor material across the sample thickness and diameter.

2. The gamma ray spectra from more than one element could be difficult to resolve, and basically a Ge(Li) detector is required. The situation in the experiment of Rao and Fink is ideal since the material to be examined is pure, as required mostly for cross-section experiments. In general cases, this situation can not be expected, such as in routine activation analysis, due to the impurities present in the sample which cause interferences.

3. The choice of the standard material for flux monitoring, on gamma spectroscopy basis, is restricted to reactions leading to gamma lines that do not coincide with those of the material being examined. This restriction can be removed by employing radio-chemical separation, which is not advisable for routine activation analysis and cross-section measurement specially when short-lived radio-activity is to be examined.

CHAPTER 6

THE CONCENTRIC RING TECHNIQUE FOR THE MEASUREMENT OF FAST NEUTRON FLUXES AND ENERGIES

6.1 Fast Neutron Flux Measurement

The recommendations made by different researchers in the field of fast neutron flux monitoring have been generally toward establishing some neutron cross-sections as standards. As we have indicated earlier, this approach has been followed without taking into account the different experimental conditions. Also, no recommendations have been made so far toward establishing a universal activation technique as a standard for fast neutron flux monitoring to overcome the variation in irradiation conditions effect.

The limitations mentioned previously for separate foil, sandwich foil, and mixed powder techniques cast doubts on their use as the basis of a standard technique in fast neutron monitoring. Therefore, it seems that an alternative technique is required as a standard for use by different laboratories. Such a technique should require minimum

number of corrections and yields negligible errors to improve the accuracy of fast neutron activation analysis and minimize the discrepancies in fast neutron cross-section data.

Accordingly, we present here a summary of the characteristics that we propose for new sample/monitor geometry to obtain improved fast neutron flux monitoring.

1. Sample and monitor are placed at the same distance from the source to eliminate the flux gradient corrections due to sample/source and monitor/source separation difference.

2. They are exposed to neutrons with approximately the same average energy to eliminate the errors due to different excitation functions of monitor and sample. The neutron energy should be above the reactions thresholds unless appropriate correction due to threshold energy difference is introduced.

3. They can be transferred to the counting equipment so that their activities can be measured simultaneously, or they can be separated easily for subsequent counting.

4. They should have equal thickness and distinct boundaries to minimise the corrections due to self-absorption. The advantage of this is also reflected on matching the flux gradients and calculating the average neutron fluxes.

5. No neutron screening effect should be presented by either the monitor or the sample upon the other.

These conditions appear to be satisfied by using a sample in the form of a disc surrounded by a concentric ring of the flux monitoring material. In this thesis, the term thickness will represent the distance traversed by the incident fast neutron beam, and width

will represent the difference between the outer and inner radii of the ring.

6.2 Accuracy of the Technique

The accuracy of fast neutron flux measurement by the concentric ring technique is determined by the ring's width and its corresponding subtended angle on the neutron source. A photograph of a concentric ring/disc set is presented in Fig. (6.1). Also an illustration of the relative dimensions of the ring and disc system is given on a neutron energy scale for 0^{o} and 90^{o} and shown in Fig. (6.2). This is for E_d = 0.3 MeV on a thick T-Ti target.

For a given sensitivity the dimensions of the ring are determined by the neutron flux, disc dimensions and the monitoring reaction cross-section. For reasonably high reaction cross-section, the amount of the monitoring material required to obtain good gamma counting statistics is usually small. Therefore, for ideal conditions, the width of the ring is expected to be very small and the additional θ-ψ angle subtended by the ring is negligible compared with that subtended by the disc (Fig. 6.2). For the experiments which we have performed using a copper flux monitoring ring and aluminium disc, the experimental geometry was such that ψ = 12.32 degrees and θ = 13.0 degrees. In fact, this represents an angular spread of only about 5% which corresponds to a neutron energy spread of $\pm$ 5 keV at 90^{o}. At other laboratory angles where the neutron energy variation with angle is lower than 90^{o}, the energy spread will be smaller.

Only the outer edges of the monitoring ring are exposed to neutrons of higher or lower energy than is the sample, and as this represents

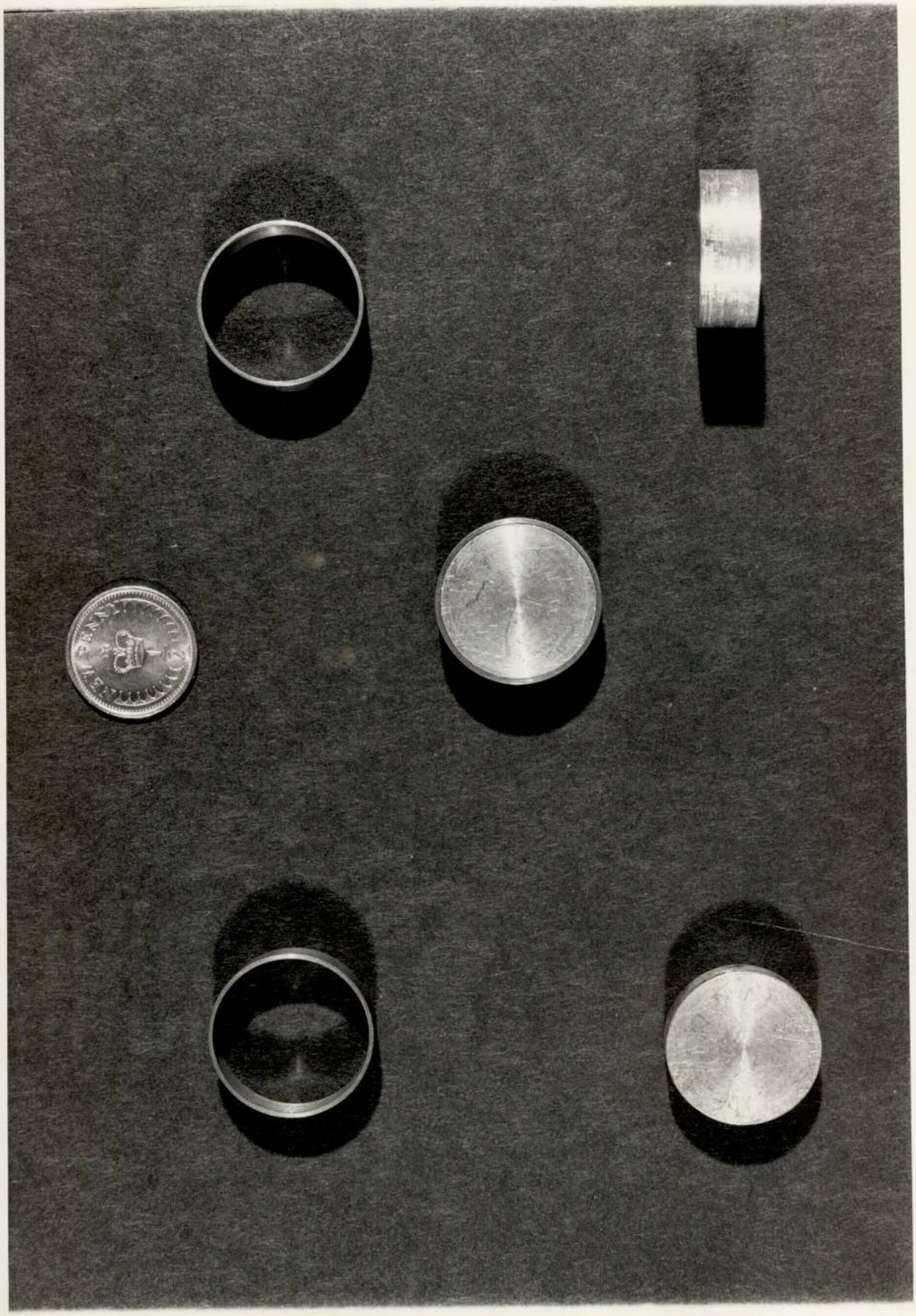

Fig. 6.1 Concentric Ring/Disc Samples

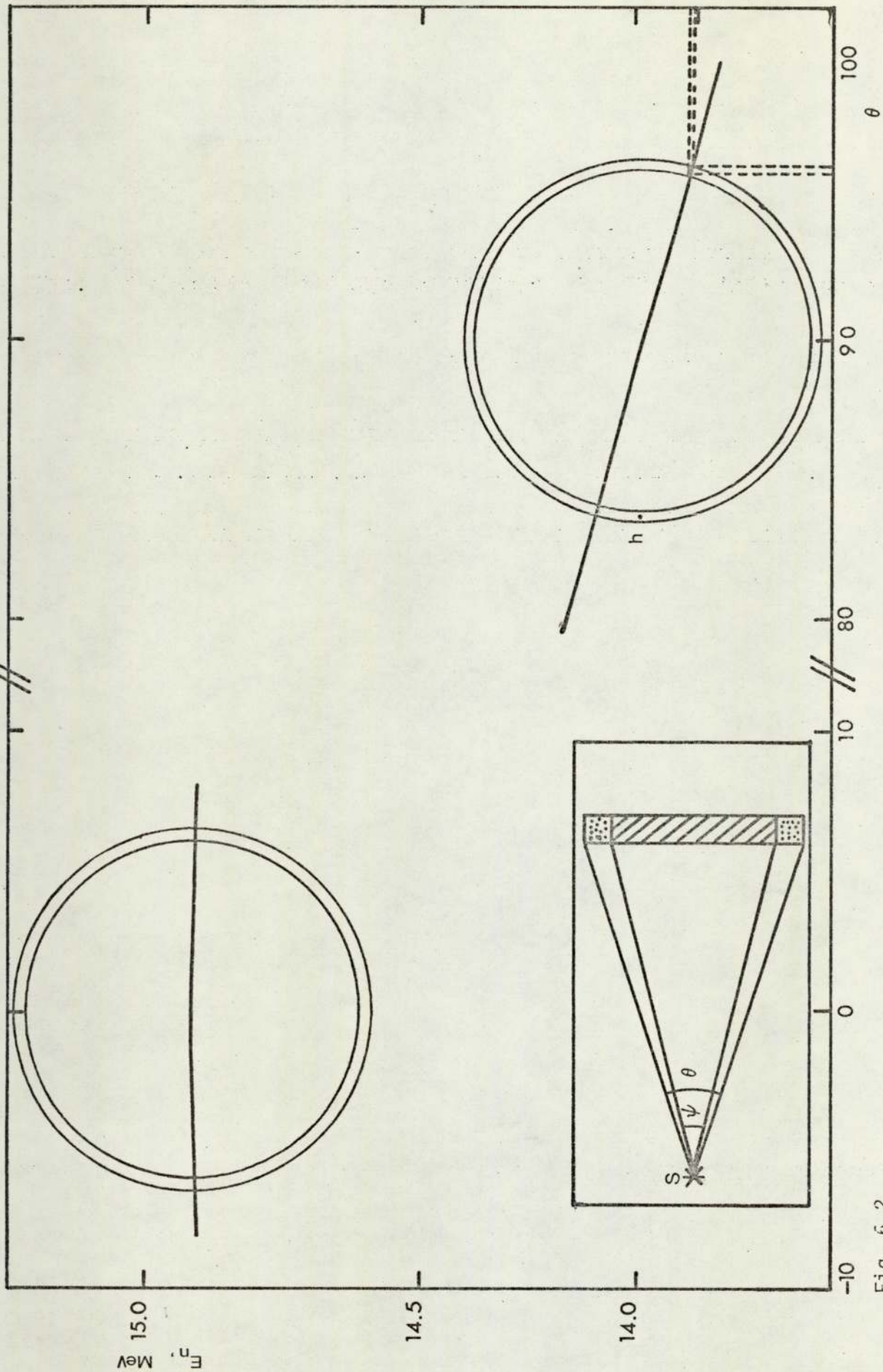

Fig. 6.2
A Concentric Ring/Disc Sample on a Neutron Energy Scale

a small fraction of the total ring area, the error is not great. Let us consider for example a point at half the ring's width, i.e. point h at the 90^{o} position as shown in Fig. (6.2). This point will be then corresponding to an energy spread of approximately 2.5 keV compared with the nearest point of the disc.

Suppose we have now an excitation function with a positive slope of 20% MeV^{-1}; therefore point h will exhibit a cross-section variation of 0.05% only compared with the disc edge, and the cross-section variation is even smaller for other laboratory angles. It should be kept in mind here that with such geometry, the small additional neutron energy spreads are actually experienced by very small fractions of the ring and therefore the overall effect is even less. Corrections for wider rings can be calculated mathematically. Also, we have produced an experimental method to estimate this correction as shown in the next chapter.

It has already been proposed that the disc and ring should have equal thicknesses and the importance of this can be demonstrated if we try to calculate the average neutron fluxes. Let us assume a homogeneous unidirectional neutron flux incident perpendicularly on a concentric ring/disc sample. Therefore, the average neutron flux within the sample can be expressed in terms of the incident neutron flux (ϕ_o), material linear thickness ($\chi = \chi_r = \chi_d$) and the macroscopic cross-section (Σ_r or Σ_d). Here, r and d are corresponding to the ring and disc.

$$\bar{\phi} = \phi_o [1 - \exp(-\Sigma x)] / \Sigma x \qquad (6.1)$$

The average neutron flux can also be represented by the local neutron flux at a depth equal to px for $0 \leq p \leq 0.5$, by using the basic exponential relation.

Therefore,

$$\phi_o[1 - \exp(-\Sigma x)]/\Sigma x = \phi_o \exp(-\Sigma p x) \qquad (6.2)$$

This solution can be then simplified to yield the required value of p.

$$\text{i.e.} \qquad p = \frac{2.302}{\Sigma x} \log \frac{\Sigma x}{1 - \exp(-\Sigma x)} \qquad (6.3)$$

For our concentric ring configuration the magnitudes of $(\Sigma_r x)$ and $(\Sigma_d x)$ are less than unity due to the small macroscopic cross-sections for 14 MeV neutrons. Obviously, this means that $p \sim 0.5$ and the average neutron flux is given by the local flux at a point which is half the way along the material thickness.

$$\text{i.e.} \qquad \bar{\phi}_r = \phi_o \exp(-\Sigma_r \tfrac{x}{2}) \qquad (6.4)$$

$$\text{and} \qquad \bar{\phi}_d = \phi_o \exp(-\Sigma_d \tfrac{x}{2}) \qquad (6.5)$$

This leads finally to the following expression for a disc and ring of equal thickness.

$$\frac{\bar{\phi}_d}{\bar{\phi}_r} = \exp[(\Sigma_r - \Sigma_d) \tfrac{x}{2}] \qquad (6.6)$$

6.3 Fast Neutron Energy Measurement

The discrepancies in fast neutron cross-section data can partially be attributed to the inaccurate estimation of incident neutron energy. The impact of this inaccuracy is expected to be pronounced for these measurements which are sensitive functions of neutron energy. For measurements that include steep excitation functions or fine structure

investigations, accurate values of the neutron energies are required, and errors due to monitor and sample positioning have to be eliminated.

Measurement of fast neutron energies in the 14 MeV region is difficult to carry out compared with lower energy regions. These measurements have to be carried out at the sample position and they have to be made during sample irradiation to eliminate positioning errors and take into account time and geometrical variations of neutron beam.

Cox and Jarjis [126] have suggested that the variation in the ratio of the absolute activities of two materials could be used to measure neutron energy, if the slopes of their excitation functions were different. Their experiment was based on irradiating a compressed powder composite made of two different materials and they determined an accuracy of 2.1% in the 14 MeV neutron energy measurements. The use of the concentric ring configuration appreciably extends the application of this technique and increases its accuracy. Also, by activating two concentric rings of selected materials either alone or surrounding a disc of the material under investigation it is possible to measure fast neutron flux and energy simultaneously.

The two materials selected for flux and energy measurement by this technique should have the following properties:-

1. They should have reasonably high cross-sections for good sensitivity, and their excitation functions should be well-known.

2. The ratio of cross-sections for the two materials should be a steep function of neutron energy to obtain high sensitivity to energy changes with sample position. For example, ideally one excitation function should have a large positive gradient and the other a large

negative gradient.

3. The two materials should have nearly equal half-lives to reduce the effects of any instabilities in neutron production.

4. The gamma rays emitted by the two materials and used for the calculations should be well separated in energy if the induced activities are required to be counted simultaneously.

5. The properties for ideal standard flux monitoring material, (Section 4.3), should also be applied to the standard energy measuring materials.

6. The cross-section ratio curves, determined by using the accurate excitation functions, are required to establish good reference standards.

6.4 Modification of the Technique

The errors introduced by using concentric ring monitors for large target to specimen separations are small but for small target to specimen separation the increased spread in neutron energies experienced by a uniform ring becomes noticeable. This is shown in Fig. 6.3, and in this case the areas A and B of the ring are exposed to wider ranges of neutron energies than the rest of the ring and the circular disc. For example, let us consider a sample consisting of a 3 cm diameter disc surrounded by a 1 cm wide ring. Therefore, for a separation of 2 cm from the neutron source a specimen in the forward direction would be exposed to a range of neutron energies from 14.74 to 14.91 MeV, and the monitoring ring to a range from 14.60 to 14.91 MeV. These are data for 0.3 MeV deuterons on thick

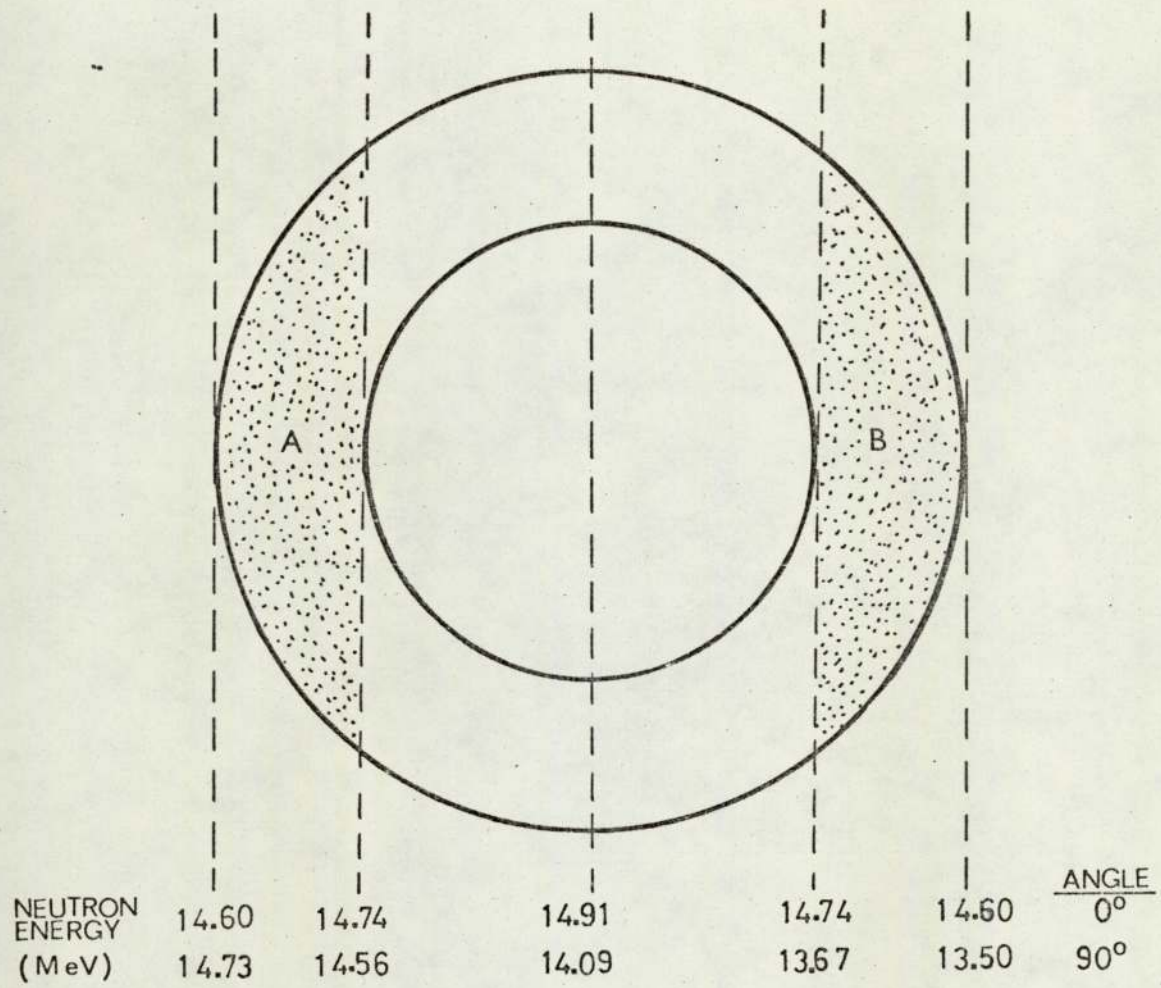

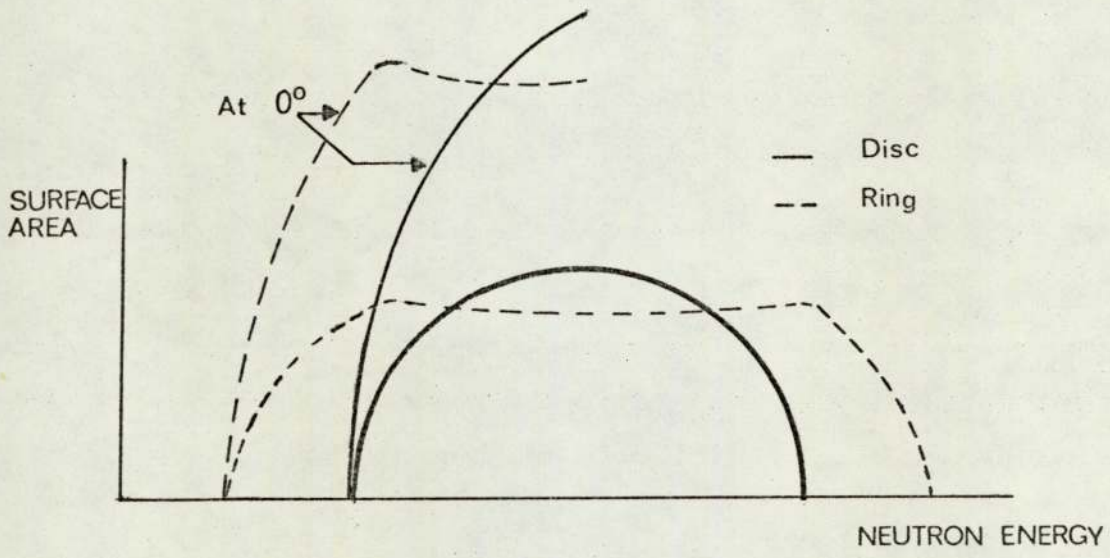

FIG.(63) THE CONCENTRIC RING/DISC SAMPLE AT A SHORT SEPARATION FROM THE TARGET.

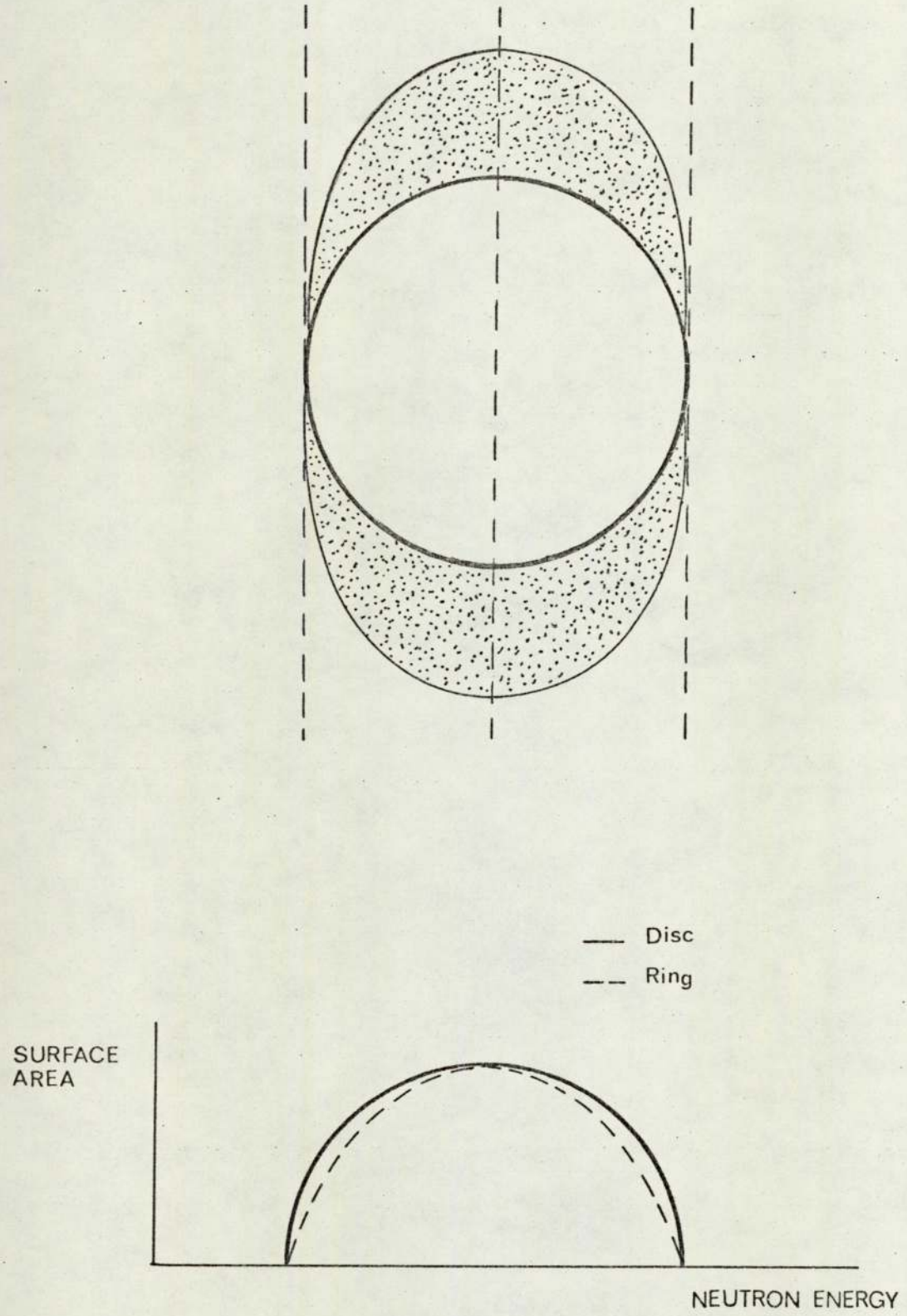

FIG.64) THE MODIFIED CONCENTRIC RING.

tritium target. At 90^{o} the corresponding energies will be 13.67 - 14.56 MeV for the specimen and 13.50 - 14.73 MeV for the ring.

The effect will be small for smooth excitation functions and can be minimised by using a specially designed ring as shown in Fig. 6.4 such that the area of the ring exposed to neutrons of particular energy is proportional to that of the disc exposed to those neutrons.

6.5 Some Potential Applications of the Concentric Ring Technique

The concentric ring technique could have the following applications in neutron irradiation work which are thought to be worthy of further investigation.

1. For multielemental activation analysis, standard flux monitoring rings matched as closely as possible to the excitation functions and half-lives of each of the constituent elements would enable their concentrations to be determined very accurately.

2. The comparator technique used for activation analysis can be improved if the comparator which contains a known concentration of the material is used in ring geometry. For experiments involving more than one constituent in a composite sample, we suggest the use of comparator concentric rings each corresponding to a certain element.

3. If the comparator is in the form of a disc placed at a laboratory angle different from that of the sample, a set of standard concentric rings for fast neutron fluxes and energies measurement can be very useful to reduce the errors due to relative flux and energy variations. The introduction of the concentric ring technique could possibly minimise the role of sample/standard spinning approach, although disc/

ring spinning mechanism could also be introduced.

4. The D-T neutron source is often used as a standard for determining the efficiencies for neutron detectors which are used in neutron spectroscopy. Therefore the results obtained by concentric ring detectors specially at the detector position can yield some local information which the associated particle technique fails to predict, e.g. neutron attenuation in the target assembly. The technique can also be used over wider neutron energy ranges, in which "point source" geometry is used, by a suitable choice of detector materials.

6.6 A Possible System for the Standardisation of Neutron Cross-Section Data

Neutron cross-section data are usually presented in terms of the corresponding neutron energies as calculated from the $T(d,n)^4He$ reaction kinematics. Often, specially in the early publications, no information is given to indicate the procedure used for estimating fast neutron energies. In several cases, no corrections due to T-Ti target thicknesses and sample/monitor positioning have been made.

Therefore, we suggest presenting the cross-section data together with the corresponding estimated neutron energies which could be calculated from the irradiation angle, but more conveniently they can be found in terms of the induced activity ratios of the internationally accepted neutron monitors at sample position. Such system would be feasible if standardisation of the neutron energy measurement by the concentric ring technique is established.

CHAPTER 7

EXPERIMENTAL PROCEDURE

7.1 Neutron Irradiation

A moderated BF_3 detector was used during the irradiation to record the fluctuations in neutron production. This was useful for estimating the appropriate corrections due to flux variation, and also to ensure good accelerator operation. Experiments involving large neutron flux variations have been excluded from the calculations and each of the reported data is an average value obtained from more than one irradiation. Absolute neutron flux was determined in terms of the induced activities on stanadrd materials of known cross-sections.

To minimize the background of lower energy neutrons the following procedures were followed:- 1) new tritium targets were used to obtain minimum D-D neutron yield for those measurements which involve reactions with low thresholds. 2) the design of our target assemblies was such that the cooling water path does not coincide with target/sample direct line. 3) a specially designed sample holder was introduced to ensure minimum neutron scattering.

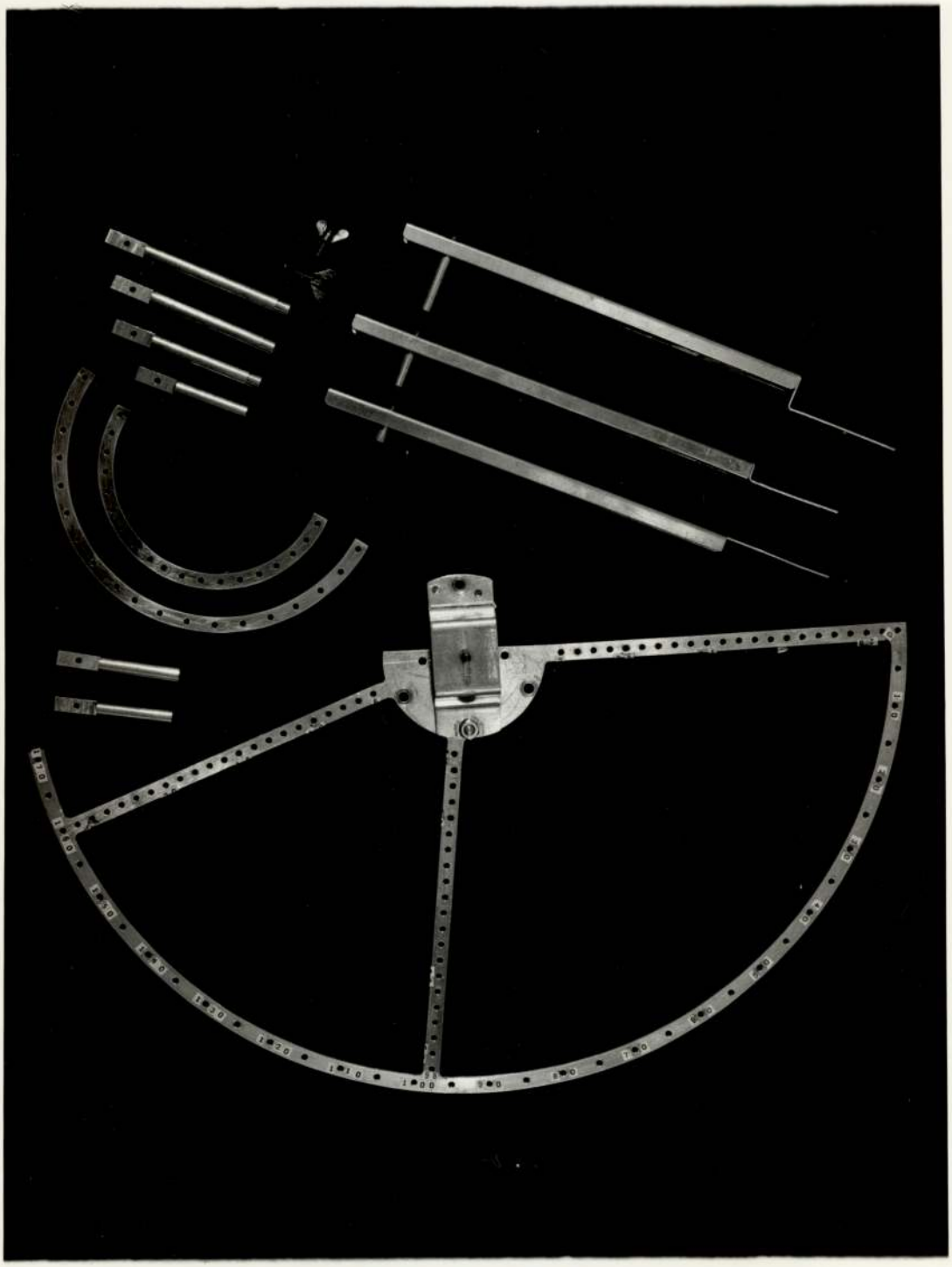

Fig. 7.1 Components of the Sample Holder

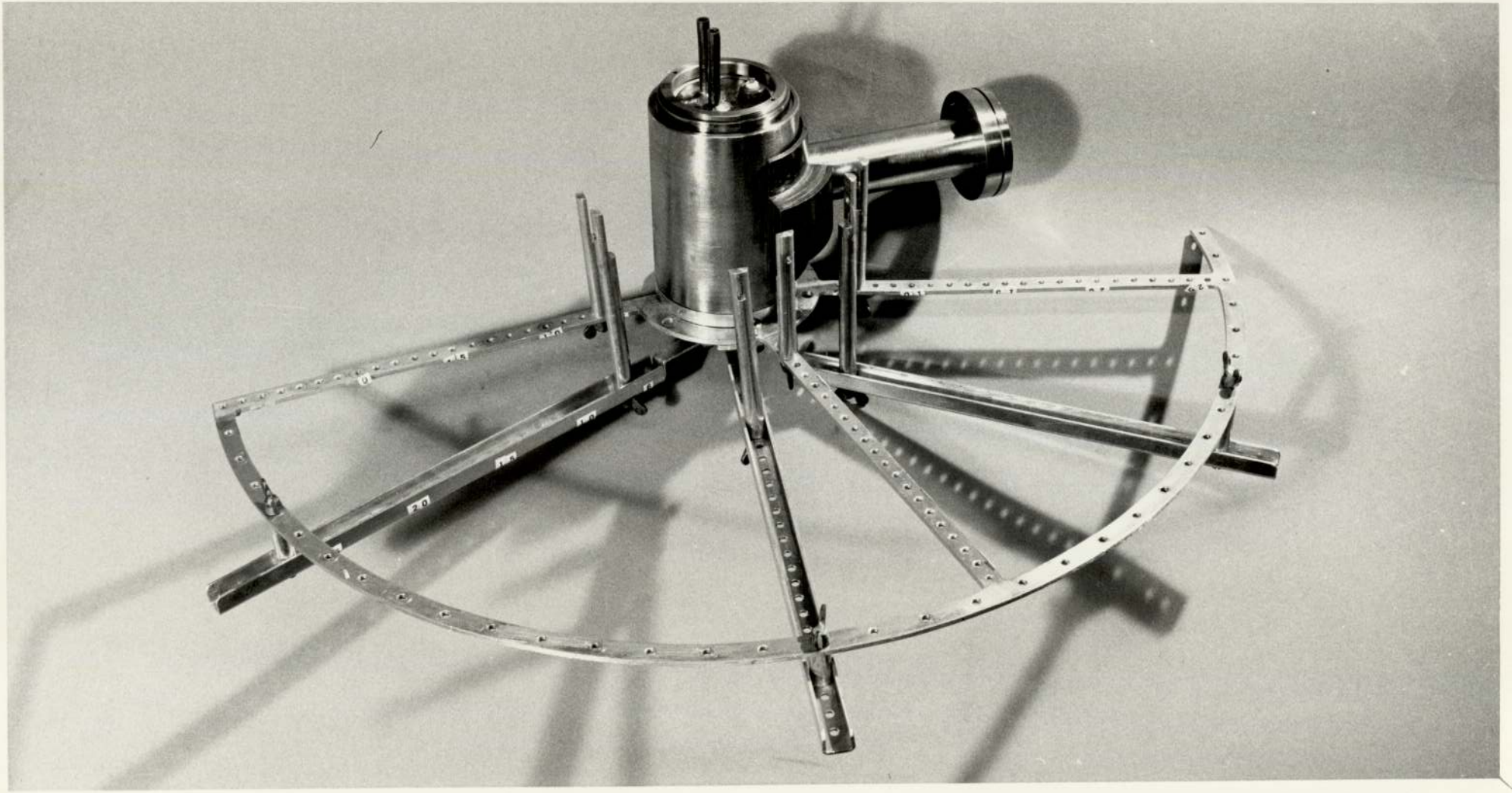

Fig. 7.2 The Target Assembly and Sample Holder

Design of the light sample holder's various components, Fig. 7.1, can be explained as follows:-

1. It is made of aluminium, and basically it consists of a thin arc which is 27 cm in radius, supported by three stationary arms at 0^{o}, 98^{o} and 160^{o} to be used for sample mounting and also to provide a support on the target assembly, Fig. 7.2.

2. Three mobile arms are provided for positioning purposes at different angles with respect to the deuteron beam. They are pivoted at the target centre for rotating and fixing in 5^{o} intervals from 0^{o} to 160^{o}. They can also be removed if necessary to reduce neutron scattering.

3. Several arcs of different radii are also available to be fixed on the stationary arms for some special experiments.

4. Samples are attached to thin aluminium rods which can be moved radially along the arms. To produce the same source/sample geometry, these rods were made of different lengths to compensate for the special design features of the mobile arms.

With such sample holder, samples can be placed at 5^{o} and 1 cm intervals along a source/sample distance of up to 30 cms by effecting a compromise between the requirements for low neutron energy spread and high flux, and varied with the magnitude of the cross-section of the sample. Estimation of the additional neutron energy spread due to sample/source geometry was obtained by using the neutron energy curves of Chapter 3. The evaluated neutron energy spread due to the subtended angle of the sample was then added quadratically to the energy spread due to the deuteron beam energy loss in the tritium target. In most of the experiments, a separation distance of 10 cms was found

to be satisfactory and an accuracy of about 1% in sample positioning was obtained.

7.2 Gamma-Ray Spectrometry

In this investigation, standard materials for fast neutron monitoring are studied. These materials have the advantage of producing simple gamma spectra which make the analysis procedure relatively simple and does not require the use of high resolution Ge(Li) detectors. Therefore, a shielded 3" x 3" NaI(Tl) detector was adopted for gamma detection in the present work. In comparison with Ge(Li) detectors, NaI(Tl) detectors have much better efficiency, require negligible care, and can operate at room temperature.

The electric pulses from the photomultiplier tube were amplified by using a CANBERRA 1417 spectroscopy amplifier whose output was then fed to the multichannel analyser. 400 channel RIDLE and 1000 channel NUCLEAR DATA ND 101 multichannel analysers were used, and the counting system was periodically calibrated by using standard gamma sources.

Gamma counting was carried out in a low background room, and the measured count rates were then corrected for dead time, background counts, irradiation time and decay. Half-lives were also measured when necessary, and detector efficiency was estimated from the tables of Grosjean and Bossert [127].

Sample separation from the NaI(Tl) crystal was determined by the counting statistics and in most of the experiments, placing the sample at a 3 cm distance was found to be satisfactory. For positron emitters, the annihilation 0.511 MeV radiations were counted by enclosing the

radioactive sample in a positron absorber of an appropriate thickness.

The counting sequence selected to get good statistical accuracy varied from one experiment to the other. But generally, the monitoring rings were used to be counted first such as for the case of $^{121}Sb(n,2n)^{120g}Sb$ excitation function due to their shorter half-lives, i.e. 9.5 and 9.8 m for aluminium and copper compared with 15.9 m for antimony. On the other hand, for the silicon experiments the situation used to be reversed due to the shorter lived product of silicon, i.e. $T_{\frac{1}{2}}$ = 2.27 m.

To get good statistical accuracy, a sequence for gamma counting was followed. The procedure depended on the material half-life, its cross-section and its weight. For example, for measuring the cross-section for $^{121}Sb(n,2n)^{120g}Sb$ reaction, aluminium and copper rings were used for neutron monitoring. In this case the rings have less weights compared with the antimony sample. They have lower cross-sections, and also lower half-lives. Accordingly, the induced activities on the rings were counted first and then followed by the antimony sample. For measuring $^{28}Si(n,p)^{28}Al$ cross-section the situation was the reverse due to the relatively short half-life of $^{28}Al(T_{\frac{1}{2}}$ = 2.27 m).

For each nucleus the number of radioactive nuclei present at the end of the irradiation depends on the one hand on the cross-section σ; on the other hand, n may be expressed in terms of the number of gamma ray counts A:

$$\frac{\phi\sigma LWsa}{G} = n = \frac{Ae^{\lambda te}(1 - e^{-\lambda tc})^{-1}}{b\varepsilon} \qquad (7.1)$$

where ϕ = the time-integrated neutron flux density at the midplane of the sample,

L = Avogadro's number,

W = the weight of the sample,

s = the fraction of the created radioactive nuclei which survive until the end of the irradiation,

a = the relative isotopic abundance of the target isotope,

G = the target gram atomic weight,

λ = the radioactive decay constant

t_e = the time elapsed between the end of the irradiation and the start of the gamma-ray counting,

b = the number of gamma rays per disintegration,

ε = the efficiency of the NaI(Tl) detector for total absorption,

and t_c = the length of time that the gamma rays are counted.

Equation 7.1 was used to evaluate the cross-sections, and information about the decay schemes were obtained from reference 128.

CHAPTER 8

EXPERIMENTAL RESULTS AND DISCUSSION

8.1 $^{63}Cu(n,2n)^{62}Cu$ Excitation Function

The variation of cross-section with neutron energy for the $^{63}Cu(n,2n)^{62}Cu$ reaction was measured in the usual manner by counting the annihilation (0.511 MeV) gammas due to the decay by positron emission of ^{62}Cu ($T_{\frac{1}{2}}$ = 9.8 m). Samples were placed at different laboratory angles with respect to the deuteron beam direction, and therefore subjected to neutrons of different mean energies. The results were obtained relative to the recommended value of 558 mb at 14.7 MeV as proposed by Body and Csikai [129]. Fig. (8.1a) shows our experimental cross-section data which were made by using the Van de Graaff and Dynamitron accelerators, (E_d = 0.3 MeV and 0.7 MeV). A smooth variation of the cross-section with neutron energy can be observed.

$^{63}Cu(n,2n)^{62}Cu$ absolute cross-section and its variation with neutron energy have been measured by several workers [90,130-141]. For comparison some of these data are plotted in Fig. (8.1b) with our

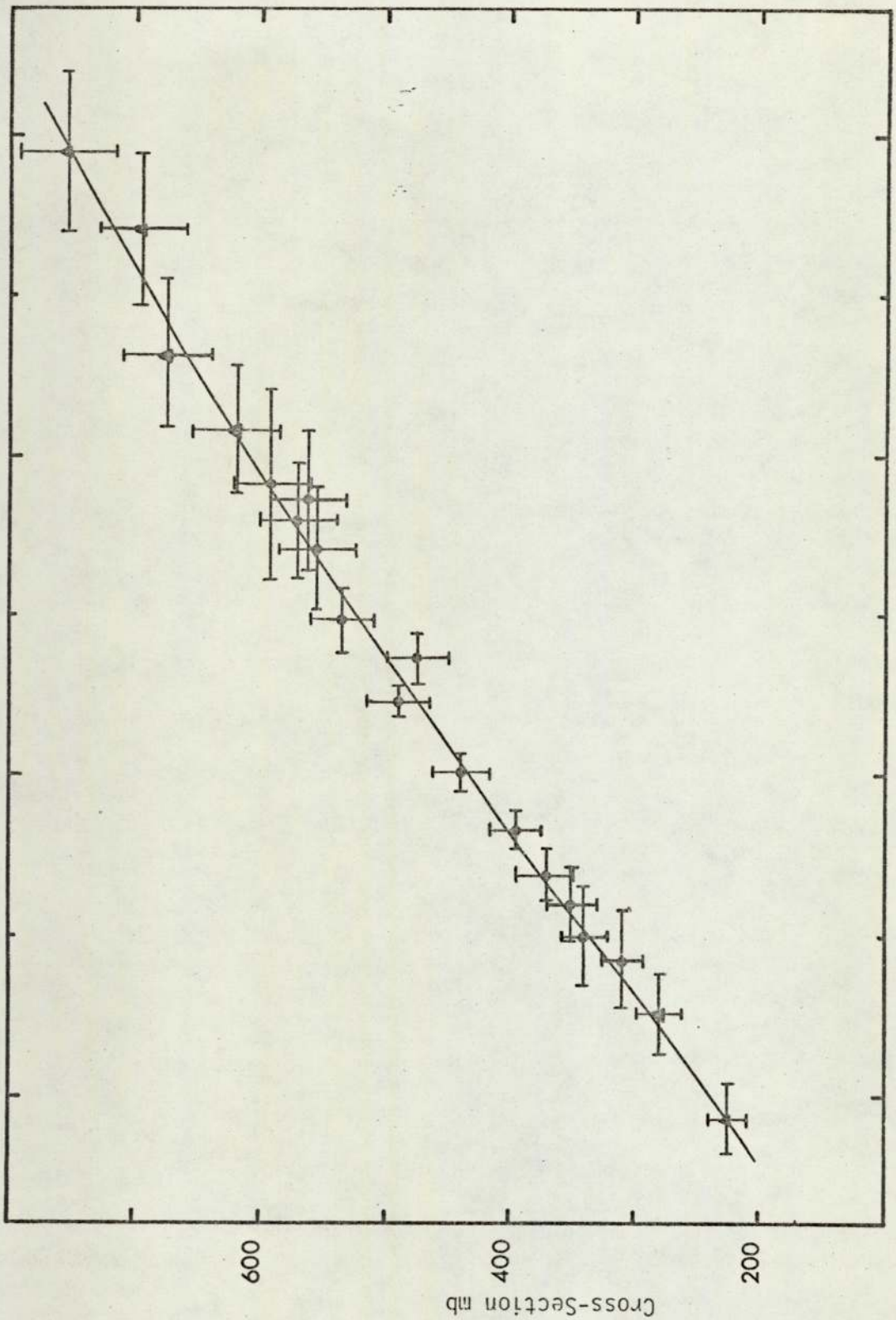

Fig. 8.1a
$^{63}Cu(n,2n)^{62}Cu$ Excitation Function

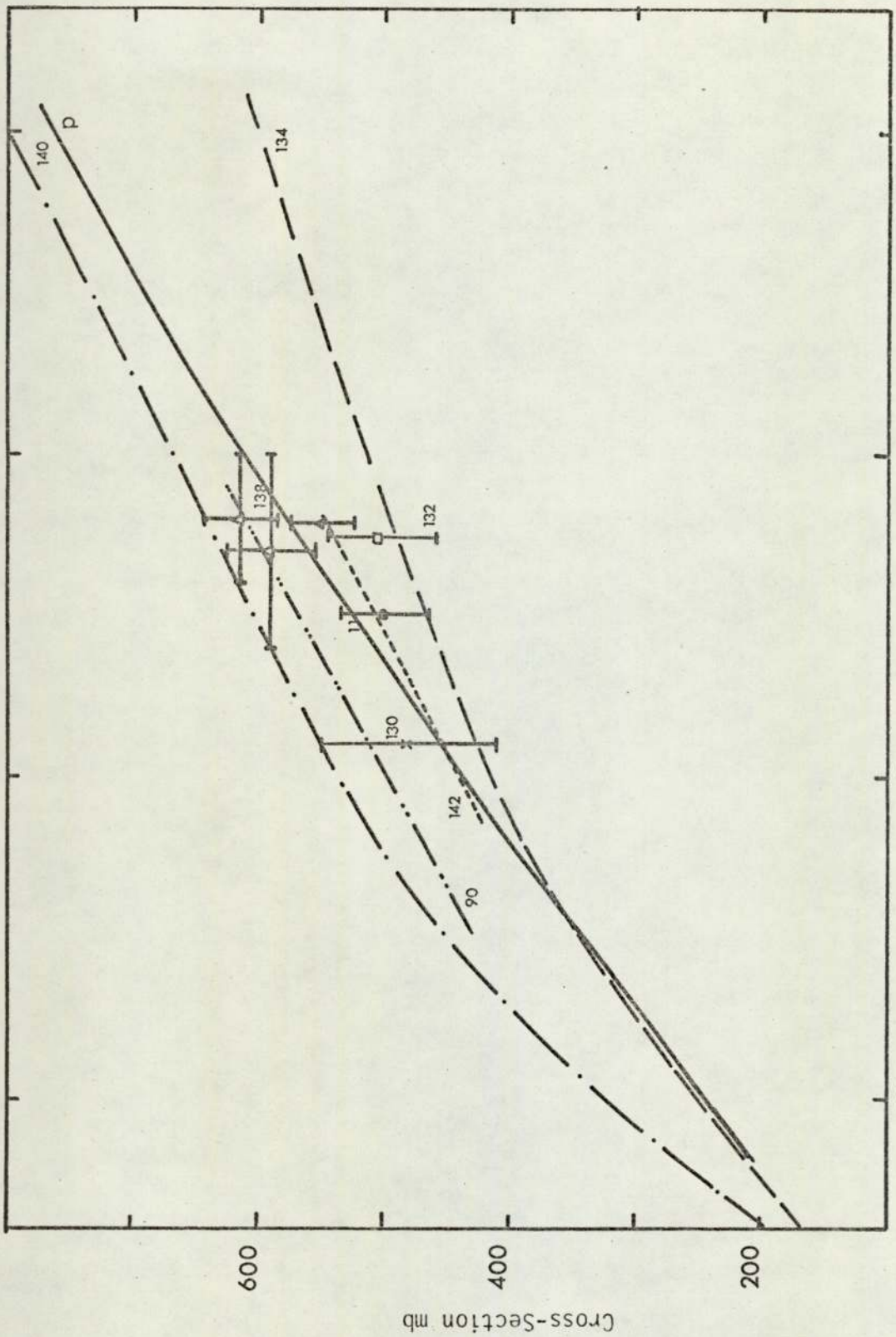

Fig. 8.1b
$^{63}Cu(n,2n)^{62}$ Cross-Section Data

excitation curve (solid curve), and a good general agreement can be observed. A weighted average value from the published experimental data at 14.5 ± 0.4 MeV (σ = 501 ± 36 mb) is also shown. This value and a theoretical value based on the statistical model predictions (σ = 481 mb) are taken from the work of Kondiah [11]. Similarly at 14.7 ± 0.3 MeV the values obtained by Qaim [138] are in good agreement with our data (σ_{exp} = 593 ± 36 mb and σ_{theor} = 543 mb). These results indicate that this reaction proceeds mainly via compound nucleus formation.

8.2 $^{27}Al(n,p)^{27}Mg$ Excitation Function

$^{27}Al(n,p)^{27}Mg$ excitation function was measured by detecting the 0.842 MeV gammas which are produced due to 70% of the β-decay of ^{27}Mg ($T_{\frac{1}{2}}$ = 9.5m). Samples were designed in the form of circular aluminium disc surrounded by very thin ring of copper which was used as the flux monitor. These concentric samples were irradiated together, and for checking purposes a single copper sample was also exposed at the same distance from the tritium target and at the angle which corresponds to 14.7 MeV neutrons, (40^{o} for E_d = 0.3 MeV).

The determination of the $^{27}Al(n,p)^{27}Mg$ excitation function was related to the measured copper excitation function, Fig. 8.1a, and the results are shown in Fig. 8.2a. A further check was carried out by measuring the aluminium (n,p) excitation function relative to the 558 mb value of $^{63}Cu(n,2n)^{62}Cu$ at 14.7 MeV by using separate single aluminium and copper samples. The results show similar behaviour to Fig. 8.2a but with higher standard deviation.

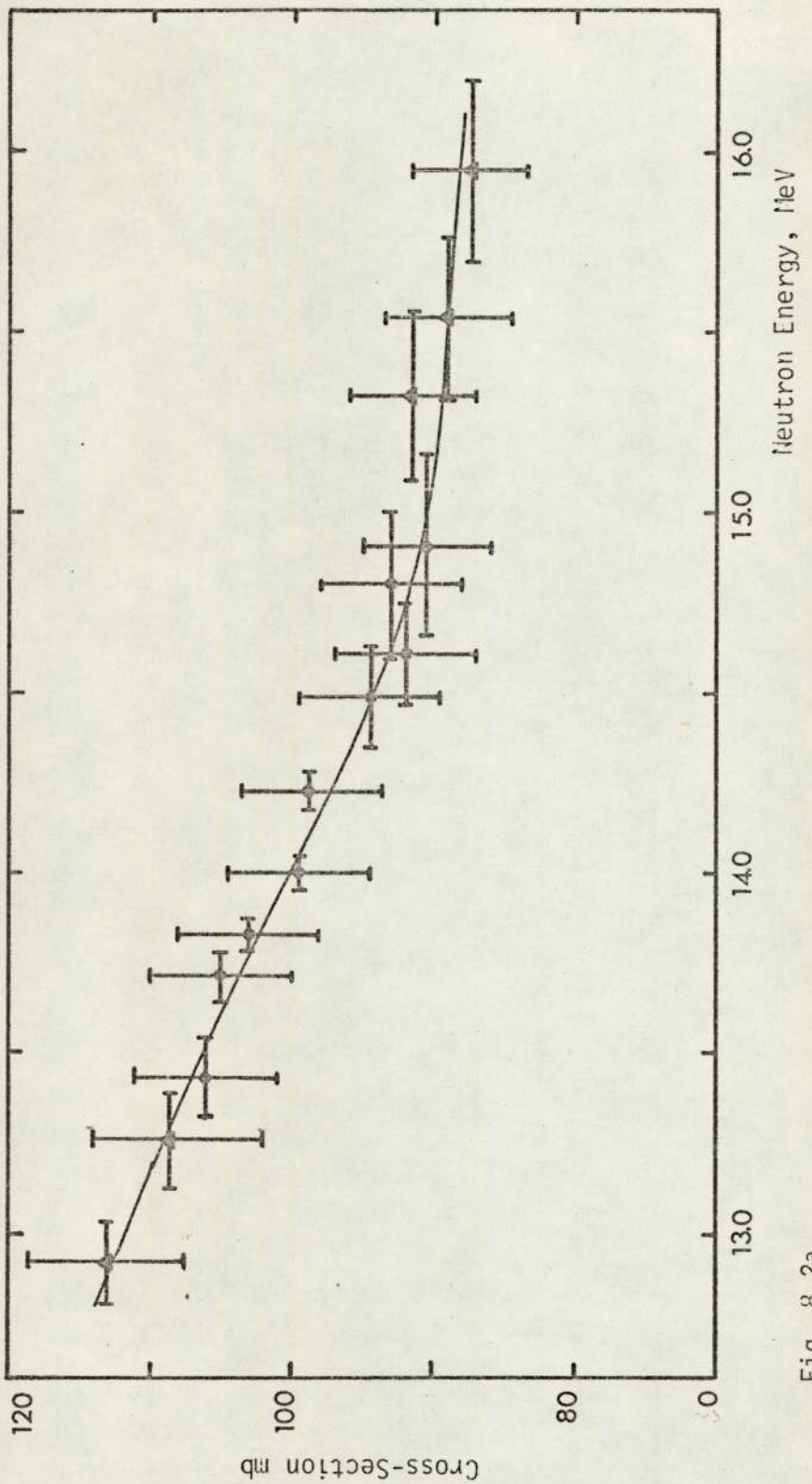

Fig. 8.2a
$^{27}Al(n,p)^{27}Mg$ Excitation Function

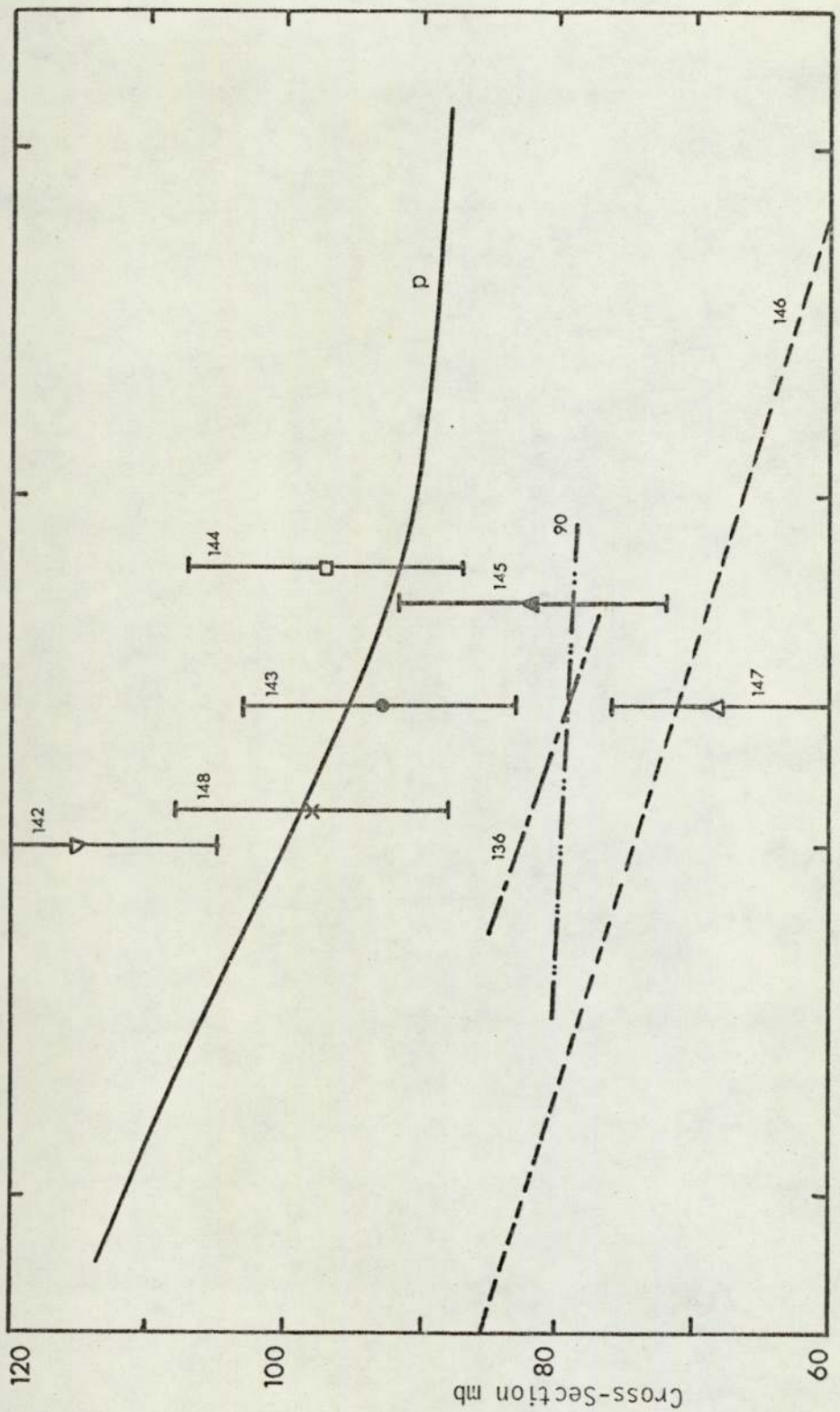

Fig. 8.2b
$^{27}Al(n,p)^{27}Mg$ Cross-Section Data

A phenomenological formula based on the neutron excess concept has been produced by Eder et al [149] to predict (n,p) cross-section values for neutron energies between 14 and 15 MeV, and it is shown below

$$\log_{10}(\sigma_{n,p}/\text{mb}) = 0.2 + 0.4A^{1/2} - 4.6(N-Z)/A^{2/3} \qquad (8.1)$$

By using this formula we obtained a cross-section value of 58.1 mb which is slightly lower than most of the experimental results.

For low mass nuclei, it was found that (n,p) cross-sections could be reproduced by the compound nucleus theory with the values of the level density parameter a = A/8.7 [148]. For ^{27}Al nucleus the theoretically calculated value is 70.5 mb at 14.1 MeV, (shown in Fig. 8.2b).

The general trend of our excitation function is approximately similar to the published data, but it does not agree with the results of Partington et al [90], which show a much lower slope in the 13.5 - 14.9 MeV region.

8.3 The Cross-Section Ratio Curve for Fast Neutron Energy Measurement

It has been proposed in Chapter 6, that the selection of standard materials for neutron energy measurement should be based on the similarity in half-lives and on the strong variation of the cross-section ratio with neutron energy. Therefore, $^{63}Cu(n,2n)^{62}Cu$ and $^{27}Al(n,p)^{27}Mg$ reactions have been selected as standards for the energy measurement due to their similar half lives and the slopes of this excitation function. Our measured excitation function indicate that in the 13-15 MeV region, copper cross-section increases approximately linearly with neutron energy with a slope of 28 per cent MeV^{-1}, whilst aluminium cross-section

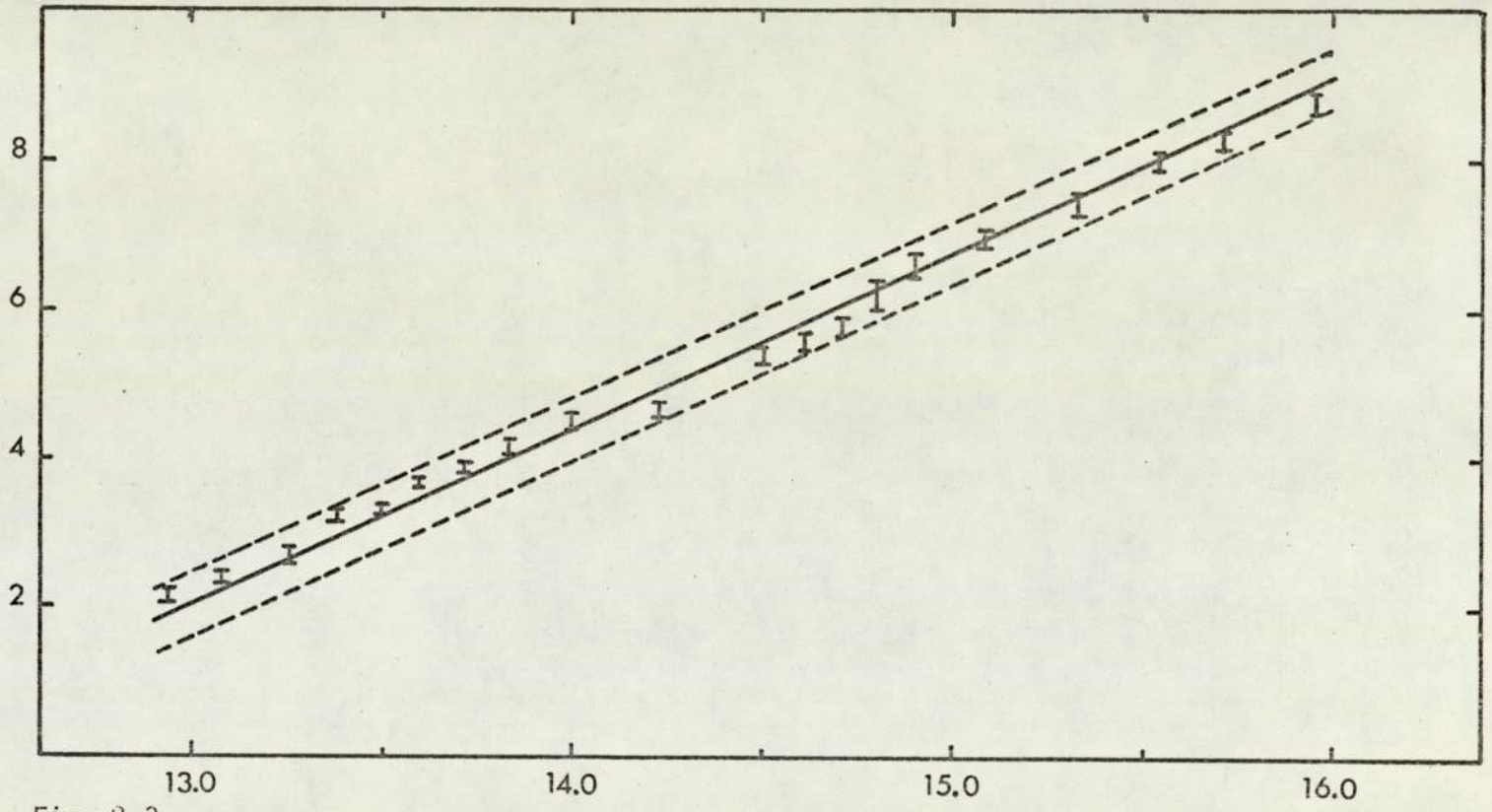

Fig. 8.3

The Ratio of Cross-Sections as a Function of Neutron Energy

decreases with a slope of -9 per cent MeV^{-1}.

Samples were made in the form of circular aluminium disc surrounded by a thin ring of copper. The samples were irradiated with different mean energy neutrons and at large and equal distance from the D-T neutron source, and the induced activities were measured for a range of neutron energies from 12.9 to 15.9 MeV.

The ratio of our copper and aluminium excitation functions has been plotted as a solid line in Fig. 8.3, the experimental uncertainties being indicated by the dotted lines. The concentric ring technique was used to establish the cross-section ratio at specific energies and these are shown in the form of points in Fig. 8.3. The results reveal a slight non linearity in the activation ratios, although there is good general agreement between the two sets of results. The accuracy of the neutron energy measurement is $\pm$ 1.2 per cent by the concentric ring technique.

The results obtained by using the Van de Graaff and Dynamitron accelerators are consistent and this is in support of the proposed use of the cross-section ratio curve as a reference for fast neutron energy measurement.

8.4 Accuracy of Fast Neutron Flux Measurement by the Concentric Ring Technique

To estimate the accuracy of the concentric ring technique, concentric copper samples consisting of a circular disc surrounded by two rings were used. The concentric copper samples were positioned at different angles with respect to the deuteron beam direction, and

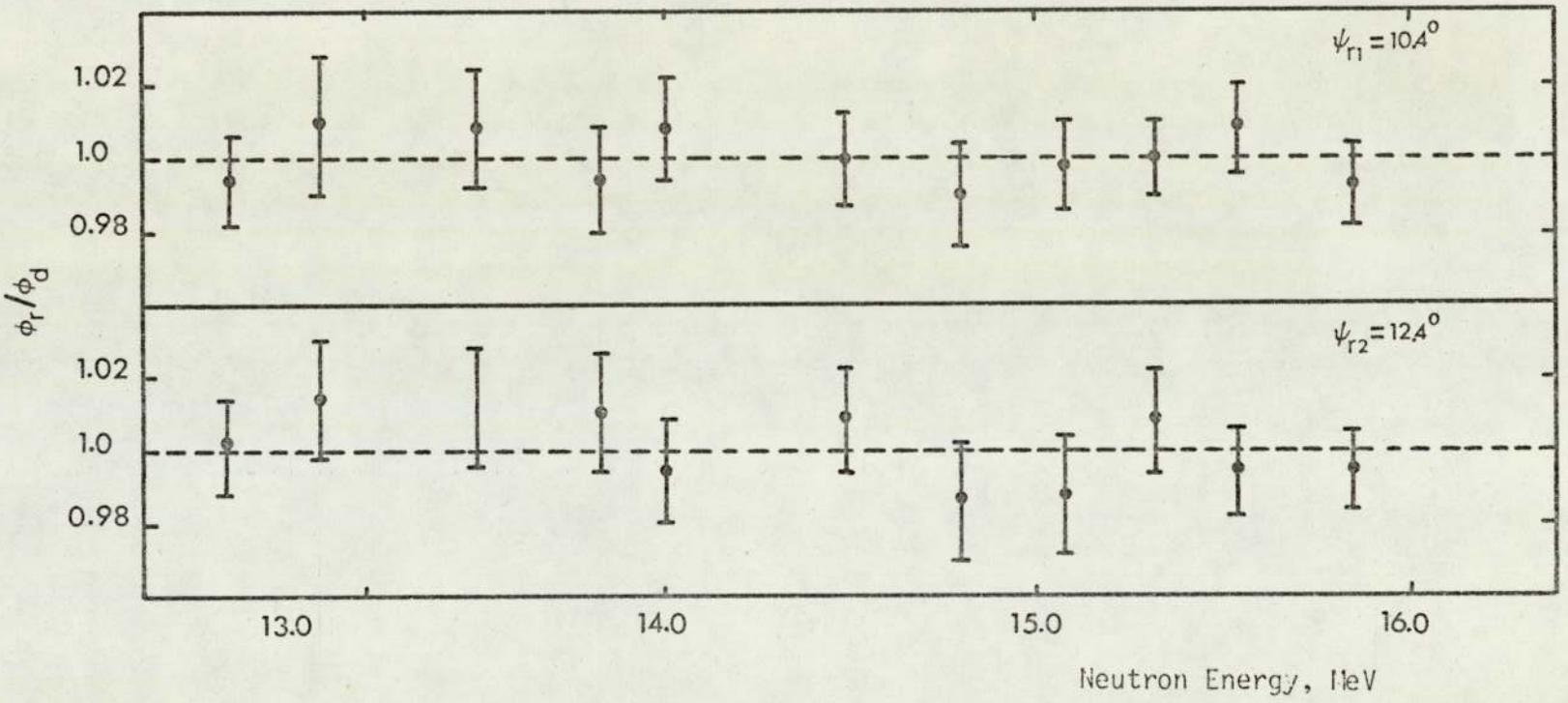

Fig. 8.4

The ratios of neutron fluxes measured by using the $^{63}Cu\ (n,2n)^{62}Cu$ reaction on concentric copper ring/disc samples.

in such a geometry that the angles subtended by the disc (θ_d) and the two rings (ψ_{r_1}, ψ_{r_2}) on the target are 10.2, 10.4 and 12.4 degrees respectively.

Following the irradiation, the components of the concentric samples were counted separately, and the corrected ratios of the determined induced activities in the rings and disc were proportional to the ratios of neutron fluxes to which they were exposed. Fig. 8.4 shows two plots of the flux ratio results against neutron mean energy for the two rings. The experimental results, as obtained by using the Dynamitron and Van de Graaff accelerators, indicate that a 1 per cent average accuracy in fast neutron flux measurement can be obtained by using the concentric ring technique.

8.5 $^{28}Si(n,p)^{28}Al$ Excitation Function

The samples used for this experiment were made of a circular disc made of a compressed silicon powder, surrounded by two copper and aluminium rings. Fast neutron flux was determined in terms of the induced activity on the aluminium ring and was obtained ~~absolutely~~ relative to the $^{27}Al(n,p)^{27}Mg$ excitation function of the present work. Neutron energy at the sample position was evaluated from the cross-section ratio curve of copper and aluminium.

The cross-section data of silicon in the 13.4 - 14.9 MeV region, Fig. 8.5a, were obtained by irradiating the concentric samples for 10 m and 30 m. The gamma activities which were produced in the silicon samples are due to 100 per cent of the decay of $^{28}Al(T_{\frac{1}{2}}=2.27\ m)$ to the 1.78 MeV excitation level. Silicon activities were the first

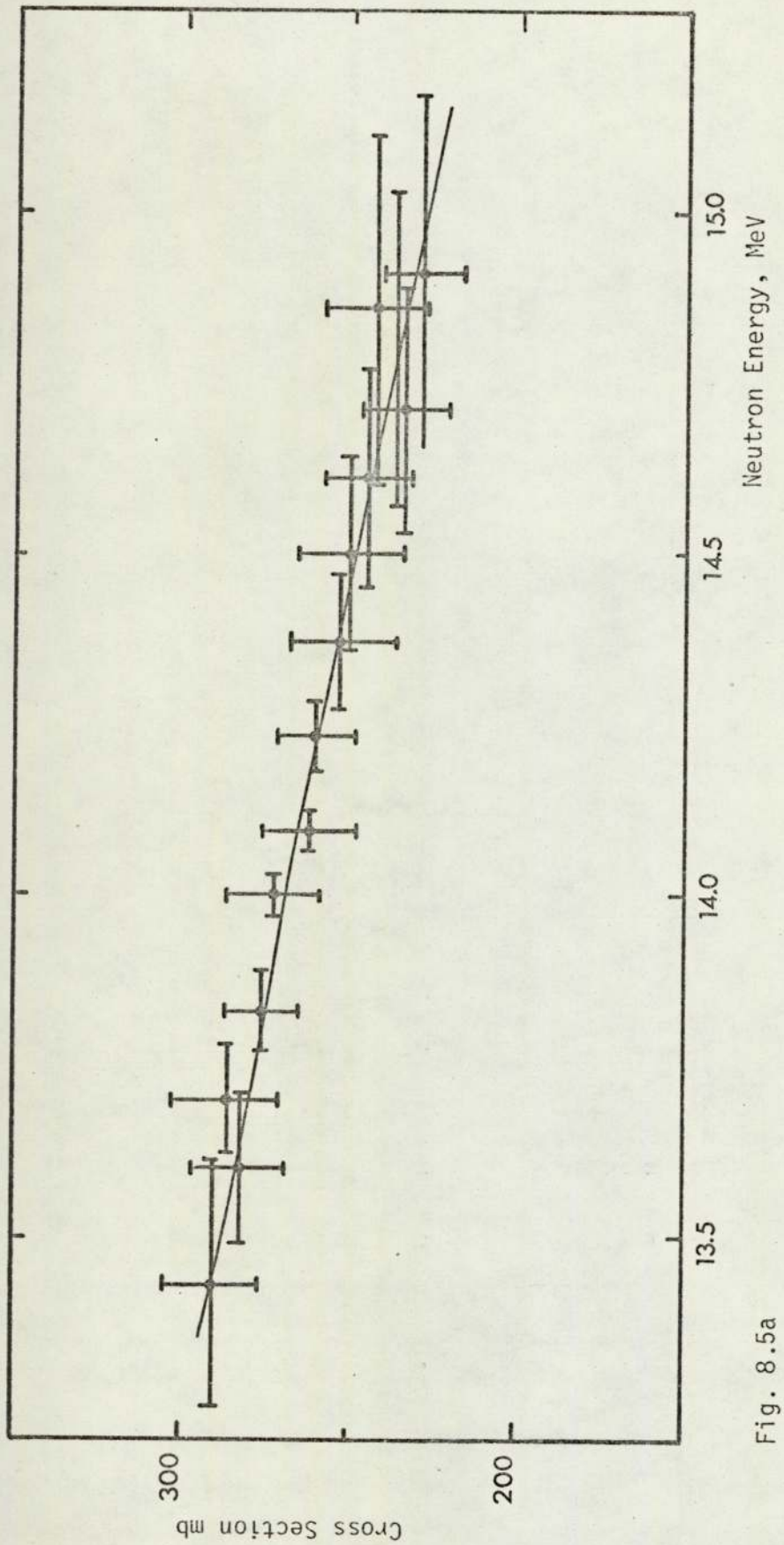

Fig. 8.5a
$^{28}Si(n,p)^{28}Al$ Excitation Function

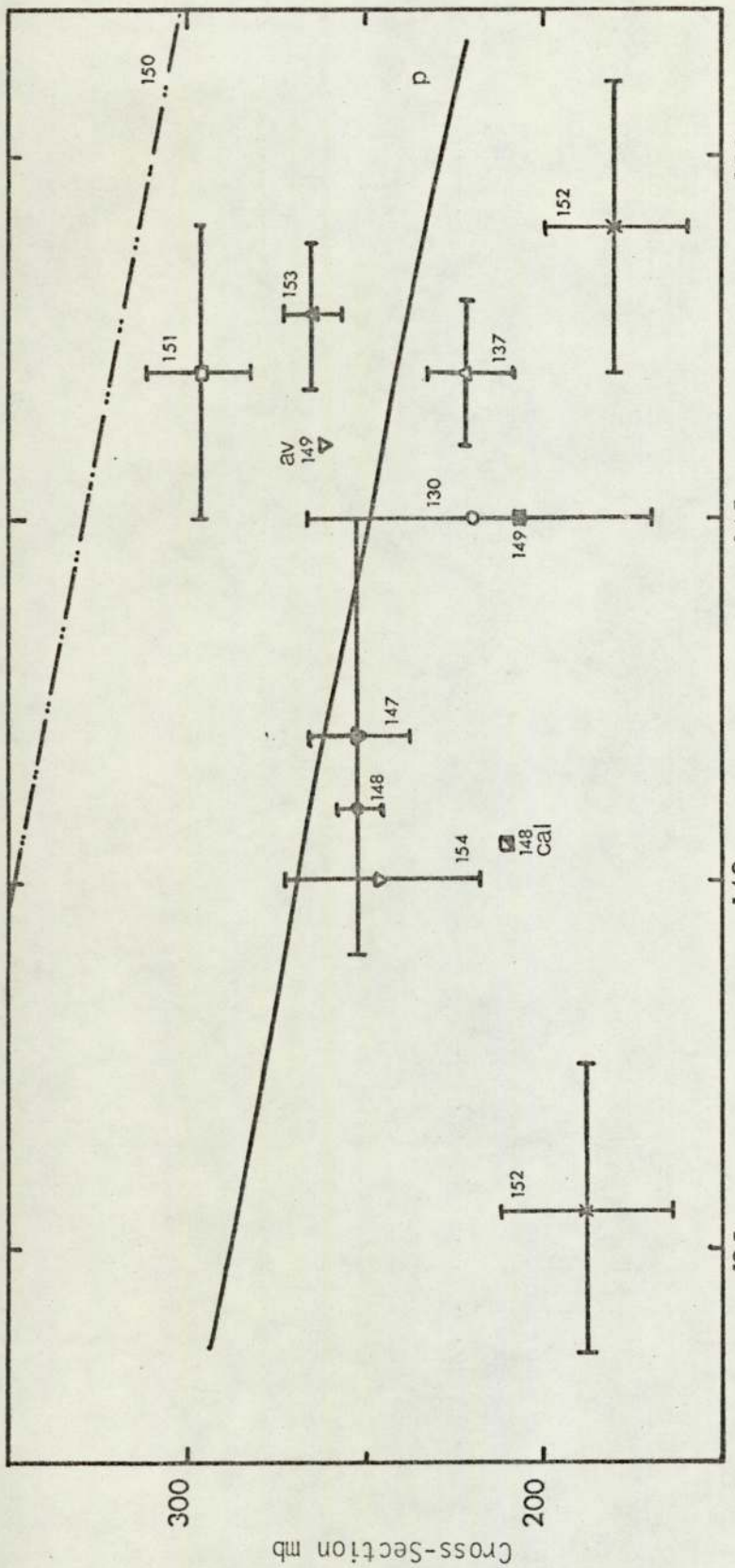

Fig. 8.5b
$^{28}Si(n,p)^{28}Al$ Cross-Section Data

to be counted after the irradiation, then they were followed by the aluminium and copper rings.

The cross-section value at 14.5 MeV that we have calculated from eq. (8.1) is 207 mb which is slightly lower than our experimental results. An average experimental cross-section value of 260 mb at 14.7 $\pm$ 0.15 MeV was reported by Eder et al [149]; this was obtained by taking into account the data of Schantl [155]. On the other hand, the compound nucleus calculations made by Kaji et al [148] have produced a cross-section value of 210 mb at 14.1 MeV, but a higher value is expected if the direct interaction contribution was taken into account.

8.6 $^{64}Zn(n,2n)^{63}Zn$ Excitation Function

This excitation function was measured by irradiating concentric samples made of a zinc disc and aluminium/copper rings for 1h and 1.5h. The neutron energy and absolute neutron flux were estimated by using the copper/aluminium cross-section curve and our $^{63}Cu(n,2n)^{62}Cu$ excitation function.

The cross-section data which are shown in Fig. 8.6a were obtained by the integration under the annihilation gamma ray peak which corresponds to $^{63}Zn(T_{\frac{1}{2}} = 30\ min)$. This was preceeded by the measurement of the induced activities on the copper and aluminium rings separately. The general agreement between the present and published data is relatively good, and in particular the recent measurements by Kaji et al. [161].

Kaji et al [161] have carried out theoretical calculations for the $^{64}Zn(n,2n)^{63}Zn$ reaction by using 1.2 and 4.7 MeV^{-1} values for the level density parameter, whilst Khurana and Hans [162] made a use of the level

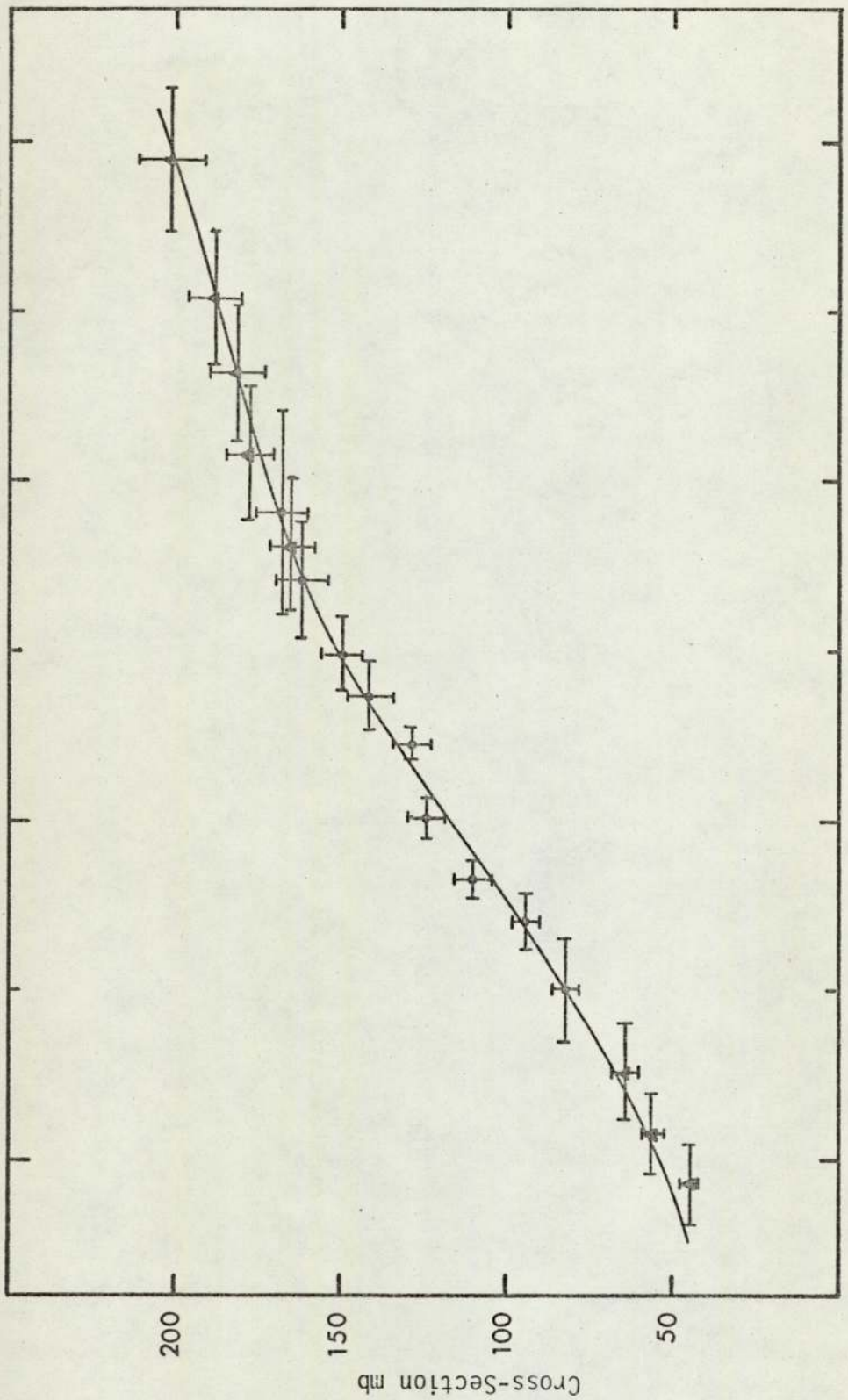

Fig. 8.6a
$^{64}Zn(n,2n)^{63}Zn$ Excitation Function

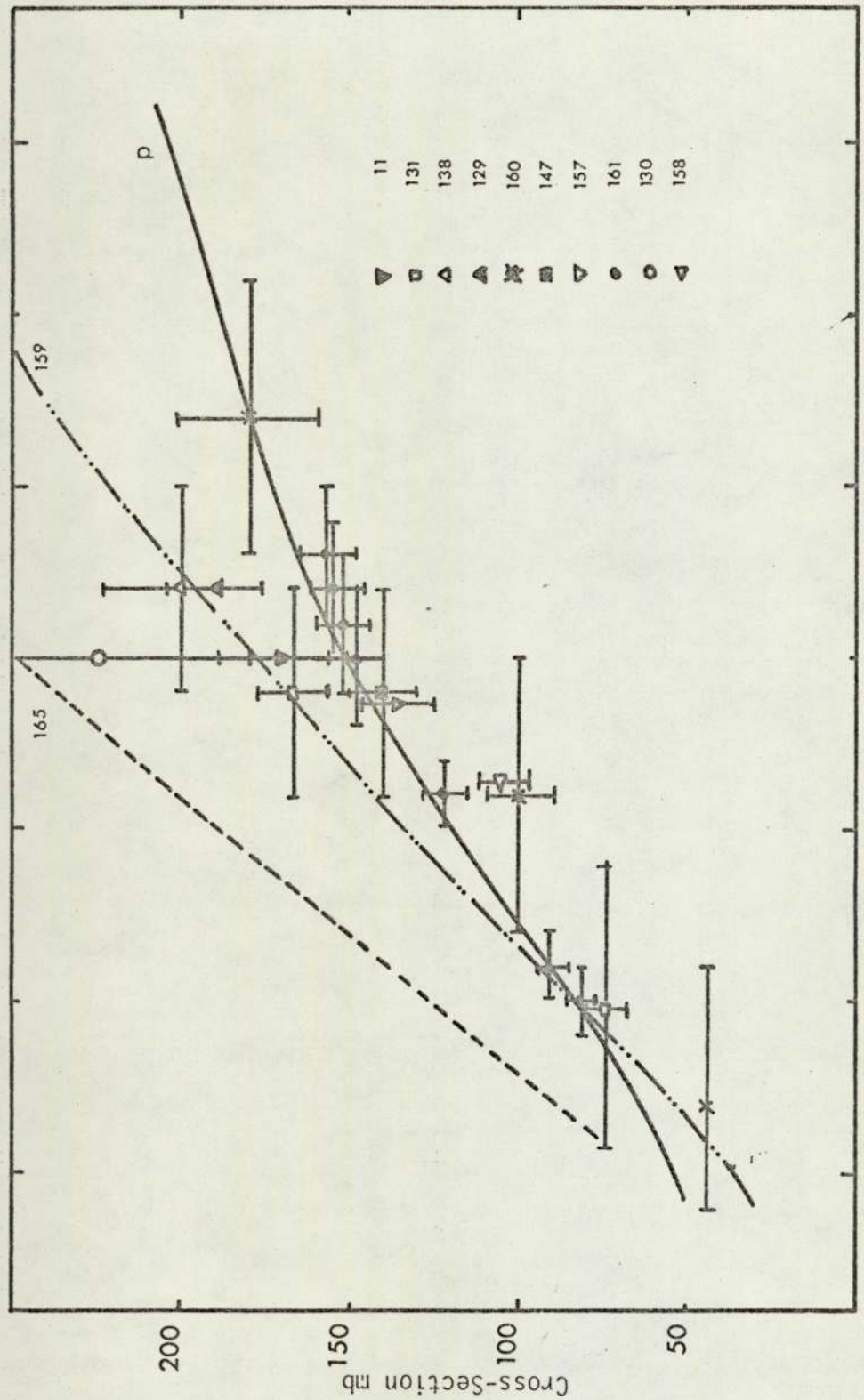

Fig. 8.6b
$^{64}Zn(n,2n)^{63}Zn$ Cross-Section Data

density formula of Newton [166] in their calculations, which takes into account the shell effects. Both calculations have produced results which are much higher than the experimental results, and this can be attributed to the fact that these calculations were made under the assumption that the $^{64}Zn(n,p)^{64}Cu$ competing reaction can be neglected.

8.7 $^{121}Sb(n,2n)^{120g}Sb$ Excitation Function

The residual nucleus of the total (n,2n) reaction on ^{121}Sb can decay in two ways, one with a half-life of 15.9 m leading to the formation of ^{120}Sb in its ground state, the other with a half-life of 5.8 days which leads to the formation of the metastable state ^{120m}Sb.

Determination of the isomeric cross-section ratios is useful for understanding the kind of mechanism governing the reactions. This is being due to its dependence on the angular momenta in various stages of the reaction which in turn depend on the mechanism of the reaction.

In the present work, we report the absolute cross-section data for the $^{121}Sb(n,2n)^{120g}Sb$ reaction in the neutron energy region between 9.29 and 15.9 MeV, which are useful for estimating the extent to which the isomer is populated in the total (n,2n) reaction. Since we are to a large extent interested in the applications of the excitation functions, cross-section measurements for the isomeric state were not carried out. On the other hand, total cross-sections and isomeric cross-sections can be estimated from the previous publications.

The experimental results in Fig. (8.7a) were obtained by irradiating a pure antimony sample surrounded by two concentric rings made of copper and aluminium for the measurement of fast neutron flux and

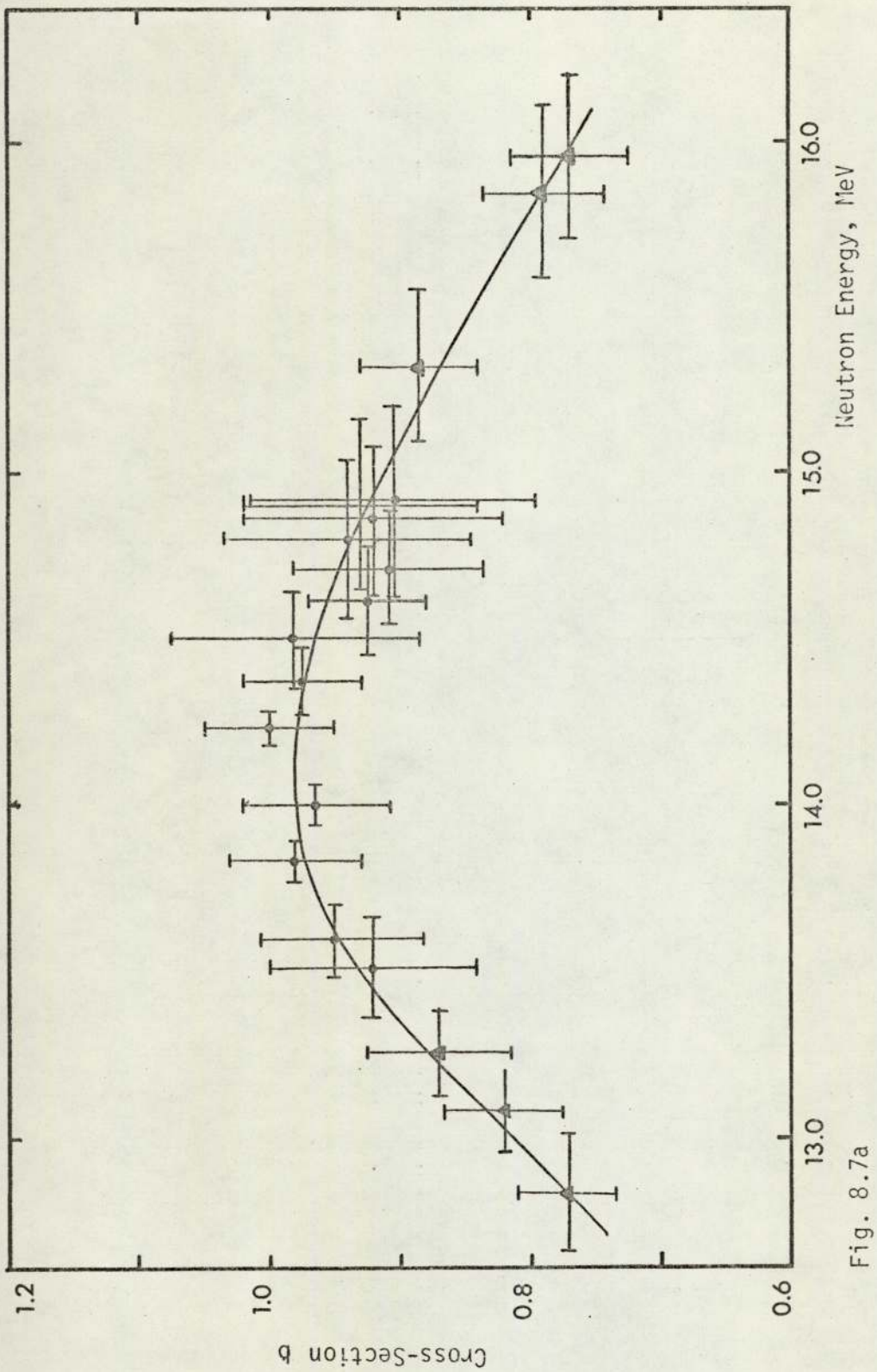

Fig. 8.7a

$^{121}Sb(n,2n)^{120g}Sb$ Excitation Function

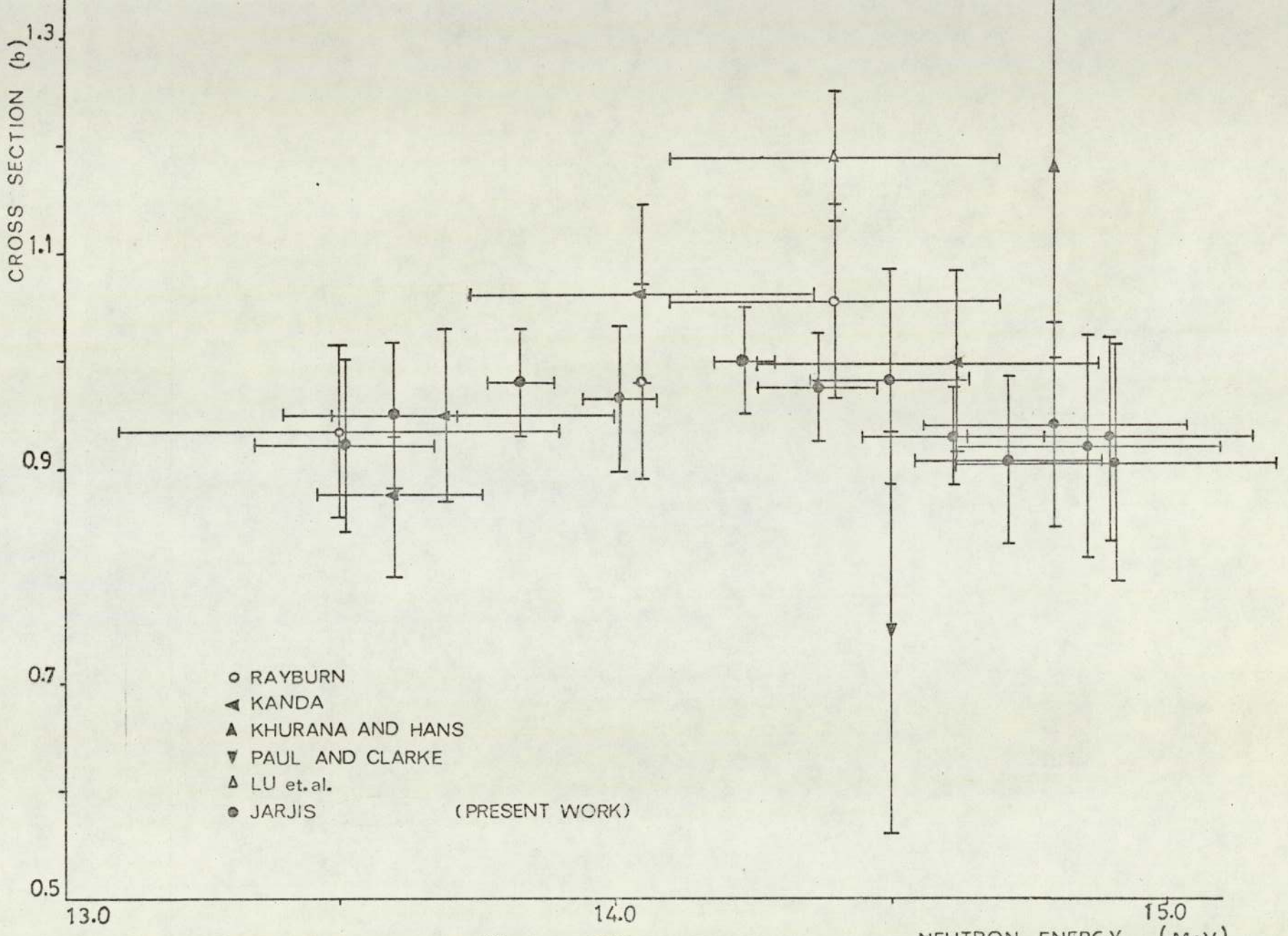

Fig. 8.7b $^{121}Sb(n,2n)^{120g}Sb$ Cross-Section Data

energy. The cross-section data were obtained relative to $^{63}Cu(n,2n)^{62}Cu$ excitation function by counting the annihilation gamma rays from the decay of ^{62}Cu and ^{120g}Sb by positron emission, separately.

It is worthwhile indicating that $^{121}Sb(n,2n)^{120g}Sb$ cross-section data of Kanda [163] were obtained by the mixed powder technique. The induced activities on copper and antimony were counted simultaneously and in comparison with our method, Kanda had to carry out the necessary analysis of the decay curve to obtain the yield ratio of ^{120g}Sb and ^{62}Cu.

Our results indicate that $^{121}Sb(n,2n)^{120g}Sb$ excitation function has a broad peak in the 13-15 MeV region. The results obtained on the Van de Graaff and Dynamitron accelerators confirm each other and indicate the occurence of some competing reaction above 15 MeV. The total reaction cross-section determined from our ^{120g}Sb results and an average isomeric cross-section of 770 mb is 1760 mb at about 14.5 MeV, compared with a weighted average value of 1741 mb [11]. The statistical model calculations by Kanda [163] predicted a value of 1880 mb using Blatt and Weisskopf formula [2]. The calculations of Pearlstein [165], which are based on an empirical expression for inelastic cross-sections and level density, gave total cross-section values of 1486 mb and 1715 mb at 13.1 MeV and 15.1 MeV respectively. On the other hand by using more accurate optical model values for non-elastic cross-sections, Kondaiah [11] obtained 1401 mb at 14.5 MeV.

To carry out an appropriate test for the empirical systematic method that has been discussed in Chapter 1, a FWHM value of 9.6 MeV was obtained for the (n,2n) reaction on ^{121}Sb, see Fig. 1.5. An extrapolation of our excitation curve yields a FWHM value of 6.2 MeV whilst the corresponding value from the early measurements by Rayburn was found to be 14.2 MeV [131].

Finally, Antimony is suggested as a very suitable flux monitor for 14 MeV neutrons when used to produce activities with half-lives in the 10 - 30 min region. It has the advantage of having a relatively high cross-section, its radioactive product has a reasonable half-life of 15.9 min and its excitation function is smooth and almost flat in the 13.5 - 15 MeV region.

8.8 $^{56}Fe(n,p)^{56}Mn$ Excitation Function

The experimental cross-section data for $^{56}Fe(n,p)^{56}Mn$, Fig. 8.8a, were measured relative to the cross-section data of $^{121}Sb(n,2n)^{120g}Sb$ reaction. The irradiated samples consisted of an iron sample surrounded by a flux monitoring ring made by compressing pure antimony powder. Measurement of the induced activity on the antimony ring was followed by detecting the 0.847 MeV gammas emitted due to the decay of $^{56}Mn(T_{\frac{1}{2}} = 9.58h)$.

It has been shown by Levkovskii [171] that for a broad range of (A) values, the (n,p) cross-sections can be described by a single exponential formula containing the neutron asymmetry parameter.

$$\frac{\sigma_{n,p}}{\sigma_{ne}} = 0.73 \exp(-33 \frac{N-Z}{N+Z}) \qquad (8.2)$$

By using this formula for 14-15 MeV neutrons, Levkovskii[172] has estimated a cross-section of 100 mb for $^{56}Fe(n,p)^{56}Mn$ which is in a very good agreement with the experimental data. On the other hand, we have obtained a low value of 86.0 mb by using eq. 8.1 which was proposed by Eder et al [149]. Also, a low cross-section of 25 mb at 14.1 has been obtained theoretically by Kaji et al [148], and this was interpreted by the presence of the direct process.

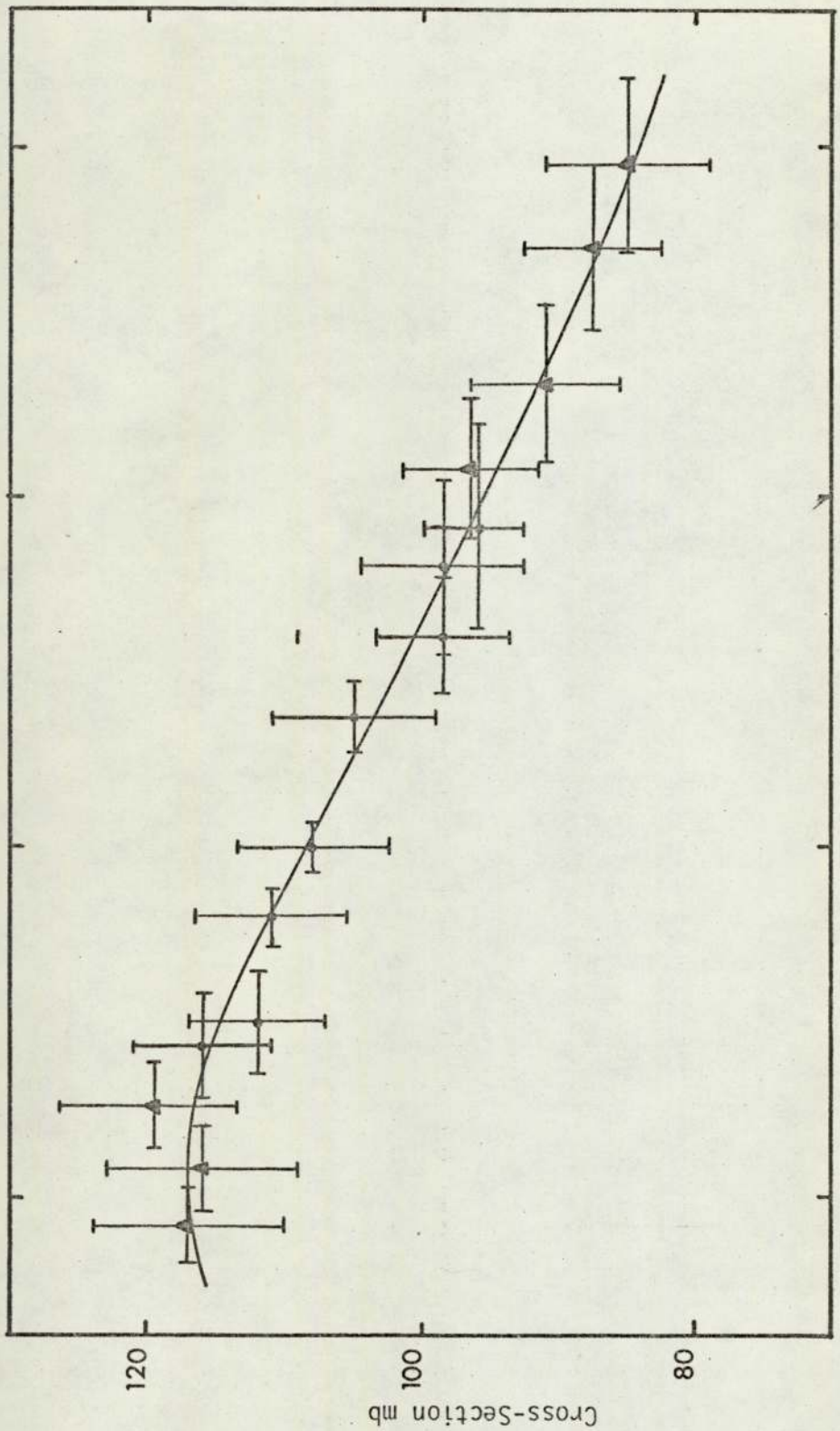

Fig. 8.8a

$^{56}Fe(n,p)^{56}Mn$ Excitation Function

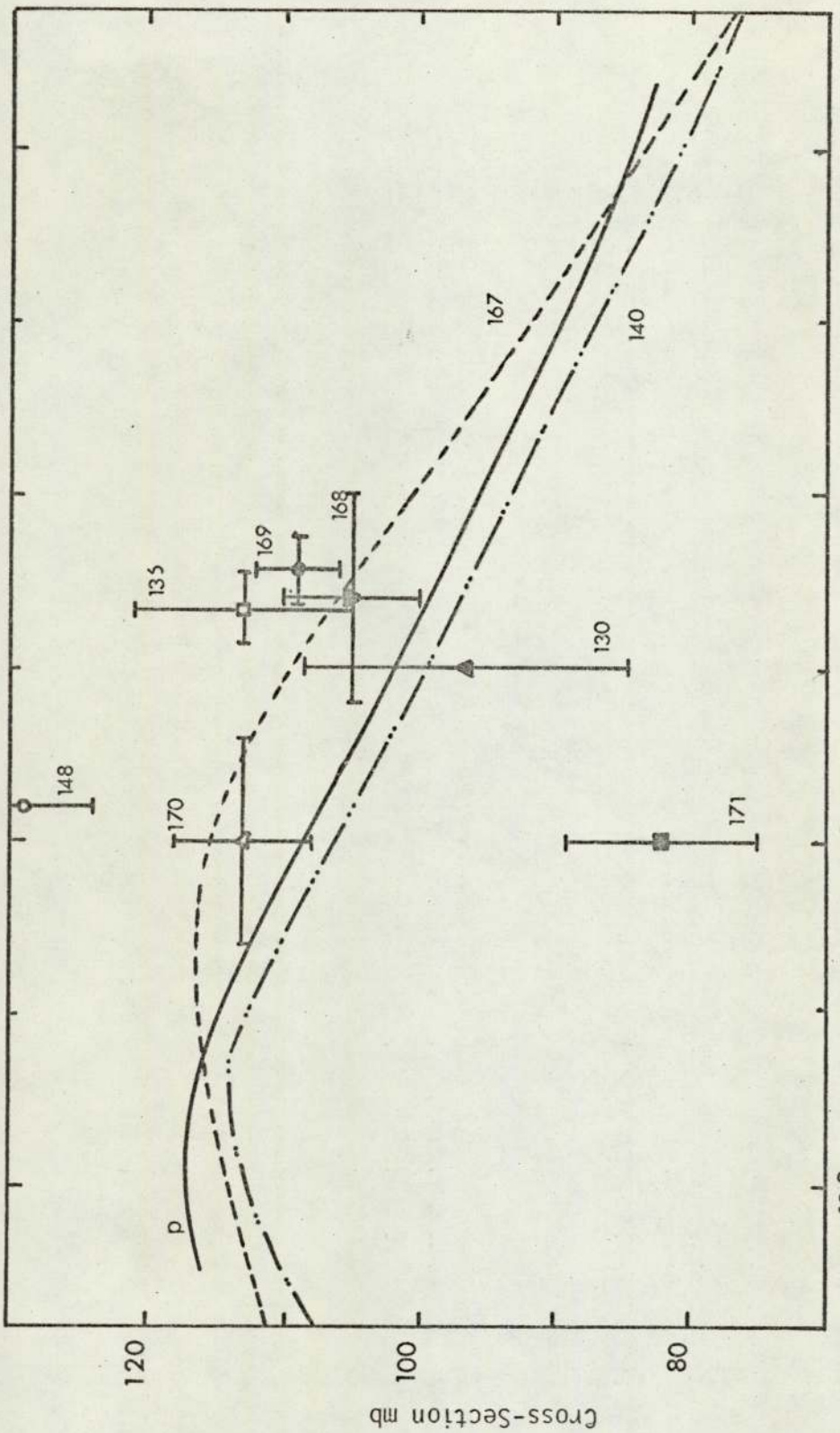

Fig. 8.8b

$^{56}Fe(n,p)^{56}Mn$ Cross-Section Data

8.9 $^{59}Co(n,\alpha)^{56}Mn$

The excitation function for $^{59}Co(n,\alpha)^{56}Mn$ reaction was determined relative to the excitation function of $^{121}Sb(n,2n)^{120g}Sb$ by using Antimony rings for flux monitoring. Additional check was provided by employing iron rings and the $^{56}Fe(n,p)^{56}Mn$ excitation function to obtain the absolute cross-section data. Both sets of data were found to be consistent and average values were plotted in Fig. 8.9a.

According to Levkovskii [172], for A > 40, the value of $\sigma_{n,\alpha}$ is about 2.5 times smaller than that of $\sigma_{n,p}$ for the same nucleus and in the 14-15 MeV region. Accordingly, a new formula for $\sigma_{n,\alpha}$, based on eq. (8.2), has been proposed.

$$\frac{\sigma_{n,\alpha}}{\sigma_{ne}} = 0.29 \exp(-33\frac{N-Z}{N+Z}) \qquad (8.3)$$

A cross-section of 26 mb for ^{59}Co nucleus has been estimated from this equation, which is very close to the experimental data. This value for ^{59}Co is actually very close also to that obtained using the statistical model analysis by Milano group [177,178]. In this case, a cross-section of 27 mb has been obtained by analysing the (n,α) excitation functions and energy spectra to evaluate the appropriate level density values.

8.10 $^{27}Al(n,\alpha)^{24}Na$ Excitation Function

The (n,α) cross-section on ^{27}Al is being used very often as a flux monitoring standard, specially for long irradiation times since the product nucleus ^{24}Na has a half-life of 15h. In addition, the cross-section variation with energy has been subjected to several fine structure investigations as it has been discussed in Chapter 1.

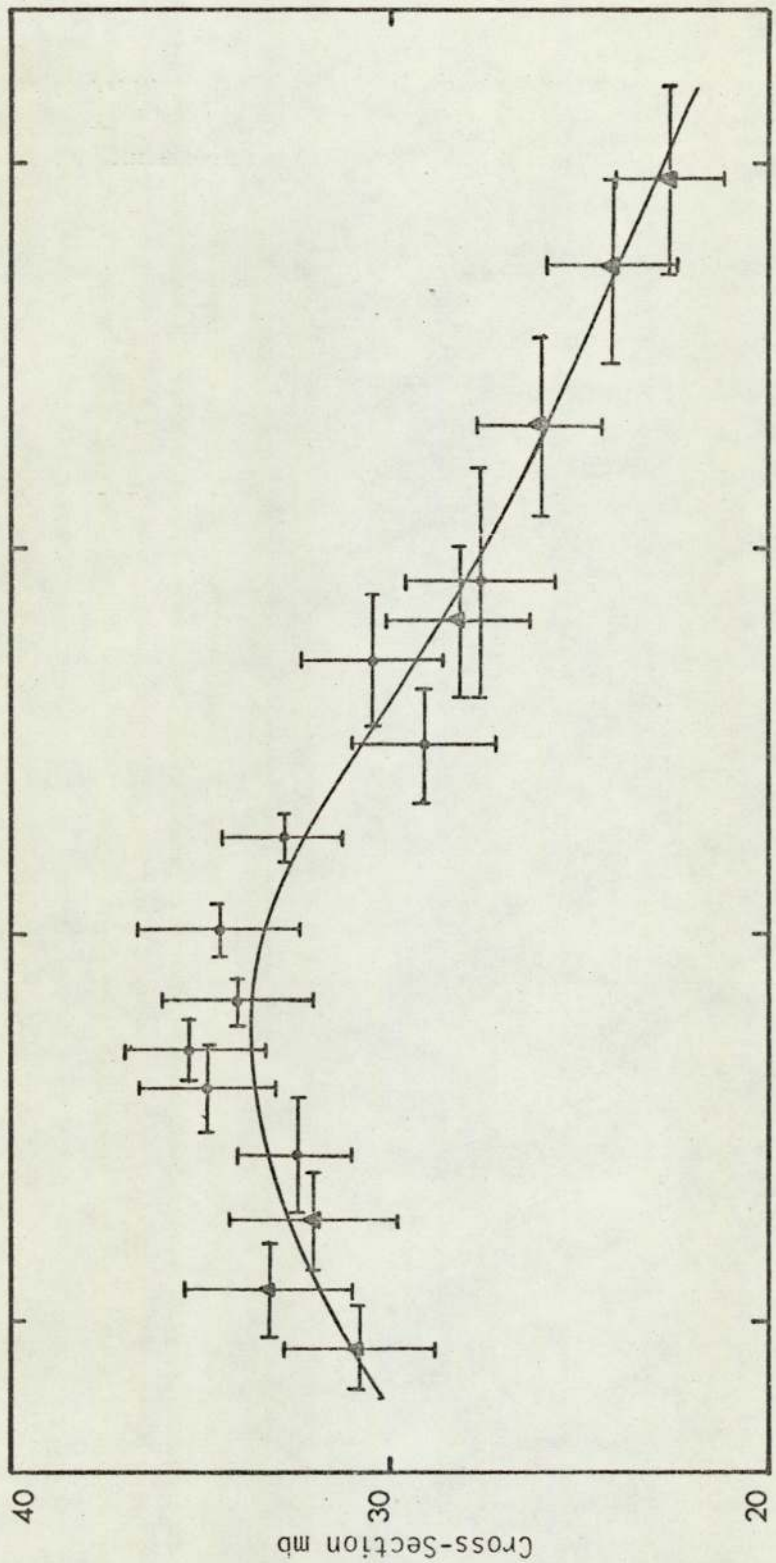

Fig. 8.9 a
$^{59}Co(n,\alpha)^{56}Mn$ Excitation Function

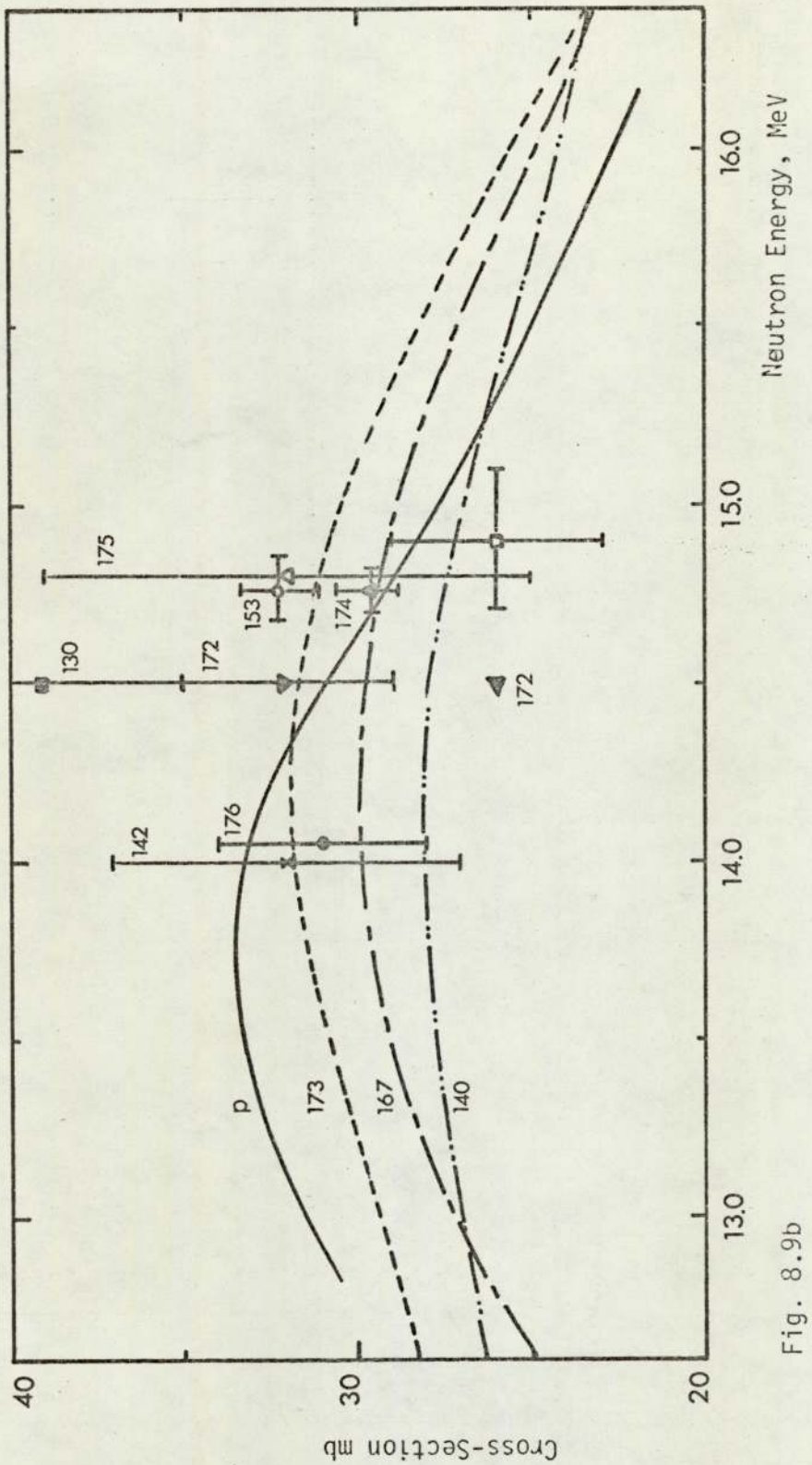

Fig. 8.9b
$^{59}Co(n,\alpha)^{56}Mn$ Cross-Section Data

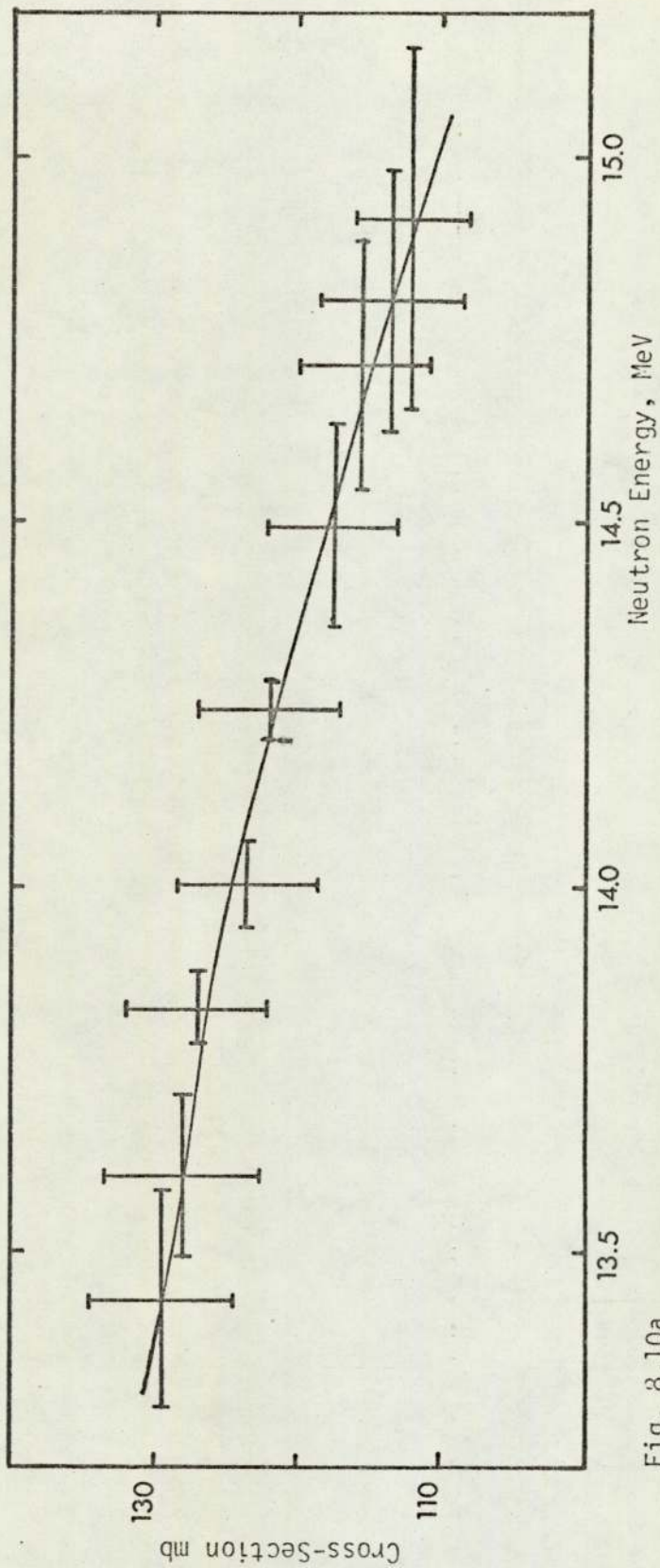

Fig. 8.10a

$^{27}Al(n,\alpha)^{24}Na$ Excitation Function

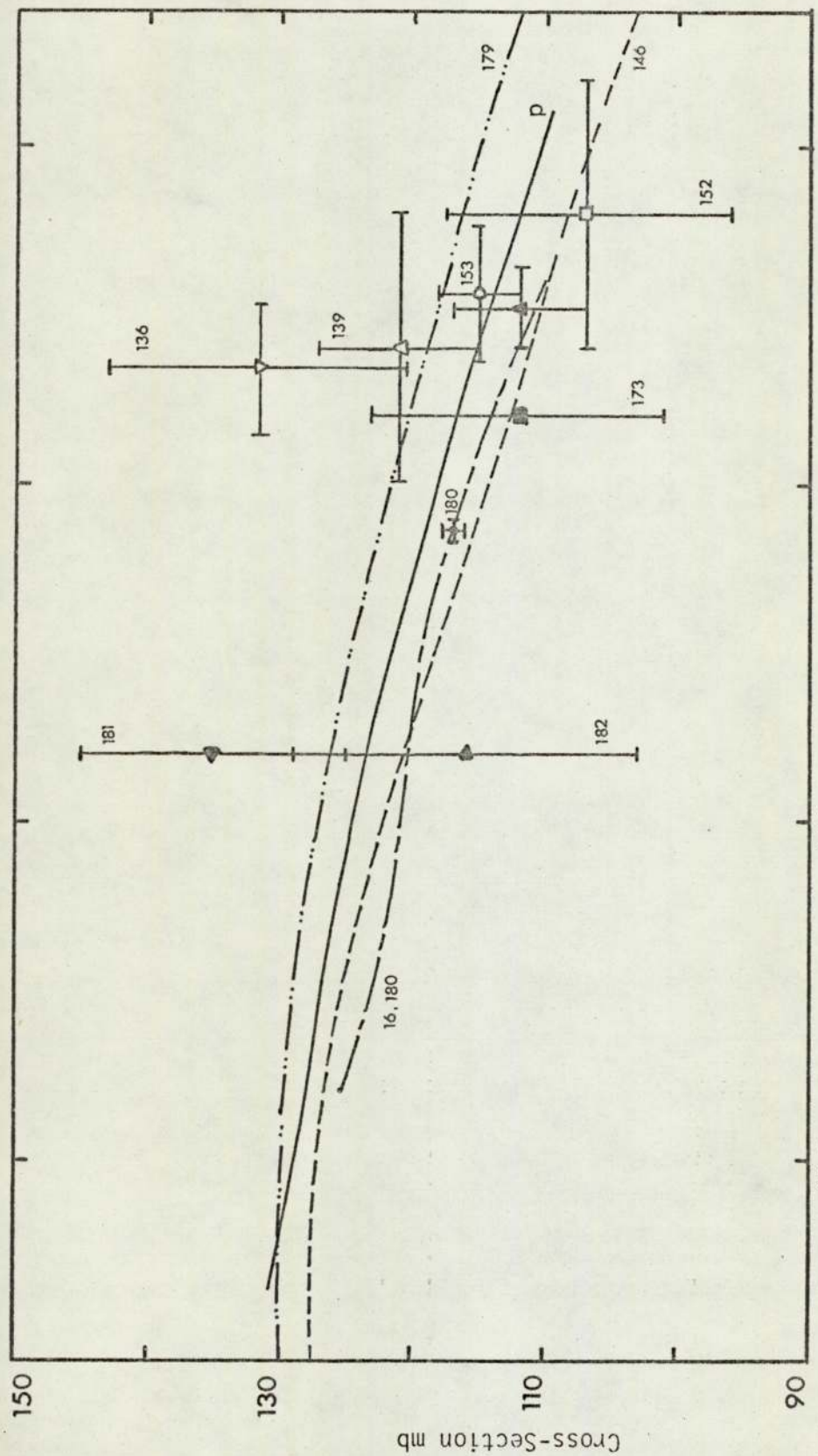

Fig. 8.10b
$^{27}Al(n,\alpha)^{24}Na$ Cross-Section Data

In the present study, investigation of Ericson's fluctuations was not possible mainly due to the deuteron beam energy loss in the used tritiated targets which results in neutron energy spreads wider than the expected fluctuation average width. On the other hand, an accurate determination of the general trend of the excitation function was required for absolute neutron flux monitoring.

The ~~absolute~~ cross-section data presented in Fig. 8.10a were determined relative to an accurate cross-section of 1170 $\pm$ 0.8 mb at 14.43 $\pm$ 0.015 MeV, which was recently measured by Vorach et al.[180] The required information about neutron anisotropy etc. were obtained from our reported results in Chapter 3.

Apart from some odd data, the present data and most of the published data are in good agreement. The reported evaporation model theoretical cross-section is 125 mb for 14 MeV neutrons [178]. This is consistent with the experimental data, as was the case of ^{59}Co, which indicate the validity of the evaporation model calculations for predicting the (n,α) cross-sections at least within the 27-59 target mass region.

8.11 $^{64}Zn(n,p)^{64}Cu$ Excitation Function

In this experiment, samples made of a zinc disc and aluminium ring were used, and the cross-section results were obtained relative to $^{27}Al(n,\alpha)^{24}Na$ excitation function. Following the irradiation, a decay time of about 4h was introduced to allow the interference from $^{63}Zn(T_{\frac{1}{2}} = 38m)$ to reach a negligible level. The cross-section was then determined by integrating under the annhilation peak of $^{64}Cu(T_{\frac{1}{2}} = 12.9h)$.

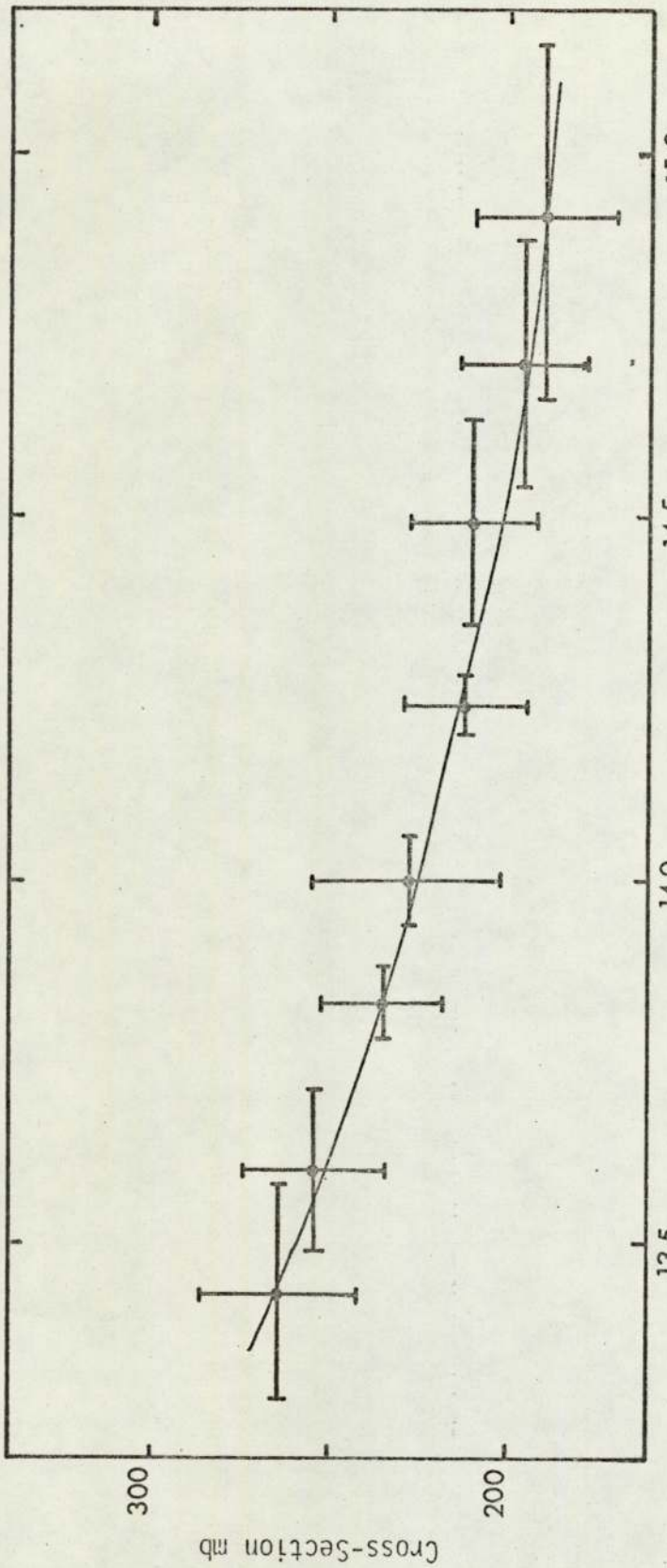

Fig. 8.11a
$^{64}Zn(n,p)^{64}Cu$ Excitation Function

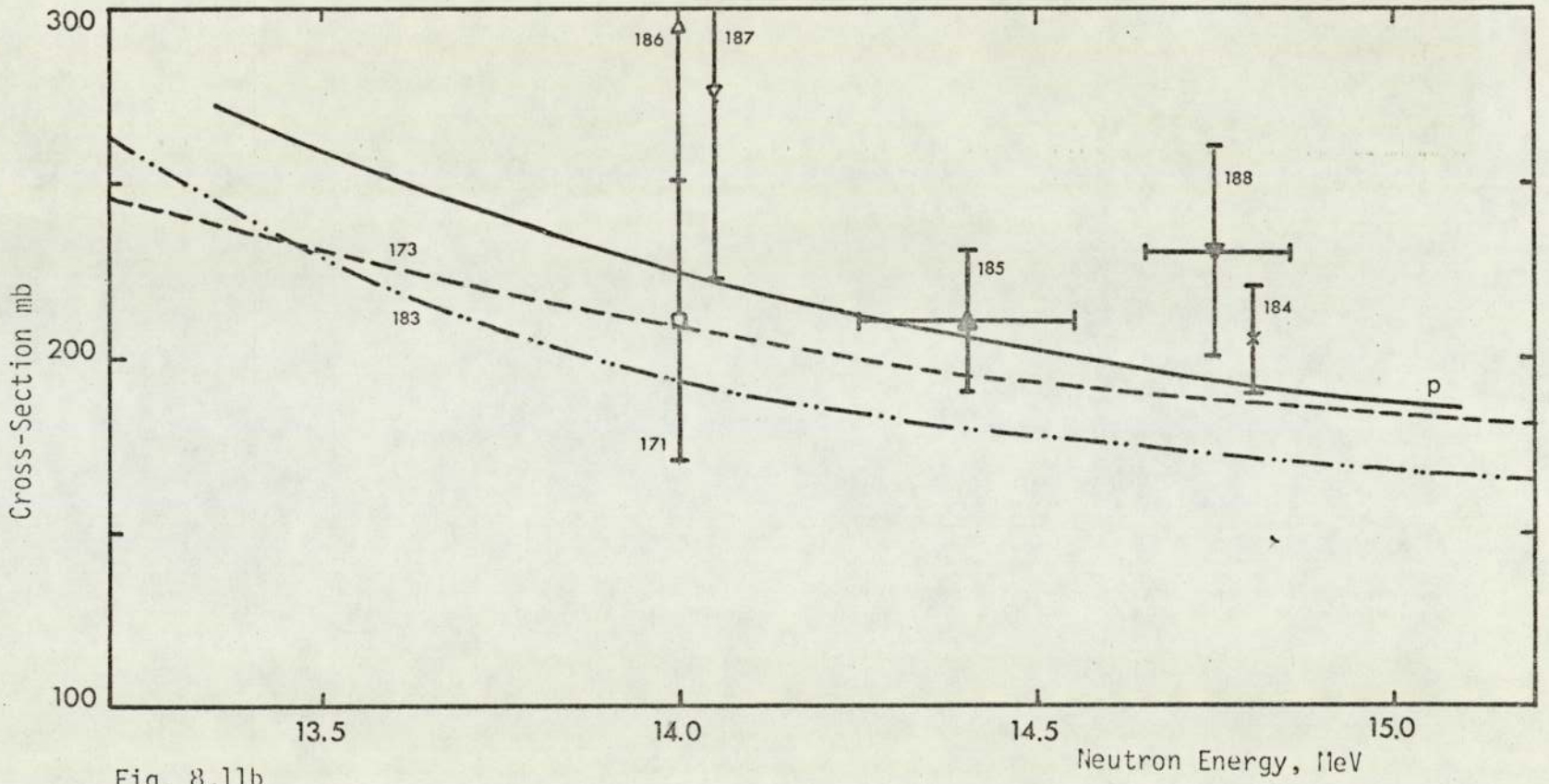

Fig. 8.11b

$^{64}Zn(n,p)^{64}Cu$ Cross-Section Data

The cross-section variation with energy of the present work is in a good agreement with the experimental data by Gabbard and Kern [173], and by Santry and Butler [183]. The calculated cross-section from Levkovskii's formula, eq. 8.2, is 140 mb for 14-15 MeV neutrons, which is in this case very close to the experimental values. Furthermore, the recent statistical model calculations by Kaji et al [148] have produced a cross-section of 180 mb for 14.1 MeV, but the experimental cross-section by the same authors was 325 $\pm$ 38 mb which is higher than the rest of the experimental data.

8.12 $^{65}Cu(n,2n)^{64}Cu$ Excitation Function

Aluminium ring was again used for measuring the neutron flux, but the data were normalized to the recommended cross-section of 965 mb at 14.7 MeV for the $^{65}Cu(n,2n)^{64}Cu$ reaction [129]. A suitable decay time was allowed after the irradiation to eliminate the interference from ^{62}Cu, and the cross-section was determined in terms of the integrated area under the annihilation peak for ^{64}Cu ($T_{\frac{1}{2}}$ = 12.8h).

The shape of the present excitation function is very similar to those which have been obtained by the other researchers. The statistical model calculations by Kondaiah [11] have produced a value of 752 mb for 14.5 MeV neutrons.

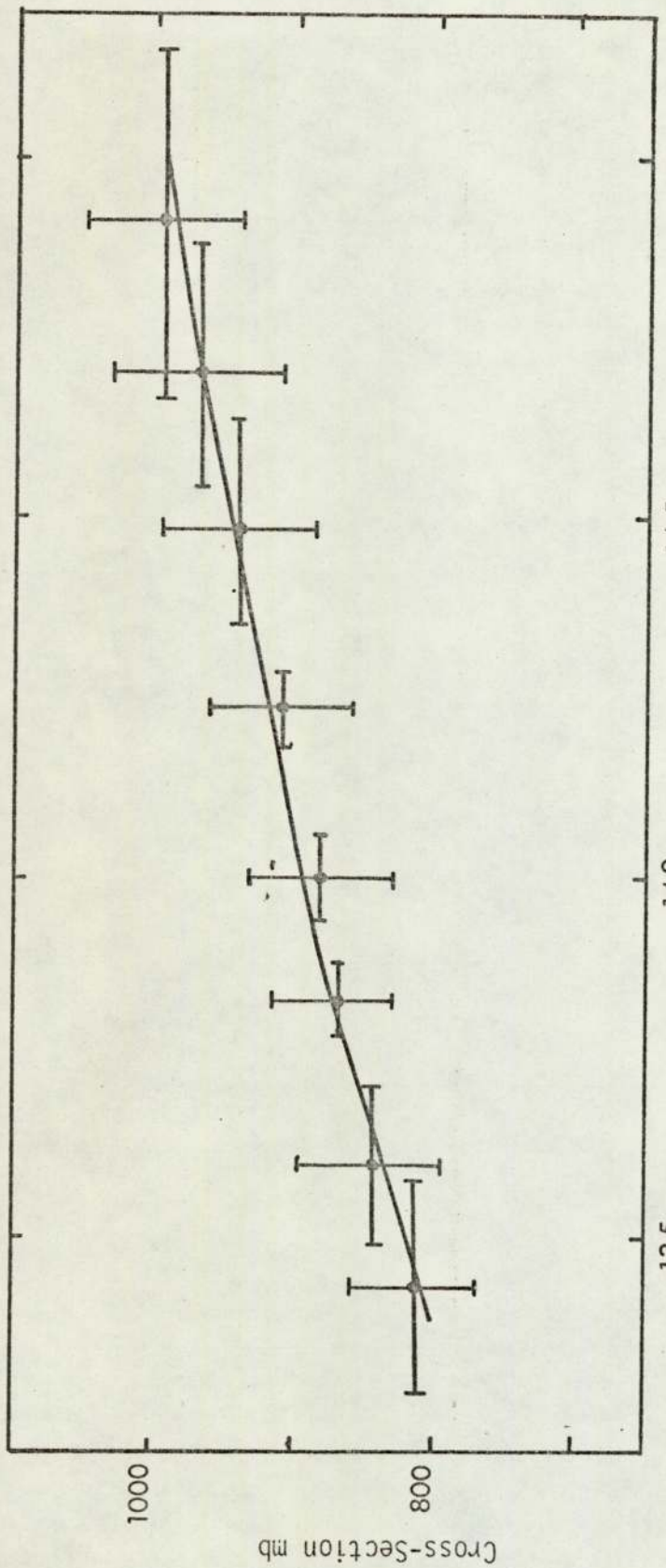

Fig. 8.12a

$^{65}Cu(n,2n)^{64}Cu$ Excitation Function

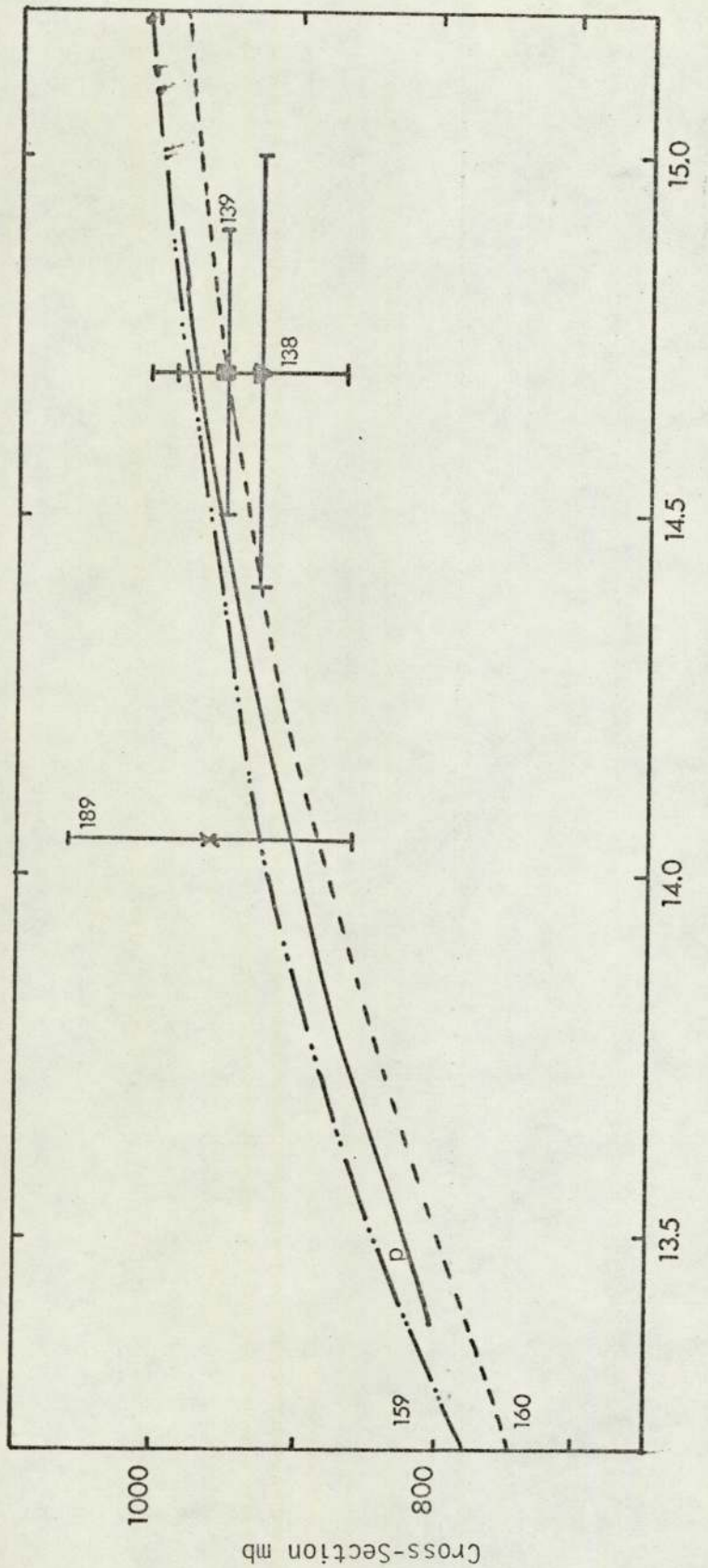

Fig. 8.12b

$^{65}Cu(n,2n)^{64}Cu$ Cross-Section Data

CONCLUSIONS

The concentric ring technique appears to be sufficiently accurate for producing good results for standard excitation functions. Therefore, it can also be used for measuring cross-section data for rare reactions, and for studying the effects of the overlapping of excitation levels. The use of the concentric ring technique will minimize the errors due to neutron flux measurement and energy estimation.

Our experimental results indicate that better information about the actual shape of the excitation function can be obtained by expanding the incident neutron energy range. Cross-section systematics should be based on a neutron energy region wider than 14-15 MeV to reduce the effect of cross-section peak position which varies by varying the mass of target nucleus, i.e. cross-sections of nuclei with a peak position within the 14-15 MeV region are underestimated. In addition to this, it will be possible to study the cross-sections for (n,xn) reactions, and learn more about the high energy ~~ring~~ tail portion of the (n,2n) excitation functions [190,191].

Accelerator neutron sources with high neutron production rate are required for obtaining advanced information about these reactions which have low cross-sections e.g. (n,t) and (n,^{3}He) and therefore improve their systematics [192-195]. Such data are important in both nuclear physics and in estimating light elements concentration build-up in future fusion reactors. The other advantage of high neutron source strength is in studying the fluctuations in neutron cross-sections as a function of energy, since samples can be placed at longer distances from the source to reduce the spread due to sample subtended angle.

REFERENCES

(1) S.M. Qaim, Proc. Int. Conf. Nuclear Cross-Sections and Technology, N.B.S. SP 425 (1975). (R.A. Schrack and C.D. Bowman, eds.)

(2) J.M. Blatt and V.C. Weisskopf, Theoretical Nuclear Physics (John Wiley & Sons, Inc., New York 1952), p.336

(3) A.S. Divatia et al., Nuclear Data for Reactors, I.A.E.A. Publications, Vol. 1

(4) J.H. Gibbons and R.L. Macklin, Phys. Rev. 114 (1959) 571

(5) A. Chatterjee, Nucl. Phys. 60 (1963) 273

(6) A. Chatterjee, Nucl. Phys. 49 (1963) 686

(7) D.G. Gardner, Nucl. Phys. 29 (1962) 383

(8) M. Bormann, Nucl. Phys. 65 (1965) 257

(9) R.K. Mohindra and S.K. Gupta, J. Phys. Soc. Jap. 39 (1975) 1147

(10) S.M. Qaim, Nucl. Phys. A185 (1972) 614

(11) E. Kondaiah, J. Phys. A: Math., Nucl. Gen., 7 (1974) 1457

(12) E. Holub and N. Cindro, J. Phys. G: Nucl. Phys. 2 (1976) 405

(13) J. Csikai and G. Peto, Phys. Lett. 20 (1966) 52

(14) T. Ericson, Ann. Phys. 23 (1963) 390

(15) W.H. Breunlich, Proc. Int. Conf. on the study of nuclear structure with neutrons (1965) p.100

(16) H.K. Vorach et al., Proc. Int. Conf. on the study of nuclear structure with neutrons (1965) p.885

(17) N. Cindro et al., Phys. Lett. 6 (1963) 205

(18) P. Strohal et al., Phys. Lett. 10 (1964) 104

(19) J. Csikai, Proc. Int. Conf. on the study of nuclear structure with neutrons (1965)

(20) J.M. Ferguson et al., Nucl. Phys. A98 (1967) 65

(21) M. Bormann and I. Riehle, Z.f. Physik 207 (1967) 64

(22) M.A. Gardner and D.G. Gardner, Nucl. Phys. A265 (1976) 77

(23) L. Colli et al, Phys. Lett. 1 (1962) 120

(24) L. Colli et al, Phys. Lett. 2 (1962) 12

(25) L. Colli et al., Nucl. Phys. 43 (1963) 529

(26) A.K.M. Siddiq et al., Indian J. Phys. 48 (1974) 318

(27) M. Bormann et al., Nuclear Data for Reactors, I.A.E.A. Publications

(28) V. Krivan and H. Munzel, J. Inorg. Nucl. Chem. 33 (1971) 1233

(29) V. Krivan and H. Munzel, J. Inorg. Nucl. Chem. 34 (1972) 2093

(30) V. Krivan and H. Munzel, J. Inorg. Nucl. Chem. 34 (1972) 2989

(31) V. Krivan and H. Munzel, J. Radioanalyt. Chem. 15 (1973) 575

(32) H.L. Rook et al., Int. Conf. Modern Trends in Activation Analysis, NBS, Washington, 1969

(33) H.P. Ule and V.P. Guinn, Proc. Int. Conf. on Peaceful Uses of Atomic Energy, I.A.E.A. Vienna, II, 111 (1964)

(34) D.C. Borg et al., Int. J. App. Radiat. Isotopes 11 (1961) 30

(35) N.A. Frigerio, Meeting on Radiological Applications of Neutron Irradiation, I.A.E.A., STI/PUB-325, Vienna, 1971

(36) S. Taczanoski, Nucl. Inst. and Meth. 104 (1972) 219

(37) L.C. Pasztor and D.E. Wood, Talanta 13 (1966) 389

(38) J. Csikai et al., Atomic Energy Review 7 (1969) 93

(39) E.L. Steele et al., Variable Energy Neutron Activation Analysis, AEC Report GA-6691, 1965

(40) O.N. Jarvis et al., Nucl. Instr. and Meth. 112 (1973) 559

(41) H. Liskein and A. Paulsen, Nuclear Data Tables 11 (1973) 569

(42) E. Magiera et al., Nucl. Phys. A246 (1975) 413

(43) H.H. Barschall, Nuclear Structure Study with Neutrons, J. Ero and J. Szucs (Eds.), Plenum Press, London, (1974),

(44) M.R. Cleland and K.H. Morganstein, Nucleonics 18 (1960) 52

(45) J.B.A. England, Techniques in Nuclear Structure Physics (I), Macmillan Press Limited, (1974).

(46) Amersham Radiation Sources for Industry and Research Catalogue (1971)

(47) J. Hoste et al., The Determination of Oxygen in Metals by 14 MeV Neutron Activation Analysis, E.U.R. 3565.e (1967)

(48) J.J. Broerse et al., Int. J. Appl. Radiation and Isotopes 22 (1971) 486

(49) D.M. Bibby et al., Nuclear Energy 11 (1970) 68

(50) J.J. Broerse, Conf. Accelerator Targets designed for the production of neutrons, E.U.R. 2641.e (1965)

(51) H. Fabian, Conf. Accelerator Targets designed for the production of neutrons, E.U.R. 2641.1 (1966)

(52) J. Pivarc, Wiss. Z. Techn. Univers. Dresden 21 (1972) 694

(53) G. Stengl et al., Nucl. Instr. and Meth. 126 (1975) 235

(54) D.M. Bibby et al., Nucl. Instr. and Meth. 94 (1971) 397

(55) D. Cossutta, Conf. Accelerator Targets designed for the production of Neutrons, E.U.R. 2641.e (1965).

(56) J. Laverlochere, Accelerator Targets designed for the production of neutrons. E.U.R. - 3895, Brussels 1968 p.202

(57) O. Reifenschweiller, Philips Res. Depts. 16 (1961) 401

(58) E. Hara, Jap. J. Appl. Phys. 7 (1968) 70

(59) J. Benveniste and J. Zenger, Information on the neutrons produced by the $^{3}H(d,n)^{4}He$ Reaction, UCRL - 4266 (1954)

(60) E.W. Saker and J.D.L.H. Wood, S.E.R.L. Tech. Report No. 61 (1958)

(61) E.M. Gunnersen and G. James, Nucl. Inst. and Meth. 8 (1960) 173

(62) S.D. Warshaw, Phys. Rev. 76 (1949) 1759

(63) N. Bohr, Mat. Fys. Medd. Dan. Vid. Selsk. 18, No. 8 (1948)

(64) J. Lindhard and M. Scharff, Mat. Fys. Medd. Dan. Vid. Selsk. 27 No. 15 (1953)

(65) L.N. Rothenberg, Phys. Rev. C1 (1970) 1226

(66) J.A. Cookson et al., Proc. Int. Conf. Nuclear Cross-Sections and Technology, N.B.S. SP425 (1975). (R.A. Schrack and C.D. Bowman, eds.)

(67) D.J. Hughes, Pile Neutron Research, Addison-Wesley Cambridge/Mass., (1953)

(68) I. Heertje, Thesis, University of Amsterdam (1963)

(69) I. Heertje et al., Physica 30 (1964) 1762

(70) E. Bruninx and J. Crombeen, Int. J. Appl. Radiat. Isotopes 20 (1969) 255

(71) R.C. Lawson et al., Radiochem. Radiological Lett. 10 (1972) 323

(72) R.C. Lawson et al., Phys. Med. Biol. 17 (1972) 771

(73) G. Oldham and K.G. Darrall, Int. J. Appl. Radiat. Isotopes 20 (1969) 255

(74) M.C. Scott, J. Nucl. Energy 35 (1971) 405

(75) De Volpi and Porges, Proc. 2nd Int. Conf. Neutron Cross-Sections and Technology, NBS Special Bulletin (1968)

(76) A.M. Atta and M.C. Scott, J. Nucl. Energy 27 (1973) 875

(77) E. Bruninx, Proc. Int. Conf. Modern Trends in Activation Analysis, NBS Publication 312 (1969)

(78) E. Bruninx, Int. J. Appl. Radiat. Isotopes 21 (1970) 657

(79) E. Bruninx, Uses of Cyclotron in Chemistry, Metallurgy and Biology, C.B. Amphett (ed.), Butterworth and Co. Ltd., London (1970)

(80) L.D. Stephens and A.R. Smith, U.S. Atomic Energy Commission Report, U.C.R.L. 8418 (1958)

(81) C.A. Feu Alvin and A.N. Das Santos, Nucl. Inst. and Meth. 105 (1972) 289

(82) W.W. Meinke and R.W. Shideler, Nucleonics 20 (3) (1962) 60

(83) F.A. Iddings, Anal. Chem. Acta. 31 (1964) 206

(84) M. Ahmad et al., Nucl. Inst. and Meth. 126 (1975) 309

(85) J.C. Robertson and K.J. Zieba, Nucl. Inst. and Meth. 45 (1966) 179

(86) P. Fieldhouse et al., Conf. Accelerator Targets Designed for the Production of Neutrons, EUR - 2641 (1966)

(87) Proc. 1965 Int. Conf. Modern Trends in Activation Analysis, College Station, Texas, April (1965)

(88) R.L. Heath, Proc. Conf. Accelerator Targets Designed for the Production of Neutrons, EUR - 2641, Brussels (1966)

(89) T. Shiokawa et al., J. Inorg. Nucl. Chem. 30 (1968) 1

(90) D. Partington et al., Analyst 95 (1970) 257

(91) B.T. Kenna and F.J. Conrad, Health Physics 12 (1966) 564

(92) K.G. Darrall and G. Oldham, Nuclear Energy (1967) 104

(93) H.F. Priest et al., Nucl. Inst. and Meth. 50 (1967) 141

(94) G. Oldham and D.M. Bibby, Nuclear Energy (1968) 167

(95) J.P. Op de Beeck, J. Radioanal. Chem. 1 (1968) 313

(96) J.P. Op de Beeck, Radiochem. Radioanal. Lett. 1 (1969) 281

(97) J. Janczyszyn and L. Loska, Radiochem. Radioanal. Lett. 3 (1970) 343

(98) T. Kishikawa, and C. Shinomiya, Radiochem. Radioanal. Lett. 7 (1971) 15

(99) J. Janczyszyn and S. Taczanowski, Radiochem. Radioanal. Lett. 9 (1972) 143

(100) D. Crumpton, Nucl. Inst. and Meth. 55 (1967) 198

(101) P. Oblozinsky and I. Ribansky, Nucl. Inst. and Meth. 7 (1971) 139

(102) S. Taczanowski, J. Radioanal. Chem. 12 (1972) 535

(103) H. Gotoh et al., Nucl. Inst. and Meth. 100 (1972) 473

(104) H. Gotoh et al., Nucl. Inst. and Meth. 116 (1974) 361

(105) E. Ricci, J. Inorg. Nucl. Chem. 27 (1965) 41

(106) H. Hollister, Nucleonics, 22 (No.6) (1964) 68

(107) S. Glasstone and M.C. Edlund, The Elements of Nuclear Reactor Technology, Van Nostrand, New Jersey (1958)

(108) M.D. Goldberg et al., USAEC Report BNL-400 (1962)

(109) D. Drake et al., Phys. Lett. 36B (1971) 557

(110) M. Valkonen and J. Kantele, Nucl. Inst. and Meth. 103 (1972) 549

(111) K. Ponnert et al., Physica Scripta 10 (1974) 35

(112) H.J. Price, "Graphical Analysis of Theoretical Neutron Flux Produced by Fast-Neutron Generators", Kaman Nuclear Corporation, Colorado Springs, Colorado (1964)

(113) S. Vass et al., Nucl. Inst. and Meth. 130 (1975) 271

(114) O.U. Anders and D.W. Briden, Anal. Chem. 3 (1964) 287

(115) J.R. Vogt and W.D. Ehman, Radiochem. Acta 4 (1965) 24

(116) V.P. Guinn and C.D. Wagner, Anal. Chem. 32 (1960) 317

(117) W.E. Mott and J.M. Orange, Anal. Chem. 37 (1965) 1338

(118) D.G. Wood et al., Conf. Anal. Chem. and Appl. Spec., Feb. (1966)

(119) S.S. Nargolwalla et al., Anal. Chem. 40 (1968) 666

(120) S.S. Nargolwalla et al., Anal. Chim. Acta, 49 (1970) 425

(121) F. Adams et al., "Instrumental and Radiochemical Activation Analysis", Monotopic Series, Butterworth, London (1971)

(122) R. Gijbels et al., Anal. Chim. Acta. 43 (1968) 183

(123) R. Gijbels et al., Proc. Int. Conf. Modern Trends in Activation Analysis, NBS Special Publication 312 (1969)

(124) R. Gijbels et al, The Industrialization of 14 MeV Neutron Activation Analysis of Oxygen in Steel, EUR-4297, Luxemburg (1969)

(125) P. Venugopala Rao and R.W. Fink, Phys. Rev. 154 (1967) 1023

(126) A.J. Cox and R.A. Jarjis, Int. J. Appl. Radiat. Isotopes 23 (1972) 301

(127) C.C. Grosjean and W. Bossert, Computing Laboratory, Ghent University, Belgium, 1965

(128) C.M. Lederer et al, Table of Isotopes, 6th Ed. (1967)

(129) Z.T. Body and T. Csikai, Atomic Energy Rev., 11 (1973) 153

(130) E.B. Paul and R.L. Clarke, Can. J. Phys. 31 (1953) 267

(131) L.A. Rayburn, Phys. Rev., 122 (1961) 168

(132) J.M. Ferguson and W.E. Thompson, Phys. Rev., 118 (1960) 228

(133) S. Yasumi, J. Phys. Soc. Japan, 12 (1957) 443

(134) L.A. Rayburn, Phys. Rev., 130 (1963) 731

(135) B. Grimeland et al., Phys. Rev. 137 (1965) B8878

(136) P. Cuzzocrea et al, Nuovo Cimento, 54B (1968) 53

(137) A. Pasquarelli, Nucl. Phys., A185 (1972) 614

(138) S.M. Qaim, Nucl. Phys., A185 (1972) 614

(139) D. Crumpton et al., J. Inorg. Nucl. Chem., 31 (1969) 1

(140) H. Kiskien, A. Paulsen, J. Nucl. Energy, A/B19(1965)73

(141) R.N. Glover and E. Weigold, Nucl. Phys. 29 (1962) 309

(142) C.S. Khurana and H.S. Hans, Proc. 4th Symp. on Low Energy Nuclear Physics, Bombay 1960

(143) F.L. Hassler and R.A. Peck, Jr., Phys. Rev. 125 (1962) 1011

(144) B. Mitra and A.M. Ghose, Nucl. Phys. 83 (1966) 157

(145) J. Kantele and D.G. Gardner, Nucl. Phys. 35 (1962) 354

(146) G.S. Mani et al, Nucl. Phys. 19 (1960) 535

(147) N. Ranakumar et al, Nucl. Phys. A122 (1968) 679

(148) H. Kaji et al, The Science Reports of the Tohoku University 58 (1975) 54

(149) G. Eder et al, Z. Physik 253 (1972) 335

(150) B.D. Kern et al, Nucl. Phys. 10 (1959) 226

(151) D. Crumpton, J. Inorg. Nucl. Chem. 31 (1969) 157

(152) J.M. Jeronymo et al, Nucl. Phys. 47 (1963) 157

(153) J.C. Robertson et al, J. Nucl. Energy 27 (1973) 531

(154) D.L. Allan, Nucl. Phys. 24 (1961) 274

(155) W. Schantle, Thesis, Vienna University, (1970)

(156) M. Bormann et al, Z. Phys. 174 (1963) 1

(157) E. Weigold and R.N. Glover, Nucl. Phys. 32 (1962) 106

(186) L. Rosen and A. Armstrong, Bull. Am. Phys. Soc. 1 (1956) 224

(187) R.S. Storey et al, Proc. Phys. Soc. A75 (1960) 526

(188) E.T. Bramlitt and R.W. Fink, Phys. Rev. 131 (1963) 2649

(189) S.G. Forbes, Phys. Rev. 88 (1952) 1309

(190) H. Liskien, Nucl. Phys., A118 (1968) 379

(191) B.P. Bayhurst et al, Phys. Rev. C12 (1975) 451

(192) S.M. Qaim et al, Proc. Int. Conf. on Chemical Nuclear Data; Measurements and Applications, Canterbury, 1971, p.12

(193) S.M. Qaim, Proc. Int. Conf. Nuclear Structure Study with Neutrons, Budapest 1972

(194) S.M. Qaim and G. Stocklin, J. Inorg. Nucl. Chem. 35 (1973) 19

(195) S.M. Qaim and G. Stocklin, Nucl. Phys. A257 (1976) 233.

ACKNOWLEDGEMENTS

I would like to thank my supervisor, Professor S.E. Hunt for his enthusiasm and guidance over the last five years, which made my research in neutron physics a memorable experience. His support over the past two years whilst I was working at Manchester University, and his valuable suggestions about the manuscript of this thesis are very much appreciated.

Among the other people I would like to acknowledge, are the department's secretary Mrs. I. Neal for her friendship and assistance, Mr. Biggs and Mr. Phull for their technical help in the nuclear physics laboratory, and the staff of the physics department's workshop for making the sample holder and target assemblies.

I would like also to thank my colleagues at Manchester University for their understanding, Mr. K. Conway for his assistance in the computer data fitting program and Miss E. Rich for the efficient typing of this thesis.

Finally, I would like to express my gratitude to my family abroad for their moral support, and my girlfriend Angela for her patience and understanding.

APPENDIX 1

```
C                    (( N E U T R E D ))
C
C
C       ( PROGRAM FOR STUDYING THE D-T NEUTRON BEAM CHARACTERISTICS )
C
    ( 0.7 MEV DEUTRONS ON A THICK TRITIATED TITANIUM TARGET OF T/TI=1.2 )
      INTEGER ELSTI, ELST, NNCL, NNN, LC, NNLL
      REAL DTCRS, DEL, EN, RN, EMAX, EMIN, EMEAN, EDMAX, EDMIN, DR, AND
      DIMENSION DTCRS(224),AND(200),ELSTI(34),ELST(34),NNCL(34),LLCL(20)
     1,NNN(34,20),EMAX(20),EMIN(20),EMEAN(20),EDMAX(20),EDMIN(20),ANISO(
     234,20),EN(34,20),TNE(20),TRN(20),DD(34),GAM(34),LLL(34,20),DEL(34)
     3,PARTNE(34,20),LC(400),NNLL(20,20),RTRN(20,20),RN(34,20),DR(24)
C
C
      READ(1,2)(DR(M),M=1,24)
    2 FORMAT(12(1X,F5.1))
C
      READ(1,3)(AND(M),M=1,200)
    3 FORMAT(6X,10(1X,F5.1))
C
      READ(1,4)(ELSTI(M),M=1,34)
    4 FORMAT(18(1X,I3))
C
      READ(1,6)(ELST(M),M=1,34)
    6 FORMAT(14(1X,I4))
C
C
      A = 3.1417/180
      I = -10
      DO 600 L = 1, 20
      B = 0.0
      C = 0.0
      IF (L - 20) 8, 7, 8
    7 I = 98
      GO TO 9
    8 I = I + 10
    9 KL = 11
      KK = 50
      KN = 1.0
      KP = 1.0
      M = 0
      ATNE = 0.0
      ATRN = 0.0
      N = 0
      DO 500 J=10,700,5
>
```

```
100 IF(J-200) 101,101,106
101 IF(J-55) 160,102,102
102 F = J/KL
103 IF(F-5) 160,104,160
104 KL = KL+2
105 GO TO 500
106 IF(J-205) 101,107,107
107 H = J/KK
108 IF(H-5) 111,109,111
109 KK = KK+10
110 GO TO 160
111 GO TO 500
160 N = N+1
    M = M+1
    IF (I-0) 25, 18, 25
 18 NNCL(N) = J
    DEL(N) = 48*ELSTI(M)/(48+3*1.2)+3*1.2*ELST(M)/(48+3*1.2)
    DD(N) = (4.00260361*(2.01410219+3.01602994)/(1.00866544*2.0141021
   19))*(3.01602994/(2.01410219+3.01602994)+(17578.5/J))
    GAM(N) = SQRT(1/DD(N))
 25 EN(N,L) = 0.001*(0.080307*J*COS(2*I*A)+0.798676*(0.599615*J+17578
   15)+0.795126*COS(I*A)*(SQRT(0.405783*J*(0.599615*J+17578.5)*(1-0.10
   20925*J*(SIN(I*A))**2/(0.599615*J+17578.5))))
    ANISO(N,L) = GAM(N)*(COS(I*A)+SQRT(DD(N)-(SIN(I*A))**2))**2/SQRT(D
   1D(N)-(SIN(I*A))**2)
    IF(J-200) 27,27,30
 27 DTCRS(M) = DR(KN)
    KN = KN+1
    GO TO 32
 30 DTCRS(M) = AND(KP)
    KP = KP+1
 32 RN(N,L) = ANISO(N,L)*DTCRS(M)/DEL(N)
    PARTNE(N,L) = RN(N,L)*EN(N,L)
    TNE(L) = ATNE+PARTNE(N,L)
    ATNE = TNE(L)
    TRN(L) = ATRN+RN(N,L)
    ATRN = TRN(L)
    LLL(N,L) = I
    NNN(N,L) = J
    IF (PARTNE(N,L)-C) 50, 41, 37
 37 EMAX(L) = EN(N,L)
    IF (N-1) 40, 40, 41
 40 B = PARTNE(N,L)
 41 C = PARTNE(N,L)
 50 IF (PARTNE(N,L)-B) 52, 52, 500
 52 EMIN(L) = EN(N,L)
    B = PARTNE(N,L)
500 CONTINUE
    EMEAN(L) = TNE(L)/TRN(L)
    EDMAX(L) = EMAX(L)-EMEAN(L)
    EDMIN(L) = EMIN(L)-EMEAN(L)
    LLCL(L) = I
    M = L
    IF (M-20) 60,65,65
>
```

```
   60 LC(M) = LLCL(L)
      GO TO 600
   65 DO 570 M=20,400
      LC(M) = LC(M-19)
  570 CONTINUE
  600 CONTINUE
      DO 900 KL=1,20
      DO 850 K=1,20
      NNLL(K,KL) = LLCL(KL)
      RTRN(K,KL) = TRN(K)/TRN(KL)
  850 CONTINUE
  900 CONTINUE
C
C
      WRITE(2,605)(NNCL(N), DEL(N),N=1,34)
  605 FORMAT(1H1,///,9X,105H300KEV  DEUTERON  BEAM  ENERGY  LOSS  IN  TI
     1TANIUM  TRITIATED  TARGET  OF  TRITIUM  ATOMIC  RATIO  =  1.2,////
     2/,17H(D ENERGY IN KEV),///,5(4X,4HDEL(,I3,3H)= ,F8.3))
C
      WRITE(2,609)((NNN(N,L), LLL(N,L), ANISO(N,L),N=1,34),L=1,20)
  609 FORMAT(1H1,///,50X,20HNEUTRON   ANISOTROPY,////,35H(D ENERGY IN KE
     1V , ANGLE IN DEGREE),///,4(5X,6HANISO(,I3,1H,,I3,2H)=,F8.4))
C
      WRITE(2,612)((NNN(N,L),LLL(N,L),EN(N,L),N=1,34),L=1,20)
  612 FORMAT(1H1,///,15X,90HENERGY  OF  NEUTRONS  AS  A  FUNCTION  OF EM
     1ISSION  ANGLE  AND  INCIDENT  DEUTERON  ENERGY,////,35H(D ENERGY I
     2N KEV , ANGLE IN DEGREE),///,4(5X,3HEN(,I3,1H,,I3,2H)=,F8.4))
C
      WRITE(2,650)((NNN(N,L),LLL(N,L),EN(N,L),RN(N,L),N=1,34),L=1,20)
  650 FORMAT(1H1,///,26X,67HENERGY  DISTRIBUTION  OF  THE  NEUTRONS  AT
     1 DIFFERENT  LAB  ANGLES,////,35H(D ENERGY IN KEV , ANGLE IN DEGREE
     2),///,2(10X,1H(,I3,1H,,I3,1H),5X,6HEN =  ,F8.4,5X,6HRN =  ,F8.4),
     3//)
C
      WRITE(2,700)(LLCL(L),EMAX(L),EMIN(L),EMEAN(L),EDMAX(L),EDMIN(L),L=
     11,20)
  700 FORMAT(1H1,///,25X,70HMEAN  NEUTRON  ENERGY  AND  ENERGY  SPREAD
     1AT  DIFFERENT  LAB  ANGLES,/////,21X,11HMAX. ENERGY,5X,11HMIN. ENE
     2RGY,15X,11HMEAN ENERGY,5X,11HENERGY DIV.,5X,11HENERGY DIV.,4X,5H(M
     3EV),///,(5X,8HANGLE = ,I3,2(7X,F9.4),10X,3(7X,F9.4),//))
C
      WRITE(2,800)(LLCL(L), TRN(L), L=1,20)
  800 FORMAT(1H1,///,30X,47HFAST  NEUTRON  FLUX  AT  DIFFERENT  LAB  ANG
     1LES,////,2(20X,8HANGLE = ,I3,7X,7HFLUX = ,F8.4),//)
C
      WRITE(2,999)(((LC(M),NNLL(K,L),RTRN(K,L),K=1,20),L=1,20),M=1,400)
  999 FORMAT(1H1,///,87HANGULAR  VARIATION  OF  NEUTRON  FLUX  RELATIVE
     1 TO  THE  FLUXES  AT  REFERENCE  ANGLES,////,40X,34H( ACTUAL ANGLE
     2 ,REFERENCE ANGLE ),///,2(3X,2H( ,I3,3H , ,I3,6H )    ,16HRELATIVE
     3 FLUX = ,F7.3,12X),//)
C
      STOP
      END
>
```

International Journal of Applied Radiation and Isotopes, 1975, Vol. 26, pp. 57–60. Pergamon Press. Printed in Northern Ireland

A Concentric Ring Technique for the Measurement of Fast Neutron Fluxes and Energies

R. A. JARJIS and S. E. HUNT

Department of Physics, The University of Aston in Birmingham, Birmingham B47 ET, England

(*Received* 1 *May* 1974)

The limitations imposed by fixed foil, mixed powder and sandwich foil techniques for fast neutron flux measurement led the authors previously to suggest a concentric ring monitoring technique. This technique can be extended to measure neutron energies if excitation functions of the two materials are known.

The method is verified by using concentric copper monitoring rings with aluminium discs. The ratios of activities of copper and aluminium enable the neutron energy to be measured to $\pm 1{\cdot}2$ per cent.

The advantages and applications of the technique are discussed and a modified design is suggested for very short target to specimen separation.

An antimony disc with concentric copper and aluminium rings was used to measure the $^{121}Sb(n, 2n)^{120g}Sb$ excitation function, the copper and aluminium rings being used to measure both fast neutron flux and energy. It is suggested that the $^{121}Sb(n, 2n)^{120g}Sb$ reaction would be very useful as a standard for flux monitoring in the 14 MeV region since its excitation function is relatively flat between 13·5 and 15 MeV.

INTRODUCTION

Low energy particle accelerators are being used extensively in pure and applied nuclear science for the production of neutrons using the $^{3}T(d, n)^{4}He$ reaction. The fast neutrons so produced have variable energies and fluxes due to such factors as the variations in sample to target geometry, neutron scatter and absorption, non uniform loading of tritium in the target,[1] build up of deuterium and depletion of tritium in the target;[2] so it is very important to have a simple and accurate technique for the measurement of these two variable parameters at any specific point and time.

Fast neutron fluxes are usually estimated by using a single separate monitor foil, sandwich foils or the mixed powder technique, but each of these has disadvantages. The single foil cannot monitor the flux precisely at the specimen position, the sandwich technique may involve a large self absorption correction and errors introduced by the non uniform mixing of powders can be appreciable. These problems have been considered in more detail by the authors in a previous paper[3] in which a suggestion has been made for the use of a concentric ring technique. The monitor ring subtends a slightly larger angle on the target than the sample, but the increased spread in neutron energies is usually negligible; there is no "shielding effect" as in the sandwich technique, and by comparison with the mixed powders technique the monitoring ring and sample can easily be separated for subsequent counting.

In a previous communication by Cox and Jarjis[4] the use of a mixed powder sample to measure neutron energies was proposed. Use was made of the different excitation functions of the two materials for neutrons in the 14 MeV region and the ratio of activities was used to measure neutron energies to an accuracy of about .2·1 per cent. The use of the concentric ring configuration appreciably extends the

* Present address; van de Graaff Laboratory, the University, Manchester M13 9PL, England.

application of this technique. By activating two concentric rings of selected materials either alone or surrounding a disc of the sample under investigation it is possible to measure fast neutron flux and energy simultaneously.

EXPERIMENTAL PROCEDURE

Fast neutrons were produced by the D–T reaction on tritiated titanium target by its bombardment with an 0·3 MeV deuteron beam from a Van de Graaff accelerator. The target assembly was fitted with a thin flexible sample holder made of aluminium, and the specimens were subjected to neutrons of varying mean energy by altering the angular position with respect to the incident deuteron beam.[5]

The first set of experiments was on copper and aluminium which undergo the reactions ^{62}Cu(n, 2n)^{63}Cu and ^{27}Al(n, p)^{27}Mg, the products of which have half-lives of 9·8 and 9·4 min respectively. Samples were in the form of circular aluminium disc surrounded by a thin ring of copper. The samples were irradiated with different mean energy neutrons and at large and equal distance from the D–T neutron source, and the induced activities were measured for a range of mean neutron energies from 13·3 to 15 MeV.

In order to measure the ^{121}Sb(n, 2n)^{120g}Sb excitation cross section a method of measuring neutron energy and flux simultaneously was established by using a configuration of concentric rings of copper and aluminium surrounding a circular disc of pure antimony.

A 3-in. × 3-in. NaI(Tl) detector coupled to a multichannel analyser was used to measure the induced activities. The cross sections were calculated from the measurements on the 0·511 MeV annihilation radiations from ^{62}Cu and ^{120g}Sb and the 0·842 MeV gammas from ^{27}Mg.

RESULTS AND DISCUSSION

The excitation functions of ^{63}Cu(n, 2n)^{62}Cu and ^{27}Al(n, p)^{27}Mg reactions have been measured previously by a number of workers including the authors.[3] Our previous measurements indicated that the copper cross section increases approximately linearly with neutron energy with a slope of 28 per cent MeV^{-1} in the 14 MeV region, whilst the aluminium cross

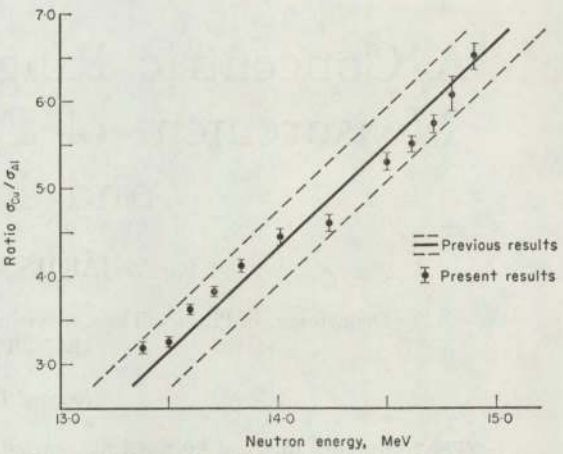

FIG. 1. The ratio of cross sections as a function of neutron energy.

section decreases with a slope of −9 per cent MeV^{-1} in this region. The ratio of these results has been plotted as a solid line in Fig. 1, the experimental uncertainties being indicated by the dotted lines. In the present work the concentric ring technique was used to establish the cross section ratios at specific energies and these are shown in the form of points in Fig. 1. The uncertainties associated with the present measurements are less due to the effective elimination of common systematic errors and they reveal a slight non linearity in the activation ratios, although there is good general agreement between the two sets of results. The accuracy of the neutron energy measurement has been improved to ±1·2 per cent by the concentric ring technique.

The neutron fluxes for the calculation of the ^{121}Sb(n, 2n)^{120g}Sb excitation curve were estimated from the activity of the copper ring, using our previously measured copper excitation curve and the recommended value of ^{63}Cu(n, 2n)^{62}Cu reaction cross section of 558 mb at 14·7 MeV proposed by BÖDY and CSIKAI,[6] this is somewhat lower than the absolute value obtained in this laboratory.[7] Neutron energies were calculated from the observed activity ratios on the copper and aluminium rings using the cross sections ratio results from Fig. 1.

The ^{121}Sb(n, 2n)^{120g}Sb cross section has been measured by few researchers,[8–12] from these only RAYBURN[8] and KANDA[9] have measured

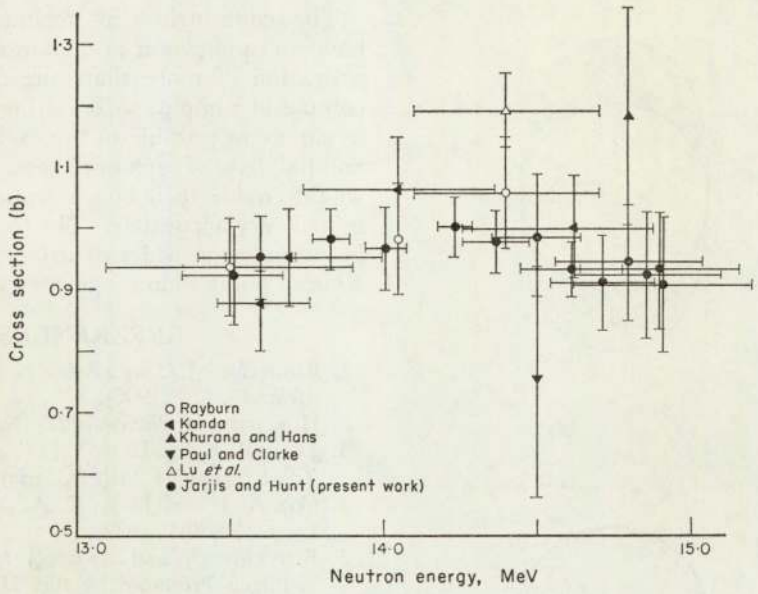

FIG. 2. $^{121}Sb(n, 2n)^{120g}Sb$ excitation function.

its variation with neutron energy. Our results are shown in Fig. 2 together with the former data and a good agreement can be noticed in the energy range which we have covered. In general the experimental uncertainties associated with the present work are less than those of previous work.

Antimony is suggested as a very suitable flux monitor for 14 MeV neutrons when used to produce activities with half lives in the 10–30 min region has the advantage of having a relatively high cross section, its radioactive product has a reasonable half life of 15·9 min and its smooth and almost flat excitation function make it suitable for many (n, p) and (n, 2n) reactions which have a similar type of excitation function.

The errors introduced by using concentric ring monitors for large target to specimen separations are small but for small target to specimen separation the increased spread in neutron energies experienced by a uniform ring becomes noticeable as shown in Fig. 3, in this case the areas A and B of the ring are exposed to wider ranges of neutron energies than the rest of the ring and the circular disc. For example if we consider a concentric sample consisting of a 3 cm diameter disc surrounded by a 1-cm thick ring, for a separation of 2 cm from the neutron source a specimen in the forward direction would be exposed to a range of neutron energies from 14·74 to 14·91 MeV, and the monitoring ring to a range from 14·60 to 14·91 MeV and at 90° the corresponding energies will be 13·67–14·56 MeV for the specimen and 13·50–14·73

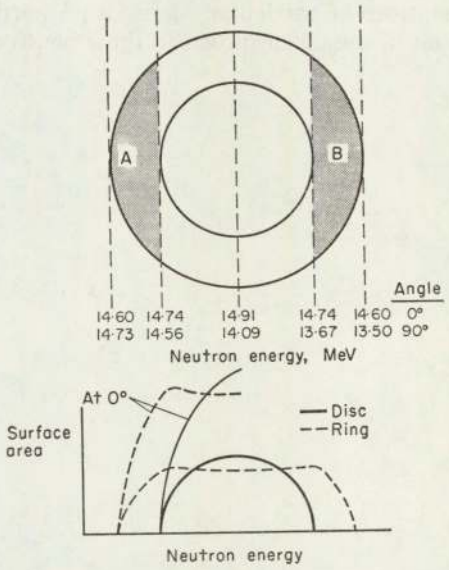

FIG. 3. The concentric ring/disc sample at a short separation from the target.

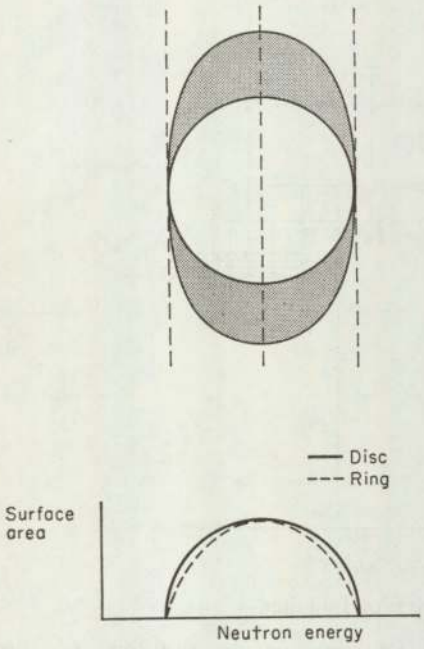

FIG. 4. The modified concentric ring.

MeV for the ring. The effect will be small for smooth excitation function and can be minimized by using a specially designed ring as shown in Fig. 4 such that the area of the ring exposed to neutrons of particular energy is proportional to that of the disc exposed to these neutrons.

The concentric ring technique could also have an application in measurements involving activation of more than one constituent in a composite sample. Monitoring rings matched as closely as possible to the excitation functions and half lives of each of the constituent elements would enable their concentrations to be determined very accurately. The technique can also be extended to wider neutron energy ranges in which "point source" geometry is used.

REFERENCES

1. ROBERTSON J. C. and ZIEBA K. J. *Nuclear Instrum. Meth.* **45,** 179 (1966).
2. HOLLISTER H. *Nucleonics* **22,** (No 6), 68 (1964).
3. JARJIS R. A. and HUNT S. E. *Proc. Int. Conf. Modern Trends Activation Analysis, Saclay, France* (1972).
4. COX A. J. and JARJIS R. A. *Int. J. appl. Radiat. Isotopes* **23,** 301 (1972).
5. BENVENISTE J. and ZENGER J. Information on the Neutrons Produced by the $^{3}H(d, n)$ ^{4}He Reaction. UCRL-4266 (1954).
6. BÖDY Z. T. and CSIKAI T. *Atomic Energy Rev.* **11,** 153 (1973).
7. CRUMPTON D. *et al. J. inorg. nucl. Chem.* **31,** 1 (1968).
8. RAYBURN L. A. *Phys. Rev.* **130,** 731 (1963).
9. KANDA Y. *J. Phys. Soc. Japan* **24,** 17 (1968).
10. KHURANA C. S. and HANS H. S. *Nucl. Phys.* **28,** 560 (1961).
11. PAUL E. B. and CLARKE R. L. *Can. J. Phys.* **31,** 267 (1953).
12. LU W. *et al. Phys. Rev.* **C1,** 350 (1970).

Journal of Radioanalytical Chemistry, Vol. 16 (1973) 611–616

AN IMPROVED NEUTRON MONITOR GEOMETRY FOR NEUTRON ACTIVATION

R. A. JARJIS, S. E. HUNT

Physics Department, University of Aston in Birmingham (England)

Introduction

A large amount of data on neutron capture cross sections and their variations with neutron energy around 14 MeV has been published during the last twenty years. The measured data are important in testing the relevant nuclear theories; and more practically in measuring neutron fluxes,[1] and in special cases neutron energies.[2] These are of great importance in the field of neutron activation analysis.

The precision of neutron activation analysis and neutron excitation function measurements depends on the accuracy of neutron flux measurements which are usually made in terms of the induced activity on standard materials, and the standards themselves can be a source of discrepancy between published data.

Errors can be introduced due to non uniform distribution of tritium in the target and the change in charged particle beam conditions which cause the neutron flux to vary in a different manner at the sample and monitor particularly if these subtend different angles to the beam.[3] In order to reduce the errors due to these factors sandwich and mixed powder methods are commonly employed. If sample and monitor are placed at different distances from the target either one behind the other or in a sandwich configuration, a correction has to be made due to the variation in flux with distance from the source[4] and this can be considerable for short sample to source distances. A correction must also be made for the flux attenuation due to absorption.

In order to reduce these errors the mixed powder technique was produced by Venugopala Rao and Fink.[5] Powders of two different materials were mixed with the powder under investigation. The powders should all have the same grain size but even so the problem of incomplete mixing and consequent difference in self absorption are difficult to eliminate. The gamma spectra for three nuclei may also be difficult to analyse. An additional improvement in the field can be made by employing a method which satisfies the conditions that sample and monitor:

(1) Are at the same distance from the neutron source but have distict boundaries between them.

(2) Are exposed to neutrons with approximately the same average energy to eliminate the errors due to the different excitation functions of monitor and sample.
(3) Can be transferred to the counting equipment so that their activites can be measured simultaneously.
(4) Have equal thickness to avoid the necessity of introducing inverse square law flux corrections.

These conditions appear to be satisfied by using a sample in the form of a disc and surrounding it by a concentric ring of the flux monitoring material.

Experimental

A Van de Graaff accelerator was used to accelerate deuterons up to an energy of 0.3 MeV. The deuteron beam was allowed to strike a tritiated titanium target, and neutrons were produced by the D — T reaction. Neutrons with different energies could be obtained by varying the angular position with respect to the deuteron beam. We have used a computer programme "NEUTRED" to provide the information concerning the neutron production by taking into account the energy loss of the deuteron beam in the target. We found that the average neutron energy varies from 13.43 MeV at 150° to 14.97 MeV at 0° with a value of 13.98 MeV at 98°. Uniform distribution of tritium throughout the target thickness was assumed.

Our sample holder was made of aluminium, and consists of a thin arc supported by three thin rigid arms at 0°, 98° and 150°; there is also a moveable arm which could be rotated through an angle of 180°, or removed if necessary, to reduce neutron scatter. This set up allows the samples to be positioned at angular interval of 5° throughout the range of 0° to 180° with respect to the incident beam. The target to specimen distance could be varied from 5 cms to 25 cms in 1 cm steps.

To count the induced gamma activities of the irradiated samples a 3" x 3" NaI(Tl) detector coupled to 400 channel RIDL multichannel analyzer were used. Crystal efficiencies were estimated from the results of Grosjean and Bossaert.[6] Each of the results obtained is based on three or more independent measurements.

Results

Excitation curve of copper standard

The excitation curve for $^{63}Cu(n, 2n)^{62}Cu$ reaction was first measured in the usual manner by counting the induced activity at each angle with respect to that at 30°. The measurements were made by counting the annihilation (0.511 MeV) gammas produced by the positron in an aluminium cover of adequate thickness. The reference cross-section value at 30° (14.8 MeV) of 558 mb[7] was used and the results are shown in Fig. 1.

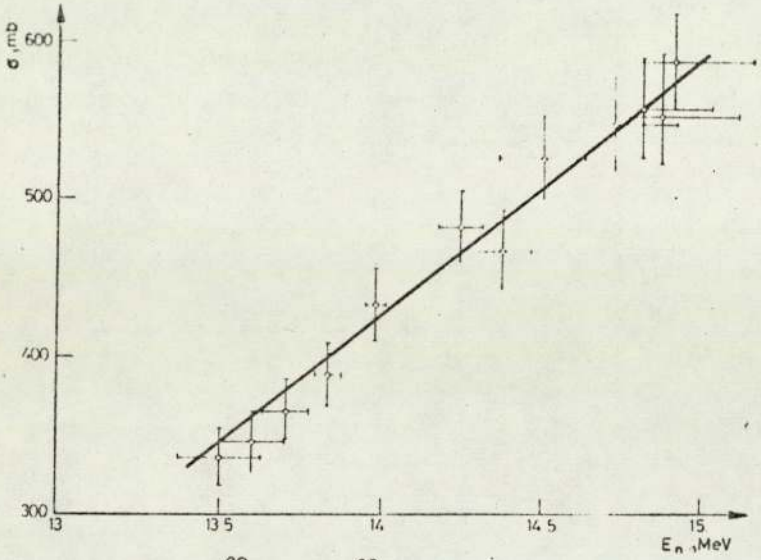

Fig. 1. $^{63}Cu(n, 2n)^{62}Cu$ excitation function

Measurement of excitation function of aluminium

^{27}Mg (T = 9. 5 m) is a beta active, it decays to various levels in ^{27}Al, a 70% of the decay leads to the 0. 842 MeV level and the rest to the 1. 015 MeV level. Measurements were made on the 0. 842 MeV γ-ray.

Samples were designed in the form of circular aluminium disc surrounded by a very thin ring of copper which was used as the monitor. The geometry was such that the additional angle subtended by the copper ring was very small and consequently the sample and monitor were exposed to neutrons of the same mean energy. These concentric samples were irradiated together, and for checking purposes a single copper sample was also exposed at the same distance from the target and at an angle of 30° to the beam direction. It was therefore exposed to neutrons of mean energy 14. 8 MeV.

The induced gamma activities in the irradiated concentric samples of aluminium and copper were counted simultaneously and a typical gammaspectrum is shown in Fig. 2.

The determination of the $^{27}Al(n, p)^{27}Mg$ excitation function was related to the measured copper excitation function Fig. 1, and the results are shown in Fig. 3. A further check was carried out by measuring the aluminium (n, p) excitation function relative to the 558 mb value of $^{63}Cu(n, 2n)^{62}Cu$ at 14. 8 MeV by using separate single aluminium and copper samples. The results showed a similar behaviour to Fig. 3, but with higher standard deviation.

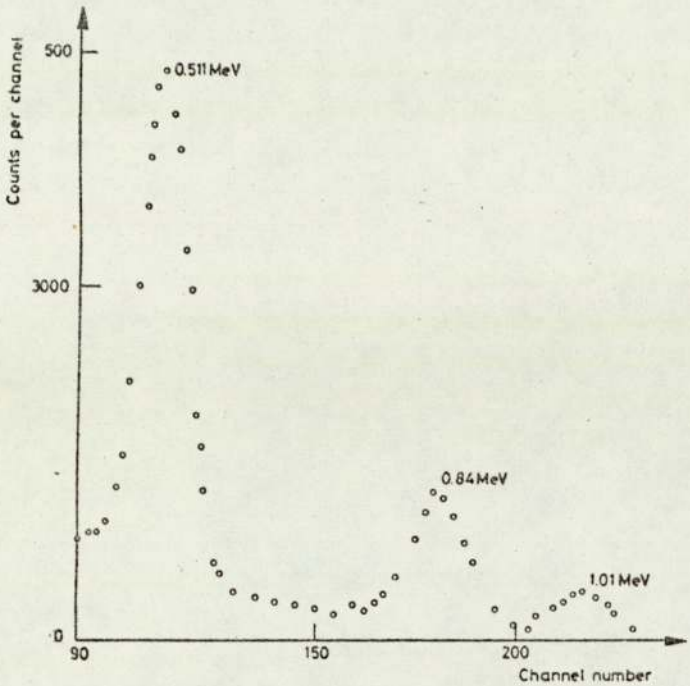

Fig. 2. Gamma-ray spectrum from the aluminium/copper sample

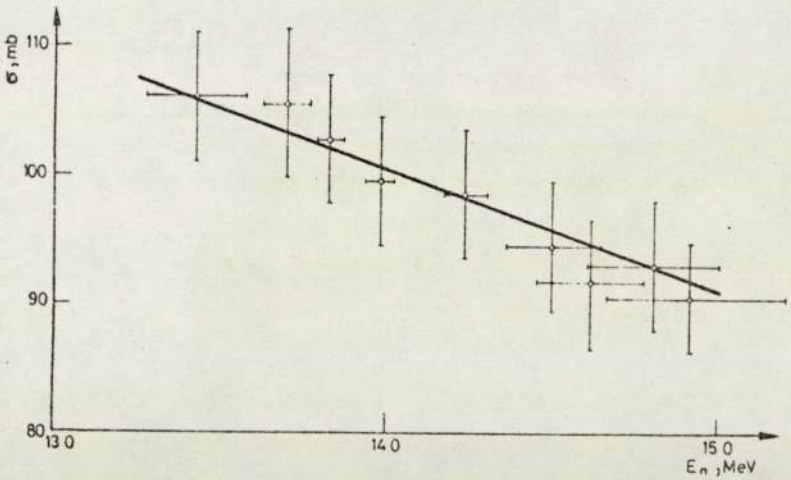

Fig. 3. $^{27}Al(n, p)^{27}Mg$ excitation function

Discussion

$^{63}Cu(n, 2n)^{62}Cu$ absolute cross-section and its variation with neutron energy have been measured by several workers.[7-16] The measured values vary from 422[8] to 469[9] mb at about 14 MeV. Between 14.7 and 14.77 MeV the published results are 577,[10] 593,[11] 507[12] and 550[13] mb, and at 14.8 MeV are 615[14] and 558[7] mb. The cross-section in the 14 MeV range increases with neutron energy and the approximate gradients of the published excitation functions vary between 25% and 26% MeV^{-1}. Our excitation function showed a slightly higher slope of 28%.

A large spread of $^{27}Al(n, p)^{27}Mg$ cross-section values at specific energies and its variation with energy can be noted from the previously published results.[17-23] Between 14 and 14.5 MeV[17-19] the cross-section values varied between 115[17] to 87[19] mb. At 14.8 MeV[20-22] the variation was between 71[20] and 97[21] mb.

Partington et al.[15] studied the variation of cross-section with neutron energy in the range 13.5–15.0 MeV and their results show a small approximate decrease in the cross-section of 3% MeV^{-1}.

Previously Cuzzocrea and Perillo[9] studied this variation in the region 13.7-14.6 MeV, their excitation function showed a larger negative slope of 12% MeV^{-1} at 14.0 MeV. Our excitation function shows a negative slope of 9% at 14.5 MeV in tne range 13.4–14.9 MeV. This value of the slope is in between the previously published results. The magnitude of the $^{27}Al(n, p)^{27}Mg$ cross-section fell from 106 millibarns to 92 millibarns in the energy range, relative to a value of 558 millibarns for the $^{63}Cu(n, 2n)^{62}Cu$ reaction at 14.8 MeV.

The smaller spread in the experimental points which was obtained using the concentric aluminium disc and copper monitoring ring indicates that random errors due to beam shift etc. were reduced.

This method of monitoring appears to have potential application in the field of fast neutron irradiation.

References

1. D. Crumpton et. al., Nucl. Instr. Methods, 92 (1971) 533.
2. A.J. Cox, R.A. Jarjis, Intern. J. Appl. Radiation Isotopes, 23 (1972) 301.
3. W.E. Mott, J.M. Orange, Proc. Intern. Conf. Modern Trends in Activation Analysis, Texas A and M University, College Station, 1965, p. 115.
4. H. F. Priest et al., Nucl. Instr. Methods, 50 (1967) 141.
5. P. Venugopala Rao, R.W. Fink, Phys. Rev., 154 (1967) 1023.
6. C.C. Grosjean, W. Bossaert, Computing Laboratory, Publication in the University Ghent, Belgium, 1965.
7. B. Grimeland et. al., Phys. Rev., 137 (1965) B8878.
8. L.A. Rayburn, Phys. Rev., 130 (1963) 731.
9. P. Cuzzocrea, E. Perillo, Nuovo Cimento, 54B (1968) 53.

10. A. Pasquarelli, Nucl. Phys., A93 (1967) 218.
11. S. M. Qain, Nucl. Phys., A185 (1972) 614.
12. J. M. Ferguson, E. Weigold, Nucl. Phys., 29 (1962) 309.
13. R. N. Glover, E. Weigold, Nucl. Phys., 29 (1962) 309.
14. D. Partington et. al., J. Inorg. Nucl. Chem., 31 (1969) 1.
15. D. Partington et. al., Analyst, 95 (1970) 257.
16. H. Liskien, A. Paulsen, J. Nucl. Energy, A/B 19 (1965) 73.
17. C. S. Kurana, H. S. Hans, Proc. 4th Symp. on Low Energy Nuclear Physics, Bombay, 1960.
18. F. L. Hassler, R. A. Reck, Jr., Phys. Rev., 167 (1968) 1091.
19. J. Kantele, D. G. Gardner, Nucl. Phys., 35 (1962) 354.
20. P. N. Tiwari, E. Kondiah, Phys. Rev., 167 (1968) 1091.
21. S. K. Mukherjjee et. al., Proc. Phys. Soc. (London), 77 (1967) 508.
22. L. Husain et. al., Phys. Rev., 1 (1970) No. 4, 1233.
23. B. Mitra, A. M. Ghose, Nucl. Phys., 83 (1966) 157.

MEASUREMENTS AND APPLICATIONS OF THE EXCITATION FUNCTIONS FOR FAST NEUTRON INDUCED REACTIONS

BY

RAIK A. JARJIS

A thesis submitted to the
University of Aston in Birmingham
for the degree of
Doctor of Philosophy in Physics

December 1976

ABSTRACT

The concentric ring technique has been devised for the measurement of fast neutron fluxes and energies by using different standard materials and their measured excitation functions. It has been shown experimentally that for the determination of flux and energy in the 14 MeV region, this novel technique can yield accuracy values of the order of 1.0% and 1.2% respectively. An experimental cross-section ratio curve for the (n,2n) reaction on ^{63}Cu and the (n,p) reaction on ^{27}Al has been established as a standard reference for fast neutron energy measurement.

The technique has been applied to the measurement of the excitation functions for the following nuclear reactions:-

a) The 12.9 to 15.9 MeV neutron energy region

(1) $^{27}Al(n,p)^{27}Mg$ (2) $^{56}Fe(n,p)^{56}Mn$ (3) $^{59}Co(n,\alpha)^{56}Mn$

(4) $^{64}Zn(n,2n)^{63}Zn$ (5) $^{63}Cu(n,2n)^{62}Cu$ (6) $^{121}Sb(n,2n)^{120g}Sb$

b) The 13.4 to 14.9 MeV neutron energy region

(7) $^{28}Si(n,p)^{28}Al$ (8) $^{27}Al(n,\alpha)^{24}Na$ (9) $^{64}Zn(n,p)^{64}Cu$

(10) $^{65}Cu(n,2n)^{64}Cu$

The cross-section data obtained by using an 0.5 MeV Van de Graaff and 3.0 MeV Dynamitron accelerators are consistent and are in good general agreement with the published data. This investigation includes also detailed studies of fast neutron production by the $T(d,n)^{4}He$ reaction, fast neutron monitoring, activation analysis and cross-section data systematics.

Some of the recommedations proposed include flux monitoring by

the $^{121}Sb(n,2n)^{120g}Sb$ reaction, further possible applications of the concentric ring technique, and a possible system for the standardization of neutron cross-section data.

CONTENTS

I N T R O D U C T I O N

The measurement of fast neutron induced reaction cross-sections and their variations with neutron energy specially around 14 MeV is an important field in nuclear science and technology. The cross section data are applied to nuclear theories to yield information about the relevant nuclear models and nuclear interaction theories, such as in testing the validity of the statistical theory and in determining the contribution of direct interaction mechanism. More practically, the measured data are extensively used in neutron spectroscopy, reactor physics, activation analysis, nuclear medicine, and in the design of D-T plasma type nuclear fusion devices.

In spite of the frequent measurements of the excitation functions for neutron induced reactions, a considerable number of the published results reveal large discrepancies on even the reactions which are used as standards. Discrepancies in the data can be mainly attributed to the undetected sources of systematic errors, inaccuracies in the values of the standard cross-sections, and also in the experimental techniques used to carry out the experiments. Furthermore, the early measurements

with the activation method include also additional errors due to β-counting, and poor gamma resolution when complex spectra are involved.

The limited yield of neutron sources plays an important role in causing the scarcity of the data for reactions of relatively small cross section. Finally, for reactions in which the cross-sections exhibit strong variations with energy, failure to estimate the incident neutron beam energies accurately is a further source of error.

CHAPTER ONE

SYSTEMATIC STUDIES OF FAST NEUTRON CROSS-SECTIONS

The fact that the neutron is electrically neutral and interacts strongly with the nucleus enables us to study nuclear structure with fast neutrons and to investigate with considerable efficiency the excited states of nuclei at energies between 10 and 20 MeV, where the Coulomb barrier complicates the use of charged particles. Several types of neutron reactions are energetically possible in the 14 MeV region and these reactions compete with each other to give variable degrees of relative contributions to the total cross-sections as shown in Fig. (1.1) [1]. Such contributions therefore determine the general shapes of the excitation functions; but more accurately, the threshold energies are determined by the negative Q-values of the various reactions and the yield curves are also controlled by the Coulomb barriers for (n, charged particle) reactions, and the positions of maximum yields are determined by the threshold of the competing reactions.

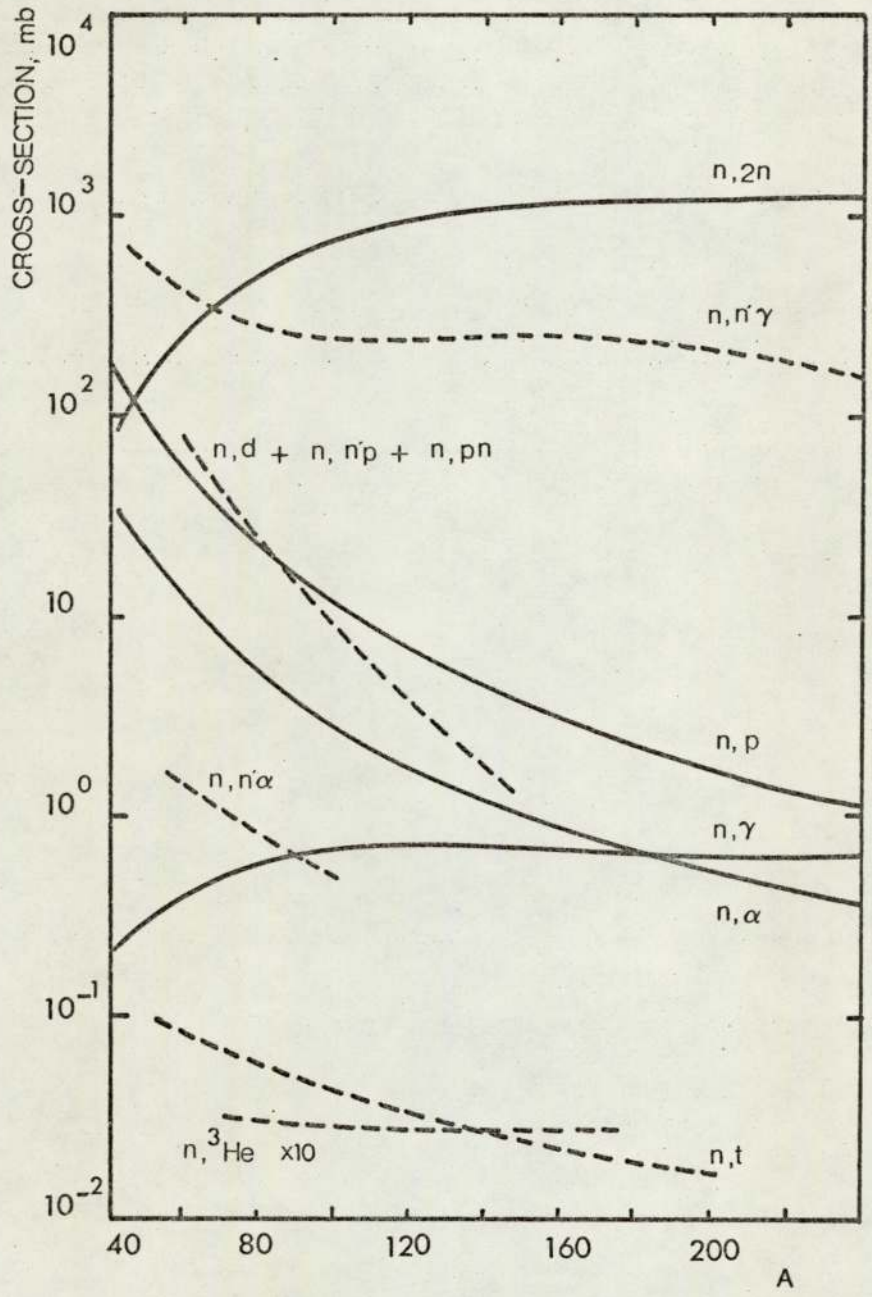

Fig. 1.1

Relative Contributions of Nuclear Reactions Produced by 14 MeV Neutrons on Medium and Heavy Mass Nuclei

1.1 Methods of Neutron Cross-Section Determination

Since the subject of neutron cross-section determination methods is very wide indeed, and its full review is beyond the scope of this thesis, we have therefore settled to only a limited discussion.

1.1.1 Activation and direct detection methods

Neutron cross-section data in the 14 MeV region are most commonly determined by using the activation method which follows the production of radioactive residual nuclei. This method has the advantage that the yields of constituent isotopes of an element can be well separated by gamma spectroscopy. Also, it is possible to irradiate large amounts of material, therefore eliminating most of the difficulties presented by the relatively low neutron cross-sections in the 14 MeV region and the limited incident neutron flux, self absorption corrections are required specially for β-counting. The progress in gamma ray spectroscopy and radiochemical separation methods have increased the reliability of this method even in the determination of rare reaction cross-sections.

The cross-sections values obtained by the activation method represent the integral values which include the sums of differential cross-sections, and the method offers no discrimination between the cross-sections for the formation of daughter nuclei in ground and very short-lived excitation states. Good separation between the induced activities on the basis of the differences in decay rates is possible and it can provide cross-section data for ground and isomeric states.

The other method of cross-section measurement is by the direct on-line detection of the emitted particles, and this method can usually yield information about the differential cross-sections and angular

distributions to study reaction mechanisms. By comparing the theoretical and experimental excitation functions, emitted particles and angular distributions, a sensitive check on the predictions of the statistical model can be made and data for the level densities and compound nucleus formation cross-sections could be obtained. If the angular distribution of the emitted particles is not symmetric about 90^{o} and the observed correlations between the particles can not be explained within the limitations of the statistical theory, direct process effect is usually introduced.

It is clear therefore, that the direct detection method can provide vast amounts of information, but if only the determination of excitation functions is required the activation method without doubt will be the right choice. The limitations presented by the direct detection method which restrict its use for the determination of neutron excitation functions can be explained as follows:

1) The measurements have to be carried out in high background environment due to the interaction of neutrons with the T-target and its backing, detector, and reaction chamber.

2) For the detection of emitted charged particles, the experiments are usually carried out under vacuum on thin targets containing small amounts of the studied materials, and accordingly small count rates are produced which limit the accuracy.

3) For reactions of small cross-sections such as the (n,α) reaction on heavy nuclei, an attempt to increase the count rate by using thicker targets would mean the complete loss of the α-spectrum.

1.1.2 The reciprocity method

The excitation functions of fast neutron induced charged particle reactions can be estimated with reasonable accuracy by using the reciprocity theorem [2] which employs the excitation functions of neutron emitting reactions. According to the theorem, the cross-section $\sigma(a,b)$ for the reaction A(a,b)B can be expressed in terms of the cross-section $\sigma(b,a)$ for the B(b,a)A reaction according to the relationship [3].

$$\frac{\sigma(a,b)(2I_A+1)(2I_a+1)}{\lambda\!\!\!^{-2}_a} = \frac{\sigma(b,a)(2I_B+1)(2I_b+1)}{\lambda\!\!\!^{-2}_b}$$

where I_A, I_B, I_a, I_b = spins of nuclei A, B, a, b and $\lambda\!\!\!^{-}_a$, $\lambda\!\!\!^{-}_b$ = $1/2\pi$ x the De Broglie wave length of the particle a, b in the centre-of-mass system.

The excitation functions for neutron producing reactions are usually known precisely due to the high resolution of the incident charged particle beams which are mainly obtained by using ripple free Van de Graaff accelerators. Thus, by using the reciprocity theorem one would expect to be able to study even the structure in fast neutron excitation functions, when they exist, where the inaccuracies due to the energy spreads of incident neutron beams are difficult to eliminate. So far, this method has been used only on a small scale for bombardment energies lower than 6.5 MeV, such as in determining the $^{16}O(n,\alpha)^{13}C$ cross-section from $^{13}C(\alpha,n)^{16}O$ cross-section [3] and the $^{3}He(n,p)T$ cross-section from $T(p,n)^{3}He$ cross-section [4].

1.2 Shell Closure Effect

The studies of shell closure effects on the systematic trends of the most common (n,2n), (n,P) and (n,α) cross-sections have been the

subject of interesting investigations in the 14 MeV region. The contradictory results obtained by the researchers so far, specially for the (n,2n) cross-sections, leaves the understanding of the subject in a rather uncertain state and indicates the necessity for further explorations in this field. Therefore, it is not possible at this stage to state whether the shell effects exist or not, but a brief review of the important results might be worthwhile, as follows.

1) By plotting (n,α) and (n,p) cross-sections against Z_R, the charge of the residual nucleus, depressions in the cross-sections are observed at just these values of Z_R corresponding to proton magic numbers [5,6], with an odd-even effect for (n,p) cross-sections between Z_R = 10 to 20.

2) By introducing the isotope effect of Gardner [7], both shell and odd-even effects become obscure, which indicates that the previous results of Chatterjee [5,6] were obtained by using the cross-sections of the most abundant isotopes. According to Gardner, for a given nuclear charge (n,p) cross-sections should differ by a factor of two between neighbouring isotopes with the isotope of higher mass number having the lower cross-section. The same considerations may well apply to the (n,α) reaction cross-section.

3) Distinctive minima and maxima in the mass dependence of (n,2n) cross-sections in the region of closed neutron and proton shells were observed by Bormann [8] when the cross-sections were plotted against the target mass number A. More recently, similar effects were confirmed by Mohindra and Gupta [9] who showed definite shell effects at N = 20, 28 and 50 when the (n,2n) cross-sections are plotted against N and (N-Z)/A for magic number nuclei in comparison with the neighbouring nuclei of same N-Z and pairing effects.

4) On the other hand, Qaim [10] plotted also the (n,2n) cross-sections versus the relative neutron excess (N-Z)/A as an asymmetry parameter and showed a complete lack of evidence for shell effects. His explanation for the formerly observed minima was attributed to the use of partial (n,2n) cross-sections in those cases in which the corresponding total cross-sections were not experimentally known. Kondaiah [11] also confirms this conclusion by observing no tangible evidence of shell effects when the weighted averages of the experimental cross-sections are compared with the theoretical predictions of the statistical model.

In view of the important role of the Q-value effect on (n,2n) cross-sections at a given incident energy, Holub and Cindro [12] lately looked at the dependence of (n,2n) cross-sections on the asymmetry parameter (N-Z) at a given maximum residual excitation energy, $U_R = E_n + Q_{n,2n}$ as suggested by Csikai and Peto [13]. The investigation indicated that the total (n,2n) cross-sections against the (N-Z)/A or $(N-Z)_R$ at a constant value of U_R follow smooth, structureless curves. Also the systematic difference of the total (n,2n) cross-sections compared with the statistical estimates would be interpreted in terms of the presence of pre-equilibrium processes, which harden the spectra of first neutrons and diminish the probability for the emission of second neutrons.

1.3 The Effect of Overlapping Excited Levels

For the standardization of 14 MeV neutron cross-section data for fast neutron flux monitoring, a smooth cross-section variation with energy is usually assumed. This procedure is valid due to the large neutron energy spreads of the incident beams and to the formation of highly excited compound nuclei with energies around 20 MeV in the continuum

regions. Even at such high excitation energies fluctuations in the cross-sections variations with energy have been observed for charged particle induced reactions, and several attempts to examine the existence of such fluctuations in neutron induced reactions have been carried out with good beam energy resolutions. The statistical fluctuations in cross-section for total and partial (n,p), (n,α) and (n,2n) reactions have to be compared, if they exist, with the relevant theory which was developed originally by Ericson [14], and this can be stated briefly as follows.

At energies where several or many channels can be contributed to a nuclear reaction cross-section, the total width of compound nucleus levels can be greater than their average spacing i.e. $\Gamma/D \gg 1$. Accordingly, in this overlapping resonance region partial cross-sections are not smooth functions of energies but fluctuate violently with amplitudes which are inversely proportional to the square roots of the numbers of the final states.

$$\overline{\{(\sigma - \bar{\sigma})^2/\sigma^2\}}^{\frac{1}{2}} = (2/n)^{\frac{1}{2}} \qquad (1.1)$$

where $\bar{\sigma}$ being the mean value of the cross-section on a large energy interval, $\overline{\{(\sigma - \bar{\sigma})^2\}}^{\frac{1}{2}}$ is the root mean square deviation of the cross-section and n the number of the final states.

Ericson's theory states also that in spite of the random nature of the overlapping of the resonances in the continuum region of the compound nucleus, the structure should reflect the average nucleus level width. The correlation width of the fluctuations Γ is related to the lifet-time τ of the compound nucleus by an uncertainty type of relation

$$\Gamma\tau \sim h \qquad (1.2)$$

The selection of the energy steps and required neutron beam resolution is very critical indeed for such measurements, and the uncertain existence of Ericson fluctuations in 14 MeV excitation functions can be attributed to incident neutron beam energy spreads. Fine structure studies require small neutron energy spreads such that $\Delta E < \Gamma$, and one has to keep in mind that the energy spread is further enhanced by the small-angle multiple scattering of deuterons in the tritium target [15] and by neutron scatter in the vicinity of the target [16]. It is worthwhile mentioning here that for studying the angular distributions symmetry or asymmetry the neutron beam energy spread should be much larger than the compound nucleus level width Γ i.e. $\Delta E >> \Gamma$ to discriminate between compound nucleus processes and direct reaction processes. According to Ericson, the $\Delta E >> \Gamma$ here is needed to average to zero the interference between compound nucleus levels and therefore eliminate any possible effect on the symmetry of the angular distribution about 90^{o}.

Both the activation and direct detection methods are being employed for the investigation of Ericson fluctuations in 14 MeV neutron cross-sections, and two examples for the (n,α) reaction are given here.

1) Whereas researchers such as Cindro et al [17], Strohal et al [18] and Csikai [19] have reported the existence of large fluctuations in $^{19}F(n,2n)^{18}F$ and $^{27}Al(n,\alpha)^{24}Mg$ cross-sections and even in those for heavier nuclei [19], others like Ferguson et al [20] disagree with that. Vonach et al [16] support Bormann and Riehle's conclusions[21] that the large fluctuations do not exist, and are probably due to systematic errors. The most recent publication [22] on this subject, however, confirms the existence of Ericson fluctuations in $^{27}Al(n,\alpha)^{24}Na$ total cross-section with the aid of a carefully evaluated neutron energy

resolution. The experiment of Gardner and Gardner[22] was done by using a high intensity insulated core transformer neutron facility operating at 4.5 kW of beam power. The neutron resolution obtained was 360 keV at 30^{o}, 10 keV at 98^{o} and 220 keV at 150^{o} for a tritium loading factor of 1.0 on an 0.05 mg / cm^{2} thick titanium layer. By making the measurements in steps of 15 keV the excitation function obtained revealed distinct fluctuations of about 1.5% in magnitude on the average with a width of under 65 keV between the neutron energies of 13.7 and 14.2 MeV. Fig. 1.2 shows Gardner and Gardner's data for the total $^{27}A\ell(n,\alpha)^{24}Na$ reaction cross-section on a relative scale together with few previously determined detailed excitation functions for comparison. The general trends of the excitation functions seem to be similar to each other, but the only conclusion we can draw from the reported fluctuations is the need for further high resolution investigations at extended energy ranges. The excitation function of Strohal et al [18], for example, covers a narrow range of about 700 keV only.

2) For an excitation energy of about 23 MeV for 14 MeV bombardment energy, the ^{29}Si compound nucleus represents a very interesting subject for studying the evaporation mechanism and Ericson fluctuations in the complete level mixing region. The direct detection method here employs silicon semiconductor detectors as both targets and detectors, and the resulting pulse height spectra contain well separated peaks which are mainly due to the proton and alpha groups from the (n,p) and (n,α) reactions on ^{28}Si. The appropriate selection of the thickness of the depletion layer provides an accurate facility for determining the $^{28}Si(n,\alpha)^{25}Mg$ excitation functions for the formation of ^{25}Mg nucleus in its various energy levels. The fluctuating excitation functions which were first measured by Collie et al [23,24,25]

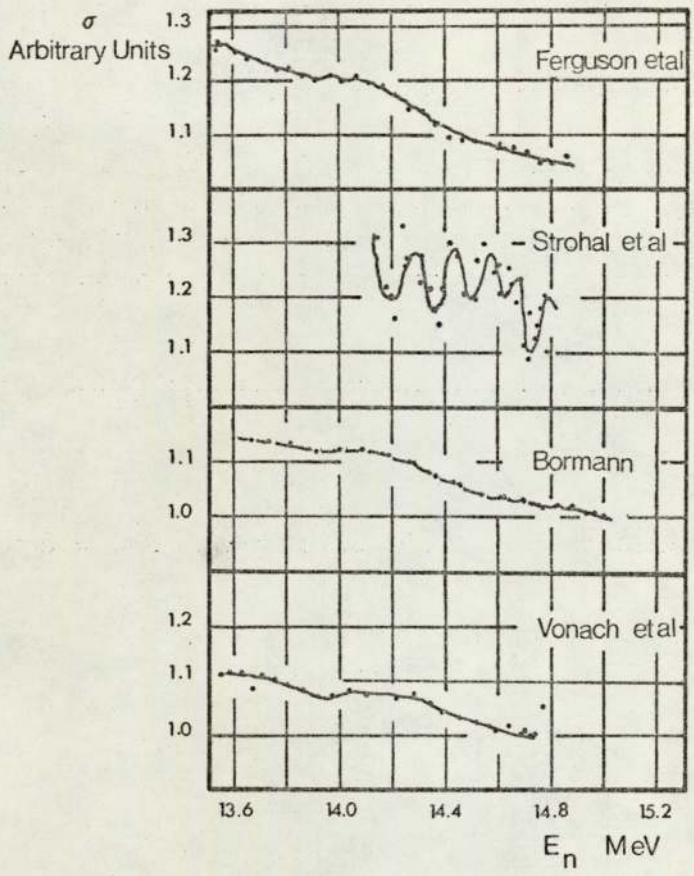

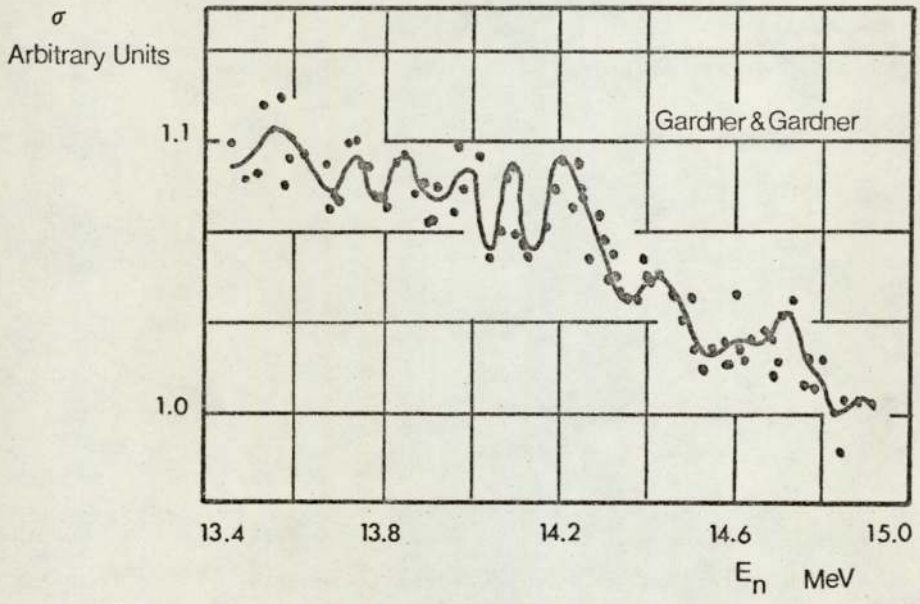

Fig. 1.2

Excitation Function for the $^{27}Al(n,\alpha)^{24}Na$ Reaction

are completely uncorrelated, showing that they are not characteristic of compound nucleus excitation energy but arise from a direct interaction interference effect. Recently, Siddiq et al [25] made similar measurements for the 12 - 18 MeV region again but with better energy resolution of values between 20 and 25 keV. Siddiq et al's excitation functions for ground, second, third and fourth excited states show strong fluctuations with amplitudes that lead to a factor of 2 agreement with Ericson predictions by using eq. 1.1. The mean lifetime of the compound nucleus as determined from the average width of the fluctuations according to eq. 1.2, is about four times smaller than that from Ericson's hypothesis, and one and a half times smaller than that of Colli et al.

1.4 Coulomb Barrier Effect

In the excitation functions for (n, charged particle) reactions a wide (8 to 10 MeV) maximum can be observed. The position of the maximum apart from several light nucleides is located between 10 and 20 MeV, and the accurate knowledge of these positions is of great practical importance.

According to the statistical theory for compound nucleus reactions, the cross-section for a given reaction depends strongly on the decay probabilities of the compound nucleus by other possible channels. At sufficient high excitation energies, the emission of a single particle may leave the nucleus still in a sufficiently high state of excitation to "boil off" a second particle. Therefore, one would expect the probability of single-particle emission to drop because of the competition of the two particle emissions. Since the neutron emission

process is relatively simple due to the lack of Coulomb barrier effect, therefore the opening of the (pn) and (αn) channels are the most competitive processes to the decay through the (p) and (α) channels. So, we should expect that the (n,p) and (n,α) reactions will reach their cross-section maxima at about the energies where the (n,pn) and (n,αn) reactions start to have noticeable yields. Bormann et al [27] have developed a simple method based on these principles to estimate the positions of (n,p) and (n,α) cross-section maxima for cases where the statistical reaction mechanism dominates, and their procedures are explained as follows.

Let us start with the reaction (n,xn), where x stands for a proton or alpha particle. Therefore the total reaction energy required to produce this reaction should be at least equal to the Coulomb barrier height $E_c(x)$ of the product nucleus for charged particle x.

$$E_n + Q_{n,xn} = E_c(x) \qquad (1.3)$$

Since the consequence of the (n,xn) reaction becoming possible is the occurrence of the maximum cross section for the (n,x) reaction, therefore the total (n,xn) reaction energy should be equal to maximum cross section.

Therefore $(E_{max})_{n,x} = E_n \simeq E_c(x) - Q_{n,xn}$

$$(E_{max})_{n,x} + Q_{n,xn} = E_c(x) \qquad (1.4)$$

If the relation (1.4) is valid, therefore the ratio $[(E_{max})_{n,x} + Q_{n,xn}]/E_c(x)$ should be unity. Fig. 1.3 shows plots of the quantities $[(E_{max})_{n,p} + Q_{n,pn}]/E_c(p)$ and $[(E_{max})_{n,\alpha} + Q_{n,\alpha n}]/E_c(\alpha)$ against the mass number A, in the mass region A = 20 to 90 as obtained from Bormann et al [27] results and the excitation function compilations of

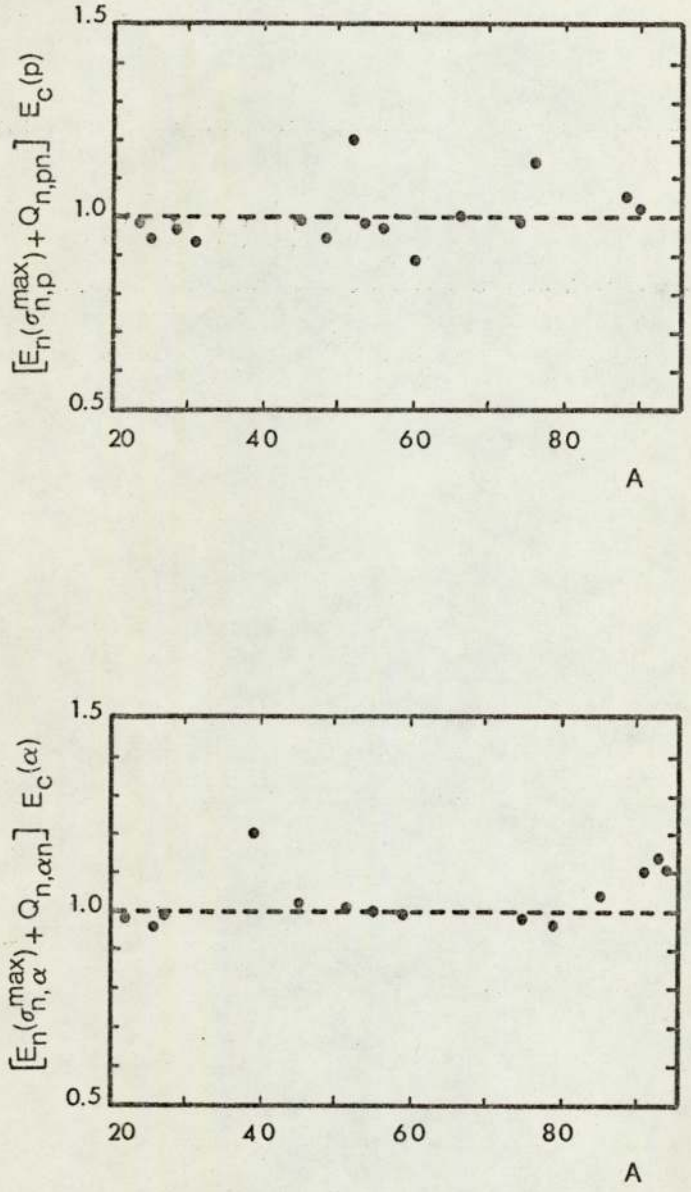

Fig. 1.3

Neutron Energy For the Maximum (n,p) and (n,α) Cross-Sections as a Function of the Target Mass Number A

Jessen et al [28]. As it can be observed from the figure, the quantities have values near to unity which proves that eq. 1.4 holds very well, and therefore can be used for the rough estimation of $(E_{max})_{n,p}$ and $(E_{max})_{n,\alpha}$.

1.5 Prediction of Fast Neutron Excitation Functions

Whereas the discrepancies in 13 - 15 MeV neutron cross-section data have already been indicated in the introduction of this thesis, the discrepancies in the excitation functions for a wider energy range of up to 20 MeV in width are even more pronounced and for many reactions no experimental data exist. Therefore, an attempt to use a neutron source of a wide continuous energy spectrum for activation purposes is limited by the lack of suitable cross-section data. Since the theoretical predictions of neutron excitation functions are not fully developed yet, empirically based estimations are therefore needed.

By using an empirical method, which was designed originally for the estimation of excitation functions for charged particle induced reactions, Krivan and Munzel [28-31] developed a rather interesting method for estimating the excitation functions for (n,p), (n,α) and (n,2n) reactions. The method is useful for predicting unknown excitation functions and extrapolating those for which data for only a narrow energy range are known. The approach of the method is interesting, but one could not expect it to be very accurate because it depends entirely on the published experimental data which is in considerable disagreement as we have explained already. Therefore, we hope that improving the accuracy of fast neutron excitation function

measurements will have a direct impact on the accuracy of this method.

According to Krivan and Munzel, the general form of the excitation functions for fast neutron induced reactions can be characterised by means of the following parameters, which are also shown in Fig. 1.4.

1) The reaction threshold energy E_{th}.

2) The maximum cross-section σ_{max}.

3) The position of maximum cross-section with respect to the Q-value of the reaction (E_{max} + Q).

4) The full and half widths at half maximum height (FWHM, HWHM) and if possible the full and half widths at tenth maximum height (FWTM,HWTM).

$$FWHM = HWHM_L + HWHM_R$$

$$FWTM = HWTM_L + HWTM_R$$

5) The asymmetry factors $F_{0.5}$ and $F_{0.1}$ at FWHM and FWTM respectively.

$$F_{0.5} = HWHM_R/HWHM_L$$

$$F_{0.1} = HWTM_R/HWTM_L$$

The analysis of the systematic trends of (n,p), (n,α) and (n,2n) reactions, as evaluated from the reported excitation functions, are shown in Fig. 1.5. This includes the three parameters (σ_{max}), (E_{max}+Q) and (FWHM), which are plotted versus the atomic number of the target nucleus. The systematic curves clearly reflect the basic differences between the reactions and are used for excitation function estimation. Finally, we would like to summarize the effects of the experimental data scatter on this method by the following points.

1) (FWHM) Curves contain relatively large standard deviations, and the determination of the trends for (FWTM), ($F_{0.5}$) and ($F_{0.1}$) is just

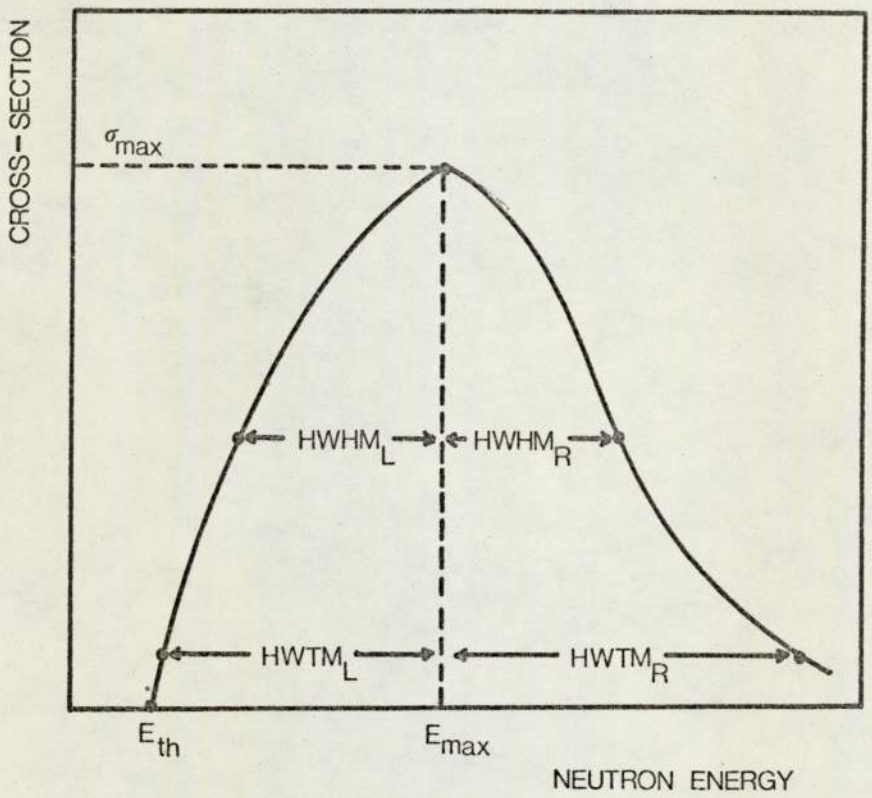

Fig. 1.4
Parameters Used to Characterize an Excitation Function

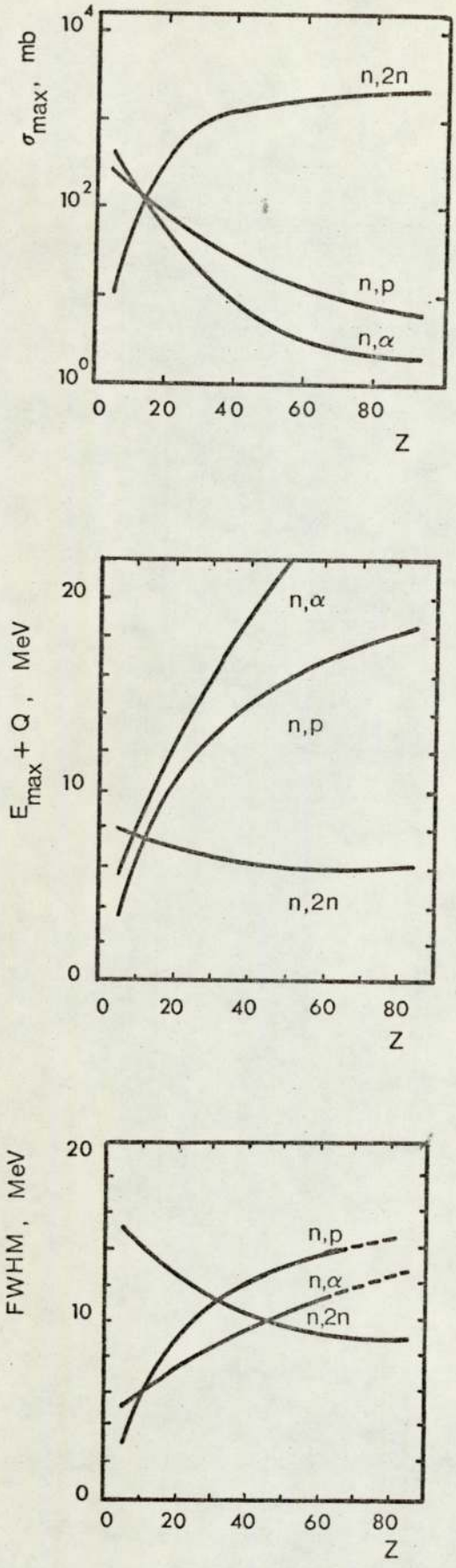

Fig. 1.5

Systematics of Excitation Functions for (n,p), (n,α) and (n,2n) Reactions

not possible. Therefore Krivan and Munzel have constructed their excitation functions by estimating the following values for ($F_{0.5}$) and ($F_{0.1}$).

Asymmetry Factor	Z = 13 - 45 (n,p)	(n,α)	Z = 27 - 69 (n,2n)
$F_{0.5}$	1.30	1.22	1.60
$F_{0.1}$	1.66	1.42	2.00

2) To a first approximation, it was assumed that the characteristics of the excitation functions depend only on the proton number Z of the target nucleus. But it is expected that the systematics will be improved if the influence of the neutron number N is taken into account by adding a correction term which depends on the neutron to proton ratio relative to that of the stability line [30]. Due to the scatter of data from published excitation functions such an approach can not be established and therefore only the target nucleus charge dependence is taken into account.

CHAPTER TWO

ACTIVATION ANALYSIS

2.1 Nuclear Analytical Techniques

An outstanding contribution to the analytical studies is being made by the non destructive nuclear techniques which are now routinely used in a wide range of disciplines in science and technology. Basically, nuclear analytical techniques require irradiating stable nuclei by a beam of photons, charged particles, or neutrons; and observing the radiation promptly emitted by the compound nuclei, or of delayed radiation from the decaying daughter nuclei. As a by-product of the nuclear power programme, activation analysis specially with neutrons advanced remarkably to a powerful analytical method for measuring the concentration of trace elements, often in amounts less than a billionth of a gram. The appropriate selection of the most efficient activation analysis method for any specific case is possibly by choosing the suitable irradiation beam and the energy of its particles or photons.

2.2 Non-Neutron Activation

2.2.1 Photon activation analysis

Activation analysis of light elements is possible by the use of photons from the heavy targets of electron accelerators. The shape of the incident gamma ray spectrum is usually a continuous bremsstrahlung spectrum of an anisotropic angular distribution, with a maximum energy value equal to the incident electron energy. The photons are emitted preferentially in the forward direction, and at low electron bombardment energies the analysis is restricted to the use of the (γ,γ') reaction which gives rise to isomeric states that decay by gamma emission. To make use of the (gamma, particle) reactions for activation analysis, the incident electron bombardment energies should be in excess of the reaction thresholds and this means that energetic electron beams from linear electron accelerators, betatrons, and electron synchrotrons are required. As in the case of neutrons, photon activation analysis leads to information about the bulk of the sample, but precise gamma absorption corrections are required. The limitations of this method are mainly the required chemical separation, and the relatively high irradiation costs when high sensitivites by using the (gamma, particle) reactions are needed.

2.2.2 Charged particle activation analysis

The relatively low operating costs and high ion beam energy resolution of Van de Graaff accelerators, make these machines very attractive tools for charged particle activation analysis. In the MeV region, analysis of light nuclei by nuclear reactions is very attractive specially when use is made of reactions which exhibit very strong resonances, typically about 1 keV wide and several keV apart. Access

to heavier elements requires higher ion bombardment energies, and this can be provided by using tandem van de graaffs with rather low beam current or cyclotrons; but increasing the bombardment energies is restricted by giving rise to spallation [32] which introduces complicated interferences. Also, information about heavy elements can be obtained even at low ion bombardment energies if backscattered ions and ion induced x-rays are observed.

Due to the short range of the incident particles, penetration depth is usually very limited, and this makes the technique very good for surface layer analysis when the ion beam energy variation with depth is taken into account. On the other hand, the technique is limited by its need of considerable care compared with neutron activation analysis and by its vacuum requirements. Also, the accuracy of charged particle activation analysis is affected by surface contamination, sample inhomogeneities, and sample overheating for large ion beam currents.

2.3 Neutron Activation Analysis

As with the other nuclear analytical techniques, activation analysis by neutrons is associated usually with high sensitivity and simplicity which puts it in a class of its own for material analysis. The transparency of samples to neutrons makes the accurate analysis of large samples quite possible, and accordingly neutron activation analysis is accepted as a standard technique for many industrial, medical and geological applications.

2.3.1 Reactor neutron source

This is the most important source of thermal neutrons for activation

analysis and other applications. Neutron thermalisation is essential to sustain the chain reaction, and the process yields thermal neutron fluxes of the order of 10^{13} - 10^{15} n/cm^2. S by fission neutron elastic collision with the moderator atoms. Fission neutrons are usually emitted in a broad spectrum which ranges approximately between 0 and 25 MeV for ^{235}U fission, but by neutron slowing down this wide energy range factor is eliminated, and the activation yields enhanced by orders of magnitude due to the large thermal neutron cross-section values. Reactors are used efficiently for long irradiation times as steady neutron sources; but with special arrangements they can also be used for pulsed activation analysis. As described by Yule and Guinn [33], a rapid removal of the main control rod causes a sudden increase in the reactivity and releases neutron fluxes of the order of 10^{16} n/cm^2 S for a few milliseconds. The sharpness of the reactor pulse duration for this special type of reactor is here determined by the temperature increase due to the reactivity build up, which makes the reactor go sub-critical automatically and shuts itself off. But, in spite of this interesting method, we can generally emphasise that the use of reactors is more reliable for activation analysis processes involving long lived isotopes. Thermal neutron activation analysis by using nuclear reactors requires a high degree of care specially to eliminate the level of interferences which affect the sensitivity of the technique. The homogeneity of the thermal neutron flux is needed of course to ensure that samples and monitors are exposed to similar neutron fluxes. Also to accomplish the activation analysis mainly by thermal neutrons, irradiations have to be carried out in the thermal column since in-core irradiations will generally yield an appreciable fission neutron contribution. Attempts to use the reactor fast neutrons for activation analysis is even more difficult, since the presence of thermal neutrons whose neutron

cross-sections may be several orders of magnitude more than fast neutrons presents a serious problem. It is obvious, therefore, that the exothermic capture reactions may very well completely overshadow the (n,p), (n,α) or (n,2n) reactions. To increase the sensitivity for the investigation of certain elements, resonance neutrons may be used by surrounding the sample with ^{10}B to absorb thermal neutrons and allow neutrons with higher energies to activate the sample [34]. But this method is limited since it requires the ratio between the resonance cross-sections of the trace element and those of the matrix to be high. On a small scale 14 MeV neutrons can be produced on the reactor site if necessary using a special arrangement. Thermal neutrons are converted to 14 MeV neutrons with an efficiency of 2.1 x 10^{-4} by using a ^{6}Li D converter [35]. The reaction sequence is as follows:

1) Tritons are produced by the $^{6}Li(n,\alpha)T$ reaction in the lithium converter which is made infinitely thick for thermal neutrons, followed by

2) Production of 14 MeV neutrons by the reaction $D(t,n)^{4}He$, the tritons from reaction (1) having an energy of 2.8 MeV.

In conclusion, if we are thinking in terms of activation analysis facilities for small laboratories, nuclear reactors do not seem to fit the requirements on the basis of complicated operating procedures. This point of view is further confirmed by taking the costs also into account, since the purchase and operation costs for a modest 100 - kW facility are well above $500,000. We can add to this other disadvantages such as heavy shielding requirements to reduce the relatively high radiation levels, handling highly radioactive spent fuel elements, and release of radioactive substances in case of an accident.

2.3.2 Isotopic neutron sources

Isotopic neutron sources are formed by using the (α,n) or (γ,n) reaction on isotopes of light elements, whose (α,n) or (γ,n) threshold is low compared with gamma or alpha energy. For example, a portable low intensity ~~zero power~~ neutron source can be produced by mixing ^{241}Am, which is an alpha emitter, with beryllium. Since the emitted alphas and gammas are not monenergetic, the emitted neutrons are not monoenergetic either; and an additional neutron energy spread occurs for (α,n) sources because alpha energies get degraded by the source materials before interacting with the beryllium. Mixing of the radio-active isotope and converter in a powder form is not essential for (γ,n) sources, e.g. $^{24}Na/Be$ or $^{24}Na/D_2O$.

The neutron output from this type of neutron source is rather low and is of the order of 10^6 n/s. c_i, but the stability of neutron production is very good specially for $^{241}Am/Be$ sources due to the long half life of ^{241}Au (248 years). The thermalization efficiencies for isotopic neutron sources are good due to their low mean neutron energies, but their reliability for accurate thermal neutron activation analysis is again affected by the low neutron output. An alternative source to provide about 4.4×10^9 n/s c_i is the ^{252}Cf which undergoes spontaneous fission and can be designed in small sizes for better geometry. But the limited commercial production of ^{252}Cf at the present time, and its short half life which is effectively 2.6 years make this source extremely expensive. The gamma ray background from ^{252}Cf source is slightly high, and it varies appreciably for (α,n) sources, where $^{241}Am/Be$ is one of the very low gamma background sources.

2.3.3 Accelerator neutron sources

2.3.3.1 14 MeV neutron generator

In spite of the important role of nuclear reactors in the activation analysis field, the development of smaller and easily operated neutron sources is extremely useful in establishing activation analysis as a more widespread analytical tool. The limitations of the isotopic neutron source that have been outlined, leaves without any doubt the so called "neutron generator" as the most promising answer.

The subject of neutron producing reactions using ion beam accelerators is well established in nuclear physics. By using low energy accelerators, occurrence of (p,n) and (d,n) reactions on several light nuclei is energetically possible, and the emitted neutrons differ in both yield and spectrum due to the difference in cross-sections, reaction Q-values and nuclear energy levels.

An ideal accelerator neutron source for activation analysis is a reaction with large positive Q-value to allow the use of low ion bombardment energies, large cross sections for good neutron yield, and also with a single neutron group emission. It is not surprising, therefore, that the $^{3}H(d,n)^{4}He$ reaction has been accepted as an excellent neutron source for activation analysis due to its unique properties. The D-T reaction has a positive Q-value of 17.59 MeV and a cross-section of 5 barns at deuteron energy of about 110 keV only. It has also the advantage of producing monoenergetic neutrons at relatively high energy (14 MeV), which is due to the high threshold for break-up of ^{4}He and the absence of excited states in this nucleus.

In neutron generators, deuterons are usually extracted from RF or PIG ion source and accelerated by using a small voltage generator such as a Van de Graaff, Cockroft-Walton, Electrostatic Rotor machine (SAMES),

or Insulating Coil Transformer to energies of the order of 120 - 200 keV. The ion beam is then allowed to strike targets in which tritium has been diffused in a thermally stable material such as titanium. By using such a simple and economical set up, intense fast neutron ~~fluxes~~ sources of 10^{11} n/mA.S are produced with a total neutron energy variation with angle of emission of about 2 MeV. The neutron beam so produced can be obtained in a continuous mode or in a pulsed mode to enhance the yield of short lived radio-isotopes. The beam pulsing can be carried out by using a common pulsing technique such as ion beam electrostatic deflection, or as suggested recently by Tazanowski [36] by using the storage ring concept to multiply the beam intensity.

Neutron generators can also be used for thermal neutron activation analysis by using an appropriate moderator surrounding the tritiated target. But, due to the steep fast neutron flux variation with distance and the low thermalization efficiency for 14 MeV neutrons, low thermal neutron flux is produced at the sample position. Monoenergetic neutrons with energies around 2.8 MeV can also be produced by using the exothermic $^{2}H(d,n)^{3}He$ reaction on deuterium targets. The D-D reaction is a better source for thermal neutrons, but for bombardment energies lower than 1.0 MeV the D-D reaction yield is much lower than that for the D-T reaction, for example for E_d = 150 keV it is 300 times lower, Fig. 3.1.

Both the variety of nuclear reactions produced by 14 MeV neutrons and the simplicity of sealed tubes for neutron generation, make the analysis by 14 MeV neutrons widely accepted specially for on-line analysis. In the steel industry, for example, the most common application of 14 MeV neutron activation analysis is the determination of oxygen [37] with a sensitivity of 5 ppm in about 1.0 minutes of analysis time. The analysis is performed by using the $^{16}O(n,p)^{16}N$ reaction and detecting

the 6.13 and 7.11 MeV gammas emitted by ^{16}N with a half-life of 7.35 S. For analysis involving very short lived radio-isotopes, cyclic activation analysis can be used to reveal their contributions. This can be achieved by accumulating in the detector the radiation induced by a number of consecutive short irradiations.

The accuracy of 14 MeV neutron activation analysis is dependent to a large extent on the accuracy of the cross-section data used in the analysis [38], and this dependence can be clearly explained as follows. 1) Neutron cross-section data are needed for determining the absolute concentrations of trace elements and also in estimating the contribution of interfering reactions. 2) For an ideal programme in activation analysis, one would also need to know the cross-section variations over an appropriate energy range to account for the neutron energy variation with angle. 3) Also positions and values of maximum energies for better reaction yields, and therefore better sensitivities. 4) The neutron flux determination for activation analysis is dependent on the excitation functions for standard reactions to whom relative measurements can be made. The use of a comparator with a known impurity concentration can avoid the requirement for precise cross-sections, but has other disadvantages. This subject will be further discussed later in this thesis.

2.3.3.2 Other accelerator neutron sources

The variety of nuclear reactions that occur under 14 MeV neutron irradiation have the disadvantage of possible creation of interferences from the matrix elements. Also, they may lead to the most serious limitation of fast neutron activation analysis which is the production of the same radio-nucleides from more than one element. By an appropriate

choice of neutron bombardment energies one can reduce the contribution made by an interfering reaction; but such requirements can not be met by using a neutron generator since the available neutron energy range is about 2 MeV only for the $T(d,n)^4He$ reaction.

By having a more powerful machine one can produce neutrons with widely varying energies using different ion beams and targets. Variable-energy cyclotrons operating at energies of about 10 MeV per nucleon can provide good selectivity for neutron activation analysis [39]. For the determination of small amounts of iron in the presence of large amounts of cobalt, 14 MeV neutrons produce the radioisotope ^{56}Mn via the $^{56}Fe(n,p)^{56}Mn$ and $^{59}Co(n,\alpha)^{56}Mn$ reactions which make the analysis impossible. The method used by Steele et al [39] to solve this problem is to use the small cyclotron and take into consideration both the reaction thresholds and the coulombic barriers. The reaction thresholds for iron and cobalt are 2.9 and zero MeV and their coulombic barriers are 4.6 and 8.3 MeV respectively. Therefore by irradiating Fe - Co samples with neutrons having energy appreciably less than 8.3 MeV, but above 2.9 MeV, ^{56}Mn activity will be produced essentially from the iron present in the samples.

By bombarding a beryllium target with deuterons of energies lower than 10 MeV stable and intense source of few MeV neutrons is produced, the $^9Be(d,n)^{10}B$ neutrons under these conditions have limited applications in fast neutron activation analysis but they offer a good source for thermal neutrons. At higher deuteron bombardment energies stripping and break-up neutrons are produced preferentially in the forward direction with a neutron flux increasing steadily by increasing the deuteron energy. The fast neutrons so produced, at deuteron energies above 10 MeV on thick beryllium targets, have energy distributions with

broad asymmetric peaks occuring at neutron energies approximately equal to 0.4 times the incident deuteron energies. By using deuteron energies varying between 16 and 53 MeV Krivan and Munzel [31] have carried out systematic studies for the detection limits of cyclotron neutrons compared with 14 MeV neutrons for (n,p), (n,α) and (n,2n) reactions. For their given experimental conditions, it was estimated that for 53 MeV deuterons the limits of detection for cyclotron-produced neutrons are lower than those for 14 MeV neutrons by a factor of 20 to 100.

By using Harwell 280 cm. synchrocylclotron, Jarvis et al [40] performed thermal neutron activation analysis on large samples by prompt and delayed gamma detection. The particle beam extracted from the synchrocyclotron was transported into the experimental area and directed towards a cylinder of natural uranium, and the neutrons were readily thermalized in a large polythene cylinder surrounding the uranium source. It is interesting to note that the proton beam intensity actually used (0.08 μA for 160 MeV) provides a neutron flux density comparable with that obtainable from a few milligrams ^{252}Cf. In spite of the prolific neutron yields produced by high energy beams, their use of course is limited; the required accelerators are expensive to install and operate and therefore they are not justified for the sole use of activation analysis.

CHAPTER THREE

THE D-T NEUTRON SOURCE

3.1 Nuclear Data for the D-T Reaction

The experimental information on absolute cross sections and angular distributions of the D-T reaction are well documented for deuteron energies up to 10 MeV [41], and with the recent measurements on Hamburg isochronous cyclotron the limit was moved to 15 MeV [42]. As shown in Fig. 3.1a [43], the average neutron energy available from the $T(d,n)^4He$ reaction is appreciably higher than those from the $D(d,n)^3He$ and $^9Be(d,n)^{10}B$ reactions throughout most of the deuteron energy range. Following a steady increase in the average neutron energy for the D-T reaction, a drop around 4 MeV is observed. This drop is explained according to the three-body system as due to the appearance of the other neutron groups above the deuteron break-up threshold. The existence of break-up neutrons presents no problem if neutron energies are below the thresholds of the neutron reactions studied. Also the energy discrimination between the two neutron groups is possible due

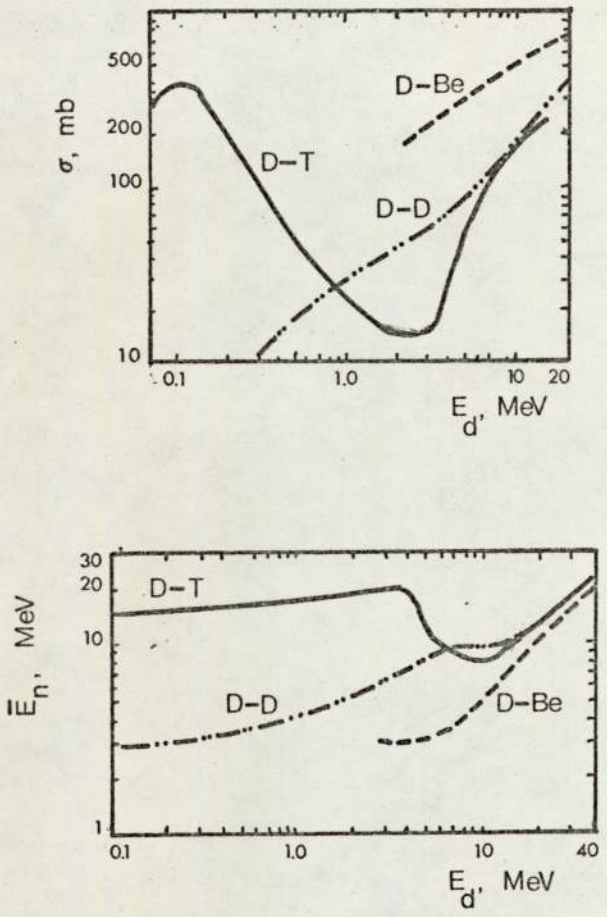

Fig. 3.1a
$D(d,n)^3He$, $T(d,n)^4He$ and $^9Be(d,n)^{10}B$ Reactions.
The Variation of Reaction Cross-Section and Average Neutron Energy with Incident Deuteron Energy.

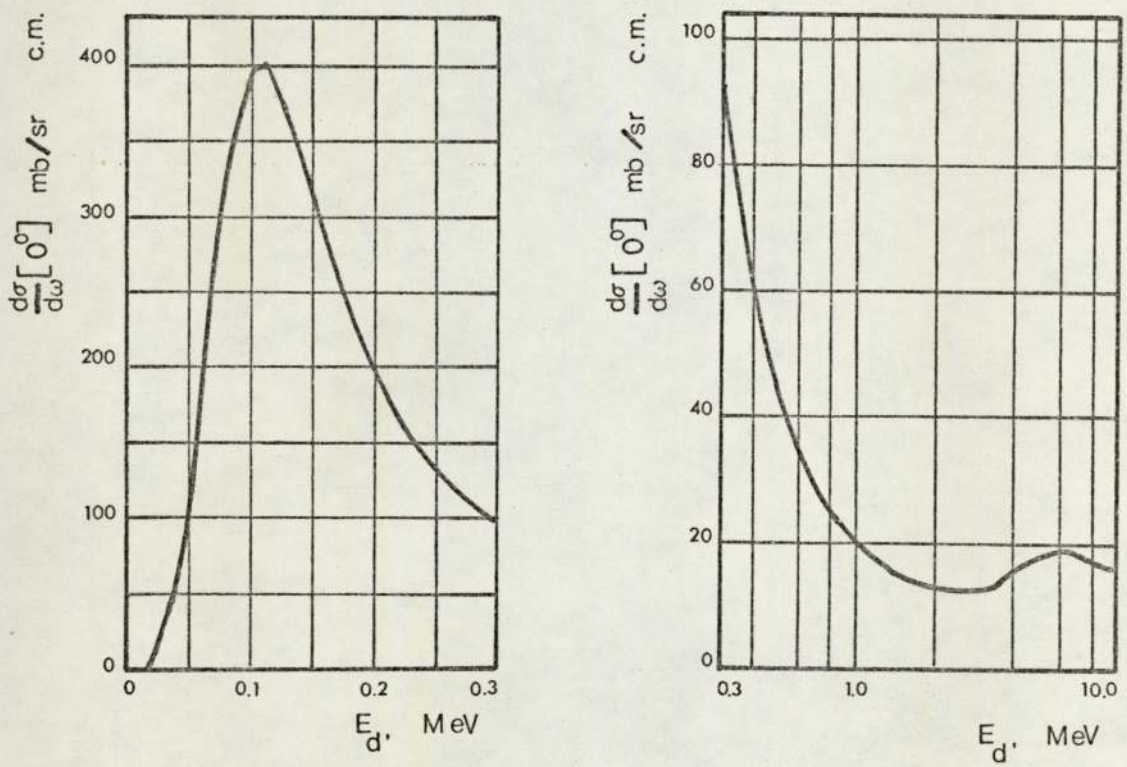

Fig. 3.1b
0^{o} Differential Cross-Section for the $T(d,n)^{4}He$ Reaction

to their large energy gap.

At low deuteron bombardment energies, the maximum neutron yield is obtained at a bombardment energy of 0.11 MeV for a thin target stopping only about 1.0 keV deuterons. This corresponds to the broad resonance peak at 0.11 MeV which has a cross section value of about 5 barns, as shown in Fig. 3.1b[41]. In practice however, thick targets are used in order to stop the whole deuteron beam, and so in this case the maximum neutron production occurs for deuteron energies higher than 0.11 MeV, Fig. 3.6.

3.2 Particle Accelerators

3.2.1 The Van de Graaff accelerator

To produce neutrons with energies ranging between 13 and 15 MeV which is the region that has the most extensive applications, low energy particle accelerators are needed. For this project, the 0.5 MeV Van de Graaff accelerator at the University of Aston in Birmingham was therefore used for the production of neutrons.

Fig. 3.2 illustrates one of the basic design features of this machine, which is the separation of the belt from the acceleration tube. The operation of this machine is similar to more modern single ended machines in which the belt and the acceleration tube are housed inside a single stack. The charging system in Astons Van de Graaff is also standard i.e. by corona discharge from a set of corona points close to the belt and situated near to the ground potential pulley. The belt charging system is dependent on the uniformity of the charge distribution which is a function of the insulation properties of the belt, (note here that this is not the case for pelletron charging system).

Fig. 3.2

The 0.5 MeV Van de Graaff Accelerator

Therefore, care in maintaining the belt was always needed; during the period in which this project was running a new belt was installed.

The neutron producing target was situated at the end of a short beam tube which was positioned directly below the acceleration tube. When beam alignment was required, a fine adjustment system was used to minimize the current readings on four slits placed at the entrance of the beam tube. The deuteron beam currents delivered by the RF source were stable and at an operating voltage of 0.3 MeV for our neutron experiments the machine conditions were satisfactory.

3.2.2 Wide neutron energy region requirements

Although much work has been done in the 13 - 15 MeV energy range because of the availability of small accelerators, excitation function measurements for neutrons having energies within a region larger than the standard 13 - 15 MeV region have certain advantages for the following reasons:-

1) Revealing the shapes of the excitation functions more clearly.

2) The possibility of making cross section measurements around σ_{max} is useful for more sensitive activation analysis work.

3) Accurate investigation of E_{max} might also lead to information about the thresholds for competing reactions.

4) By increasing the incident neutron energy above 15 MeV rare reaction investigations become much easier.

5) A good check for our own neutron monitoring technique can be obtained by working with an extended energy range and under different experimental conditions.

3.2.3 The Dynamitron accelerator

In addition to our experiments on the Van de Graaff, we have made further measurements in a wider neutron energy region. This was possible by using higher deuteron bombardment energy and a tritium target that does not stop the beam entirely. For these experiments we used a 1.4 MeV deuteron molecular beam D_2^+ which is equivalent in energy to an atomic beam D^+ of 0.7 MeV. The molecular beam was used to create a higher D^+ particle flux by breaking the molecular ions up on the tritium target. The vertical 3.0 MeV Dynamitron at Birmingham Radiation Centre was used as a source for the molecular beam and the experiments were carried out in a low scatter room.

The pressurised accelerator was manufactured by Radiation Dynamics Inc. of New York which is responsible for the development of the Dynamitron which can be considered as an R/F parallel fed Cockroft-Walton machine [44]. Basically, the accelerator design includes a resonant pressure tank circuit consisting of a toroidal coil and two electrodes. The two electrodes are C shaped and act as two capacitors, producing R.F. field between them. The induced R.F. voltages on the corona grading hoops of the acceleration stack are then transferred to the high-voltage terminal by an R.F. choke. On the Dynamitron, increase in the frequency of the driving voltage is achieved by using thermionic hard-vacuum rectifier tubes instead of the conventional rectifiers to reduce the diode shunt capacity. The required power for the thermionic rectifier at a given stage is supplied by the ripple R.F. voltage at that stage. A schematic representation of a Dynamitron accelerator is shown in Fig. 3.3 [45]. Positive ions and electron beams can be supplied with currents of the order of mA with a ripple voltage less than 3 kV peak-to-peak and a short term voltage stability of the order of 1%.

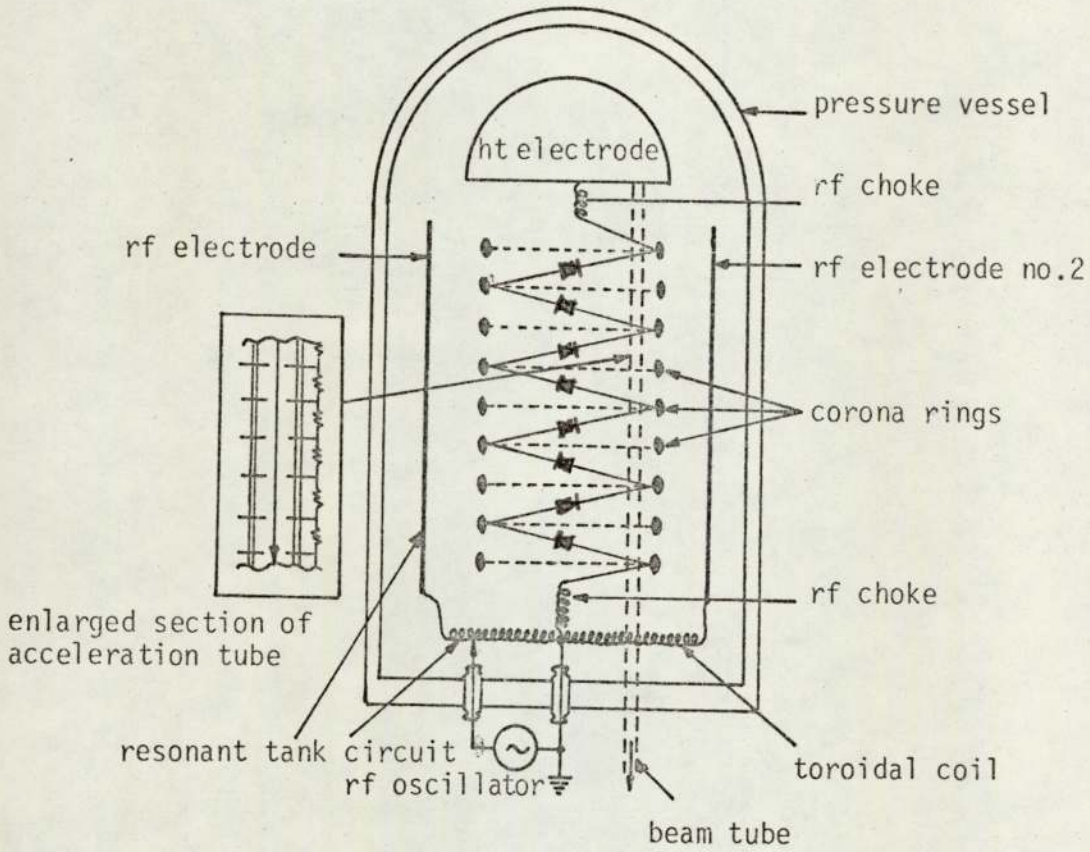

Fig. 3.3

Schematic Representation of a Vertical Section Through a Vertical Dynamitron Accelerator

The required vacuum conditions were reached by using a large diffusion pump with a cold trap for the machine and ion pumps for the beam lines. The ion beam leaving the duoplasmatron ion source is usually magnetically analysed before entering the accelerator tube. The accelerated beam then is directed towards the appropriate beam line using magnetic analysers and for our experiments a 90^{o} analyser was used.

3.3 The Tritiated Target and Target Assembly

The tritiated titanium targets used in our experiments are of the type TRT.51 and are supplied by the Radiochemical Centre at Amersham. According to the manufacturers specifications [46], these targets are made of 0.25 mm thickness and 28.17 mm diameter copper backing on which a thin titanium layer of 1.08 mg/cm^2 thickness and 2.54 cm diameter is deposited. The tritium is absorbed in the titanium layer by heating the targets to a temperature of about $400^{o}C$ and cooling them in an atmosphere of tritium. The absorbed tritium layer in our targets has a thickness of 0.77 $curies/cm^2$. The use of thick tritium targets is important for producing high neutron yields and in reducing the rate of reduction in yield. On the other hand such targets degrade the energy of incident deuteron beam and generate some spread in energies of the emitted neutrons. The TRT.51 targets are thick enough to stop the whole 0.3 MeV deuteron beam, but they present partial stopping for the 0.7 MeV beam (1.4 MeV D_2^+) which is required to expand the neutron energy range. Our measurements show that for an 0.3 MeV deuteron beam the TRT.51 target produces a neutron yield of about 10^8 n/s μA depending on the age of the target.

3.3.1 Behaviour of the neutron output from T-T_i targets

It is important to recognise that the neutron flux from gas-in-metal targets decreases with usage, and this is less pronounced for short irradiations than for longer ones. The half-life of a target is influenced by mainly deuteron bombardment time and beam current and it can be defined as the time at which the yield falls to half of the original neutron output at constant beam current. For a 2 curies target the half-life is of the order of 0.5 mA. hour, for irradiations of 5 sec at 300 μA [47]. By measuring the yield curves for a new target of uniform tritium distribution, Broerse et al [48] concluded that the curves measured after 17 and 30 hours of irradiation show that more tritium has disappeared from the front layers of the target than from the deeper layers.

It has been reported that the target deterioration with time falls in a manner defined by two exponential decays, one having a half-life of the order of 150 minutes and the other a half-life of the order of 1100 minutes [49]. These data were obtained by using 0.1 to 0.14 MeV deuteron beams with target currents of 0.25 mA to 1.0 mA, and with tritium content of 6.5 to 13.7 curies. The initial rapid fall of neutron output is explained mainly by outgassing due to local heating and positive ion bombardment, together with a limited amount of sputtering [49]. By improving the target cooling, increase of the initial half-life by 50 to 100% can be obtained [50]. The longer half-life, which takes place after about 500 min. of operating time, can be explained by the diffusion of tritium from the lower layers of the target to the region where the D-T reaction is occuring. The same mechanism applies also to a short lived increase in the neutron yield observed at the beginning of the irradiation time [51,52]. In this case

the yield proceeds by reaching a maximum after a few minutes and then follows the usual neutron yield decline ~~fasion~~ pattern in about 15 minutes. This short time interval behaviour was observed using 0.2 and 0.12 MeV deuteron beams with effective diameters of 4 and 6 mm and beam intensities of 200 and 100 μA. (51,52)

In a recent experiment by Stengle et al (53) using an analysed deuteron beam, the measured short half-lives of T-Ti targets were found to be more than an order of magnitude longer than those observed using unanalysed beams. It appeared, therefore, that the short-lives observed with unanalysed beams are mainly due to sputtering and radiation damage caused by heavy ion contaminants always present in unanalysed beams. The other improvement approach is by Bibby et al (54) who have demonstrated the effect of thermal treatment on the neutron output of used T-Ti targets. By redistributing the residual tritium a remarkable neutron output enhancement was obtained, which shows that thicker targets may be used giving a saving in running costs of a generator.

Our experience with T-Ti targets show that improved neutron outputs can be obtained by allowing the targets to rest after use for some time, this is in support of the work by Cossutta (55). To account for the neutron yield variation with irradiation time, the neutron rate of production was monitored continuously by using a BF_3 counter surrounded by a moderator. The amplified detector output was fed to a rate meter and a plotter and the cross section data were then corrected for the neutron flux variation with time.

To reduce the effect of ion beam heating on neutron production, various methods of target cooling are usually employed. Better results can be obtained if rotating targets are used, since they are capable of dissipating 600 W of power and have half-lives of up to 200 hours for

normal operation [56]. The other major development in this subject is the acceleration of a mixed deuteron-triton beam towards a metal plate and allow the ions to diffuse and reach a stage where the rate of ion loss from target is equal to the rate of ion loading. Since the acceleration of tritons is usually not desirable, hence "sealed" tubes are required to replace the pumped accelerators [57], and these are commercially available. A significant development in activation analysis can be achieved by increasing the yield of the portable sealed tubes; and a good step in this direction would be of course by increasing the beam current on self regenerating targets by using for example, a modified Duoplasmatron type ion source [58].

3.3.2 The target assembly

Various methods can be used for target cooling by water or gas, but our water cooled target assemblies were designed specially for neutron excitation function measurements. In the Van de Graaff target assembly, the T-Ti target is clamped, to ensure good thermal conductivity, on the top of a heat sink which has a cross sectional geometry of half a circle. This design was adopted so that neutrons emitted between 0^{o} and 90^{o} pass through the same thickness of material. To compensate for the neutron attenuation at angles larger than 90^{o}, calculations of the percentage of neutrons likely to interact in the backing and in the compensator were made to estimate the size of a converter which was then placed on the outside wall of the chamber. The chamber diameter was made small so that positioning the samples at short distances from the neutron source will become possible if necessary. The water cooling system was designed in a special way such that the water path does not coincide with the "direct line" of target to specimen.

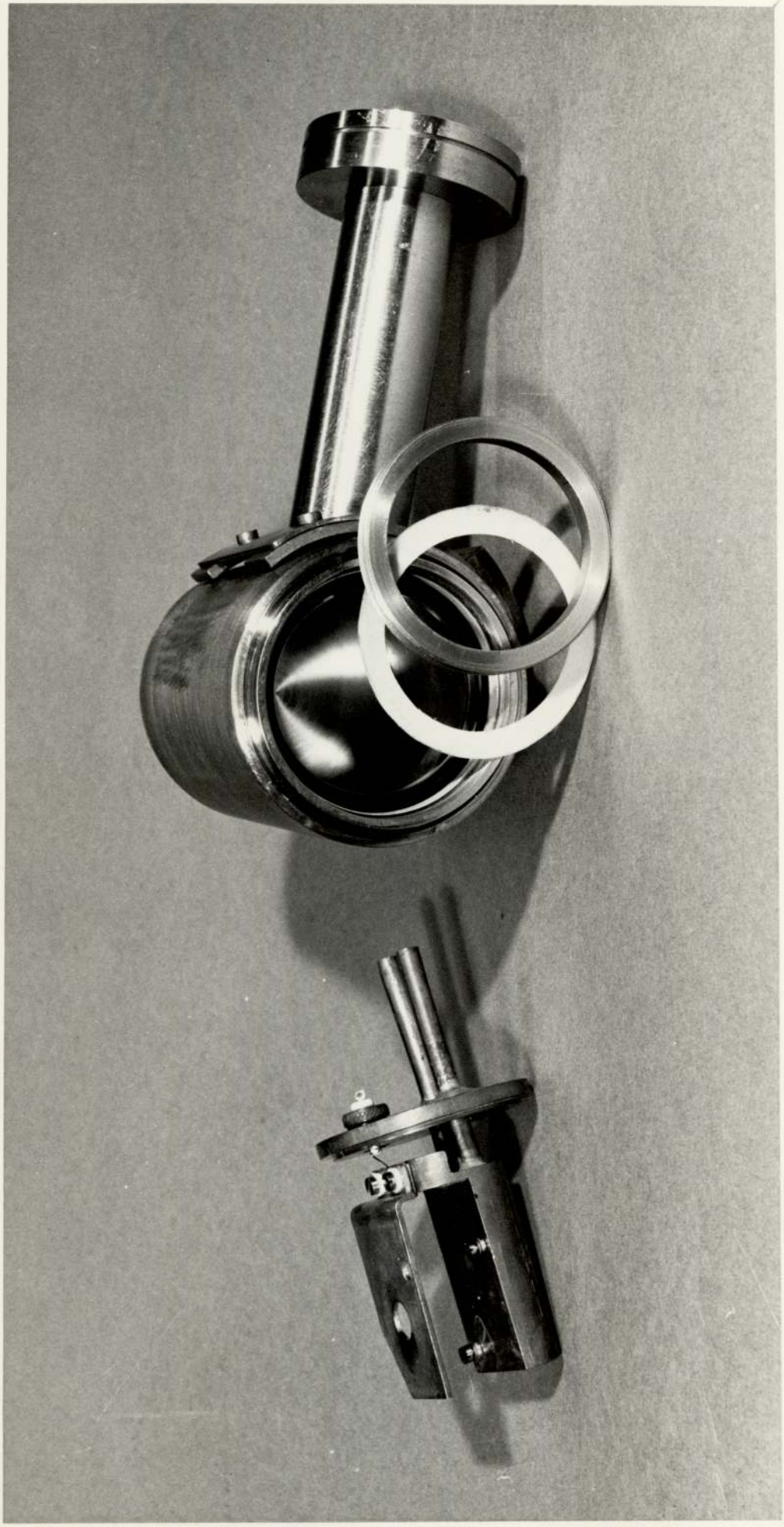

Fig. 3.4 The Water Cooled Target Assembly

A collimator of 1.2 cm diameter was used to limit the size of the deuteron beam spot on target, and by monitoring the current on this collimator efficient accelerator operation is obtained. Target current was also measured continuously on a micrometer by taking the readings from the heat sink. The heat sink is supported through the cooling water inlet and outlet on a flange which is in good electrical insulation from the rest of the chamber. The procedure used for improving the neutron yield is that another spot on the target is brought into the beam, when the former impact is exhausted.

The target assembly shown in Fig. 3.4 was used for the Dynamitron experiments. This has design features similar to the Van de Graaff target assembly, except the use of stainless steel instead of brass to satisfy the vacuum requirements on the Dynamitron. The heat sink is made of copper to obtain good thermal conductivity.

3.4 Evaluation of the D-T Source Parameters

3.4.1 Deuteron beam energy loss and straggling

Energy losses of deuteron beam in tritiated titanium targets are calculated under the assumption that Bragg's law holds, i.e. the energy loss in a compound is the sum of the energy losses in its separate constituents. Benveniste and Zenger [59] used this law and produced the following formula for T-Ti targets:

$$\left(\frac{dE}{dx}\right)_{T\text{-}Ti} = \frac{48}{48+3n}\left(\frac{dE}{dx}\right)_{Ti} + \frac{3n}{48+3n}\left(\frac{dE}{dx}\right)_{T} \qquad (3.1)$$

where (n) represents the loading factor i.e. the number of tritium atoms per titanium atom.

Due to the lack of experimental data on the energy loss of deuterons in titanium, $(\frac{dE}{dx})_{Ti}$ data for deuterons were evaluated by Benveniste and Zeneger [59], Saker and Wood [60], Gunnersen and James [61] using energy loss results of protons on different materials. Warshaw [62] has carried out experiments for the determination of $(\frac{dE}{dx})$ in aluminium, copper, silver and gold for protons in the energy region 0.05 to 0.35 MeV. By transferring Warshaw's data on aluminium and copper using an $A^{-\frac{1}{2}}$ relationship the rate of energy loss for protons in titanium was obtained. Values of $(\frac{dE}{dx})_{Ti}$ for deuterons are derived from the proton data according to the assumption that the rate of energy loss is a function only of the velocity of the particle

$$(\frac{dE}{dx})_{\text{protons}} (E) = (\frac{dE}{dx})_{\text{deuterons}} (2E) \qquad (3.2)$$

Since no results on the rate of energy loss for deuterons in tritium are available, it is therefore necessary to make a transformation from the proton energy loss data in hydrogen. The following formula is therefore valid since tritium and hydrogen have the same nuclear charge and tritium has an atomic weight equal to 3:

$$(\frac{dE}{dx})_{\text{tritium}} (\text{keV/mg/cm}^2) = \frac{1}{3} (\frac{dE}{dx})_{\text{hydrogen}} (\text{keV/mg/cm}^2) \qquad (3.3)$$

Calculations of $(\frac{dE}{dx})_{T\text{-}Ti}$ is one of the functions of the computer program which we have developed for D-T neutron production ('NEUTRED', Appendix 1). It is assumed that the energy degradation of the incident beam takes place in stages of 50 keV in the region from the incident energy to 200 keV, 10 keV in the region from 200 keV to 50 keV, and 5 keV in the region from 50 keV to 10 keV. These small steps ensure that average values for the functions $(\frac{dE}{dx})_{T}$ and $(\frac{dE}{dx})_{Ti}$ may be assumed

between energy steps. To calculate the deuteron rate of energy loss for 0.3 MeV and 0.7 MeV beams in TRT.51 T-Ti target, a loading factor of 1.2 was used. These evaluations were made by assuming a uniform tritium distribution throughout the target thickness, and the results are shown in Fig. 3.5. The accuracy of $(\frac{dE}{dx})_{T\text{-}Ti}$ results depends strongly on the accuracy of the data for its separate constituents. The uncertainties associated with each of these constituents vary with deuteron energy, but generally they are about $\pm$5% in the high energy region and rise to about $\pm$ 10% in the low energy region due to the extrapolation involved.

Deuteron beam energy spread is rather small and less than 0.1% for Van de Graaff machines. But due to the statistical nature of the energy loss processes, a deuteron experiences an energy straggling as it penetrates the target. If $f(E_d)$ denotes the energy distribution function at some depth of an initially monoenergetic beam, then energy straggling is defined as the standard deviation of $f(E_d)$ with respect to the average. If we consider the distribution to be Gaussian function of energy, therefore as the beam penetrates the distribution gets wider due to straggling.

The simplest theoretical approach to straggling is due to Bohr [63] who described the energy straggling for a given projectile as a dependent on the square root of $(Z_2 N \Delta R)$, where (Z_2) is the target atomic number, (N) is the number of target atoms per unit volume, and (R) is the thickness of the target. Bohr's theory is based on the assumptions that target atoms are randomly distributed, energy loss during single interaction is very much less than the total energy loss over the entire path, and the projectile velocity is much greater than the orbital electron velocity of the target atoms. Unfortunately, at low and medium energies the

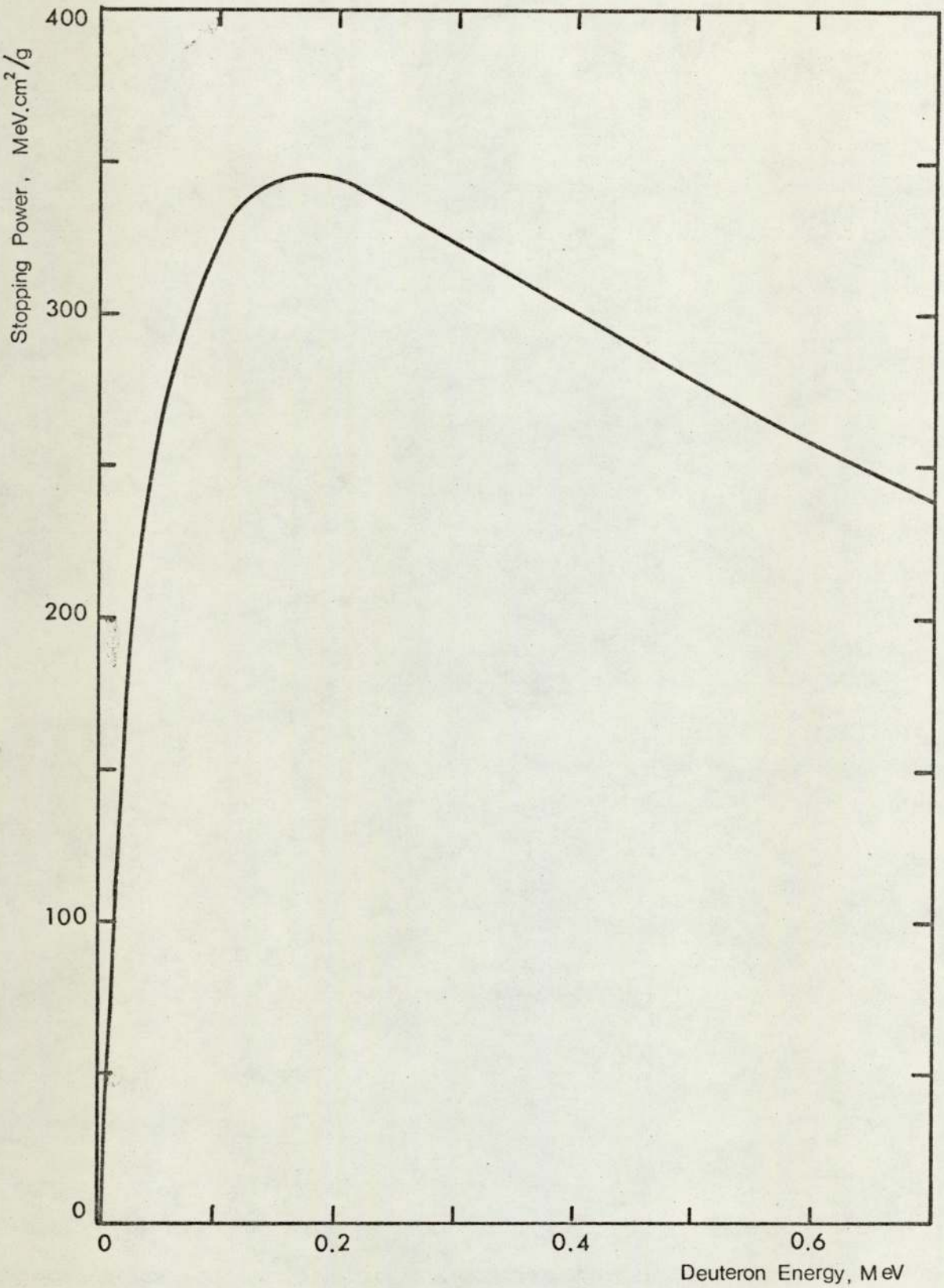

Fig. 3.5

Deuteron Rate of Energy Loss in Tritiated Titanium Target with a Loading Factor of 1.2

third assumption breaks down and the energy dependence correction of Lindhard and Scharff [64] should be considered. In addition to this it is difficult to estimate the accuracy of the theoretical calculations esepcially if a (Z_2) structure in energy straggling is present at low energies. There are no empirical values at the present time for the energy straggling in tritium or titanium to be used for the calculations. Therefore it was not possible to take the straggling factor into account.

3.4.2 Tritium target yield

Before selecting the operating conditions for neutron production it is useful to calculate the values of total neutron yield per incident deuteron of energy (E_d). The calculated values are important for choosing sample to target geometry, prediction of the magnitude of the induced activity per unit weight of the sample material, and also they are important in accelerator shielding design. The probability (P) of a deuteron undergoing a D-T reaction while travelling a distance (dx) in a T-Ti target material containing N_t tritium atoms/cm^3 is given by:

$$P = N_t \cdot \sigma \cdot dx \qquad (3.4)$$

where σ is the cross section of the D-T reaction.

Since (σ) is a strong function of deuteron energy, the following relation is used to take into account this variation effect of (σ) on (P).

$$\sigma dx = \frac{\sigma dE}{(dE/dx)_{T\text{-}Ti}} \qquad (3.5)$$

Therefore equation 3.4 will take the form

$$P = \frac{N_t \cdot \sigma \cdot dE}{(dE/dx)_{T\text{-}Ti}} \qquad (3.6)$$

For complete stopping of the deuteron beam in the target material, each deuteron will have a finite probability of reacting throughout the range of energy from zero to the accelerating energy (E_d). Thus the total probability of a deuteron reacting in the target will represent the total neutron yield per incident deuteron, (Y), and is obtained by the integration of (P) over the whole energy range.

$$Y \leq \int_0^{E_d} P.\, dE = N_t \int_0^{E_d} \frac{\sigma.\ dE}{(dE/dx)_{T-Ti}}$$

Therefore

$$Y = 4\pi N_t \int_0^{E_d} \frac{\sigma(\Omega)}{(dE/dx)_{T-Ti}}.\, dE \qquad (3.7)$$

where $\sigma(\Omega)$ represents the differential cross section for the D-T reaction given in units of barn/steradian i.e. $\sigma(\Omega) = \frac{\sigma}{4\pi}$.

The solution of eq. 3.7 produces absolute neutron yield results for thick tritium targets using the appropriate value of tritium number of atoms. The equation can also be used to calculate the depth distribution of the reactions as they occur in the target.

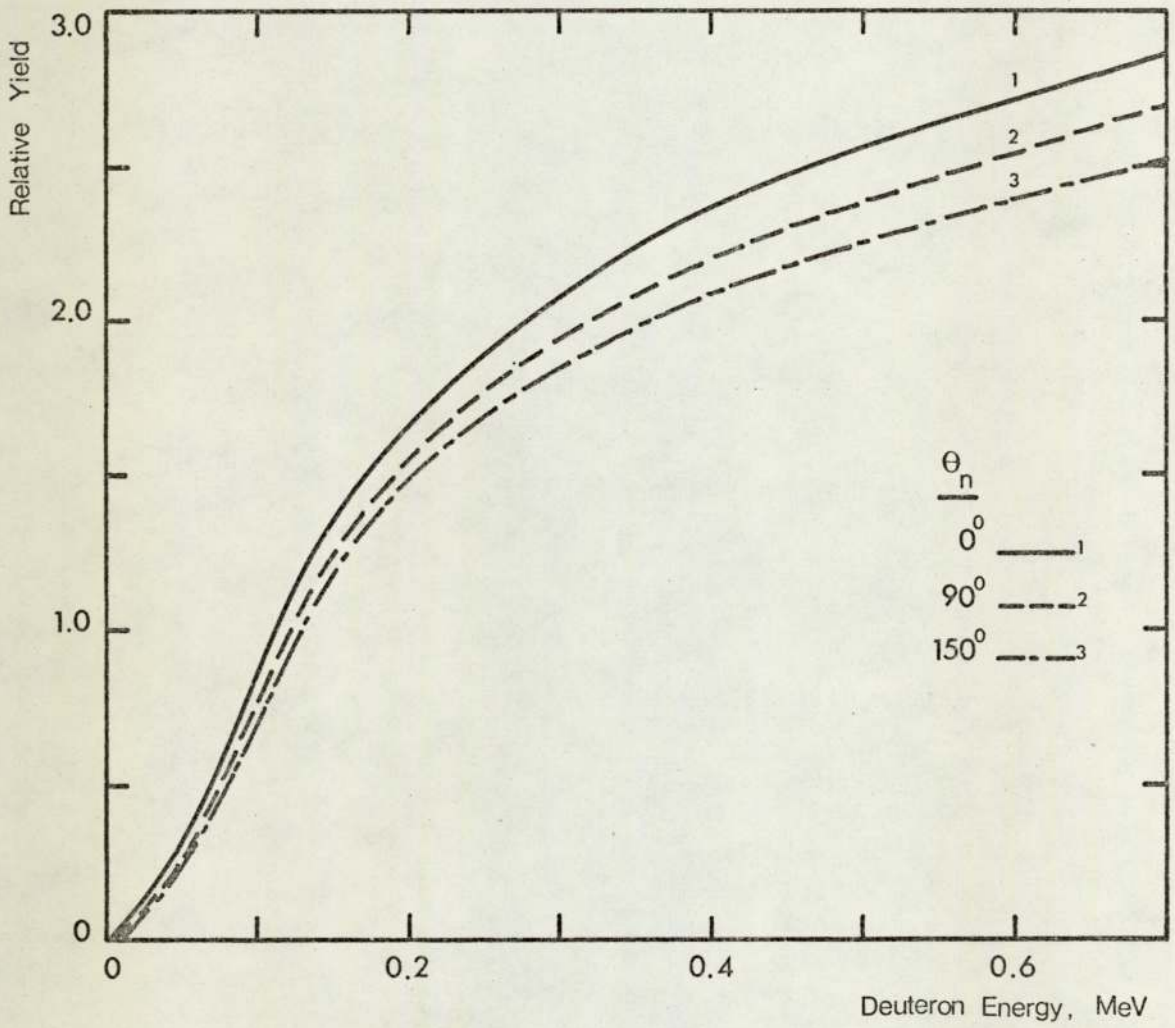

Fig. 3.6

The Variation of D-T Neutron Yield With Incident Deuteron Energy and Emission Angle for Thick T-Ti Target

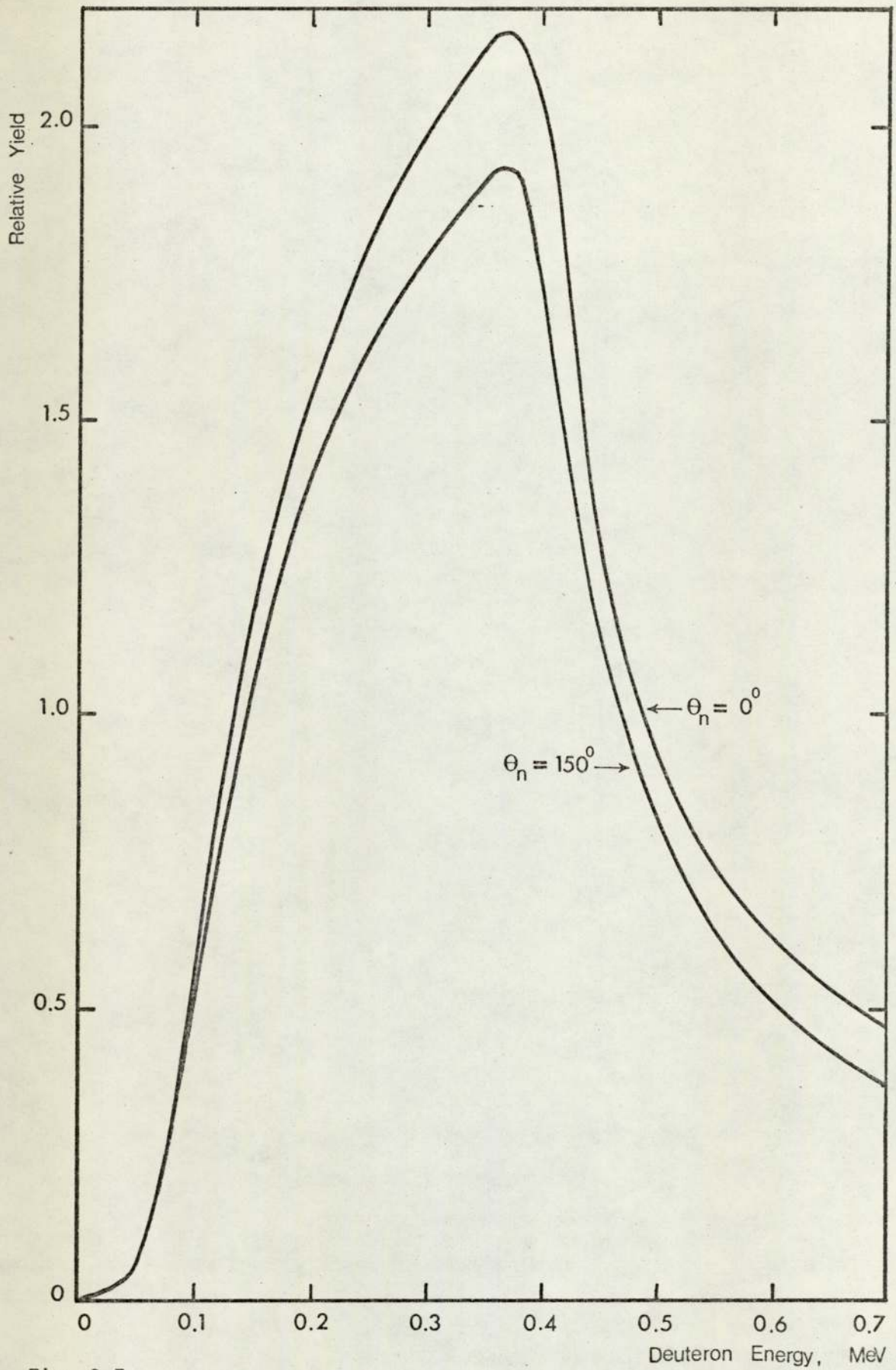

Fig. 3.7

Calculated D-T Neutron Yield Curves For a 1.08 mg/cm^2 T-Ti Target

In the present work, the absolute neutron yield curves are not required, although estimation of the neutron yield curves on a relative scale is worthwhile for calculating the neutron mean energies. This can be achieved by the integration of neutron spectra, which are evaluated on a relative scale using equation(3.15).

The yield curves for thick targets are shown in Fig.3.6 These were determined for deuteron energies up to 0.7 MeV and for different emission angles. For TRT.51 T-Ti target, the titanium layer (1.08 mg/cm^2) is not sufficiently thick to stop completely the deuteron beam above 0.37 MeV. Therefore a fall in the neutron yield is observed at higher energies as is shown in Fig.3.7.

3.4.3 Neutron anisotropy

Although in the centre of mass system of co-ordinates, the angular distribution of the reaction products from the T(d,n)^{4}He reaction is isotropic up to about 0.4 MeV; the case is different in the laboratory system. In the laboratory system the angular distribution of the reaction products is anisotropic even at lower energies, and the anisotropy increases with increasing the incident deuteron energy. Since we are dealing with the laboratory systems, a suitable transformation procedure from the centre of mass system to the laboratory system is required.

Neutron anisotropy is the ratio of neutron flux in the forward to backward directions, but since the neutron flux is isotropic in the centre of mass system, the anisotropy in the laboratory system is equal to the ratio of neutron flux in the lab. system (ϕ_ℓ) to that in the c.m. system ($\phi_{c.m.}$) over the angular range.

Let the angles made by the emitted neutron directions in the lab. and c.m. systems to be θ_ℓ and $\theta_{c.m.}$ respectively. Therefore the neutron anisotropy which equals the ratio between the solid angles in c.m. and lab. system is given by[59]:

$$\frac{dW_{c.m.}}{dW_\ell} = \frac{\phi_\ell}{\phi_{c.m.}} = \frac{\sin\theta_{c.m.}\, d\theta_{c.m.}}{\sin\theta_\ell\, d\theta_\ell} \qquad (3.11)$$

Now, if $$\gamma = \frac{V_{\ell(c.m.)}}{V_{c.m.(n)}} \qquad (3.12)$$

where $V_{\ell(c.m.)}$ = velocity of the c.m. in the lab. system,

and $V_{c.m.(n)}$ = velocity of the neutron in the c.m. system;

Therefore,

$$\cos\theta_{c.m.} = -\gamma \sin^2\theta_\ell \pm \cos\theta_\ell \sqrt{1 - \gamma^2\sin^2\theta_\ell} \qquad (3.13)$$

By differentiating eq. (3.13) we can get

$$\sin\theta_{c.m.}\, d\theta_{c.m.} = \left(2\gamma \sin\theta_\ell + \sin\theta_\ell \sqrt{1 - \gamma^2\sin^2\theta_\ell} + \frac{\gamma^2\cos^2\theta_\ell \sin\theta_\ell}{\sqrt{1 - \gamma^2\sin^2\theta_\ell}}\right) d\theta_\ell \qquad (3.14)$$

Therefore,

$$\frac{dW_{c.m.}}{dW_\ell} = \frac{\gamma(\cos\theta_\ell + 1/\gamma^2 - \sin^2\theta_\ell)^2}{\sqrt{\gamma^2 - \sin^2\theta_\ell}} \qquad (3.15)$$

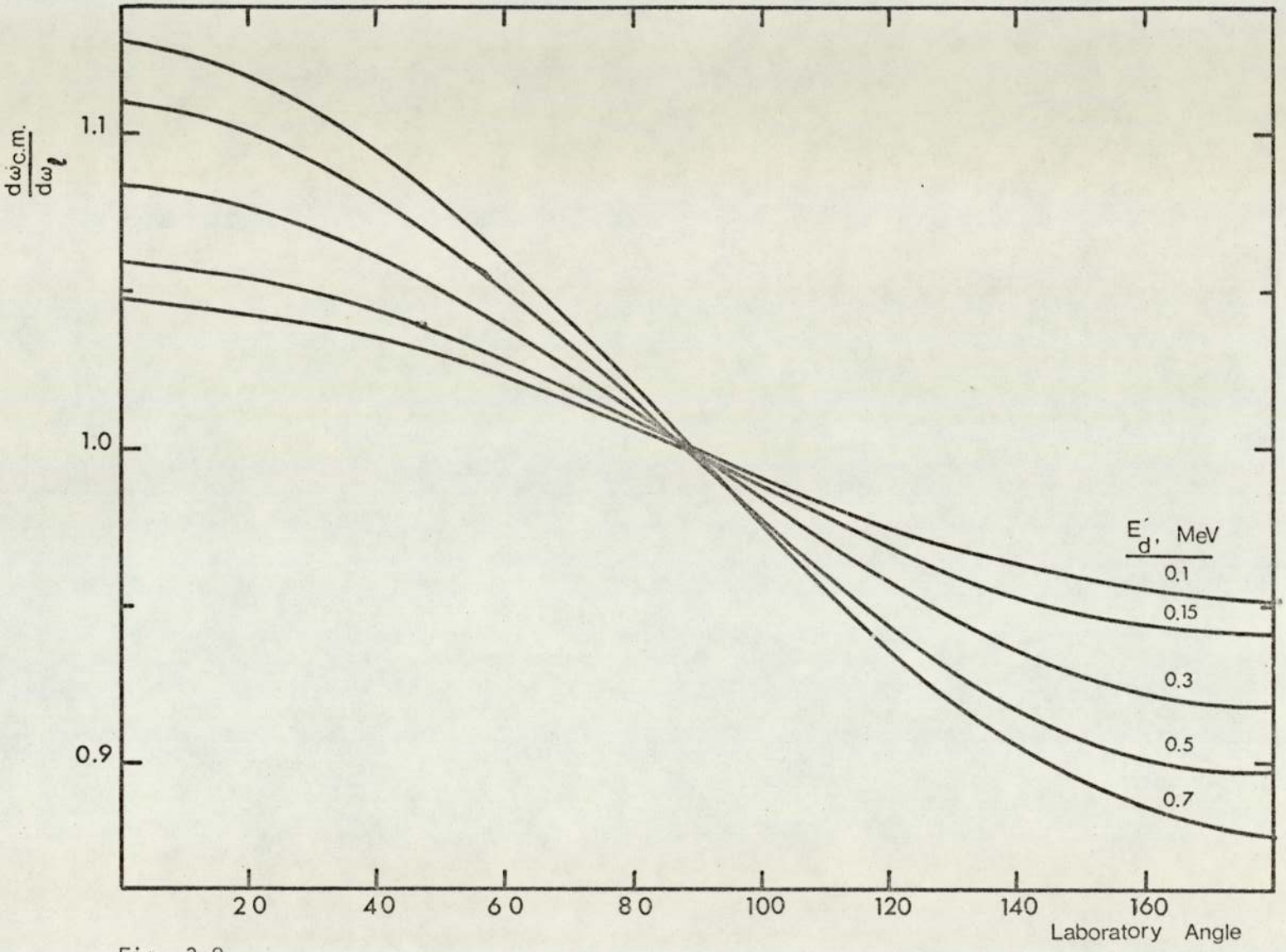

Fig. 3.8

The Ratio of the Solid Angles in the Centre of Mass and Laboratory Systems into which the Neutron is Produced as a Function of the Neutron Laboratory Angle

To evaluate the neutron anisotropy as a function of deuteron energy and lab. angle, the function $\gamma(E_d)$ has to be calculated. According to the kinematics of the reaction and according to eq. ~~3.19~~ 3.9, the following relation is obtained:

$$\frac{1}{\gamma^2} = \frac{M_\alpha}{M_n} \cdot \frac{(M_d + M_t)}{M_d} \cdot \left(\frac{M_t}{M_d+M_t} + \frac{Q}{E_d}\right) \qquad (3.18)$$

Here M_d, M_t, M_n and M_α represent the masses of incident deuteron, tritium nucleus, and the emitted neutron and alpha particles respectively. Q and E_d respresent D-T reaction Q-value and deuteron energy respectively. Fig. 3.8 shows the anisotropy plotted as a function of laboratory angle for different deuteron bombardment energies. These curves were obtained by using the computer programme 'NEUTRED'.

3.4.4 Neutron energies

For very thin targets, it is assumed that the energy spread introduced by target effects is negligible and neutron energies can be calculated from the kinematics of the two-body reaction

i.e.

$$\sqrt{E_n} = \frac{\sqrt{M_d M_n}}{(M_\alpha+M_n)} \cdot E_d \cdot \cos\theta_n \pm \sqrt{\frac{M_d M_n}{(M_\alpha+M_n)^2} \cdot E_d \cos^2\theta_n + \frac{M_\alpha - M_d}{M_\alpha+M_n} E_d + \frac{M_\alpha \cdot Q}{M_\alpha+M_n}} \qquad (3.17)$$

This consideration is not valid once thick targets are used, because of the slowing down of deuterons in the target. Fast neutrons from thick targets are produced by deuterons of energies ranging from the initial incidence energy to zero energy. Therefore the emitted neutrons at a given angle exhibit an energy distribution due to

variation in effective incident deuteron energy. Once the neutron spectra are calculated, mean neutron energies and their energy spreads can be obtained. These calculations are of great importance for the measurement of neutron cross sections where data at specific neutron energies are measured.

Neutron spectra were calculated by using 'NEUTRED' on a relative yield scale by taking into consideration anisotropy, deuteron energy loss, and D-T reaction cross section. The recommended cross section data made by Liskein and Paulsen [41] were used.

If RN = Relative number of neutrons,

ANISO = Neutron anisotropy,

DEL = Deuteron energy loss in T-Ti target,

and DTCRS = D-T reaction cross section

$$\text{Therefore, } RN(E_d,E_n,\theta_n) \alpha \frac{ANISO(E_d,\theta_n)}{DEL\ (E_d)}, DTCRS(E_d,\theta_n) \qquad (3.18)$$

Neutron spectra calculations made by using this relation were obtained in deuteron energy steps similar to those used for energy loss calculations. Laboratory angle was varied in steps of 10^o from 0^o to 180^o. The angle 98^o was also taken into account because neutrons emitted at this angle have the minimum energy spread. Neutrons emitted at 98^o have the nearest mean energy value to 14 MeV which is important as a reference at which absolute cross section results are preferably obtained.

It is clear from Fig. 3.9 that neutron spectra do not show symmetry around the peaks, but as a whole they show a symmetry around 98^o spectrum, with a decreasing peak height as we increase the neutron emission angle. The spectra peaks correspond to neutrons produced by

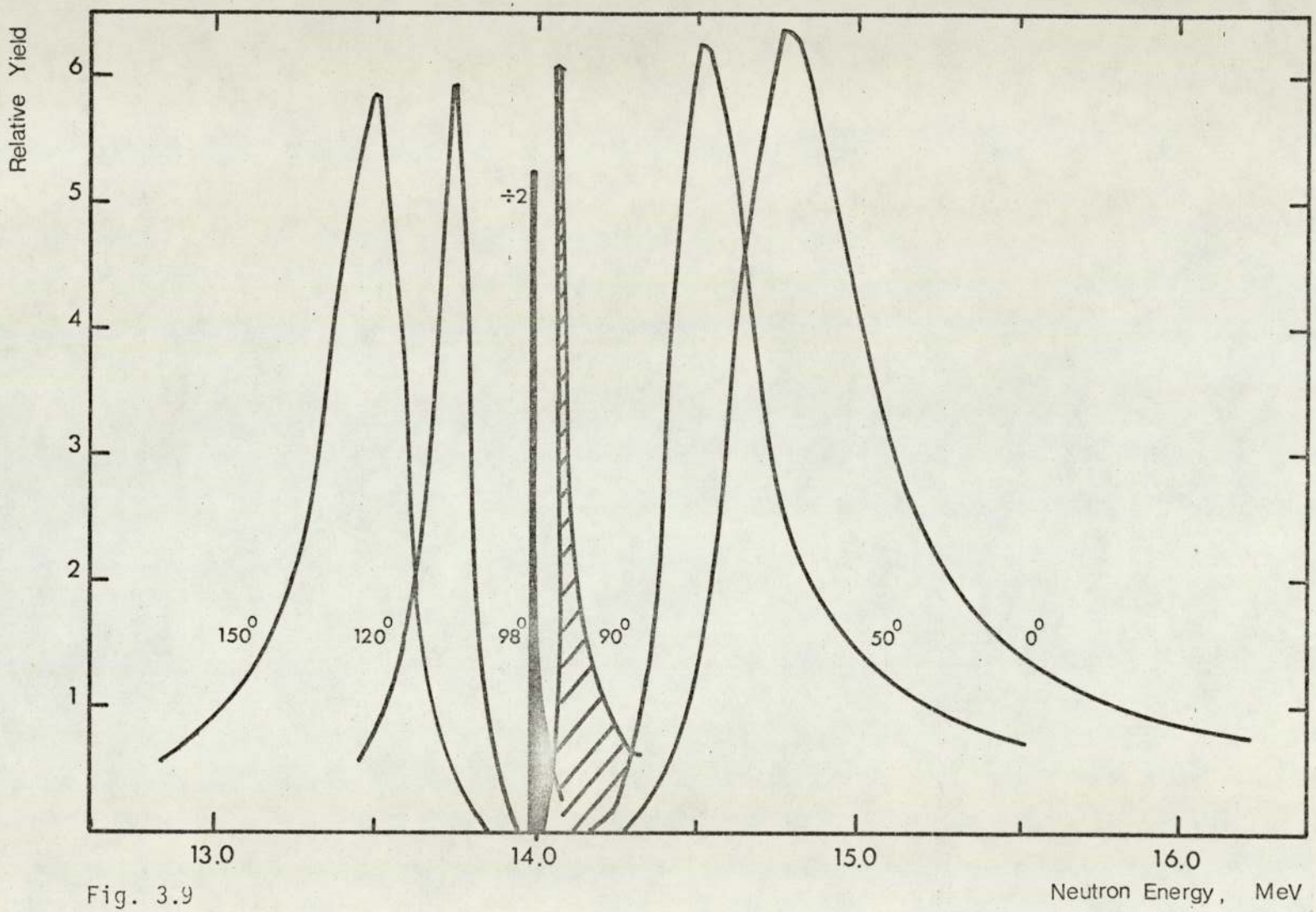

Fig. 3.9

The Energy Distributions for D-T Neutrons at Different Angles of Observation for a Thick Tritiated Titanium Target. E_d = 0.7 MeV

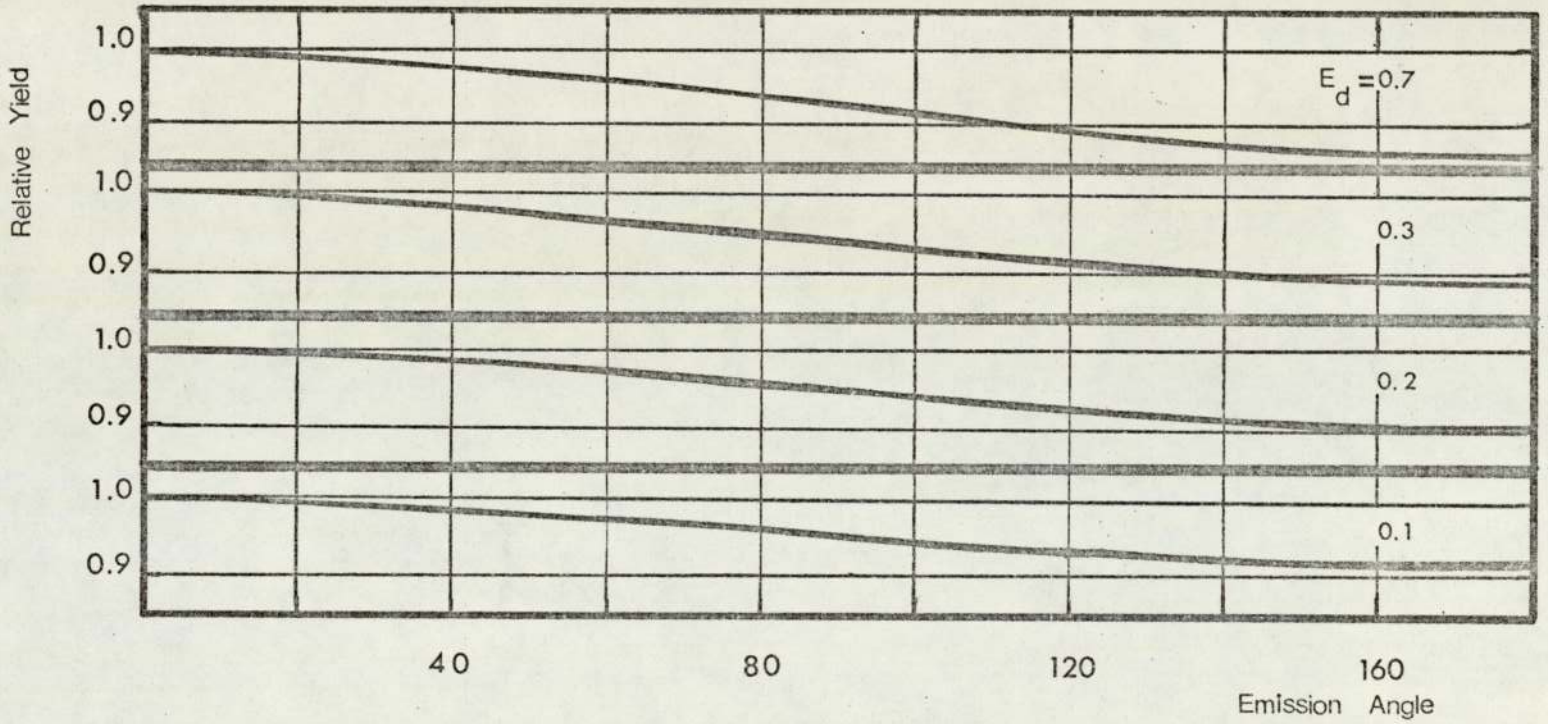

Fig. 3.10

The Relative Angular Distributions of Neutron Intensity for the (d,n) Reaction on Thick Tritiated Titanium Target

0.11 MeV deuterons; the increase in peak height by decreasing θ_n indicates that slightly more neutrons are produced by E_d = 0.11 MeV in the forward direction than in the backward direction, and the same effect ~~phenomena~~ applies to other deuteron energies. This can be demonstrated by determining the neutron angular distribution, Fig. 3.10, which is very important in making the appropriate correction for fast neutron flux slight variation with emission angle.

Neutron spectra were used to calculate the mean neutron energies numerically by using the following relationships for different angles of neutron emission.

$$\bar{E}\ (\theta_n) = \int_0^{E_d} \frac{RN(E)\ .\ E_n(E)}{TRN\ (\theta_n)}\ .\ dE \qquad (3.16)$$

where TRN is the total relative number of neutrons.

The mean neutron energy results are shown in Fig. 3.11, and here the neutron energy spreads due to deuteron energy degradation in the target are determined by the widths at half maxima for neutron spectra. The mean neutron energy range for 0.7 MeV deuteron beam on TRT.51 T-Ti target is wider than that for thicker targets. This is due to the target thickness which corresponds to an energy loss of 0.26 MeV at E_d = 0.7 MeV. Hence, for this case only the neutron groups which are due to the contributions of deuterons with energies between 0.7 and 0.44 MeV are taken into account.

In our case, the additional fractional increase in neutron energy spread due to deuteron multiple scattering has not been taken into account. This is justified because we have been interested in determining the general trends of fast neutron excitation functions. Multiple deuteron scattering effect has to be taken into account if an

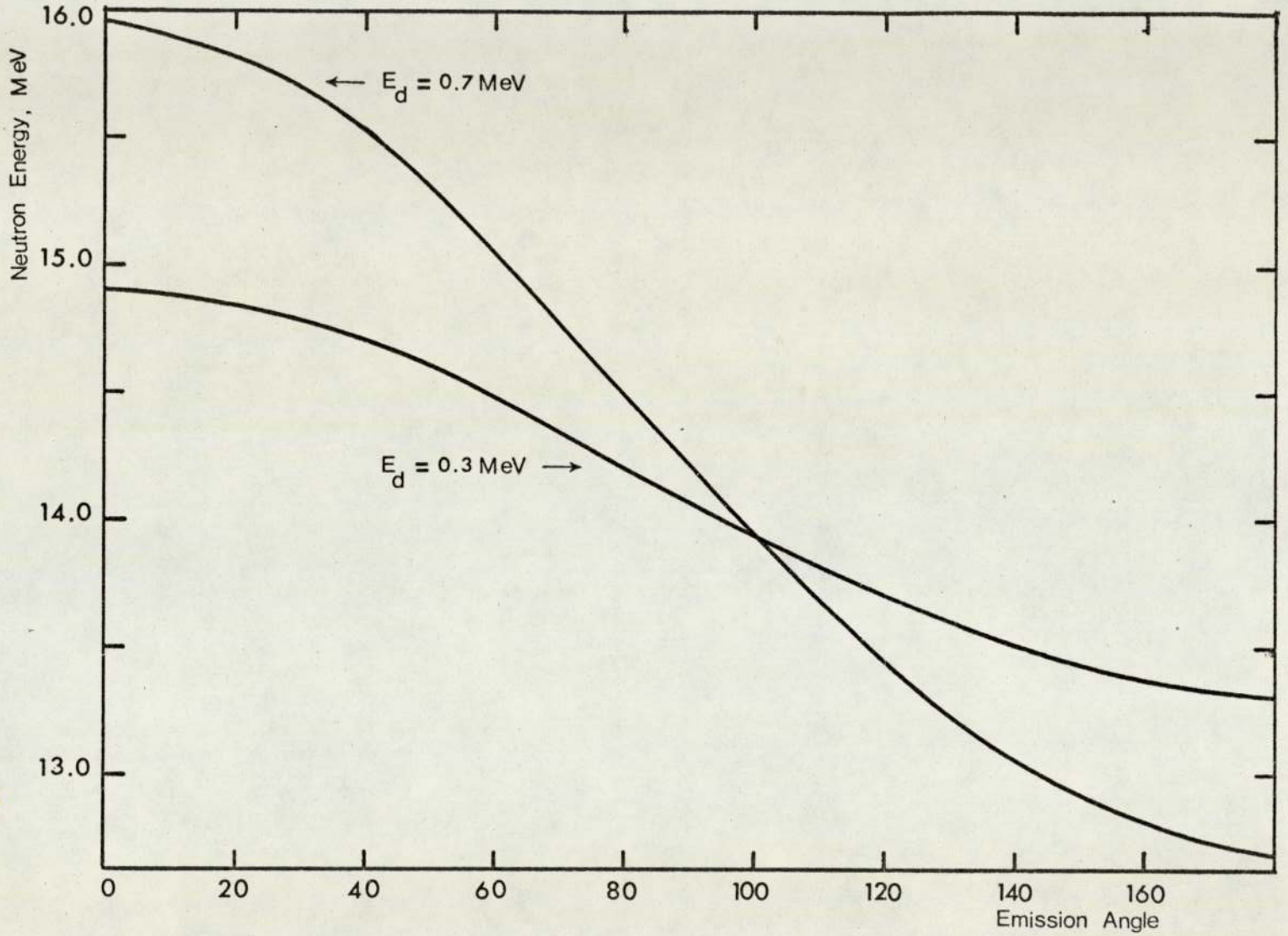

Fig. 3.11

Mean Neutron Energy as a Function of Observation Angle for a 1.08 mg/cm^2 T-Ti Target With a Loading Factor = 1.2

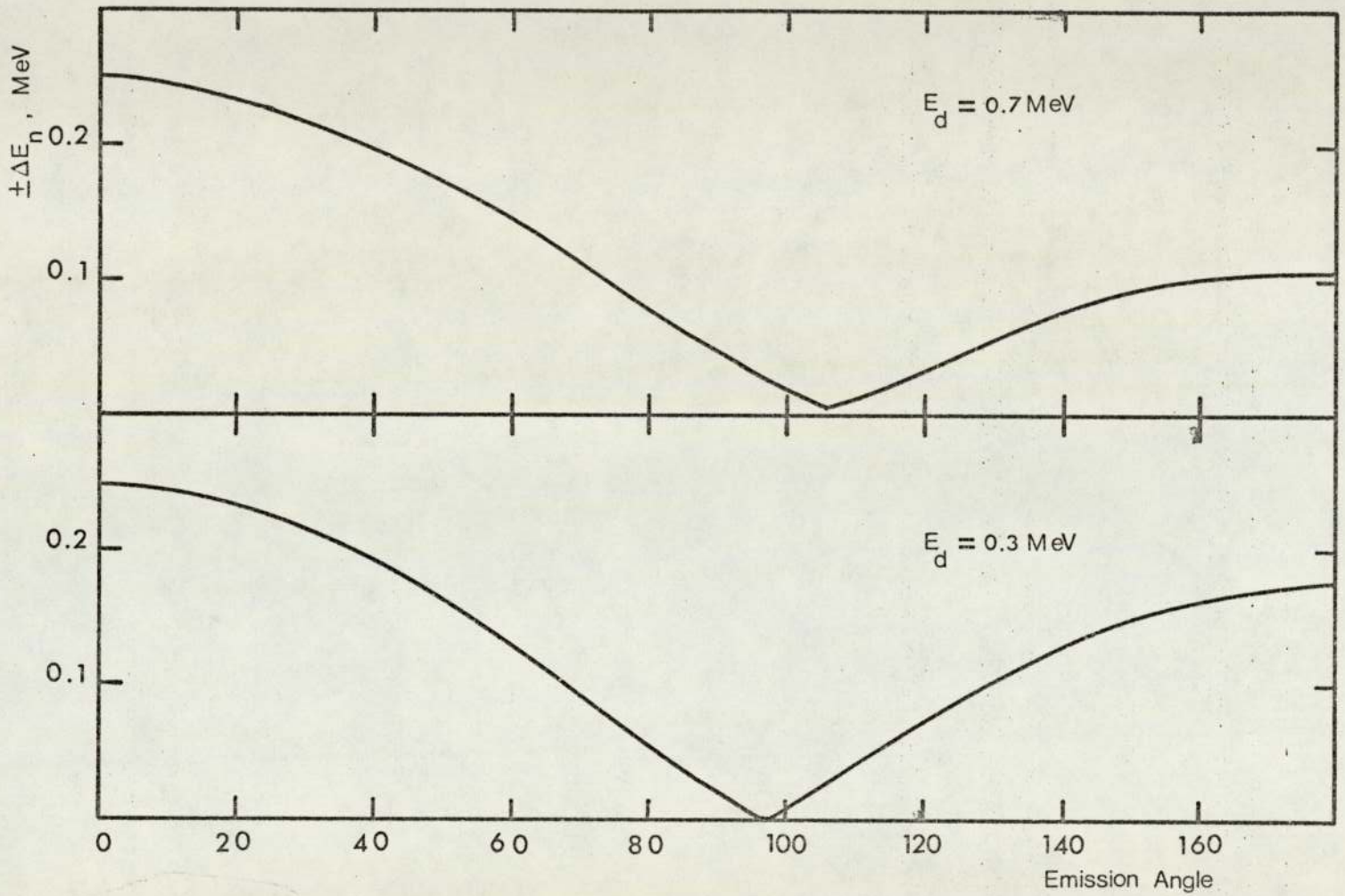

Fig. 3.12

Neutron Beam Energy Spread Due to Deuteron Energy Loss in a 1.08 mg/cm^2 T-Ti Target

attempt to investigate the fine structure in neutron excitation functions is required.

CHAPTER 4

DETERMINATION OF FAST NEUTRON BEAM PARAMETERS

4.1 Fast Neutron Detection

In neutron spectroscopy, the progress in improving neutron detection efficiencies and resolution has direct applications in studying the properties and locations of nuclear energy levels, and this information is required in nuclear terminology where accurate spectroscopic data are very important in reactor design, radiotherapy and activation analysis. Much more work is required for fast neutrons with energies up in the 14 MeV region due to the increasing interest which is being given to the controlled fusion programmes.

Generally, two principles are employed in neutron spectroscopy. The first depends on the (n,p) elastic scattering, by detecting the recoil protons produced. The second method depends on specific neutron reactions and involves determining the energies of the charged particles

produced.

The majority of fast neutron time-of-flight facilities use organic scintillators for the detection of neutrons; these scintillators have high hydrogen content and fast rise and decay times of the fluorescence output. The faster time of the scintillation pulse, with the corresponding better time resolution is an important feature of modern plastic and liquid scintillators which are excellent for coincidence measurements. The use of organic scintillators for fast neutron detection is hampered by the interferences from the gamma-ray background. The separation between neutron and gamma ray contributions is obtained by using pulse shape discrimination techniques which utilize the difference between the pulse shape of light produced by electrons and that produced by protons.

Below about 8 MeV, the (n,p) scattering is sufficiently isotropic in the centre of mass system [65], but above this energy the anisotropy begins to appear and it increases by increasing neutron energy. The lack of accurate 0^{o} differential scattering data of neutrons from protons above 8 MeV leads to uncertainties of more than 2% above 14 MeV, which is a significant contribution to the overall error in a flux measurement by recoiled protons. Therefore, the determination of detection efficiencies for such neutron spectrometers is essential. For example, Cookson et al [66] have carried out recently liquid scintillator experimental efficiency measurements below 30 MeV relative to the associated particle technique.

Generally, the use of neutron induced exoergic reactions, e.g. $^{6}Li(n,\alpha)T$, $^{10}B(n,\alpha)^{7}Li$ is primarily restricted to slow neutron detection by detecting the emitted energetic charged particles. By using neutron moderators, neutron detectors based on such reactions can also be used

for fast neutron detection, e.g. the use of BF_3 counter as a flat response Long Counter. Alternatively, fast neutron detection is more commonly carried out by using fast fission and threshold reactions in which the emitted particles are more difficult to detect. In this case the radiation emitted by the residual nuclei are detected, i.e. the activation method.

4.2 Some Activation Methods for the Measurement of Accelerator Fast Neutron Source Properties

4.2.1 Neutron spectra

Although fast neutron spectra measurements can be done by the known measuring techniques such as scintillators, solid state detectors, and proton recoil telescopes; the threshold detectors technique has been considered more reliable. The threshold detectors method, which was developed originally for reactor physics studies [67], requires a rather small amount of effort. It has also the advantages of being insensitive to non-neutron radiations and presenting negligible perturbing effects on neutron flux distributions. The technique's basic requirements are knowing the threshold energies and having sufficient accurate information about the absolute neutron cross-sections as functions of neutron energy. By covering the entire neutron energy range which is under investigation with the threshold detectros, with suitably spread thresholds, one can obtain accurate and detailed information about fast neutron yield, spectrum and angular distribution.

A proposal was made by Heertje [68] to use the threshold detectors for measuring the properties of neutrons produced by irradiating Be, Al, Co, Ag and Ta targets by 26 MeV deuterons fron a cyclotron. Although the use of threshold detectors in the early works was affected by the

limited availability of accurate data on neutron excitation functions, valuable information concerning the effect of target atomic weight and deuteron beam energy on the neutron flux and spectra were obtained. It was concluded by Heertje [68] and Heertje et al [69] that the accelerator fast neutron spectra can be described by an expression similar to that used for fission spectrum.

Also using this assumption, Bruninx and Crobeen [70] were able to study the neutron spectra of a thick beryllium target under the bombardment by 20 MeV helium-3 ions, 14 MeV protons and 7.5 MeV deuterons using the threshold detector method. Foils of carbon, aluminium, copper, silicon and indium (the reaction thresholds of which range between 0.5 MeV and 20 MeV) were irradiated as a compact sandwich at a given distance from the neutron source and in the forward direction. Following the irradiation, the corrected disintegration rate of each foil was fitted to the activation equation. The neutron flux at the sandwich position was then found by substituting the average cross-section value in the activation equation and making the appropriate corrections.

$$\phi = \frac{A}{M.\bar{\sigma}} \qquad (4.1)$$

Measurements of neutron angular distributions for each charged particle reaction were made on aluminium foils placed at different angles with respect to the incident charged particle beam direction. The activity at each angle as formed by the $^{27}Al(n,\alpha)^{24}Na$ reaction was related to the activity at (0^o) to determine the corresponding fluxes (n/sec. μA. cm^2) from the relation

$$\phi(\theta) = \frac{A(\theta^o)}{A(0^o)} . \ \phi(0^o) \qquad (4.2)$$

It should be noted here that no corrections for the $^{27}Al(n,\alpha)^{24}Na$ reaction cross-section variation with energy are given, therefore, when (r) is the distance from the neutron producing target, the total neutron yield will be given by:

$$N(n/sec.\ \mu A.\ 4\pi) = 2\pi r^2 \int_0^{\pi} \phi(\theta).\ \sin\theta\ .\ d\theta \qquad (4.3)$$

For a sealed tube D - T neutron generator, Lawson et al [71,72] established a simple activation method for measuring neutron production rate and scattered neutron fraction. The authors proposed the use of a set of threshold detectors taking into account the reaction excitation function of each detector from the threshold energies to about 15 MeV and normalizing the excitation curves to unity at 14.75 MeV. The 14.75 MeV flux densities at a given distance from the neutron source were plotted against the threshold energies and the variation trend with threshold energy indicated the presence of degraded neutrons. Also a peak centred in the region 13.5 - 15 MeV was found during spectra measurements when the response of each detector was represented by the equation:

$$\phi_{exp} = \sum_{i=1}^{n} \frac{\bar{\sigma}_i}{\sigma_{14.75}}\ \phi_i \qquad (4.4)$$

where

ϕ_{exp} = The experimental flux density deduced using the 14.75 MeV sensitivity factor,

$\bar{\sigma}_i$ = The average cross-section in the ith energy interval

n = The number of detectors used,

and ϕ_i = The mean flux density in the ith interval.

The variation of neutron flux and energy along a neutron generator axis with and without the presence of a moderating material (polythene) was the subject of an investigation by Oldham and Darrall [73]. A set

of threshold reactions with threshold energies varying between 6.3 and 15.6 MeV was used, and the method was based on suppressing the activities produced on the materials of higher threshold energies by using the moderating material. By selecting the appropriate polythene thickness the incident neutron energy was reduced by an adequate amount. The results are useful for 14 MeV activation analysis of elements which give radioactive nuclei having the same principle γ-energies and similar half-lives.

4.2.2 Neutron yields

By using the continuous flow manganese bath, which was originally produced for yield measurements of radio isotopic neutron sources, Scott [74] measured the yield of Li, Be, Co and Cu targets under the bombardment by 5 to 10 MeV protons. The neutron source was placed at the centre of an 85 cm. diameter sphere containing a solution of manganese, and the irradiation solution was then pumped continuously to a remote counting chamber containing a NaI detector. Due to the shorter half-life of ^{52}V compared with ^{56}Mn, the proposal to use vanadium as the activated element was made by De Valpi and Porges [75] for isotopic neutron sources, and later adopted for the accelerator measurements by Atta and Scott [76]. The continuous flow bath has limited applications and compared with threshold detectors it is more complicated. It provides information about neutron yields only.

To measure the neutron yield of a thick beryllium target, Bruninx [77,78,79] has used a cadmium shielded paraffin-indium detector as proposed by Stephens and Smith [80]. The method employs the activation of indium via the reaction $^{115}In(n,\gamma)^{116m}In$ by thermal neutrons resulting from the moderation of fast neutrons in a paraffin-wax sphere

shielded by cadmium foil. The detector has to be calibrated by a neutron source of known yield, and again it does not give any indication of the neutron energy spectrum. As reported by Bruninx, this detector gives higher neutron yield results compared with the threshold detectors due to the different shape of the angular distributions of neutrons with lower energies. The effect of lower energy neutrons is here more pronounced because the paraffin box is essentially an integrating device. Therefore care has to be taken to minimize the effect of lower energy neutrons in different irradiation environments.

4.3 14 MeV Neutron Flux Monitoring

4.3.1 Integral flux monitoring methods

On-line neutron integral output monitoring is useful for estimating the fast neutron flux and its changes for subsequent irradiations. It can also be utilized as the sensor for a servo-mechanism to control the neutron flux. Such flux monitoring can be achieved by using a neutron detector such as a proton recoil based detector or moderated BF_3 counter. For a good discrimination against lower energy neutrons, ZnS scintillator can be used to detect alpha particles produced by the $^{12}C(n,n')3^4He$ reaction on carbon foil, good stability and accuracy of 1% compared with standard copper foil[81] were reported. Alternatively, fast neutron flux monitoring can be done by counting the ^{16}N activity induced in the tritium target cooling water [82], although a rather poor precision is obtained due to the fluctuation in water flow rate [83].

By using the associated particle method, neutron flux determination with accuracies better than 2% is obtainable for the $T(d,n)^4He$ reaction. The α-particles produced by the reaction are counted in a well defined geometry and with very high efficiency by using an appropriate detector. At low deuteron bombardment energies the reaction angular distribution is expected to be isotropic, and therefore α-counting can serve to determine directly the neutron flux in any cone at any laboratory angle. The good energy separation between the emitted α-particles and the high yield scattered deuterons is advantageous specially for eliminating the pile-up which is introduced by the amplification system even with very short time constants. For using the associated particle method one has to take into account the interferences due to deuterium and carbon build ups which lead to the formation of new products via the (d,p) and (d,n) reactions. Furthermore, for old tritium targets α-backgrounds are produced by the (d,p) reaction on ^3He which is formed by tritium β-decay. At deuteron bombardment energies below the $^3He(d,p)^4He$ resonance at 0.44 MeV, the contribution of this interfering effect is negligible [84]. Non-uniformity of tritium loading in the target is usually considered as the most serious limitations of this method [85], and according to Fieldhouse et al [86] this effect has to be estimated by a coincidence method. In this case the tritium density distribution is determined by observing the coincidences between the emitted 14 MeV neutrons and associated alpha particles, and defining the deuteron reaction energy and hence the reaction depth according to the lab. angles of neutron and alpha detectors.

For experiments involving neutron cross-section measurements or activation analysis, the integral flux monitoring systems share generally

similar major disadvantages. As has been indicated, the D-T neutron flux changes with time during irradiation, and practically such changes are irregular and irreproducible. Therefore, magnitudes of the induced activites, specially for short-lived isotopes will be highly dependent on such changes.

4.3.2 Flux monitoring by standard materials

By monitoring the neutron flux with a standard containing an element yielding activity of a half-life approximately equal to that of the element to be analysed, the instantaneous fluctuations due to neutron production rise and fall are followed and corrected for. The standardisation of flux monitoring reactions is essential to establish interlaboratory comparison of fluxes, and establish a common basis for the determination of fast neutron fluxes for cross section measurements and activation analysis. The following set of critera is presented here to summarise the requirements for the precise selection of 14 MeV neutron flux monitoring standards.

1. The monitor material must be simple to handle, obtainable in high purity, and preferably contain predominantly one stable isotope.

2. The residual nucleus should be radioactive and must emit a γ-ray. It is very much advantageous if no chemical separation is required to count the product activity.

3. The emitted gamma rays should have a simple γ-ray spectrum and preferably it would emit only a single gamma line.

4. The γ-rays from the residual nucleus must be in the proper energy range for detection by standard gamma detectors.

5. The half-life of the residual nucleus should be of a convenient length and of a value close to that of the sample.

6. The monitor reaction cross-section variation with energy is very small or similar to that of the sample.

7. Matching the reaction thresholds for monitor and sample is beneficial to eliminate the effect of neutrons with degraded energies.

8. The excitation function of the monitor should be accurately known to take into account the neutron energy spread specially when monitor is placed close to the neutron source. This is also applied to the sample, and in both cases the incident neutron energy should be well known.

The "Texas Convention" was proposed at the 1965 Conference on Modern Trends in Activation Analysis [87], and it has stated normalized conditions for fast neutron flux measurements by a standard. A 99.9% copper disc of 1 cm or 2.5 cm diameter and 0.25 mm thick should be irradiated for 1 min. by 14 MeV neutrons. The induced β^+ activity formed by the $^{63}Cu(n,2n)^{62}Cu$ reaction, is then measured by sandwiching the monitor between two lg/cm^2 thick plastic beta absorbers for complete β^+ annihilation. After a minimum cooling time of 1 min, the sandwich is positioned along the central axis and 3 cms apart from the surface of 3" x 3" NaI(Tl) crystal. The measured flux will be then given in terms of the corrected number of disintegrations per min. per gram of Cu. Standard procedure for calculating the corrected disintegration rate for the copper standard is given by Heath [88].

Recommending the $^{63}Cu(n,2n)^{62}Cu$ reaction offers only single cross-section response with energy and single half-life. To form common basis for 14 MeV cross-section measurements and activation

analysis one has to establish a collection of standard reactions offering a wide range of excitation functions trends and half-lives. Flux monitoring by using copper standard is restricted to irradiations of less than 30 min. [$^{63}Cu(n,2n)^{62}Cu$, $T_{\frac{1}{2}}$ = 9.5 min] or for irradiations lasting more than several hours [$^{65}Cu(n,2n)^{64}Cu$, $T_{\frac{1}{2}}$=12.8h]. Accordingly, Shiokawa et al [89] have investigated the $^{19}F(n,2n)^{18}F$ excitation function on Teflon [$(CF_2)_n$] as an alternative standard. The $^{19}F(n,2n)^{18}F$ is suitable for irradiations of intermediate time ($T_{\frac{1}{2}}$ = 1.87h), but on the other hand the cross-section in the 14 MeV region is nearly one order of magnitude lower than that of the $^{63}Cu(n,2n)^{62}Cu$ reaction.

On the basis of excitation function slope, the $^{63}Cu(n,2n)^{62}Cu$ reaction does not seem to be ideal since its cross-section is a very steep function of energy. Alternatively, the use of $^{27}Al(n,p)^{27}Mg$ reaction has been suggested by Partington et al [90] due to its nearly flat response in the 14 MeV region. Actually, $^{27}Al(n,p)^{27}Mg$ cross-section is relatively low, and therefore a much more powerful standard is proposed in this thesis, i.e. $^{121}Sb(n,2n)^{120g}Sb$, and this is explained in Chapter 8.

CHAPTER 5

GEOMETRIC FACTORS AFFECTING THE D-T NEUTRON FLUX AND ITS MONITORING

5.1 The Non-Uniformity of 14 MeV Neutron Irradiation

Of more importance than time stability are D-T flux variations as a function of irradiation position. Several experimental [91-94] and theoretical [95-99] studies have been reported on the neutron flux distributions around tritium targets. Sample/target irradiation geometrical factors are also important, and these also have been the subject of several publications [100-104].

The fast neutrons produced by the D-T reaction for irradiation purposes have variable energies and fluxes due to such factors as 1) the variations in sample to target geometry, 2) neutron scattering and absorption [16,105], 3) non-uniform loading of tritium in the target [85], 4) deuteron beam diameter and conditions, 5) build-up of deuterium and depletion of tritium in target [106] and 6) scattering

from neighbouring materials. Therefore, each accelerator installation has its own neutron flux distribution patterns which are sensitive functions of several perturbing effects. This means that the use of a "universal standard" for flux estimation such as the $^{63}Cu(n,2n)^{62}Cu$ reaction can lead to inaccuracies due to anisotropy and inhomogeneity of the neutron flux. In fact the measured integrated activity on a sample must be related to a calculated average energy of the neutron flux through appropriate scattering calculations such as those proposed by Ricci [105].

5.1.1 Production of lower energy neutrons

For standard target/sample forward geometry using water cooled targets, Ricci used probability calculations to estimate the fractions of unscattered and scattered neutrons that are reaching the sample. In his particular geometry the results indicate that 58.4% of the neutrons are of the direct and unscattered type, while 27.4%, 7.6% and 6.8% are those due to scattering in target assembly aluminium and cooling water jacket hydrogen and oxygen respectively. The neutron energy ranges for the scattered neutrons are determined by taking into account first-order single scattering and using the non-relativistic scattering equation [107].

$$E_n' = E_n \cdot \frac{A^2 + 2A\,\mathrm{Cos}\theta + 1}{(A+1)^2} \qquad (5.1)$$

where A is the mass number of scattering nucleus, and θ is the scattering angle in the centre-of-mass system or the laboratory system for $A > 10$.

The neutron spectrum is formed by the direct and scattered components. While the direct component and the scattering component

from hydrogen are assumed to be rectangular within their corresponding energy ranges, the scattering components of aluminium and oxygen are assumed to be triangular. The triangular shapes with positive slope hypothenuses, are here determined by the forward peaking of the scattered neutrons angular distributions for Al and O [108] which enhance the high energy parts.

Due to the high neutron energy loss per collision with hydrogen nuclei, the presence of water in the vicinity of the neutron source will lead to the formation of a tail in the energy spectrum extending down to very low energies. Therefore 14 MeV nuetron flux measurement by $^{27}Al(n,\alpha)^{24}Na$ reaction will ~~und~~over estimate the flux by 14%, double that obtained by $^{63}Cu(n,2n)^{62}Cu$ reaction for the geometrical set-up of Ricci. This can be attributed to the threshold energy of the aluminium reaction which is much lower than that of the copper reaction. For an experimental set-up that produces 14 MeV neutrons within much narrower energy spectrum, less pronounced deviation of the results is expected due to the elimination of the threshold energy difference effect.

In most of the neutron generator facilities, the neutron producing target is housed in a limited space. In the majority of cases this is due to neutron shielding problems, and as an example we refer here to the "hole in the ground" geometry for sealed tube generators. Therefore additional low energy neutron background is expected to exist in the vicinity of the target due to neutron scattering by walls and nearby equipment. This effect is more pronounced if samples are placed far away from the target.

Interference effects due to deuterium build-up in the tritium target can be corrected for by using the corresponding element response

data for 3 MeV neutrons. It is possible to estimate the D-D neutron flux build-up which is a function of deuteron energy, integrated beam current, and target thickness.

At this point, we would like to emphasis that cross-section measurements for reactions with low thresholds should be carried out under improved irradiation conditions. This includes eliminating the effect of hydrogenous materials and the use of new tritium targets. Even then it is necessary to apply the appropriate corrections. For example, the use of the $^{27}Al(n,p)^{27}Mg$ reaction for 14 MeV flux monitoring would require full details concerning the experimental arrangements and in particular those about the cooling water and deuterium build-up. The effect of energy degraded neutrons discussed previously should also be taken into account.

The failure to fulfill such requirements will impose some doubts on the proposed use of Partington et al,[90] aluminium excitation function as a standard. Perhaps neutron scattering can also explain the rather low slope of their excitation function in the 14 MeV region.

5.1.2 Neutron flux patterns

For uniform target assemblies, like those used in this work, one would expect the fast neutron flux patterns to be nearly uniform around the neutron source, with slight anisotropy which is a basic property of the $T(d,n)^4He$ reaction in the lab. system. But, for other target assemblies larger flux pattern non-uniformities can be observed. Mapping the neutron flux distribution is useful for excitation function measurements and should materially aid the activation analyst in ensuring that the best irradiation configuration is being utilized for

the particular sample configuration being used. Simple techniques based on the use of photographic films and standard copper and teflon samples, have been studied by Priest et al. [93] to carry out such measurements. The measurements by Priest et al. [93] and Oldham and Bibby [94] indicate clearly the presence of flux angular anisotropies around the target due to angle-dependent neutron attenuation. The equiflux lines determined by Oldham and Bibby [94] reveal a "waist" effect due to neutron attenuation in the thick cooling jacket rim and target edges. As an example, by using the appropriate macroscopic cross-section it can be estimated that 1 cm of copper can be found to produce a 12% attenuation to 14 MeV neutron flux.

The neutron flux pattern properties are dependent on neutron absorption and scattering, therefore existence of enhanced scattered neutron yields can be expected at those angles which correspond to the "waist" effect. This can be estimated mathematically by means of numerical integration over the contribution of all volume elements of the target assembly and backing to the intensity for a particular angle. The scattering correction factor used by Vorach et al. [16] is based on such calculations and is given by

$$\frac{1}{(1 + \phi_{sc}(\theta)/\phi_{direct}(\theta))}$$

and for their particular experimental set-up the required corrections were up to 2.9%. For a uniform target assembly the correction factor should be nearly constant for all irradiation angles. In general, neutron flux pattern symmetry about the generator axis can be maintained if uniformity of the tritium distribution in the target is kept by using a uniform deuteron beam under good ion source operating conditions.

In fact, target deterioration leads to significant flux asymmetry of up to 30 per cent at short distances from the target [91], but the asymmetry decreases by increasing the distance. Practically, irradiation at large distances is not feasible because of the deterioration in the sensitivity due to the reduction of neutron flux with distance.

Systematic errors due to secondary neutron production by multiple reactions, i.e. (n,2n), (n,n) and (n,pn), in the target assemblies are negligible for the measurement of threshold reaction cross-sections. The situation is different for the measurement of 14 MeV neutron capture cross-sections [109], and in this case target assembly material, sample dimensions, and sample/target separation are very critical factors. Therefore, accurate relevant corrections are required for (n,γ) measurements [110,111].

5.1.3 General properties

It is obvious from the characters that we have discussed in this section that the optimization of neutron irradiation is dependent on the specific installation used. But, it will be worthwhile stressing here that neutron generating facilities share some common characters, such as neutron flux gradients. This fact has therefore prompted theoretical treatment of this general problem to the stage where its effect can be estimated with reasonable accuracy.

It is known that for a point radioactive source, the radiation intensity drop-off with distance can be well expressed by $1/R^2$ function. For 14 MeV neutron source, the $1/R^2$ relationship seems to hold at large distances but is not valid within very short distances from the tritiated metal target [92]. At such distances, a 1/R

relation is a better approximation. This is of course due to the fact that the target is not a true point source. Thus the neutrons must travel one or two target diameters before approaching the $1/R^2$ relation. Along the deuteron beam direction, the axial neutron flux distribution (ϕ_r) can be expressed in terms of the flux at target surface (ϕ), target radius (d), and distance from target (r) in the following form [95]:

$$\phi_r = 0.58\ \phi \log_{10} \frac{d^2 + r^2}{r^2} \qquad (5.2)$$

Although enhancement and time stability of neutron production are expected to take place by increasing the deuteron beam diameter, the relevant calculations by Op de Beeck [96] have shown that this increases in axial flux gradients and to a lesser extent reductions in the laterial flux gradients. To account for the effect of variation in target radius and distances from target axis and its plane, Price [112] has carried out comprehensive calculations to estimate the neutron flux.

5.1.4 Improvement of fast neutron irradiation homogenity

To establish the conditions of maximum analytical accuracy for activation analysis with 14 MeV neutrons, the effects of spatial and time fluctuation of irradiating flux on random errors have to be determined. According to the recent calculations by Vass et al. [113], random fluctuations in detected counts of an irradiated sample are related by a simple formula to the small changes in parameters describing the sample position and irradiating flux. Experimentally, effects of the changes in these parameters can be reduced by spinning the sample. In this case two major systems have been reported for reproducible routine neutron activation purposes, and have demonstrated

reasonable levels of reliability. At close separations form the target where the flux gradients are high, the concept developed by Anders and Bricken [114] depends on rotating the cylindrical sample perpendicularly to the beam axis and along its longitudinal axis. A similar system was also produced by Vogt and Ehman [115], and the rotation can be performed either mechanically or by means of an air jet.

To irradiate sample and standard simultaneously, a dual biaxial rotor system was proposed by Guinn and Wagner [116], Mott and Orange[117], and Wood et al. [118]. The suggested systems are based on rotating sample and standard simultaneously around their longitudinal axes and around the deuteron beam axis. The dual biaxial rotation systems require positioning at large distances from the target, and therefore smaller neutron fluxes are obtained. On the other hand, the longitudinal axis rotation systems do not eliminate the effect of transverse neutron flux gradients.

5.2 The Limitations of Fast Neutron Flux Monitoring Techniques

5.2.1 The separate monitoring foil technique

In this technique, fast neutron flux is measured in terms of the induced activity on a standard material placed at a laboratory angle different from that of the sample. Due to neutron anisotropy, the monitor foil will be exposed to neutrons of different energies and flux; therefore appropriate corrections should be made. Changes in deuteron beam conditions could cause the variation of neutron flux to occur in different manners at monitor and sample positions.

More accurately, the absolute neutron flux at sample position can

be estimated by averaging the activities produced in two monitor foils placed on both sides of the sample. Let us consider a sample and two monitors of identical diameters ~ 1 cm, at about 10 cm distance from the neutron source. In such geometry each of them will be subtending an angle of about 12^{o} on the target. At a mean angle of 90^{o}, Fig. 5.1, the corresponding energy spread across the triple system will be approximately $\pm$ 0.25 MeV for 0.3 MeV deuterons on the tritium target. The flux averaging procedure will be then dependent on the linear variation of neutron flux and monitor cross-section within an 0.5 MeV interval.

$$\text{i.e.} \qquad \frac{\phi_{m_1} + \phi_{m_2}}{2} \sim \phi_s \tag{5.3}$$

where ϕ_s, ϕ_{m_1} abd ϕ_{m_2} are neutron fluxes at the positions of sample, monitor no. 1 and monitor no. 2.

This assumption is not very accurate for close separation from the neutron source due to the enhanced neutron energy spread, but short distance irradiation is desirable for better sensitivity.

In the forward direction, the conditions for flux averaging at close separation from the tritium target are more complicated, see Fig. 5.1.

$$\text{Although } \phi_{m_1} \sim \phi_{m_2}, \tag{5.4}$$

$$\frac{\phi_{m_1} + \phi_{m_2}}{2} < \phi_s \tag{5.5}$$

which is due to neutron flux anisotropy.

It is advisable to replace the sample by a third monitor and compare its induced activity with the activities of the other two monitors. This is necessary for estimating the accuracy of the determined

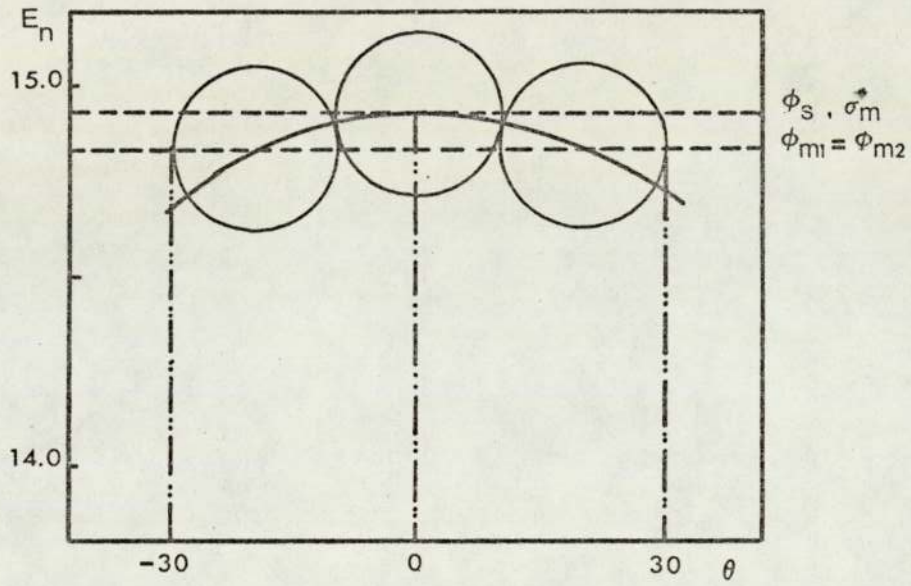

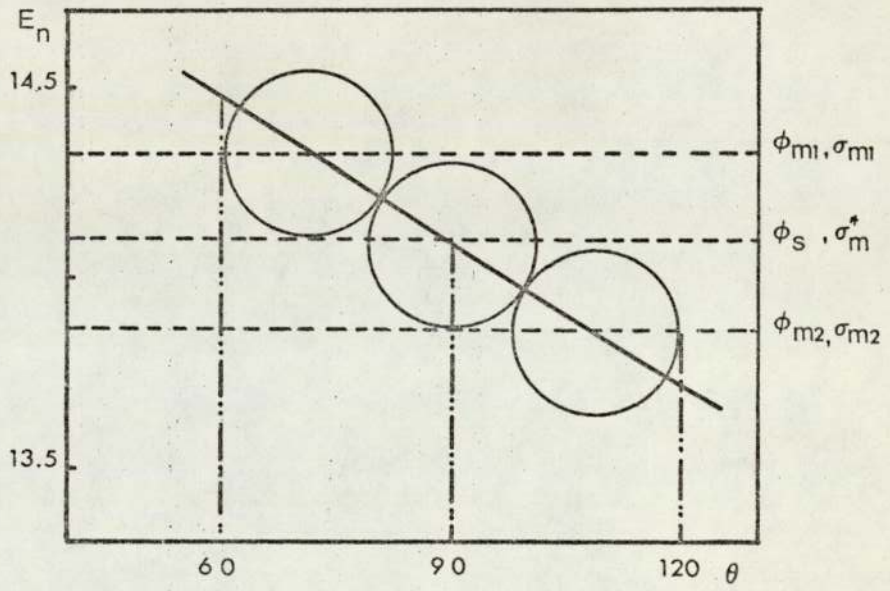

Fig. 5.1
Limitations of Neutron Flux Averaging By the Separate Foil Technique

neutron flux at sample position. The difference in the measured activities between the three monitors will be in this case due to the monitor cross-section variation with energy and due to neutron flux variations.

$$\frac{\sigma_{m_1} + \sigma_{m_2}}{2} \sim \sigma^*_m \quad \text{at } 90^o \tag{5.6}$$

$$\sigma_m = \sigma_m \neq \sigma^*_m \quad \text{at } 0^o \tag{5.7}$$

where σ_{m_1}, σ_{m_2} and σ^*_m are monitor cross-sections at the corresponding monitor 1 and 2 positions and at sample position.

This method will therefore yield information about the estimated flux at sample position, and it is dependent on the accuracy of the monitor excitation function and its slope.

Perhaps the best approach to the separate foil system is to place the two monitors on the circumference of the angle at which the sample is positioned. This method will ensure that monitors and sample are exposed to neutrons of similar mean energies. The advantages of this method will not be fully exploited unless a constant neutron attentuation is provided over the whole angular range of neutron emission by a specially designed target assembly.

By monitoring the neutron flux with a standard material, errors are usually introduced due to the uncertainties in the cross-section data of the standard. Fast neutron flux monitoring is best performed with the sample element if accurate standard cross-section data are not available, although this is no longer possible for multielemental determinations. The relative activities of comparator and sample will be then proportional to the relative concentrations by assuming the

exposure to a constant neutron flux. Although the absolute neutron cross-sections are not required in this case, the variation trends of neutron cross-sections with energy are needed.

5.2.2 The sandwich foil technique

Fast neutron flux can also be estimated by sandwiching the sample between two foils of the standard flux monitoring material. In this technique, which is widely used for cross-section measurements, corrections for the monitor reaction cross-section variation with energy are not required. This is due to the fact that the three components of the sandwich are being placed at the same mean laboratory angle. The situation for incident neutron flux measurement is rather more complicated since it is affected by the readial flux gradient and neutron screening as described below.

1. Due to the finite thickness of the sample and monitors, they will be effectively situated at different distances from the neutron source. Therefore they will be exposed to a neutron flux of negative gradient. This effect is more pronounced for short distances due to the 1/R flux dependence. The magnitude of the introduced systematic errors will be then determined by the components' thickness, and by their positions with respect to the target. From the results of Op de Beeck [95], it appears that at R = 1 cm and R = 1.8 cm, an axial displacement of 0.1 cm will correspond to a flux variation of 14% and 8.5% respectively.

2. By irradiating the sample and monitors in a sandwich geometry, a neutron screening effect will be experienced by the sample and back monitor. This is determined by the thickness (d_m) and macroscopic cross-section (Σ_m) of the front monitor in the case of the sample. Similarly, the back monitor will be screened by the front monitor plus the sample which has its own thickness (d_s) and macroscopic cross-

section (Σ_s). The estimated flux as determined by averaging those measured on the monitor foils should then be corrected for neutron screening in the sandwich. This is of course in addition to the radial flux gradient. For such calculations, removal macroscopic cross-section data are used [119,120,121]. The concept of removed cross-sections, as used in reactor shielding design, was found experimentally to yield better results for 14 MeV neutron attenuation than the use of total cross-sections [122,123].

Basically, two identical flux monitoring standards can be irradiated behind each other yielding at the end of irradiation similar activities, but with a screening effect factor due to front monitor upon back monitor, i.e. exp ($-\Sigma_m d_m$). If the monitor is now irradiated behind the sample, the screening factor will be changed to exp ($-\Sigma_s d_s$). Such experiments will therefore provide essential information for cross-section measurements by the sandwich technique, and also for activation analysis.

Several systems have been described for oxygen analysis in metals by the simultaneous irradiation of sample and standard behind each other [47,122,124]. In these cases a single comparator containing a known concentration of oxygen is irradiation behind the sample. Gijbels et al [122] have reported detailed study of this method for industrial routine analysis, and explained the necessary comparator calibration procedure to determine oxygen concentration in the sample.

5.2.3 The mixed powder technique

To eliminate the errors obtained by using the sandwich foil technique, the mixed powder technique was suggested by Rao and Fink [125] as an alternative for fast neutron cross-section measurements. In their publication, Rao and Fink applied this method for the measurement

of $^{74}Se(n,2n)^{73g}Se$ and $^{77}Se(n,2n)^{76}Se$ cross-sections at 14.4 MeV. Flux monitoring was performed internally by mixing a powder of the material under investigation with powder of the flux monitoring material. For measuring the (n,2n) reaction cross-section on ^{74}Se and ^{77}Se, the $^{56}Fe(n,p)^{56}Mn$ cross-section was used as the primary standard, and in addition $^{27}Al(n,\alpha)^{24}Na$ as the secondary standard on the other set of samples. To detect the gamma activities produced by the (n,2n), (n,p) and (n,α) reactions, it was necessary to use a Ge(Li) detector, and the known ratio of iron and aluminium cross-sections was used for checking the results. The limitations associated with this method for general applications are indicated below.

1. Materials in powder form are required, and they should have the same grain size; but even so the problems of incomplete mixing can be comparatively high. The attenuation of 14 MeV neutron beam is described by an exponential absorption law.

$$\frac{\phi}{\phi_o} = \exp(-\Sigma d) \qquad (5.8)$$

where ϕ = neutron flux after traversing the sample,

ϕ_o = neutron flux without the sample present,

d = the sample thickness,

and Σ = macroscopic cross-section for 14 MeV neutrons

Therefore attenuation of neutron flux by the sample will make the inner parts less active than the outside. In such conditions the incomplete mixing of powders will lead to the formation of variable concentration distributions of the monitor material across the sample thickness and diameter.

2. The gamma ray spectra from more than one element could be difficult to resolve, and basically a Ge(Li) detector is required. The situation in the experiment of Rao and Fink is ideal since the material to be examined is pure, as required mostly for cross-section experiments. In general cases, this situation can not be expected, such as in routine activation analysis, due to the impurities present in the sample which cause interferences.

3. The choice of the standard material for flux monitoring, on gamma spectroscopy basis, is restricted to reactions leading to gamma lines that do not coincide with those of the material being examined. This restriction can be removed by employing radio-chemical separation, which is not advisable for routine activation analysis and cross-section measurement specially when short-lived radio-activity is to be examined.

CHAPTER 6

THE CONCENTRIC RING TECHNIQUE FOR THE MEASUREMENT OF FAST NEUTRON FLUXES AND ENERGIES

6.1 Fast Neutron Flux Measurement

The recommendations made by different researchers in the field of fast neutron flux monitoring have been generally toward establishing some neutron cross-sections as standards. As we have indicated earlier, this approach has been followed without taking into account the different experimental conditions. Also, no recommendations have been made so far toward establishing a universal activation technique as a standard for fast neutron flux monitoring to overcome the variation in irradiation conditions effect.

The limitations mentioned previously for separate foil, sandwich foil, and mixed powder techniques cast doubts on their use as the basis of a standard technique in fast neutron monitoring. Therefore, it seems that an alternative technique is required as a standard for use by different laboratories. Such a technique should require minimum

number of corrections and yields negligible errors to improve the accuracy of fast neutron activation analysis and minimize the discrepancies in fast neutron cross-section data.

Accordingly, we present here a summary of the characteristics that we propose for new sample/monitor geometry to obtain improved fast neutron flux monitoring.

1. Sample and monitor are placed at the same distance from the source to eliminate the flux gradient corrections due to sample/source and monitor/source separation difference.

2. They are exposed to neutrons with approximately the same average energy to eliminate the errors due to different excitation functions of monitor and sample. The neutron energy should be above the reactions thresholds unless appropriate correction due to threshold energy difference is introduced.

3. They can be transferred to the counting equipment so that their activities can be measured simultaneously, or they can be separated easily for subsequent counting.

4. They should have equal thickness and distinct boundaries to minimise the corrections due to self-absorption. The advantage of this is also reflected on matching the flux gradients and calculating the average neutron fluxes.

5. No neutron screening effect should be presented by either the monitor or the sample upon the other.

These conditions appear to be satisfied by using a sample in the form of a disc surrounded by a concentric ring of the flux monitoring material. In this thesis, the term thickness will represent the distance traversed by the incident fast neutron beam, and width

will represent the difference between the outer and inner radii of the ring.

6.2 Accuracy of the Technique

The accuracy of fast neutron flux measurement by the concentric ring technique is determined by the ring's width and its corresponding subtended angle on the neutron source. A photograph of a concentric ring/disc set is presented in Fig. (6.1). Also an illustration of the relative dimensions of the ring and disc system is given on a neutron energy scale for 0^{o} and 90^{o} and shown in Fig. (6.2). This is for E_d = 0.3 MeV on a thick T-Ti target.

For a given sensitivity the dimensions of the ring are determined by the neutron flux, disc dimensions and the monitoring reaction cross-section. For reasonably high reaction cross-section, the amount of the monitoring material required to obtain good gamma counting statistics is usually small. Therefore, for ideal conditions, the width of the ring is expected to be very small and the additional θ-ψ angle subtended by the ring is negligible compared with that subtended by the disc (Fig. 6.2). For the experiments which we have performed using a copper flux monitoring ring and aluminium disc, the experimental geometry was such that ψ = 12.32 degrees and θ = 13.0 degrees. In fact, this represents an angular spread of only about 5% which corresponds to a neutron energy spread of $\pm$ 5 keV at 90^{o}. At other laboratory angles where the neutron energy variation with angle is lower than 90^{o}, the energy spread will be smaller.

Only the outer edges of the monitoring ring are exposed to neutrons of higher or lower energy than is the sample, and as this represents

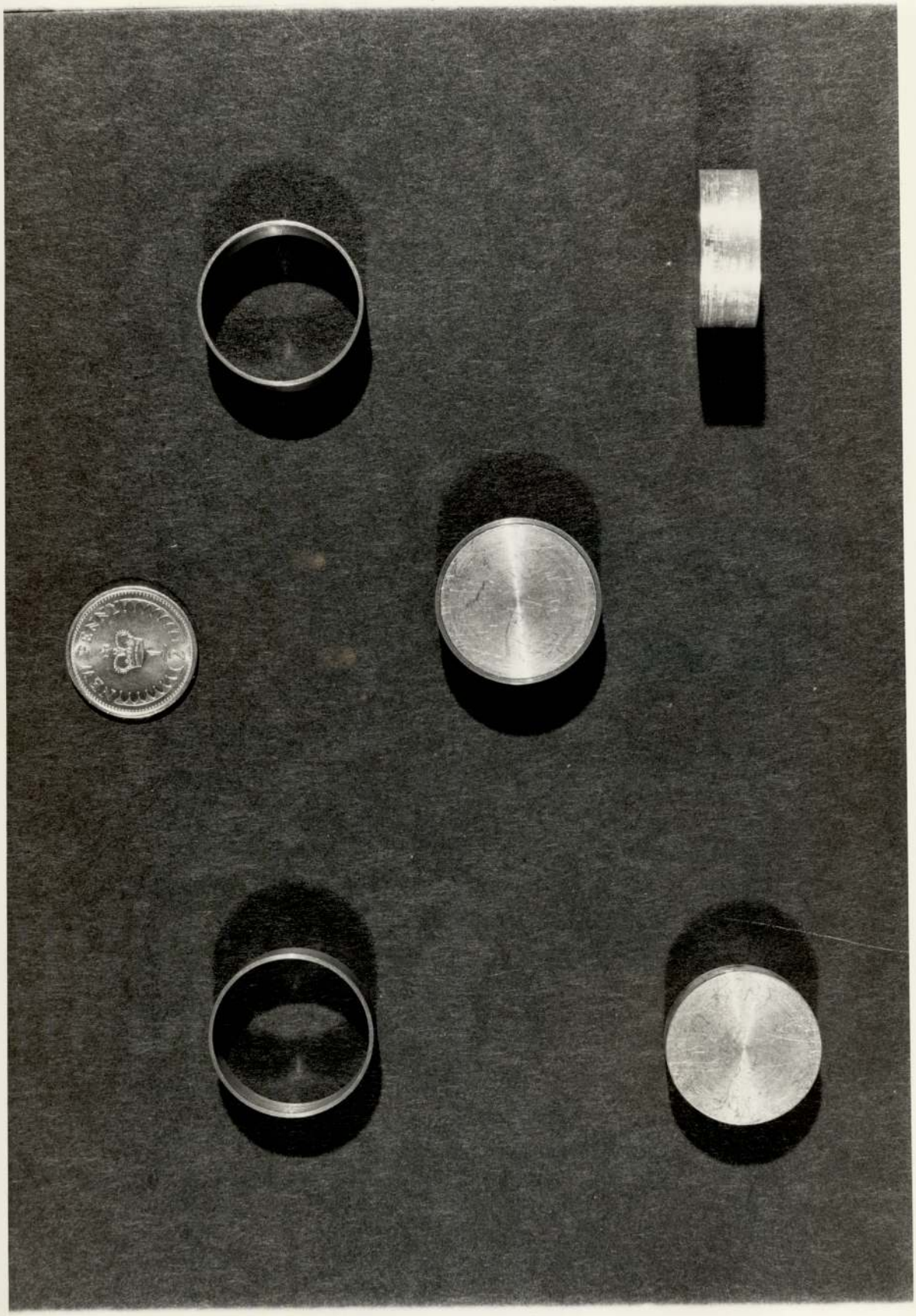

Fig. 6.1 Concentric Ring/Disc Samples

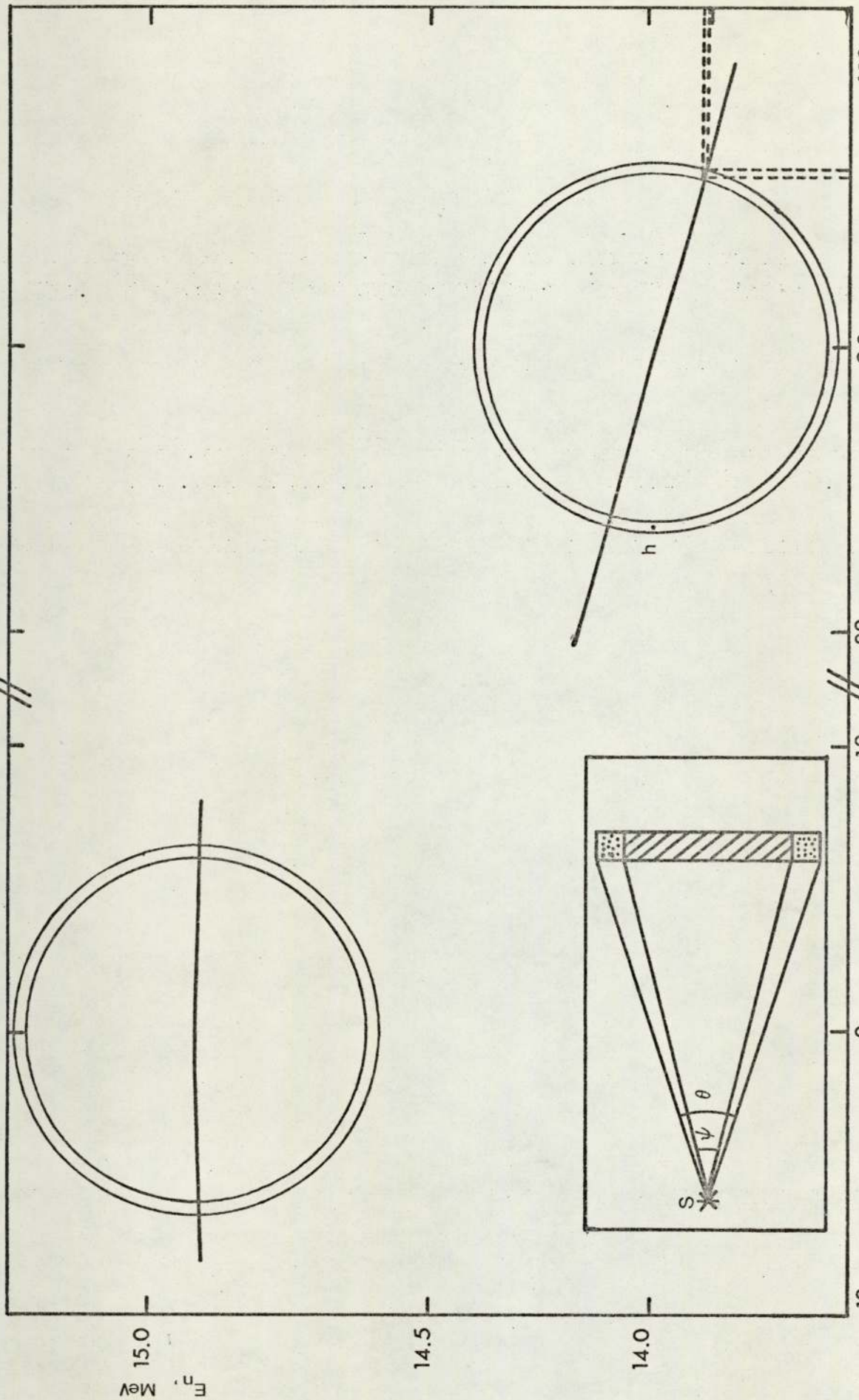

Fig. 6.2
A Concentric Ring/Disc Sample on a Neutron Energy Scale

a small fraction of the total ring area, the error is not great. Let us consider for example a point at half the ring's width, i.e. point h at the 90^{o} position as shown in Fig. (6.2). This point will be then corresponding to an energy spread of approximately 2.5 keV compared with the nearest point of the disc.

Suppose we have now an excitation function with a positive slope of 20% MeV^{-1}; therefore point h will exhibit a cross-section variation of 0.05% only compared with the disc edge, and the cross-section variation is even smaller for other laboratory angles. It should be kept in mind here that with such geometry, the small additional neutron energy spreads are actually experienced by very small fractions of the ring and therefore the overall effect is even less. Corrections for wider rings can be calculated mathematically. Also, we have produced an experimental method to estimate this correction as shown in the next chapter.

It has already been proposed that the disc and ring should have equal thicknesses and the importance of this can be demonstrated if we try to calculate the average neutron fluxes. Let us assume a homogeneous unidirectional neutron flux incident perpendicularly on a concentric ring/disc sample. Therefore, the average neutron flux within the sample can be expressed in terms of the incident neutron flux (ϕ_o), material linear thickness ($\chi = \chi_r = \chi_d$) and the macroscopic cross-section (Σ_r or Σ_d). Here, r and d are corresponding to the ring and disc.

$$\bar{\phi} = \phi_o \left[1 - \exp(-\Sigma x)\right] / \Sigma x \qquad (6.1)$$

The average neutron flux can also be represented by the local neutron flux at a depth equal to px for $0 \leq p \leq 0.5$, by using the basic exponential relation.

Therefore,

$$\phi_o[1 - \exp(-\Sigma x)]/\Sigma x = \phi_o \exp(-\Sigma p x) \qquad (6.2)$$

This solution can be then simplified to yield the required value of p.

$$\text{i.e.} \quad p = \frac{2.302}{\Sigma x} \log \frac{\Sigma x}{1 - \exp(-\Sigma x)} \qquad (6.3)$$

For our concentric ring configuration the magnitudes of $(\Sigma_r x)$ and $(\Sigma_d x)$ are less than unity due to the small macroscopic cross-sections for 14 MeV neutrons. Obviously, this means that $p \sim 0.5$ and the average neutron flux is given by the local flux at a point which is half the way along the material thickness.

$$\text{i.e.} \quad \bar{\phi}_r = \phi_o \exp(-\Sigma_r \frac{x}{2}) \qquad (6.4)$$

$$\text{and} \quad \bar{\phi}_d = \phi_o \exp(-\Sigma_d \frac{x}{2}) \qquad (6.5)$$

This leads finally to the following expression for a disc and ring of equal thickness.

$$\frac{\bar{\phi}_d}{\bar{\phi}_r} = \exp[(\Sigma_r - \Sigma_d) \frac{x}{2}] \qquad (6.6)$$

6.3 Fast Neutron Energy Measurement

The discrepancies in fast neutron cross-section data can partially be attributed to the inaccurate estimation of incident neutron energy. The impact of this inaccuracy is expected to be pronounced for these measurements which are sensitive functions of neutron energy. For measurements that include steep excitation functions or fine structure

investigations, accurate values of the neutron energies are required, and errors due to monitor and sample positioning have to be eliminated.

Measurement of fast neutron energies in the 14 MeV region is difficult to carry out compared with lower energy regions. These measurements have to be carried out at the sample position and they have to be made during sample irradiation to eliminate positioning errors and take into account time and geometrical variations of neutron beam.

Cox and Jarjis [126] have suggested that the variation in the ratio of the absolute activities of two materials could be used to measure neutron energy, if the slopes of their excitation functions were different. Their experiment was based on irradiating a compressed powder composite made of two different materials and they determined an accuracy of 2.1% in the 14 MeV neutron energy measurements. The use of the concentric ring configuration appreciably extends the application of this technique and increases its accuracy. Also, by activating two concentric rings of selected materials either alone or surrounding a disc of the material under investigation it is possible to measure fast neutron flux and energy simultaneously.

The two materials selected for flux and energy measurement by this technique should have the following properties:-

1. They should have reasonably high cross-sections for good sensitivity, and their excitation functions should be well-known.

2. The ratio of cross-sections for the two materials should be a steep function of neutron energy to obtain high sensitivity to energy changes with sample position. For example, ideally one excitation function should have a large positive gradient and the other a large

negative gradient.

3. The two materials should have nearly equal half-lives to reduce the effects of any instabilities in neutron production.

4. The gamma rays emitted by the two materials and used for the calculations should be well separated in energy if the induced activities are required to be counted simultaneously.

5. The properties for ideal standard flux monitoring material, (Section 4.3), should also be applied to the standard energy measuring materials.

6. The cross-section ratio curves, determined by using the accurate excitation functions, are required to establish good reference standards.

6.4 Modification of the Technique

The errors introduced by using concentric ring monitors for large target to specimen separations are small but for small target to specimen separation the increased spread in neutron energies experienced by a uniform ring becomes noticeable. This is shown in Fig. 6.3, and in this case the areas A and B of the ring are exposed to wider ranges of neutron energies than the rest of the ring and the circular disc. For example, let us consider a sample consisting of a 3 cm diameter disc surrounded by a 1 cm wide ring. Therefore, for a separation of 2 cm from the neutron source a specimen in the forward direction would be exposed to a range of neutron energies from 14.74 to 14.91 MeV, and the monitoring ring to a range from 14.60 to 14.91 MeV. These are data for 0.3 MeV deuterons on thick

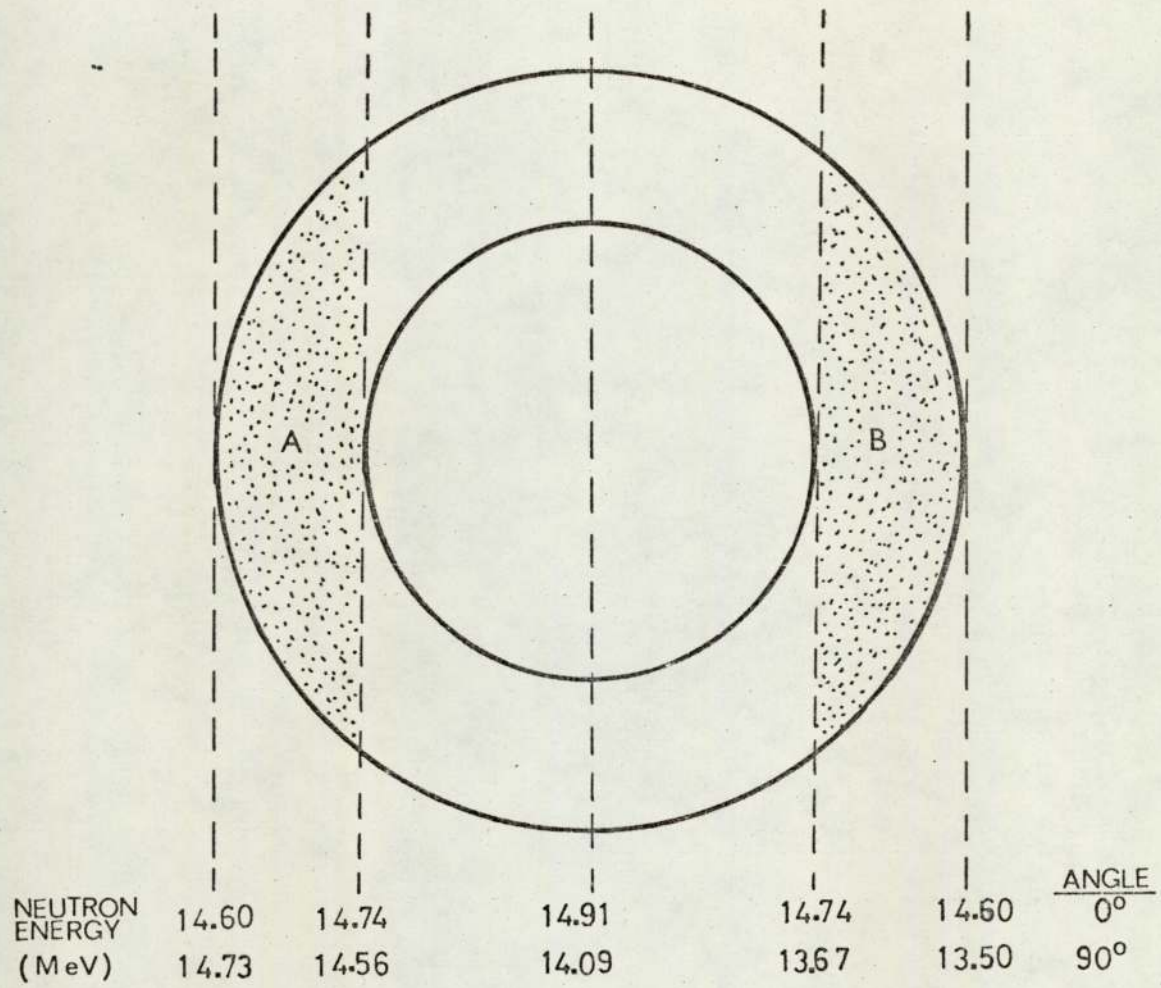

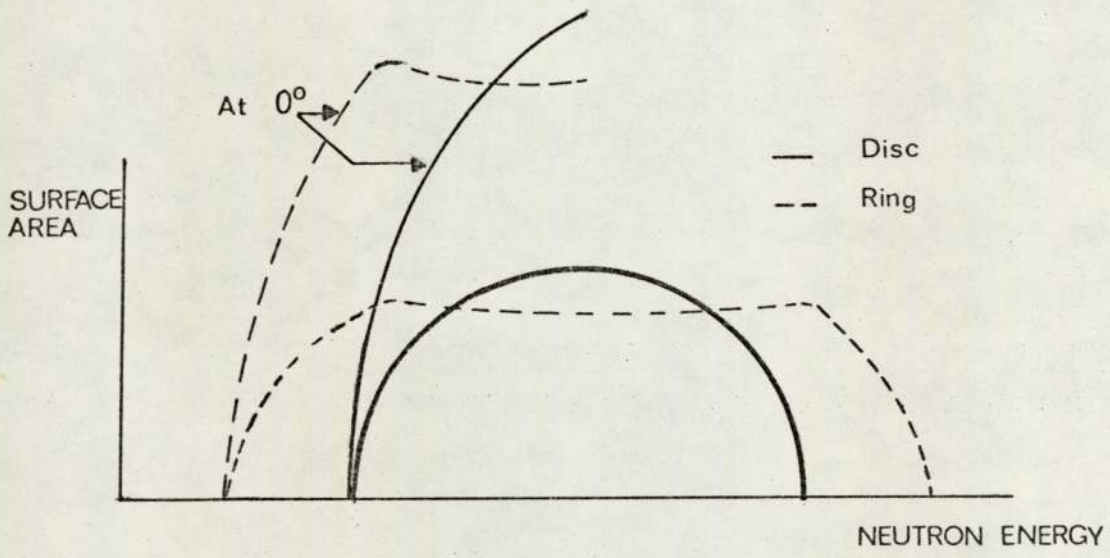

FIG. (63) THE CONCENTRIC RING/DISC SAMPLE AT A SHORT SEPARATION FROM THE TARGET.

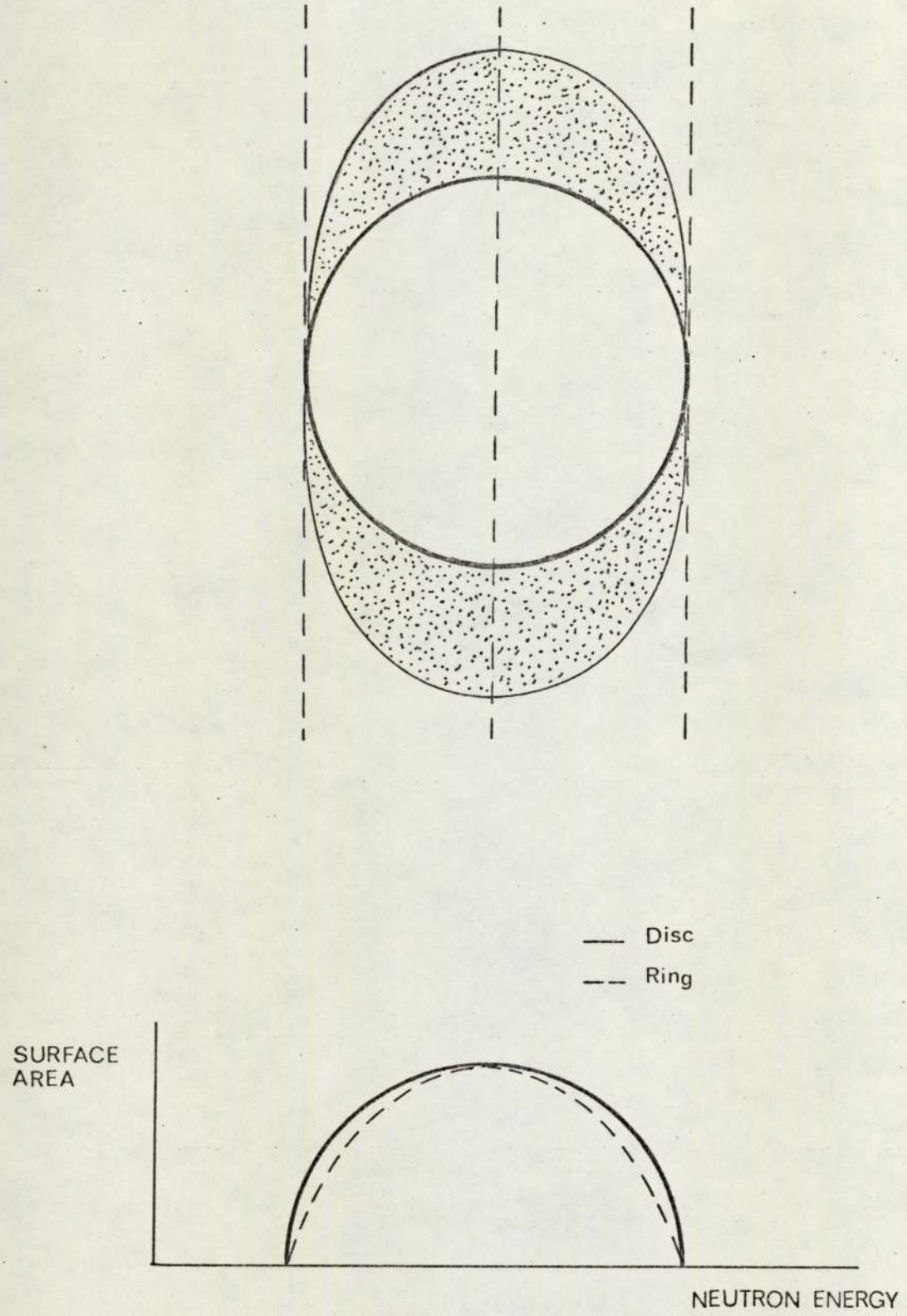

FIG.64) THE MODIFIED CONCENTRIC RING.

tritium target. At 90^{o} the corresponding energies will be 13.67 - 14.56 MeV for the specimen and 13.50 - 14.73 MeV for the ring.

The effect will be small for smooth excitation functions and can be minimised by using a specially designed ring as shown in Fig. 6.4 such that the area of the ring exposed to neutrons of particular energy is proportional to that of the disc exposed to those neutrons.

6.5 Some Potential Applications of the Concentric Ring Technique

The concentric ring technique could have the following applications in neutron irradiation work which are thought to be worthy of further investigation.

1. For multielemental activation analysis, standard flux monitoring rings matched as closely as possible to the excitation functions and half-lives of each of the constituent elements would enable their concentrations to be determined very accurately.

2. The comparator technique used for activation analysis can be improved if the comparator which contains a known concentration of the material is used in ring geometry. For experiments involving more than one constituent in a composite sample, we suggest the use of comparator concentric rings each corresponding to a certain element.

3. If the comparator is in the form of a disc placed at a laboratory angle different from that of the sample, a set of standard concentric rings for fast neutron fluxes and energies measurement can be very useful to reduce the errors due to relative flux and energy variations. The introduction of the concentric ring technique could possibly minimise the role of sample/standard spinning approach, although disc/

ring spinning mechanism could also be introduced.

4. The D-T neutron source is often used as a standard for determining the efficiencies for neutron detectors which are used in neutron spectroscopy. Therefore the results obtained by concentric ring detectors specially at the detector position can yield some local information which the associated particle technique fails to predict, e.g. neutron attenuation in the target assembly. The technique can also be used over wider neutron energy ranges, in which "point source" geometry is used, by a suitable choice of detector materials.

6.6 A Possible System for the Standardisation of Neutron Cross-Section Data

Neutron cross-section data are usually presented in terms of the corresponding neutron energies as calculated from the $T(d,n)^4He$ reaction kinematics. Often, specially in the early publications, no information is given to indicate the procedure used for estimating fast neutron energies. In several cases, no corrections due to T-Ti target thicknesses and sample/monitor positioning have been made.

Therefore, we suggest presenting the cross-section data together with the corresponding estimated neutron energies which could be calculated from the irradiation angle, but more conveniently they can be found in terms of the induced activity ratios of the internationally accepted neutron monitors at sample position. Such system would be feasible if standardisation of the neutron energy measurement by the concentric ring technique is established.

CHAPTER 7

EXPERIMENTAL PROCEDURE

7.1 Neutron Irradiation

A moderated BF_3 detector was used during the irradiation to record the fluctuations in neutron production. This was useful for estimating the appropriate corrections due to flux variation, and also to ensure good accelerator operation. Experiments involving large neutron flux variations have been excluded from the calculations and each of the reported data is an average value obtained from more than one irradiation. Absolute neutron flux was determined in terms of the induced activities on stanadrd materials of known cross-sections.

To minimize the background of lower energy neutrons the following procedures were followed:- 1) new tritium targets were used to obtain minimum D-D neutron yield for those measurements which involve reactions with low thresholds. 2) the design of our target assemblies was such that the cooling water path does not coincide with target/sample direct line. 3) a specially designed sample holder was introduced to ensure minimum neutron scattering.

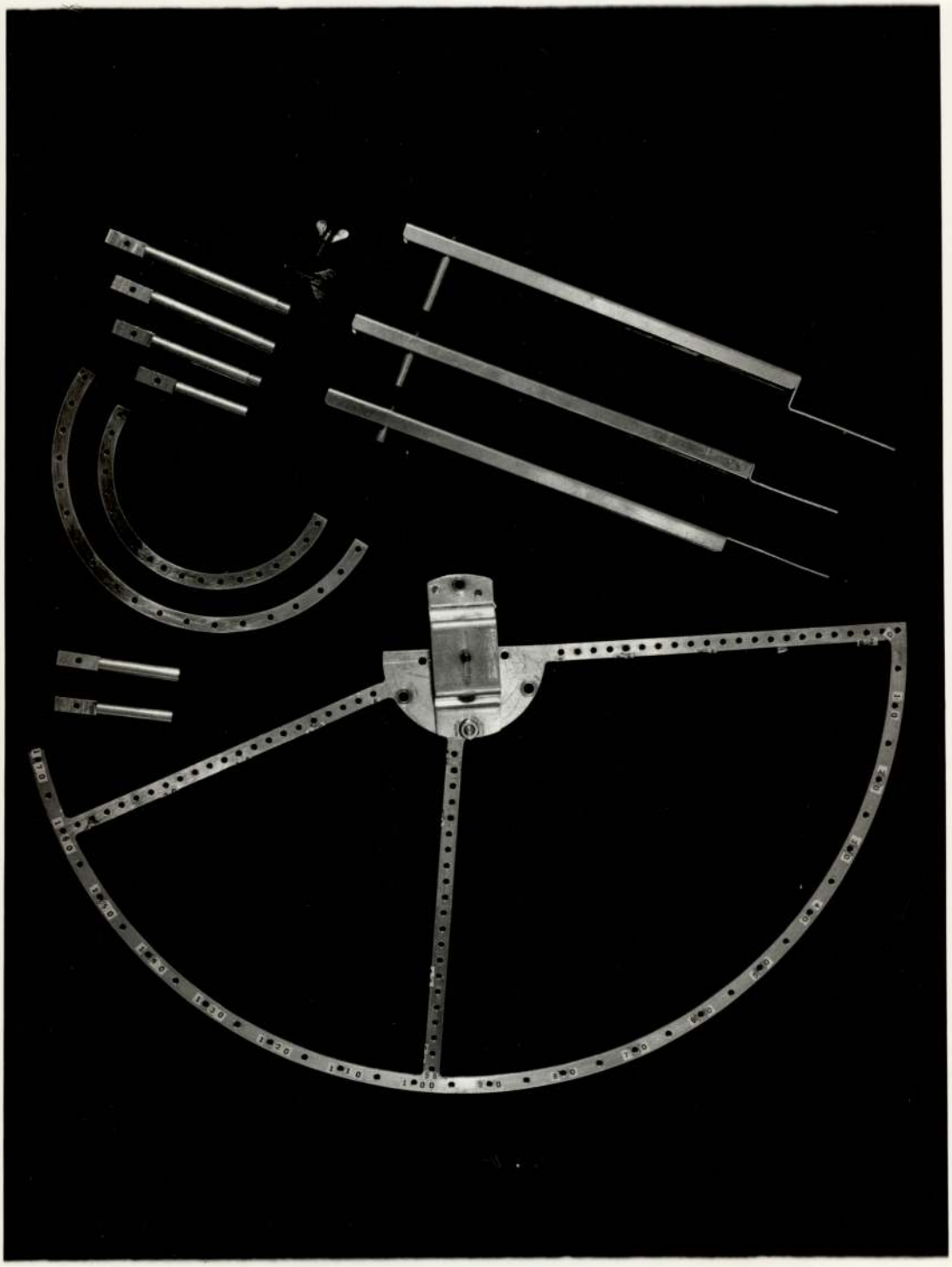

Fig. 7.1 Components of the Sample Holder

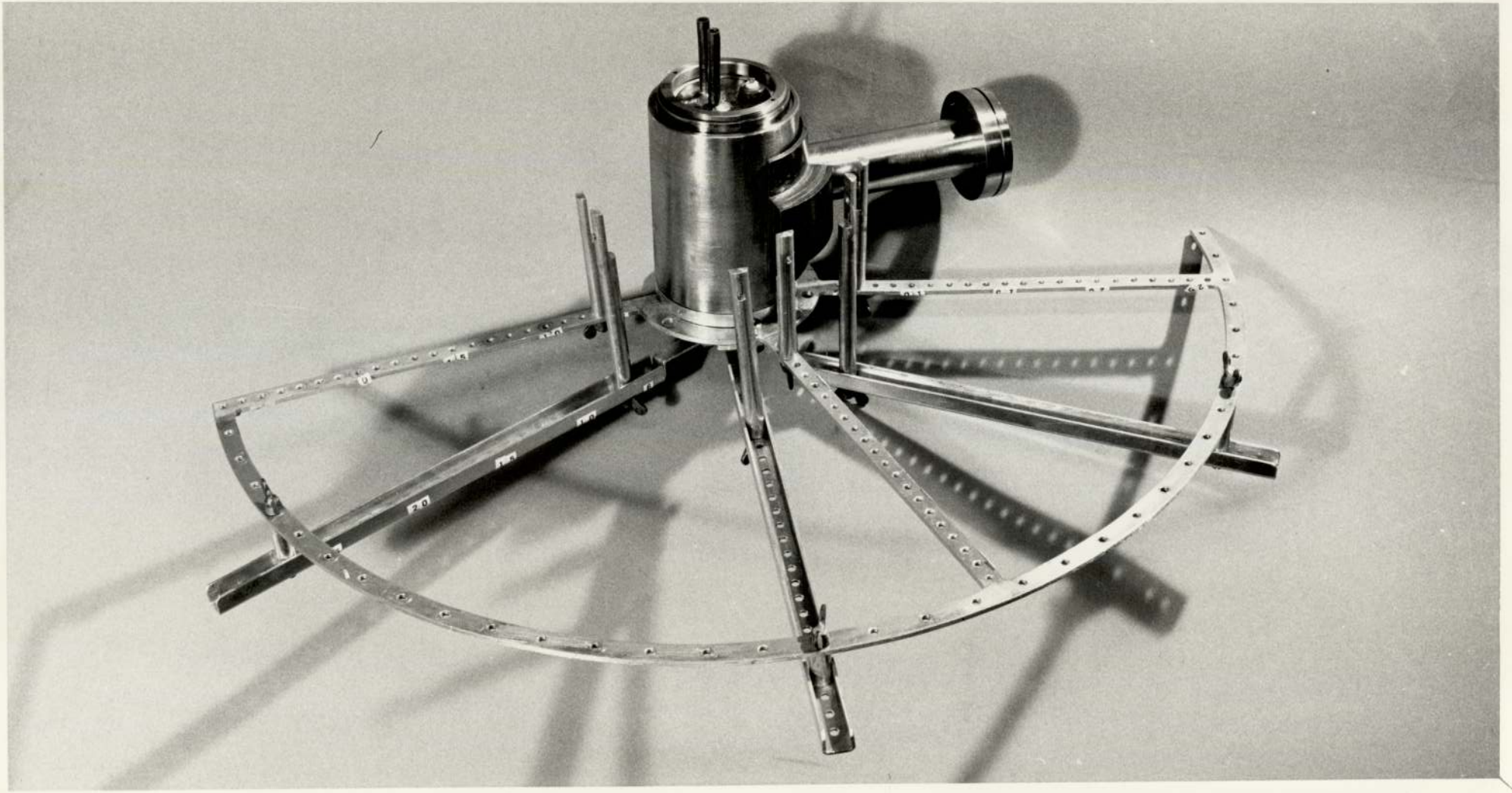

Fig. 7.2 The Target Assembly and Sample Holder

Design of the light sample holder's various components, Fig. 7.1, can be explained as follows:-

1. It is made of aluminium, and basically it consists of a thin arc which is 27 cm in radius, supported by three stationary arms at 0^{o}, 98^{o} and 160^{o} to be used for sample mounting and also to provide a support on the target assembly, Fig. 7.2.

2. Three mobile arms are provided for positioning purposes at different angles with respect to the deuteron beam. They are pivoted at the target centre for rotating and fixing in 5^{o} intervals from 0^{o} to 160^{o}. They can also be removed if necessary to reduce neutron scattering.

3. Several arcs of different radii are also available to be fixed on the stationary arms for some special experiments.

4. Samples are attached to thin aluminium rods which can be moved radially along the arms. To produce the same source/sample geometry, these rods were made of different lengths to compensate for the special design features of the mobile arms.

With such sample holder, samples can be placed at 5^{o} and 1 cm intervals along a source/sample distance of up to 30 cms by effecting a compromise between the requirements for low neutron energy spread and high flux, and varied with the magnitude of the cross-section of the sample. Estimation of the additional neutron energy spread due to sample/source geometry was obtained by using the neutron energy curves of Chapter 3. The evaluated neutron energy spread due to the subtended angle of the sample was then added quadratically to the energy spread due to the deuteron beam energy loss in the tritium target. In most of the experiments, a separation distance of 10 cms was found

to be satisfactory and an accuracy of about 1% in sample positioning was obtained.

7.2 Gamma-Ray Spectrometry

In this investigation, standard materials for fast neutron monitoring are studied. These materials have the advantage of producing simple gamma spectra which make the analysis procedure relatively simple and does not require the use of high resolution Ge(Li) detectors. Therefore, a shielded 3" x 3" NaI(Tl) detector was adopted for gamma detection in the present work. In comparison with Ge(Li) detectors, NaI(Tl) detectors have much better efficiency, require negligible care, and can operate at room temperature.

The electric pulses from the photomultiplier tube were amplified by using a CANBERRA 1417 spectroscopy amplifier whose output was then fed to the multichannel analyser. 400 channel RIDLE and 1000 channel NUCLEAR DATA ND 101 multichannel analysers were used, and the counting system was periodically calibrated by using standard gamma sources.

Gamma counting was carried out in a low background room, and the measured count rates were then corrected for dead time, background counts, irradiation time and decay. Half-lives were also measured when necessary, and detector efficiency was estimated from the tables of Grosjean and Bossert [127].

Sample separation from the NaI(Tl) crystal was determined by the counting statistics and in most of the experiments, placing the sample at a 3 cm distance was found to be satisfactory. For positron emitters, the annihilation 0.511 MeV radiations were counted by enclosing the

radioactive sample in a positron absorber of an appropriate thickness.

The counting sequence selected to get good statistical accuracy varied from one experiment to the other. But generally, the monitoring rings were used to be counted first such as for the case of $^{121}Sb(n,2n)^{120g}Sb$ excitation function due to their shorter half-lives, i.e. 9.5 and 9.8 m for aluminium and copper compared with 15.9 m for antimony. On the other hand, for the silicon experiments the situation used to be reversed due to the shorter lived product of silicon, i.e. $T_{\frac{1}{2}}$ = 2.27 m.

To get good statistical accuracy, a sequence for gamma counting was followed. The procedure depended on the material half-life, its cross-section and its weight. For example, for measuring the cross-section for $^{121}Sb(n,2n)^{120g}Sb$ reaction, aluminium and copper rings were used for neutron monitoring. In this case the rings have less weights compared with the antimony sample. They have lower cross-sections, and also lower half-lives. Accordingly, the induced activities on the rings were counted first and then followed by the antimony sample. For measuring $^{28}Si(n,p)^{28}Al$ cross-section the situation was the reverse due to the relatively short half-life of $^{28}Al(T_{\frac{1}{2}}$ = 2.27 m).

For each nucleus the number of radioactive nuclei present at the end of the irradiation depends on the one hand on the cross-section σ; on the other hand, n may be expressed in terms of the number of gamma ray counts A:

$$\frac{\phi\sigma LWsa}{G} = n = \frac{Ae^{\lambda te}(1 - e^{-\lambda tc})^{-1}}{b\varepsilon} \qquad (7.1)$$

where ϕ = the time-integrated neutron flux density at the midplane of the sample,

L = Avogadro's number,

W = the weight of the sample,

s = the fraction of the created radioactive nuclei which survive until the end of the irradiation,

a = the relative isotopic abundance of the target isotope,

G = the target gram atomic weight,

λ = the radioactive decay constant

t_e = the time elapsed between the end of the irradiation and the start of the gamma-ray counting,

b = the number of gamma rays per disintegration,

ε = the efficiency of the NaI(Tl) detector for total absorption,

and t_c = the length of time that the gamma rays are counted.

Equation 7.1 was used to evaluate the cross-sections, and information about the decay schemes were obtained from reference 128.

CHAPTER 8

EXPERIMENTAL RESULTS AND DISCUSSION

8.1 $^{63}Cu(n,2n)^{62}Cu$ Excitation Function

The variation of cross-section with neutron energy for the $^{63}Cu(n,2n)^{62}Cu$ reaction was measured in the usual manner by counting the annihilation (0.511 MeV) gammas due to the decay by positron emission of ^{62}Cu ($T_{\frac{1}{2}}$ = 9.8 m). Samples were placed at different laboratory angles with respect to the deuteron beam direction, and therefore subjected to neutrons of different mean energies. The results were obtained relative to the recommended value of 558 mb at 14.7 MeV as proposed by Body and Csikai [129]. Fig. (8.1a) shows our experimental cross-section data which were made by using the Van de Graaff and Dynamitron accelerators, (E_d = 0.3 MeV and 0.7 MeV). A smooth variation of the cross-section with neutron energy can be observed.

$^{63}Cu(n,2n)^{62}Cu$ absolute cross-section and its variation with neutron energy have been measured by several workers [90,130-141]. For comparison some of these data are plotted in Fig. (8.1b) with our

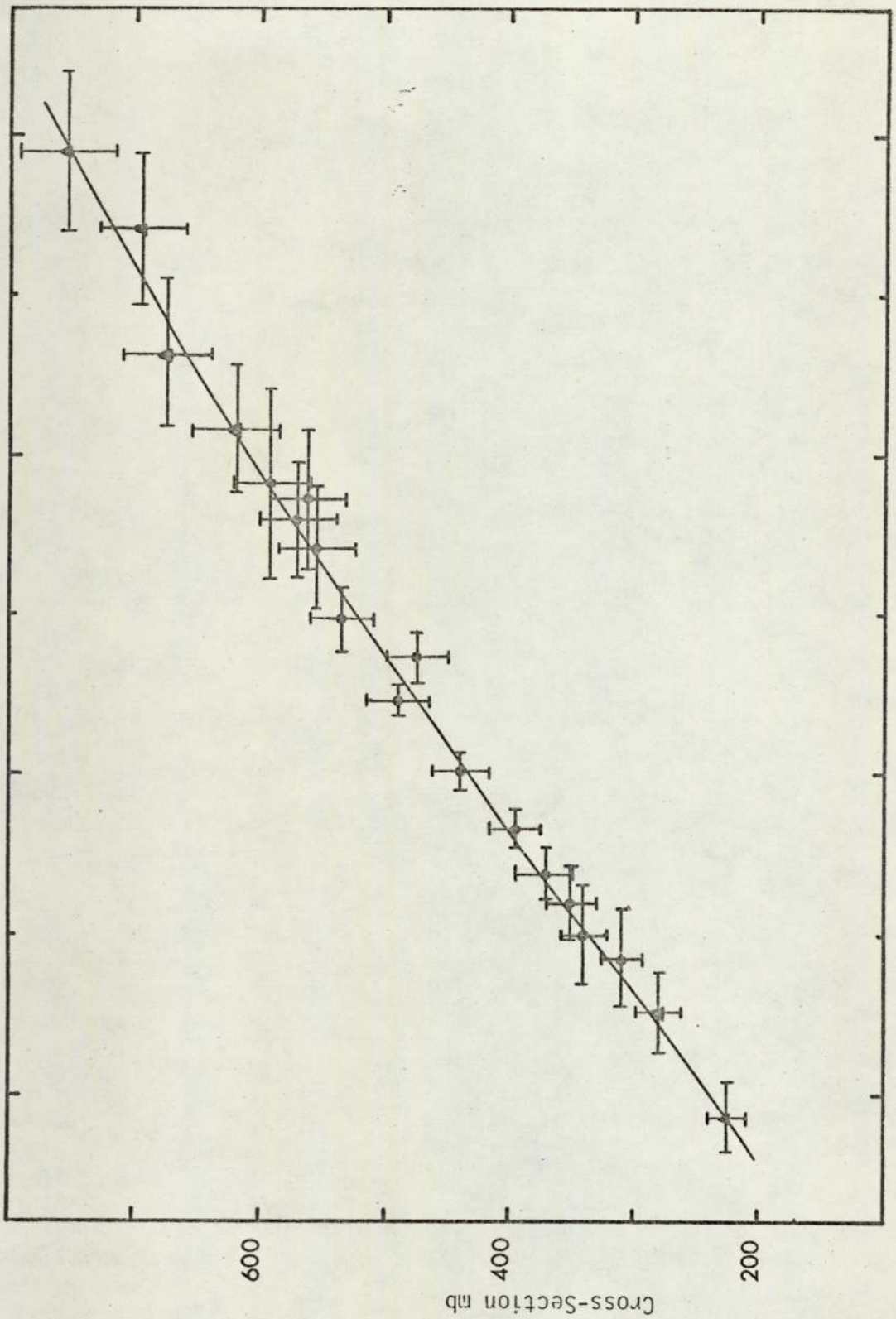

Fig. 8.1a
$^{63}Cu(n,2n)^{62}Cu$ Excitation Function

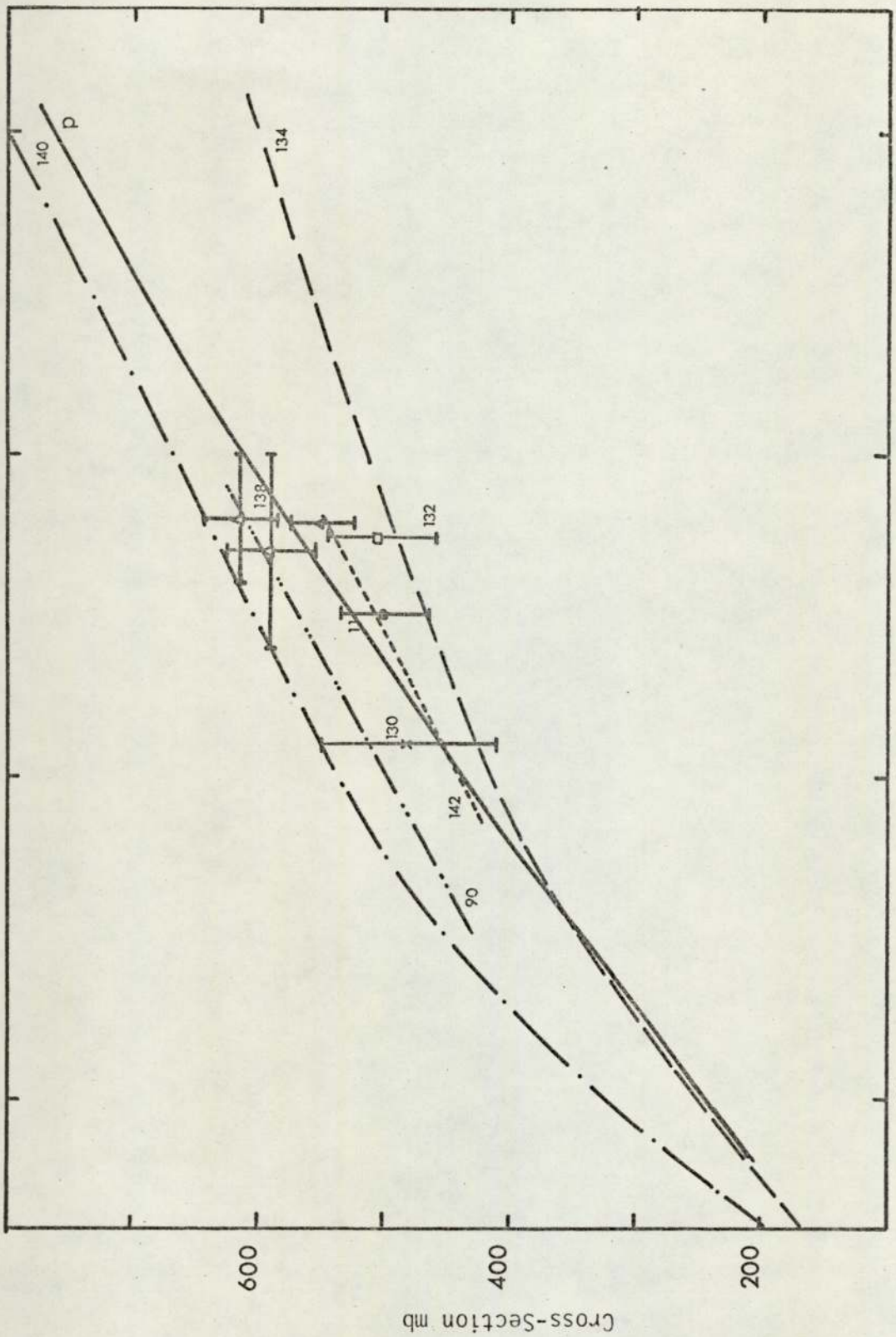

Fig. 8.1b
$^{63}Cu(n,2n)^{62}$ Cross-Section Data

excitation curve (solid curve), and a good general agreement can be observed. A weighted average value from the published experimental data at 14.5 ± 0.4 MeV (σ = 501 ± 36 mb) is also shown. This value and a theoretical value based on the statistical model predictions (σ = 481 mb) are taken from the work of Kondiah [11]. Similarly at 14.7 ± 0.3 MeV the values obtained by Qaim [138] are in good agreement with our data (σ_{exp} = 593 ± 36 mb and σ_{theor} = 543 mb). These results indicate that this reaction proceeds mainly via compound nucleus formation.

8.2 $^{27}Al(n,p)^{27}Mg$ Excitation Function

$^{27}Al(n,p)^{27}Mg$ excitation function was measured by detecting the 0.842 MeV gammas which are produced due to 70% of the β-decay of ^{27}Mg ($T_{\frac{1}{2}}$ = 9.5m). Samples were designed in the form of circular aluminium disc surrounded by very thin ring of copper which was used as the flux monitor. These concentric samples were irradiated together, and for checking purposes a single copper sample was also exposed at the same distance from the tritium target and at the angle which corresponds to 14.7 MeV neutrons, (40^{o} for E_d = 0.3 MeV).

The determination of the $^{27}Al(n,p)^{27}Mg$ excitation function was related to the measured copper excitation function, Fig. 8.1a, and the results are shown in Fig. 8.2a. A further check was carried out by measuring the aluminium (n,p) excitation function relative to the 558 mb value of $^{63}Cu(n,2n)^{62}Cu$ at 14.7 MeV by using separate single aluminium and copper samples. The results show similar behaviour to Fig. 8.2a but with higher standard deviation.

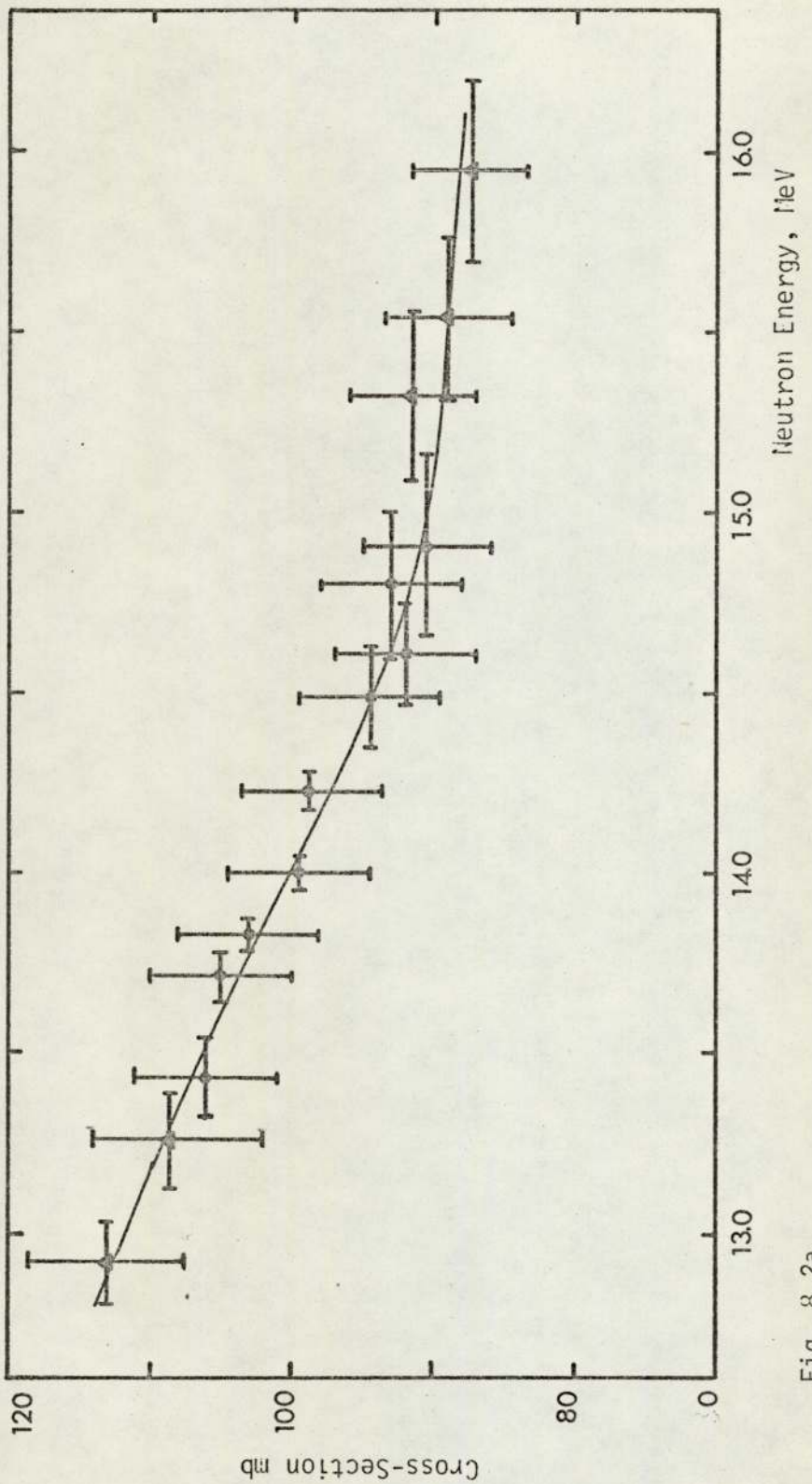

Fig. 8.2a
$^{27}Al(n,p)^{27}Mg$ Excitation Function

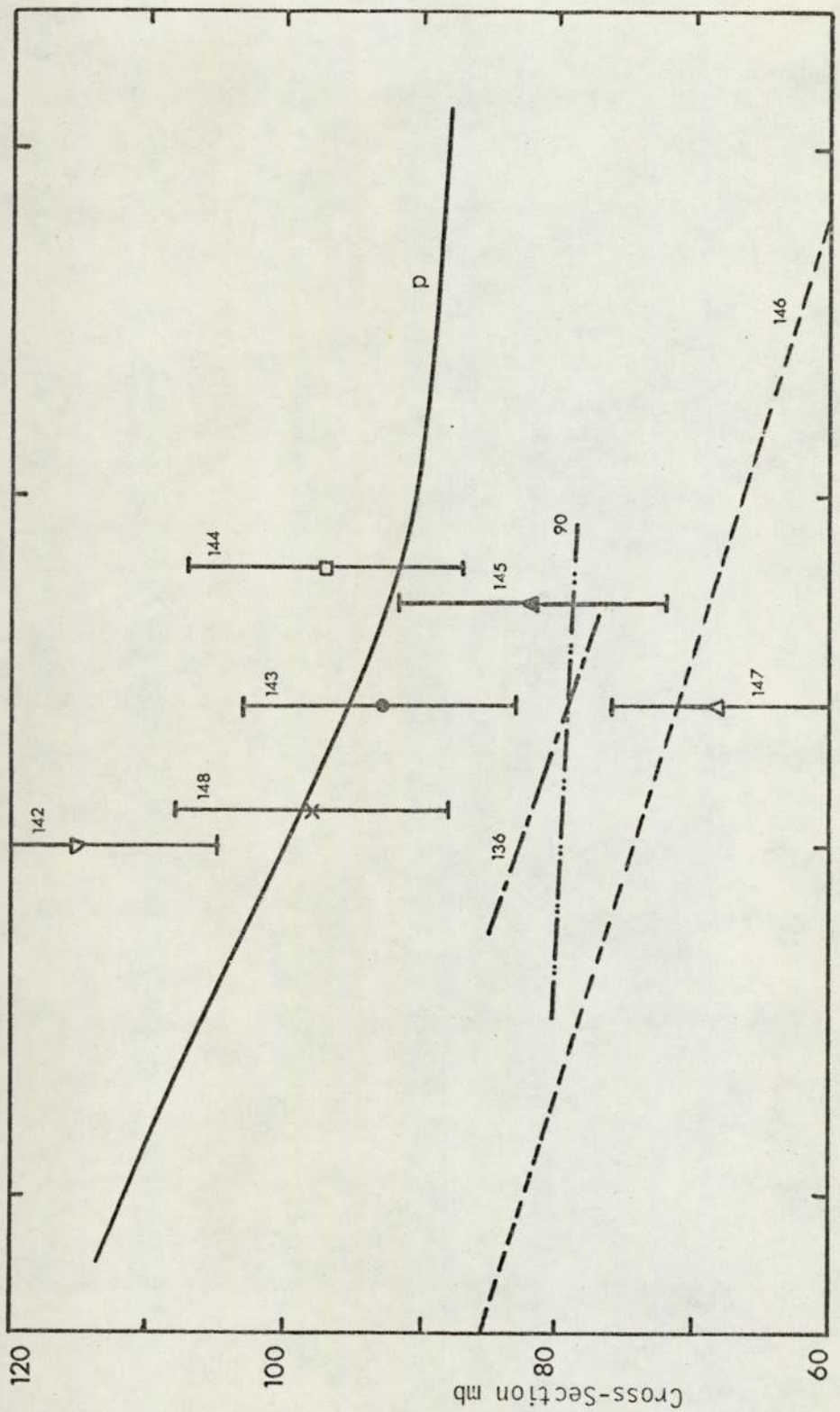

Fig. 8.2b
$^{27}Al(n,p)^{27}Mg$ Cross-Section Data

A phenomenological formula based on the neutron excess concept has been produced by Eder et al [149] to predict (n,p) cross-section values for neutron energies between 14 and 15 MeV, and it is shown below

$$\log_{10}(\sigma_{n,p}/\text{mb}) = 0.2 + 0.4A^{1/2} - 4.6(N-Z)/A^{2/3} \qquad (8.1)$$

By using this formula we obtained a cross-section value of 58.1 mb which is slightly lower than most of the experimental results.

For low mass nuclei, it was found that (n,p) cross-sections could be reproduced by the compound nucleus theory with the values of the level density parameter a = A/8.7 [148]. For ^{27}Al nucleus the theoretically calculated value is 70.5 mb at 14.1 MeV, (shown in Fig. 8.2b).

The general trend of our excitation function is approximately similar to the published data, but it does not agree with the results of Partington et al [90], which show a much lower slope in the 13.5 - 14.9 MeV region.

8.3 The Cross-Section Ratio Curve for Fast Neutron Energy Measurement

It has been proposed in Chapter 6, that the selection of standard materials for neutron energy measurement should be based on the similarity in half-lives and on the strong variation of the cross-section ratio with neutron energy. Therefore, ^{63}Cu(n,2n)^{62}Cu and ^{27}Al(n,p)^{27}Mg reactions have been selected as standards for the energy measurement due to their similar half lives and the slopes of this excitation function. Our measured excitation function indicate that in the 13-15 MeV region, copper cross-section increases approximately linearly with neutron energy with a slope of 28 per cent MeV^{-1}, whilst aluminium cross-section

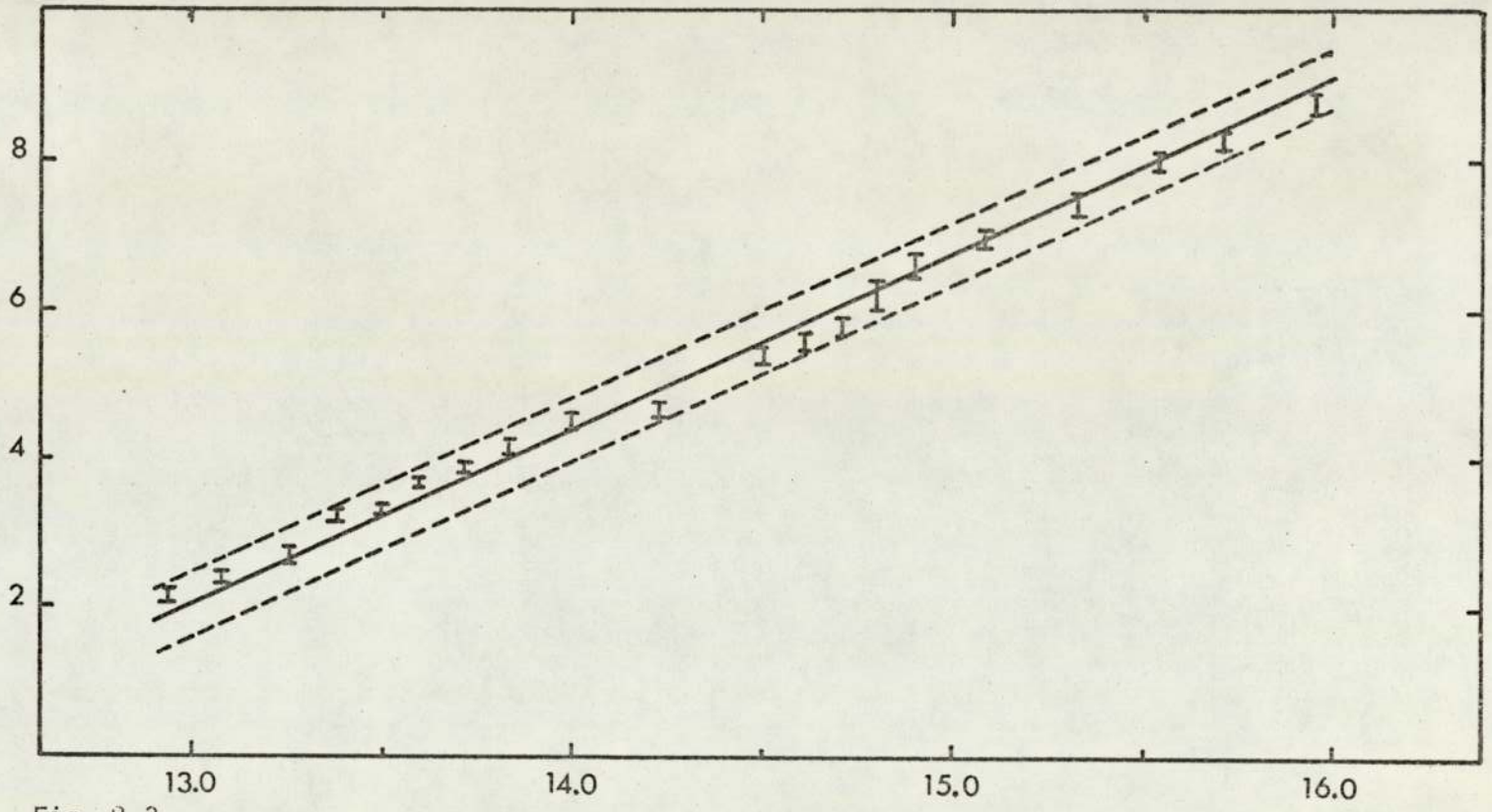

Fig. 8.3

The Ratio of Cross-Sections as a Function of Neutron Energy

decreases with a slope of -9 per cent MeV^{-1}.

Samples were made in the form of circular aluminium disc surrounded by a thin ring of copper. The samples were irradiated with different mean energy neutrons and at large and equal distance from the D-T neutron source, and the induced activities were measured for a range of neutron energies from 12.9 to 15.9 MeV.

The ratio of our copper and aluminium excitation functions has been plotted as a solid line in Fig. 8.3, the experimental uncertainties being indicated by the dotted lines. The concentric ring technique was used to establish the cross-section ratio at specific energies and these are shown in the form of points in Fig. 8.3. The results reveal a slight non linearity in the activation ratios, although there is good general agreement between the two sets of results. The accuracy of the neutron energy measurement is $\pm$ 1.2 per cent by the concentric ring technique.

The results obtained by using the Van de Graaff and Dynamitron accelerators are consistent and this is in support of the proposed use of the cross-section ratio curve as a reference for fast neutron energy measurement.

8.4 Accuracy of Fast Neutron Flux Measurement by the Concentric Ring Technique

To estimate the accuracy of the concentric ring technique, concentric copper samples consisting of a circular disc surrounded by two rings were used. The concentric copper samples were positioned at different angles with respect to the deuteron beam direction, and

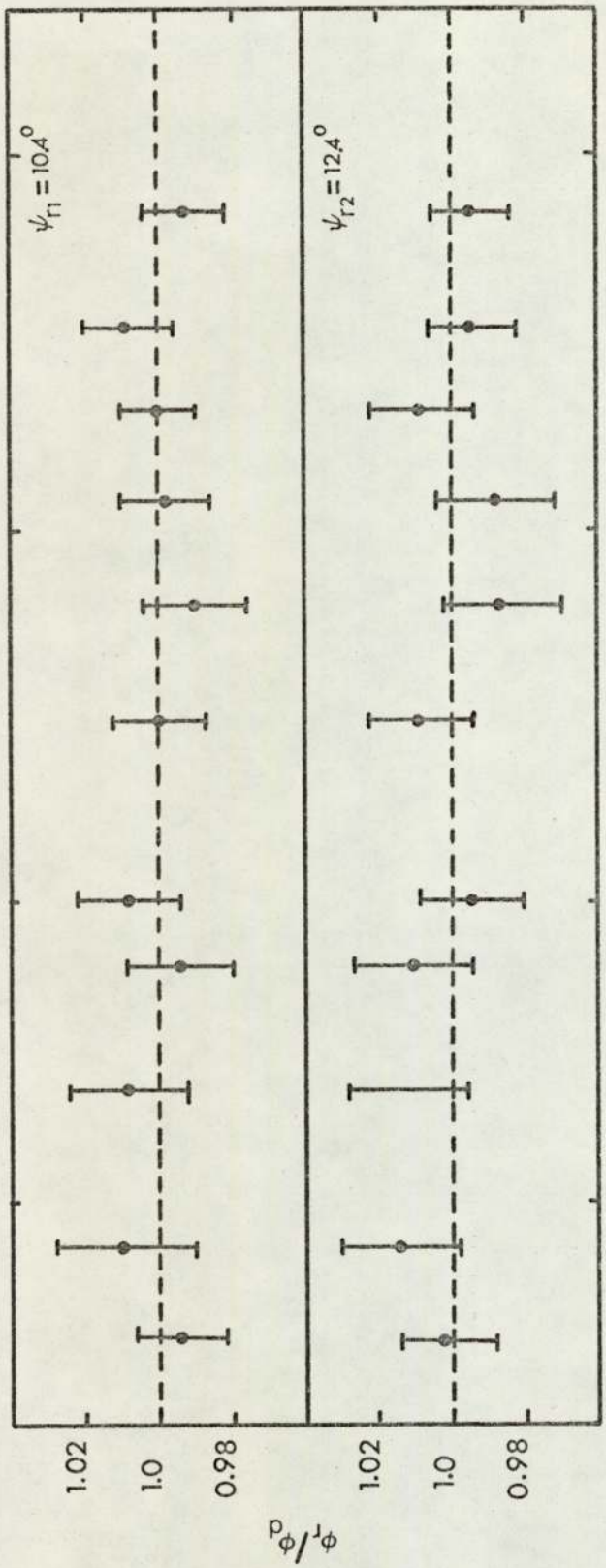

Fig. 8.4
The ratios of neutron fluxes measured by using the ^{63}Cu (n,2n)^{62}Cu reaction on concentric copper ring/disc samples.

in such a geometry that the angles subtended by the disc (θ_d) and the two rings (ψ_{r_1}, ψ_{r_2}) on the target are 10.2, 10.4 and 12.4 degrees respectively.

Following the irradiation, the components of the concentric samples were counted separately, and the corrected ratios of the determined induced activities in the rings and disc were proportional to the ratios of neutron fluxes to which they were exposed. Fig. 8.4 shows two plots of the flux ratio results against neutron mean energy for the two rings. The experimental results, as obtained by using the Dynamitron and Van de Graaff accelerators, indicate that a 1 per cent average accuracy in fast neutron flux measurement can be obtained by using the concentric ring technique.

8.5 $^{28}Si(n,p)^{28}Al$ Excitation Function

The samples used for this experiment were made of a circular disc made of a compressed silicon powder, surrounded by two copper and aluminium rings. Fast neutron flux was determined in terms of the induced activity on the aluminium ring and was obtained ~~absolutely~~ relative to the $^{27}Al(n,p)^{27}Mg$ excitation function of the present work. Neutron energy at the sample position was evaluated from the cross-section ratio curve of copper and aluminium.

The cross-section data of silicon in the 13.4 - 14.9 MeV region, Fig. 8.5a, were obtained by irradiating the concentric samples for 10 m and 30 m. The gamma activities which were produced in the silicon samples are due to 100 per cent of the decay of $^{28}Al(T_{\frac{1}{2}}=2.27$ m) to the 1.78 MeV excitation level. Silicon activities were the first

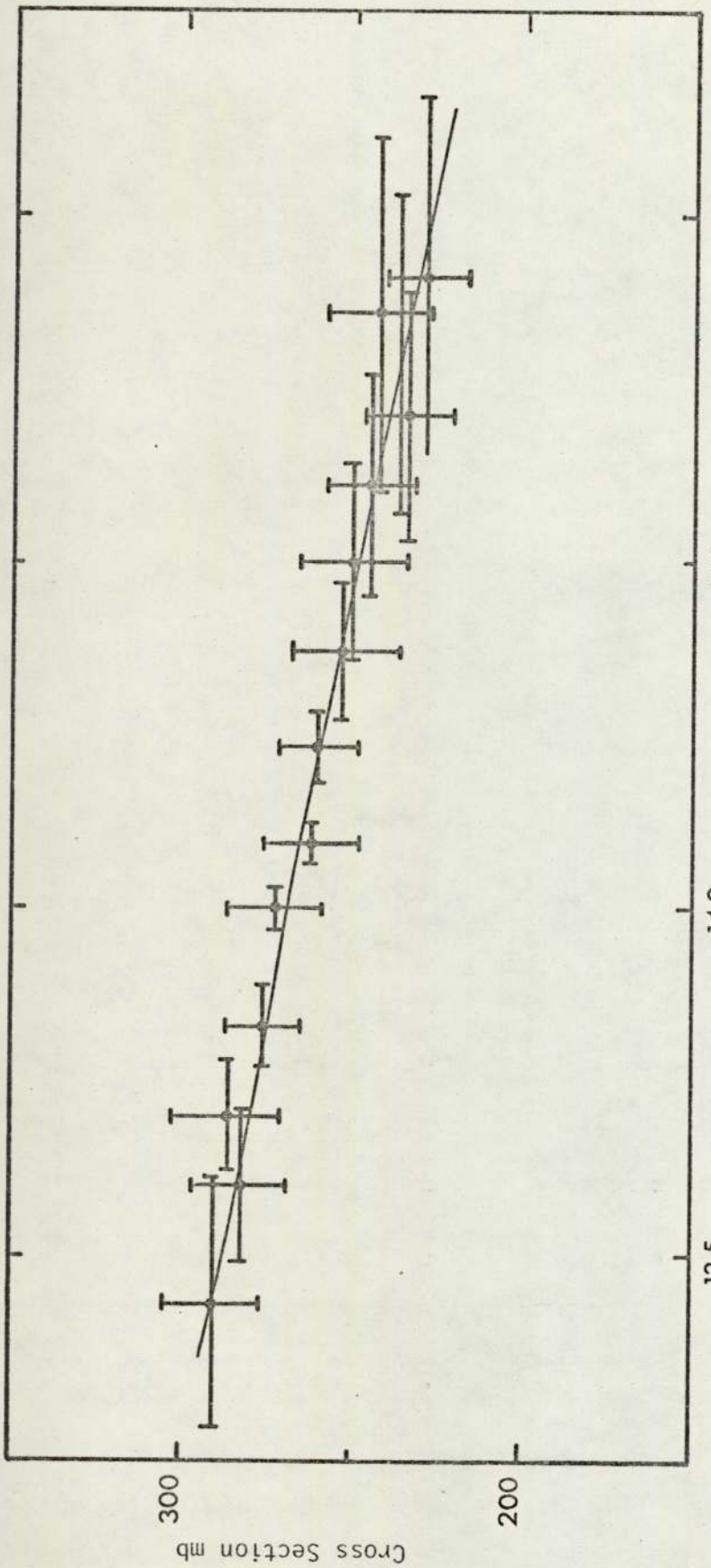

Fig. 8.5a
$^{28}Si(n,p)^{28}Al$ Excitation Function

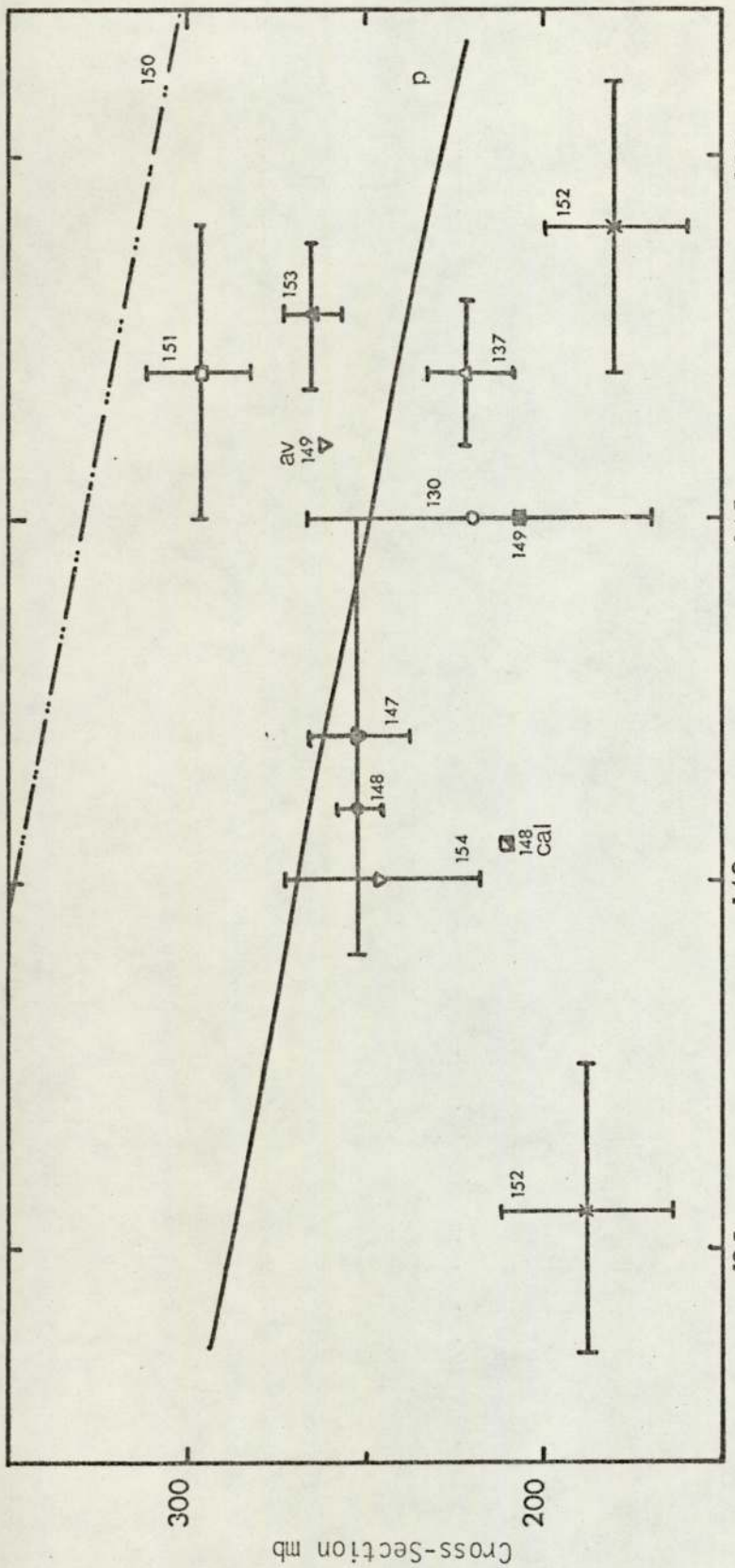

Fig. 8.5b
$^{28}Si(n,p)^{28}Al$ Cross-Section Data

to be counted after the irradiation, then they were followed by the aluminium and copper rings.

The cross-section value at 14.5 MeV that we have calculated from eq. (8.1) is 207 mb which is slightly lower than our experimental results. An average experimental cross-section value of 260 mb at 14.7 $\pm$ 0.15 MeV was reported by Eder et al [149]; this was obtained by taking into account the data of Schantl [155]. On the other hand, the compound nucleus calculations made by Kaji et al [148] have produced a cross-section value of 210 mb at 14.1 MeV, but a higher value is expected if the direct interaction contribution was taken into account.

8.6 $^{64}Zn(n,2n)^{63}Zn$ Excitation Function

This excitation function was measured by irradiating concentric samples made of a zinc disc and aluminium/copper rings for 1h and 1.5h. The neutron energy and absolute neutron flux were estimated by using the copper/aluminium cross-section curve and our $^{63}Cu(n,2n)^{62}Cu$ excitation function.

The cross-section data which are shown in Fig. 8.6a were obtained by the integration under the annihilation gamma ray peak which corresponds to $^{63}Zn(T_{\frac{1}{2}} = 30\ min)$. This was preceeded by the measurement of the induced activities on the copper and aluminium rings separately. The general agreement between the present and published data is relatively good, and in particular the recent measurements by Kaji et al. [161].

Kaji et al [161] have carried out theoretical calculations for the $^{64}Zn(n,2n)^{63}Zn$ reaction by using 1.2 and 4.7 MeV^{-1} values for the level density parameter, whilst Khurana and Hans [162] made a use of the level

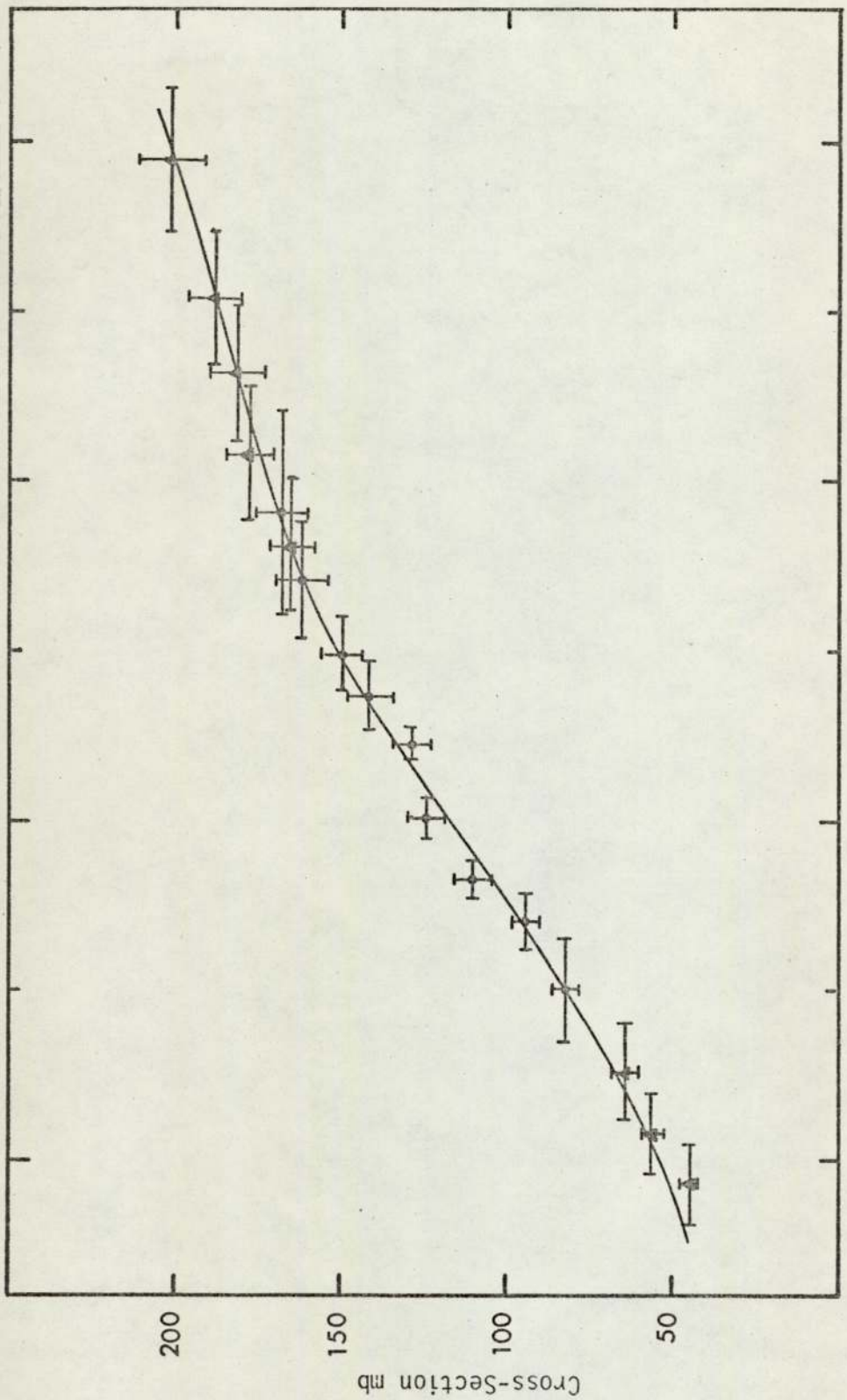

Fig. 8.6a
$^{64}Zn(n,2n)^{63}Zn$ Excitation Function

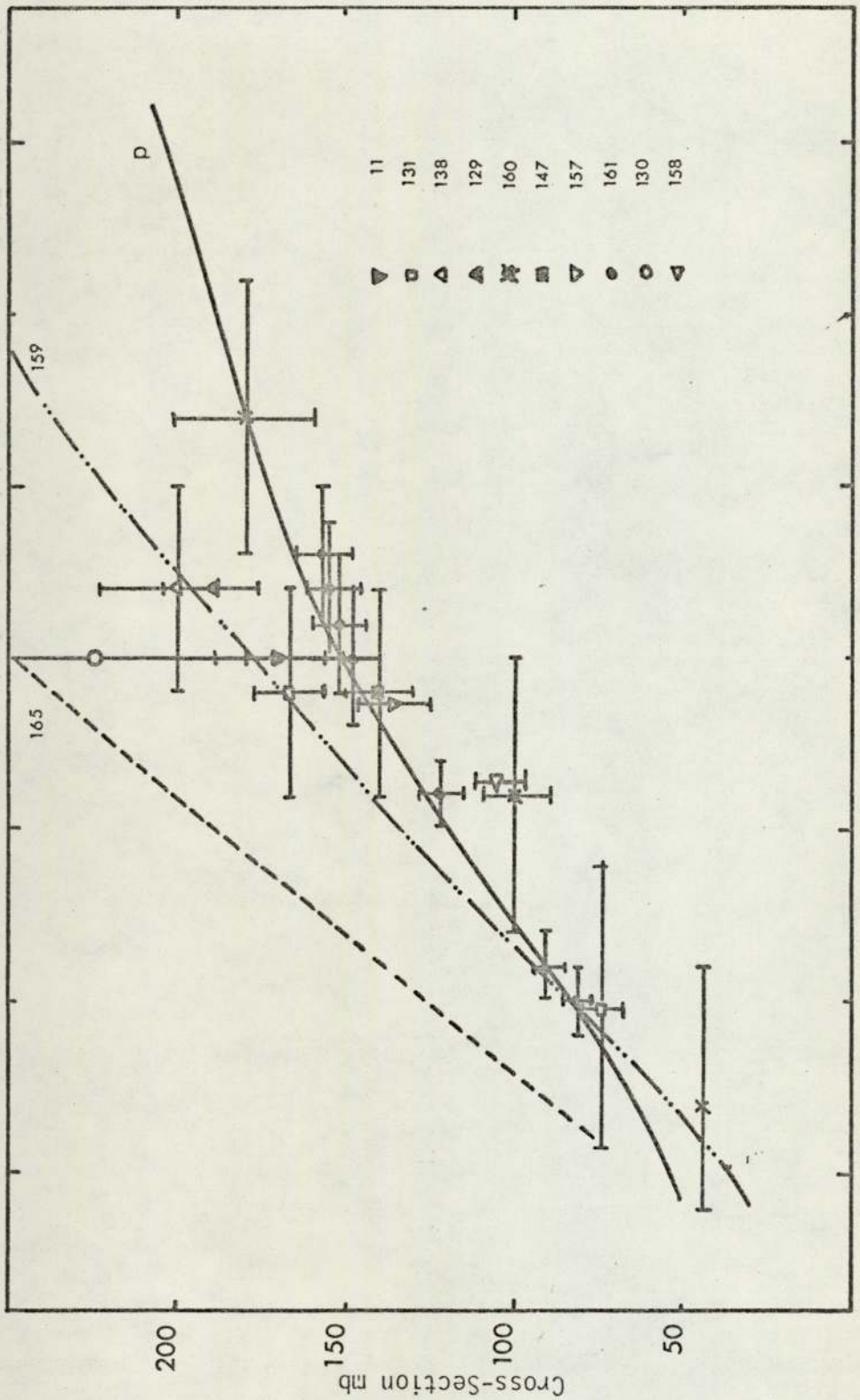

Fig. 8.6b
$^{64}Zn(n,2n)^{63}Zn$ Cross-Section Data

density formula of Newton [166] in their calculations, which takes into account the shell effects. Both calculations have produced results which are much higher than the experimental results, and this can be attributed to the fact that these calculations were made under the assumption that the $^{64}Zn(n,p)^{64}Cu$ competing reaction can be neglected.

8.7 $^{121}Sb(n,2n)^{120g}Sb$ Excitation Function

The residual nucleus of the total (n,2n) reaction on ^{121}Sb can decay in two ways, one with a half-life of 15.9 m leading to the formation of ^{120}Sb in its ground state, the other with a half-life of 5.8 days which leads to the formation of the metastable state ^{120m}Sb.

Determination of the isomeric cross-section ratios is useful for understanding the kind of mechanism governing the reactions. This is being due to its dependence on the angular momenta in various stages of the reaction which in turn depend on the mechanism of the reaction.

In the present work, we report the absolute cross-section data for the $^{121}Sb(n,2n)^{120g}Sb$ reaction in the neutron energy region between 9.29 and 15.9 MeV, which are useful for estimating the extent to which the isomer is populated in the total (n,2n) reaction. Since we are to a large extent interested in the applications of the excitation functions, cross-section measurements for the isomeric state were not carried out. On the other hand, total cross-sections and isomeric cross-sections can be estimated from the previous publications.

The experimental results in Fig. (8.7a) were obtained by irradiating a pure antimony sample surrounded by two concentric rings made of copper and aluminium for the measurement of fast neutron flux and

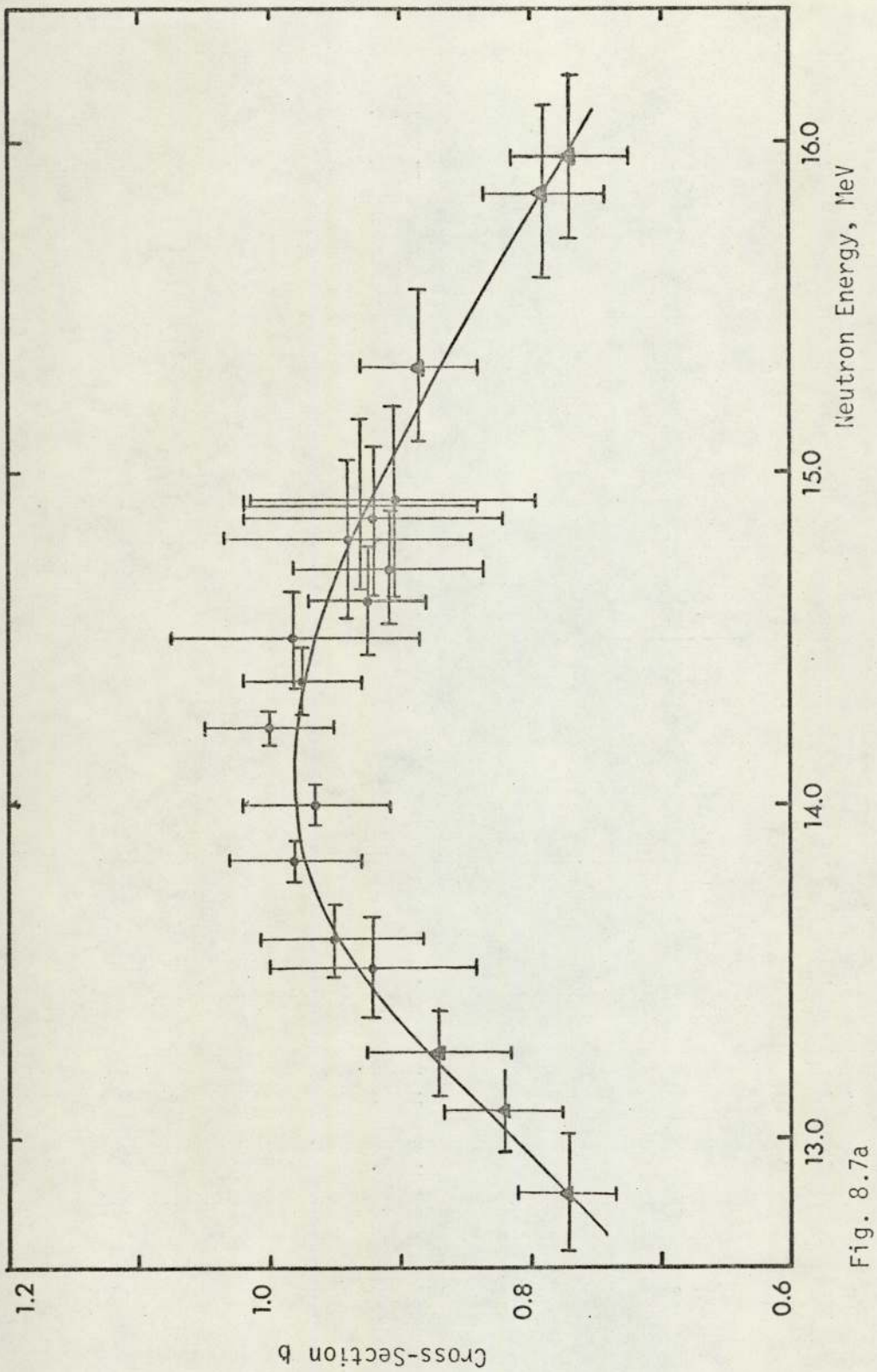

Fig. 8.7a

$^{121}Sb(n,2n)^{120g}Sb$ Excitation Function

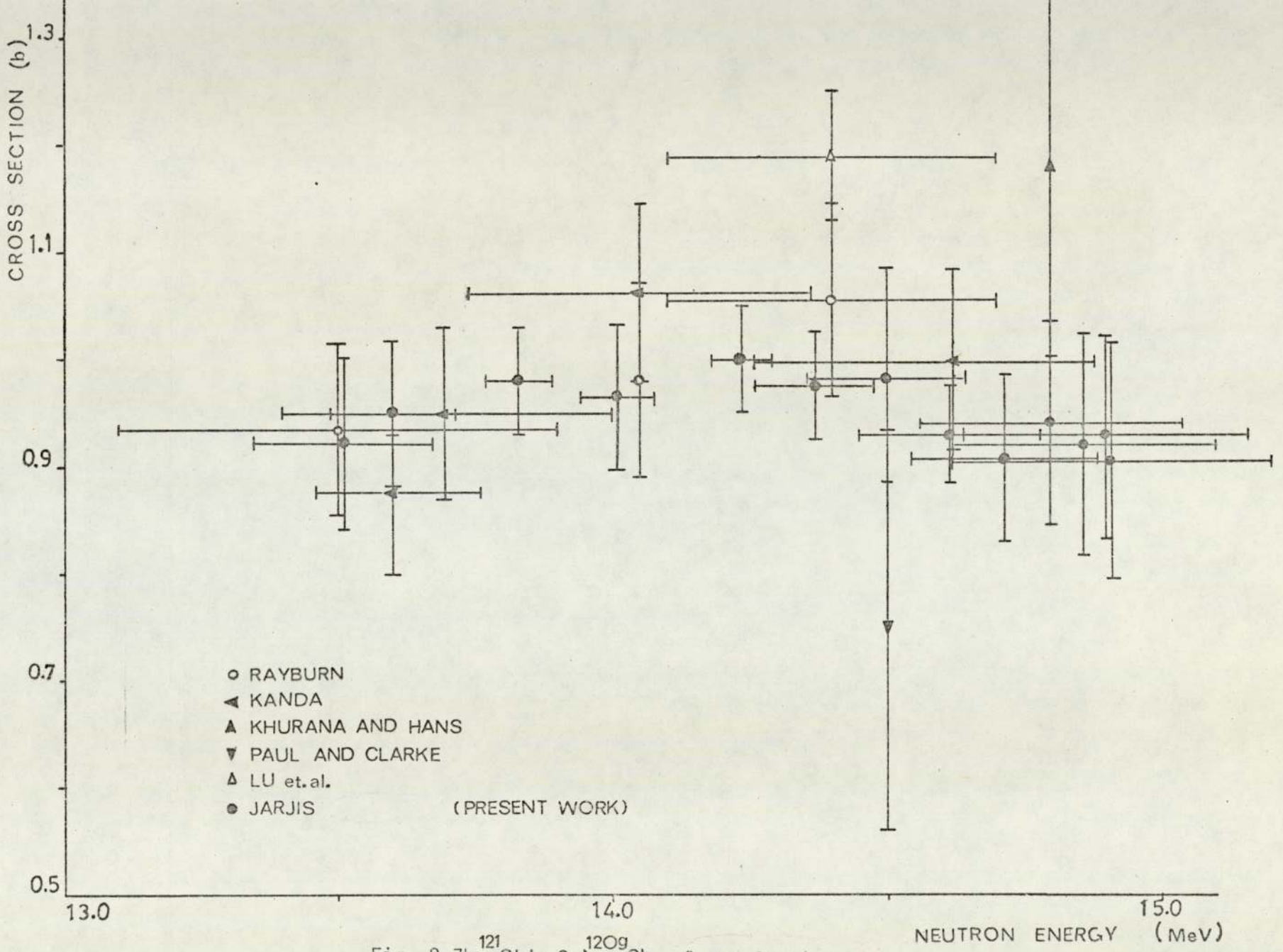

Fig. 8.7b $^{121}Sb(n,2n)^{120g}Sb$ Cross-Section Data

energy. The cross-section data were obtained relative to $^{63}Cu(n,2n)^{62}Cu$ excitation function by counting the annihilation gamma rays from the decay of ^{62}Cu and ^{120g}Sb by positron emission, separately.

It is worthwhile indicating that $^{121}Sb(n,2n)^{120g}Sb$ cross-section data of Kanda [163] were obtained by the mixed powder technique. The induced activities on copper and antimony were counted simultaneously and in comparison with our method, Kanda had to carry out the necessary analysis of the decay curve to obtain the yield ratio of ^{120g}Sb and ^{62}Cu.

Our results indicate that $^{121}Sb(n,2n)^{120g}Sb$ excitation function has a broad peak in the 13-15 MeV region. The results obtained on the Van de Graaff and Dynamitron accelerators confirm each other and indicate the occurence of some competing reaction above 15 MeV. The total reaction cross-section determined from our ^{120g}Sb results and an average isomeric cross-section of 770 mb is 1760 mb at about 14.5 MeV, compared with a weighted average value of 1741 mb [11]. The statistical model calculations by Kanda [163] predicted a value of 1880 mb using Blatt and Weisskopf formula [2]. The calculations of Pearlstein [165], which are based on an empirical expression for inelastic cross-sections and level density, gave total cross-section values of 1486 mb and 1715 mb at 13.1 MeV and 15.1 MeV respectively. On the other hand by using more accurate optical model values for non-elastic cross-sections, Kondaiah [11] obtained 1401 mb at 14.5 MeV.

To carry out an appropriate test for the empirical systematic method that has been discussed in Chapter 1, a FWHM value of 9.6 MeV was obtained for the (n,2n) reaction on ^{121}Sb, see Fig. 1.5. An extrapolation of our excitation curve yields a FWHM value of 6.2 MeV whilst the corresponding value from the early measurements by Rayburn was found to be 14.2 MeV [131].

Finally, Antimony is suggested as a very suitable flux monitor for 14 MeV neutrons when used to produce activities with half-lives in the 10 - 30 min region. It has the advantage of having a relatively high cross-section, its radioactive product has a reasonable half-life of 15.9 min and its excitation function is smooth and almost flat in the 13.5 - 15 MeV region.

8.8 $^{56}Fe(n,p)^{56}Mn$ Excitation Function

The experimental cross-section data for $^{56}Fe(n,p)^{56}Mn$, Fig. 8.8a, were measured relative to the cross-section data of $^{121}Sb(n,2n)^{120g}Sb$ reaction. The irradiated samples consisted of an iron sample surrounded by a flux monitoring ring made by compressing pure antimony powder. Measurement of the induced activity on the antimony ring was followed by detecting the 0.847 MeV gammas emitted due to the decay of $^{56}Mn(T_{\frac{1}{2}} = 9.58h)$.

It has been shown by Levkovskii [171] that for a broad range of (A) values, the (n,p) cross-sections can be described by a single exponential formula containing the neutron asymmetry parameter.

$$\frac{\sigma_{n,p}}{\sigma_{ne}} = 0.73 \exp(-33 \frac{N-Z}{N+Z}) \qquad (8.2)$$

By using this formula for 14-15 MeV neutrons, Levkovskii[172] has estimated a cross-section of 100 mb for $^{56}Fe(n,p)^{56}Mn$ which is in a very good agreement with the experimental data. On the other hand, we have obtained a low value of 86.0 mb by using eq. 8.1 which was proposed by Eder et al [149]. Also, a low cross-section of 25 mb at 14.1 has been obtained theoretically by Kaji et al [148], and this was interpreted by the presence of the direct process.

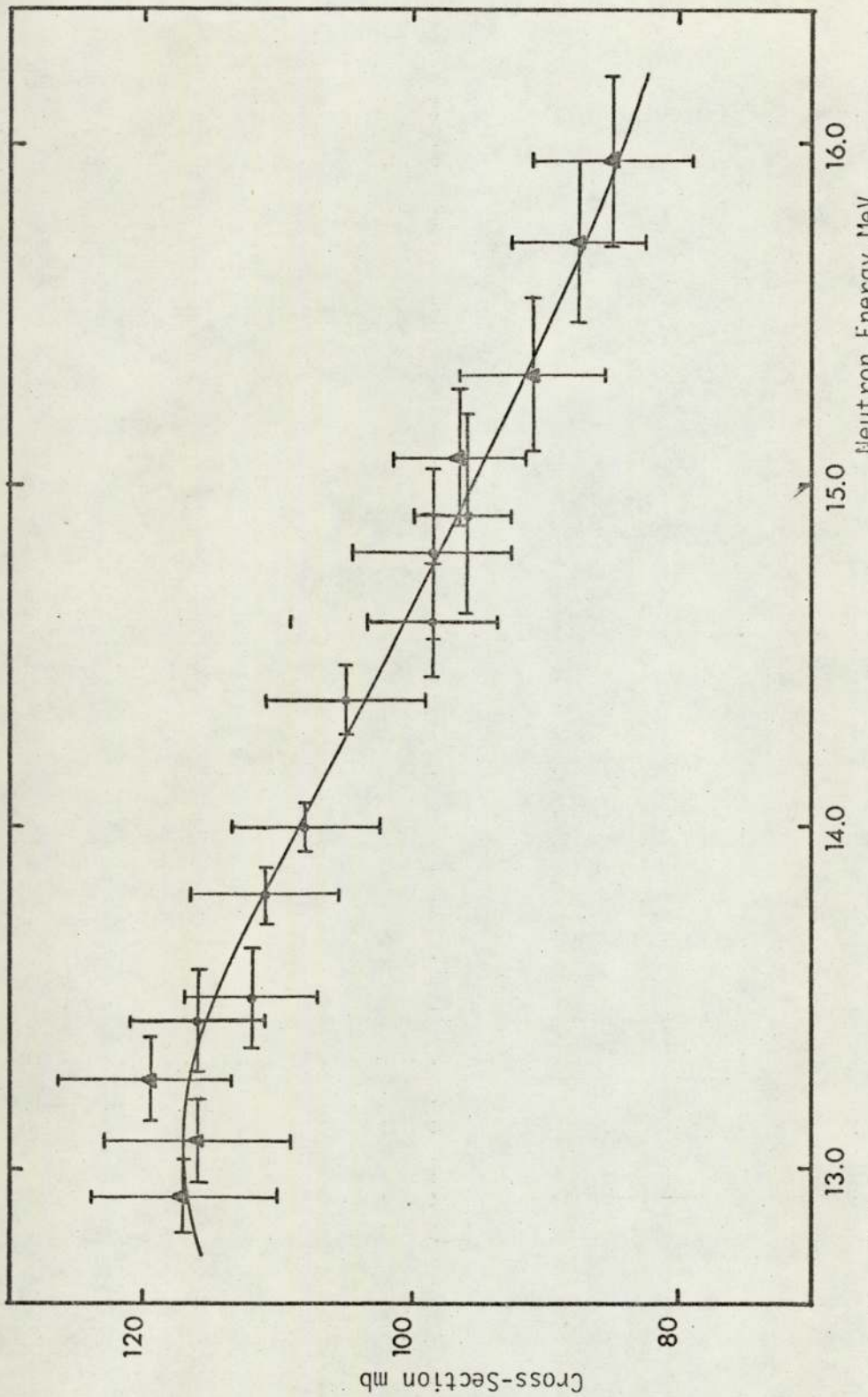

Fig. 8.8a

$^{56}Fe(n,p)^{56}Mn$ Excitation Function

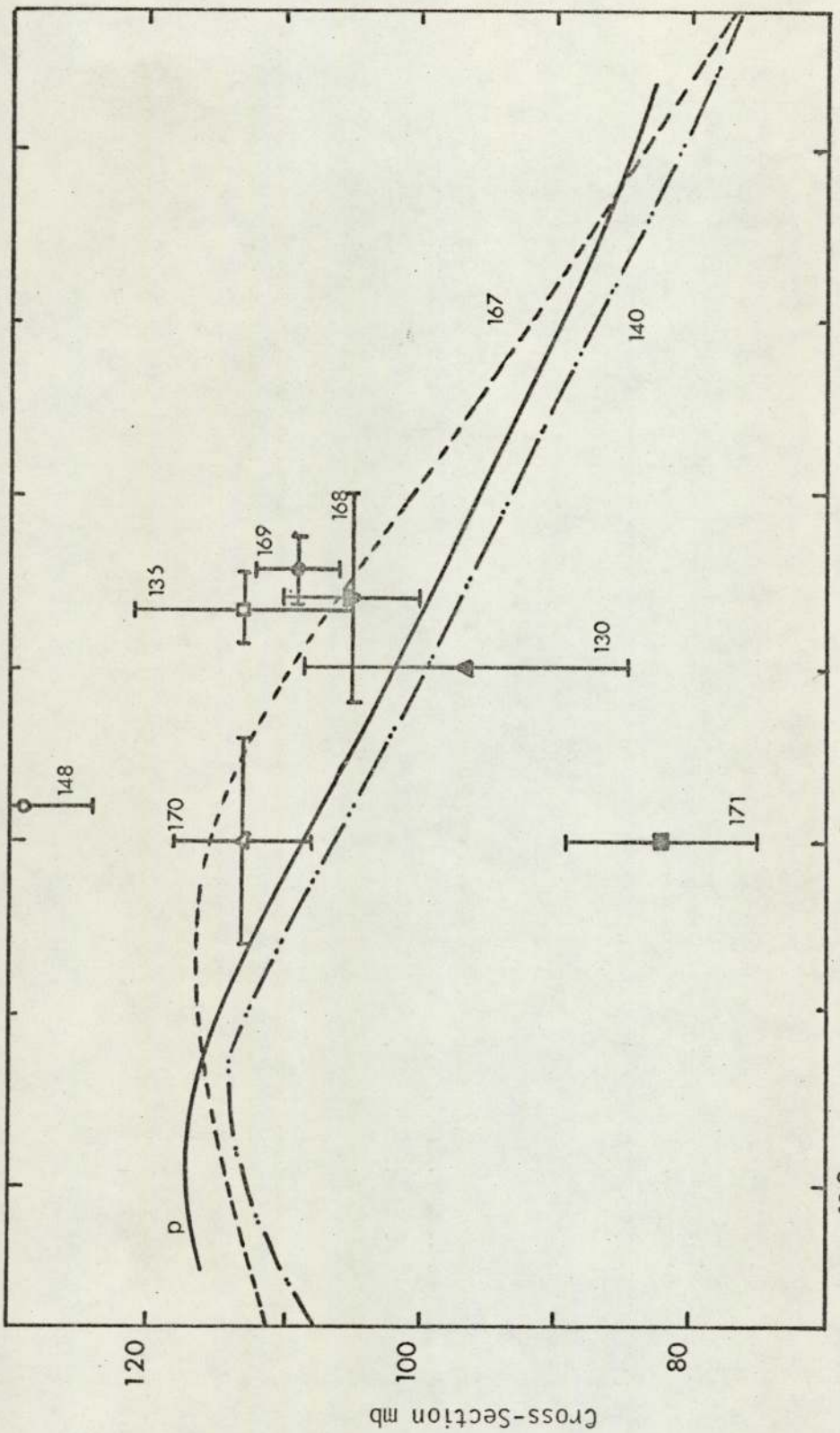

Fig. 8.8b

$^{56}Fe(n,p)^{56}Mn$ Cross-Section Data

8.9 $^{59}Co(n,\alpha)^{56}Mn$

The excitation function for $^{59}Co(n,\alpha)^{56}Mn$ reaction was determined relative to the excitation function of $^{121}Sb(n,2n)^{120g}Sb$ by using Antimony rings for flux monitoring. Additional check was provided by employing iron rings and the $^{56}Fe(n,p)^{56}Mn$ excitation function to obtain the absolute cross-section data. Both sets of data were found to be consistent and average values were plotted in Fig. 8.9a.

According to Levkovskii [172], for A > 40, the value of $\sigma_{n,\alpha}$ is about 2.5 times smaller than that of $\sigma_{n,p}$ for the same nucleus and in the 14-15 MeV region. Accordingly, a new formula for $\sigma_{n,\alpha}$, based on eq. (8.2), has been proposed.

$$\frac{\sigma_{n,\alpha}}{\sigma_{ne}} = 0.29 \exp(-33\frac{N-Z}{N+Z}) \qquad (8.3)$$

A cross-section of 26 mb for ^{59}Co nucleus has been estimated from this equation, which is very close to the experimental data. This value for ^{59}Co is actually very close also to that obtained using the statistical model analysis by Milano group [177,178]. In this case, a cross-section of 27 mb has been obtained by analysing the (n,α) excitation functions and energy spectra to evaluate the appropriate level density values.

8.10 $^{27}Al(n,\alpha)^{24}Na$ Excitation Function

The (n,α) cross-section on ^{27}Al is being used very often as a flux monitoring standard, specially for long irradiation times since the product nucleus ^{24}Na has a half-life of 15h. In addition, the cross-section variation with energy has been subjected to several fine structure investigations as it has been discussed in Chapter 1.

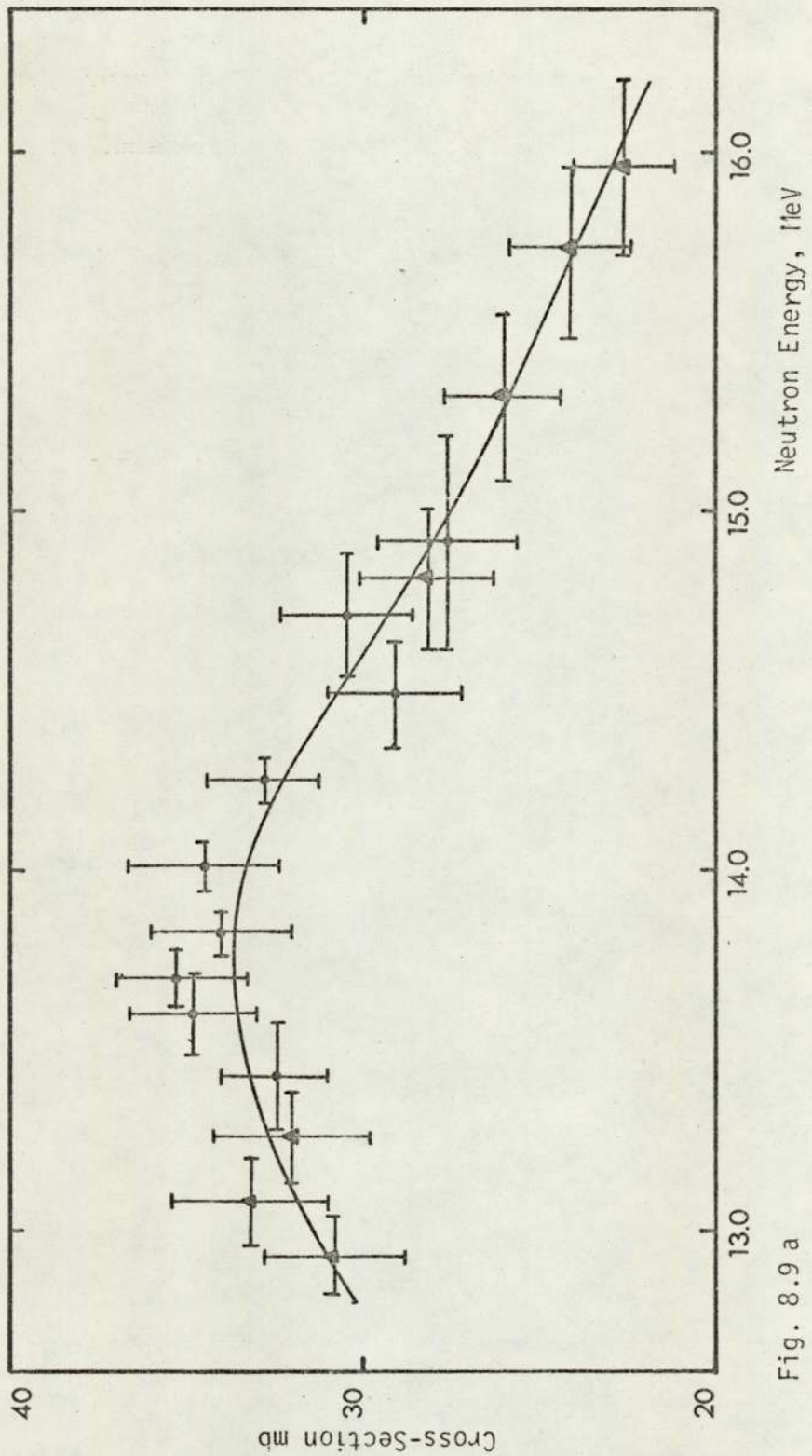

Fig. 8.9 a
$^{59}Co(n,\alpha)^{56}Mn$ Excitation Function

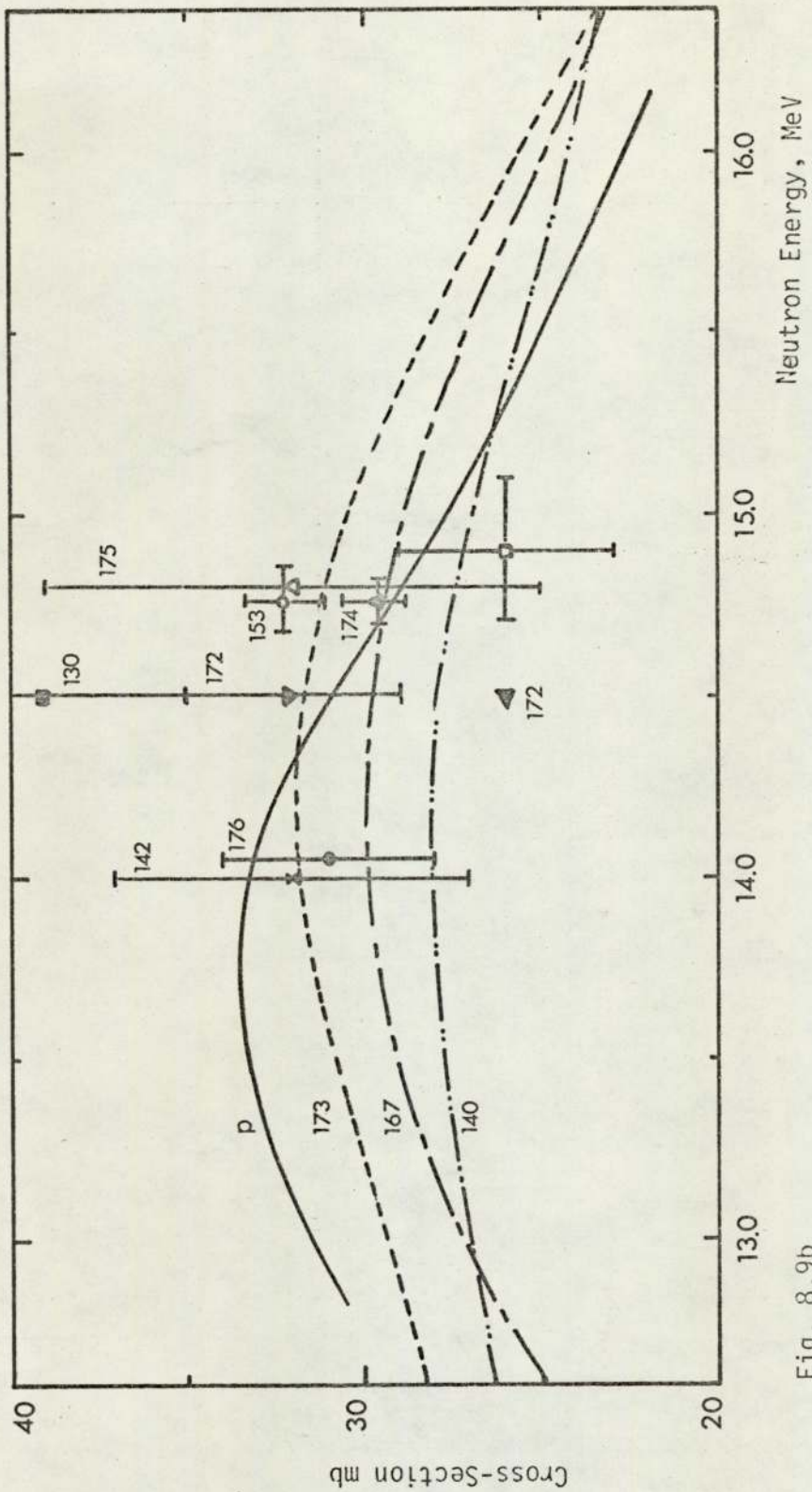

Fig. 8.9b
$^{59}Co(n,\alpha)^{56}Mn$ Cross-Section Data

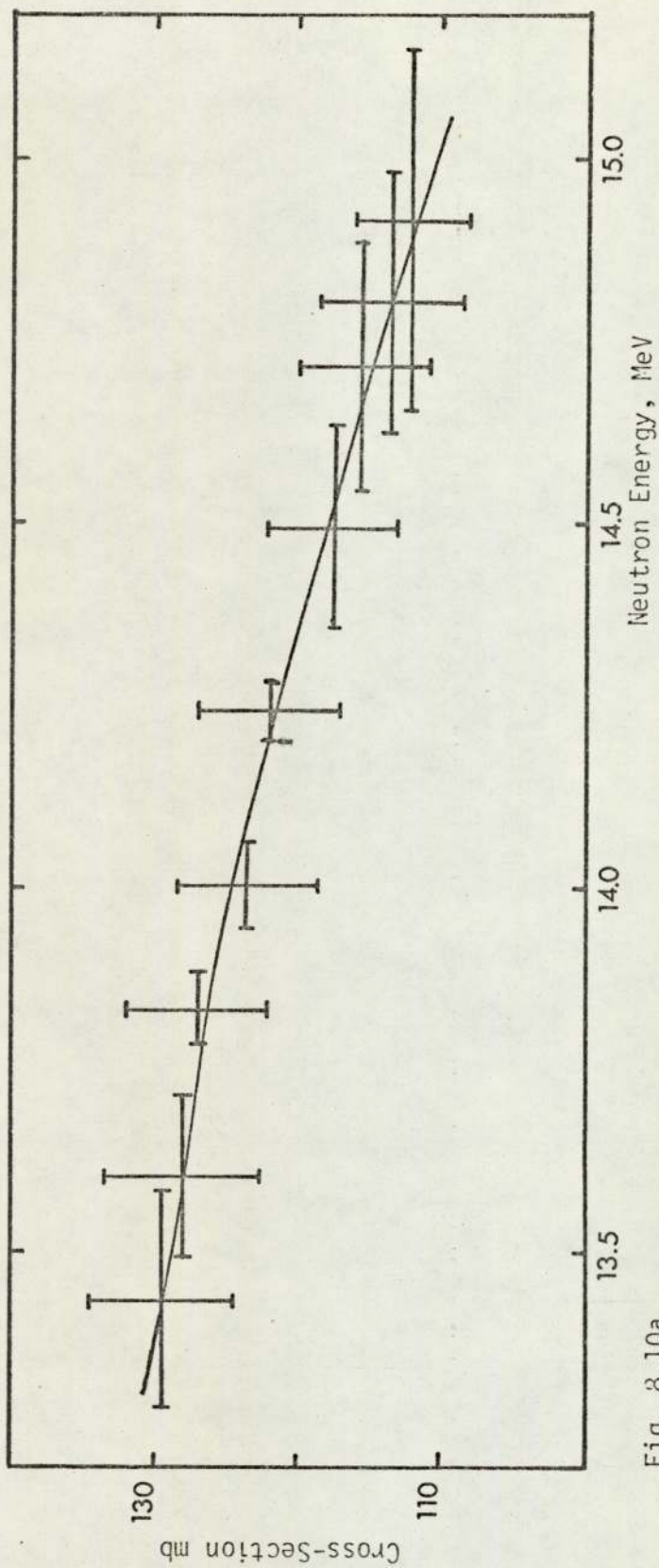

Fig. 8.10a

$^{27}Al(n,\alpha)^{24}Na$ Excitation Function

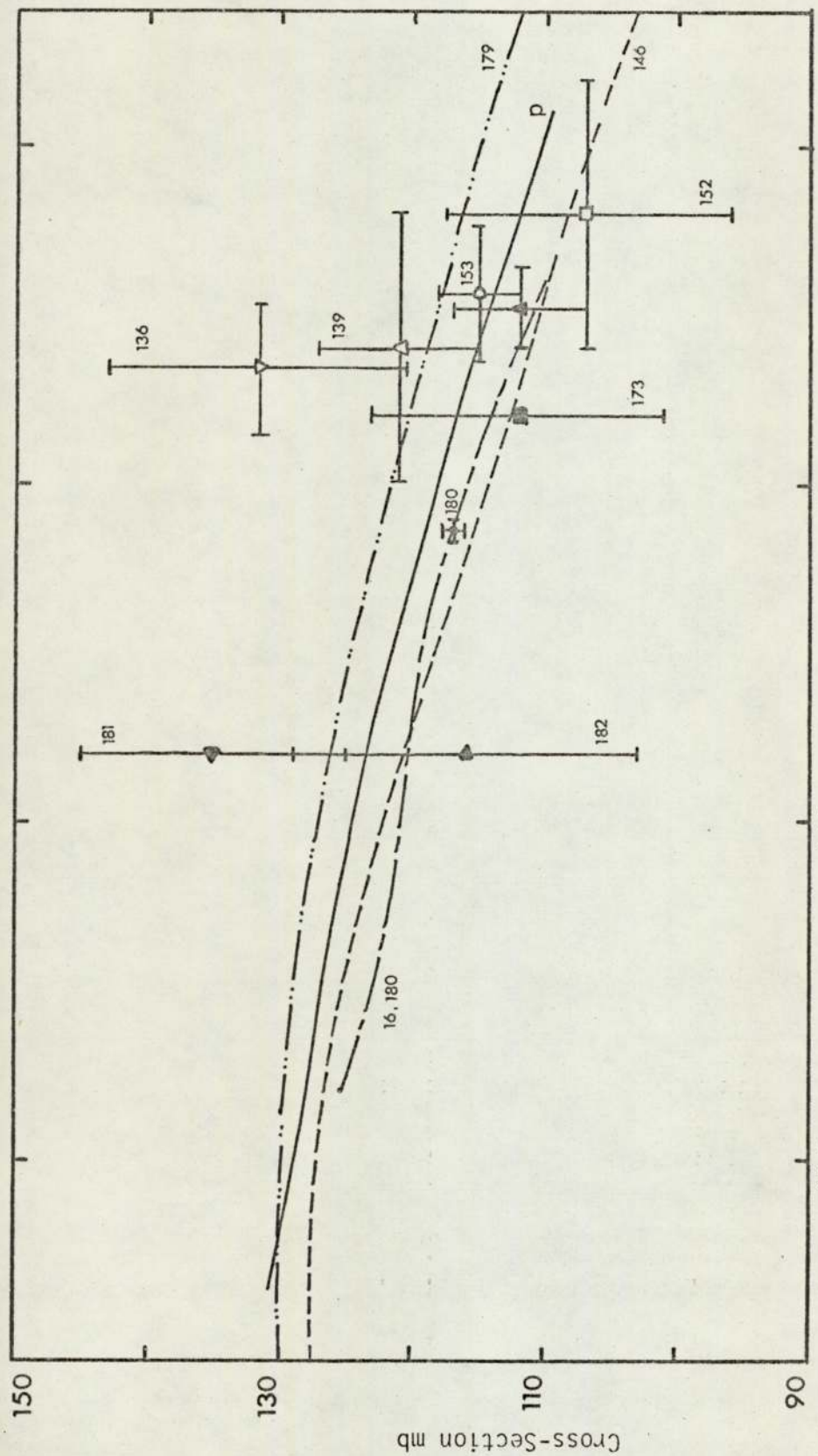

Fig. 8.10b
$^{27}Al(n,\alpha)^{24}Na$ Cross-Section Data

In the present study, investigation of Ericson's fluctuations was not possible mainly due to the deuteron beam energy loss in the used tritiated targets which results in neutron energy spreads wider than the expected fluctuation average width. On the other hand, an accurate determination of the general trend of the excitation function was required for absolute neutron flux monitoring.

The ~~absolute~~ cross-section data presented in Fig. 8.10a were determined relative to an accurate cross-section of 1170 $\pm$ 0.8 mb at 14.43 $\pm$ 0.015 MeV, which was recently measured by Vorach et al.[180] The required information about neutron anisotropy etc. were obtained from our reported results in Chapter 3.

Apart from some odd data, the present data and most of the published data are in good agreement. The reported evaporation model theoretical cross-section is 125 mb for 14 MeV neutrons [178]. This is consistent with the experimental data, as was the case of ^{59}Co, which indicate the validity of the evaporation model calculations for predicting the (n,α) cross-sections at least within the 27-59 target mass region.

8.11 $^{64}Zn(n,p)^{64}Cu$ Excitation Function

In this experiment, samples made of a zinc disc and aluminium ring were used, and the cross-section results were obtained relative to $^{27}Al(n,\alpha)^{24}Na$ excitation function. Following the irradiation, a decay time of about 4h was introduced to allow the interference from $^{63}Zn(T_{\frac{1}{2}} = 38m)$ to reach a negligible level. The cross-section was then determined by integrating under the annhilation peak of $^{64}Cu(T_{\frac{1}{2}} = 12.9h)$.

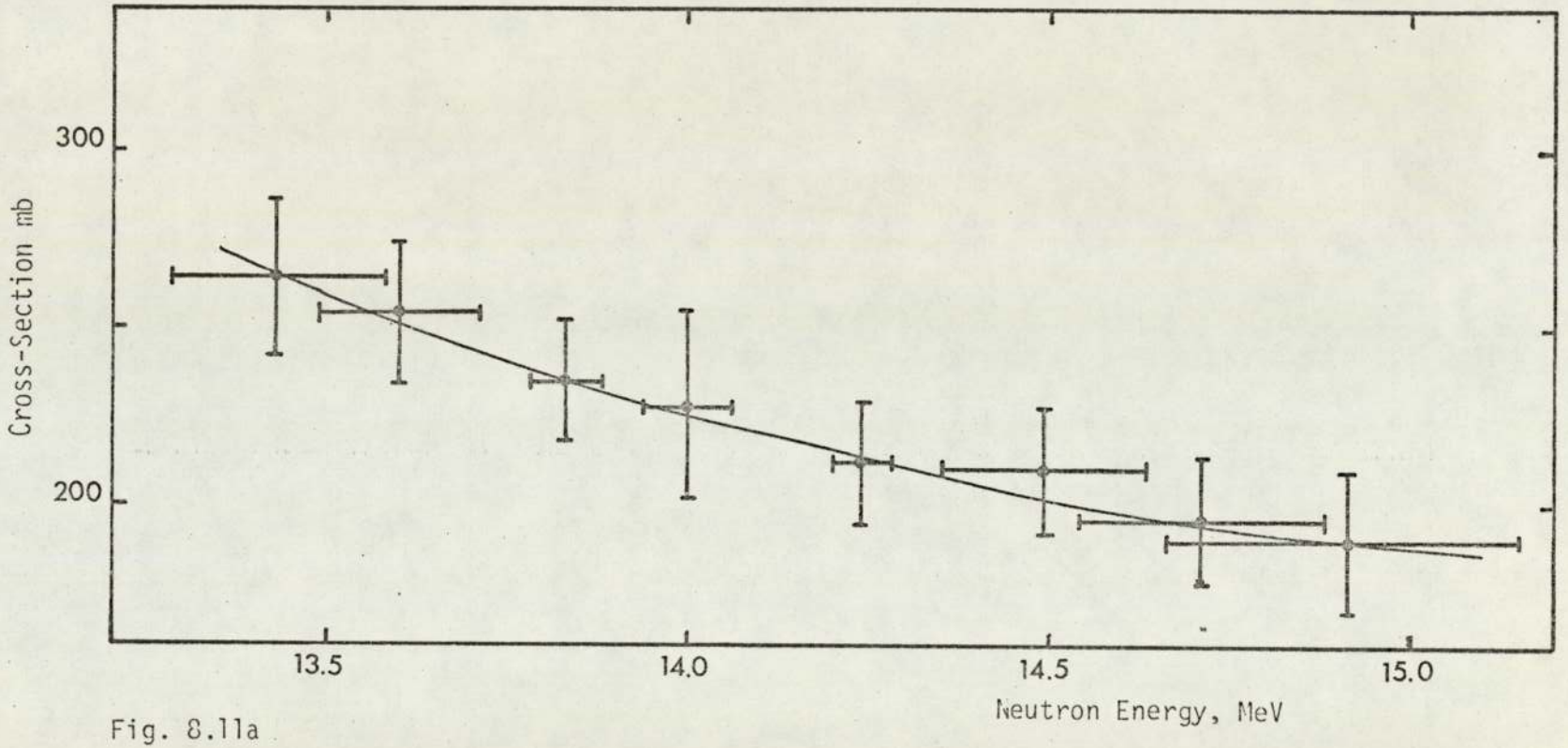

Fig. 8.11a

$^{64}Zn(n,p)^{64}Cu$ Excitation Function

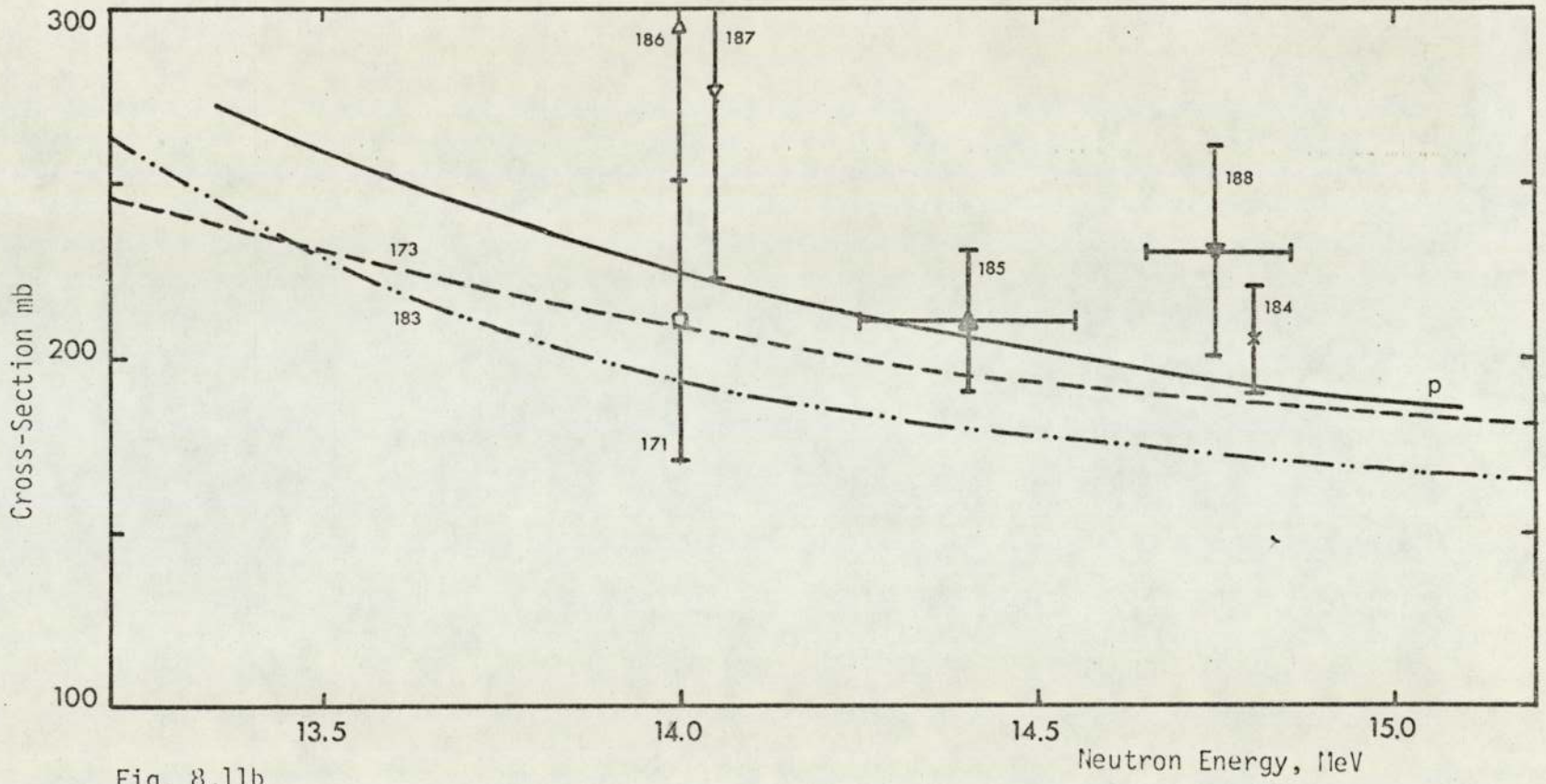

Fig. 8.11b

$^{64}Zn(n,p)^{64}Cu$ Cross-Section Data

The cross-section variation with energy of the present work is in a good agreement with the experimental data by Gabbard and Kern [173], and by Santry and Butler [183]. The calculated cross-section from Levkovskii's formula, eq. 8.2, is 140 mb for 14-15 MeV neutrons, which is in this case very close to the experimental values. Furthermore, the recent statistical model calculations by Kaji et al [148] have produced a cross-section of 180 mb for 14.1 MeV, but the experimental cross-section by the same authors was 325 ± 38 mb which is higher than the rest of the experimental data.

8.12 $^{65}Cu(n,2n)^{64}Cu$ Excitation Function

Aluminium ring was again used for measuring the neutron flux, but the data were normalized to the recommended cross-section of 965 mb at 14.7 MeV for the $^{65}Cu(n,2n)^{64}Cu$ reaction [129]. A suitable decay time was allowed after the irradiation to eliminate the interference from ^{62}Cu, and the cross-section was determined in terms of the integrated area under the annihilation peak for ^{64}Cu ($T_{\frac{1}{2}}$ = 12.8h).

The shape of the present excitation function is very similar to those which have been obtained by the other researchers. The statistical model calculations by Kondaiah [11] have produced a value of 752 mb for 14.5 MeV neutrons.

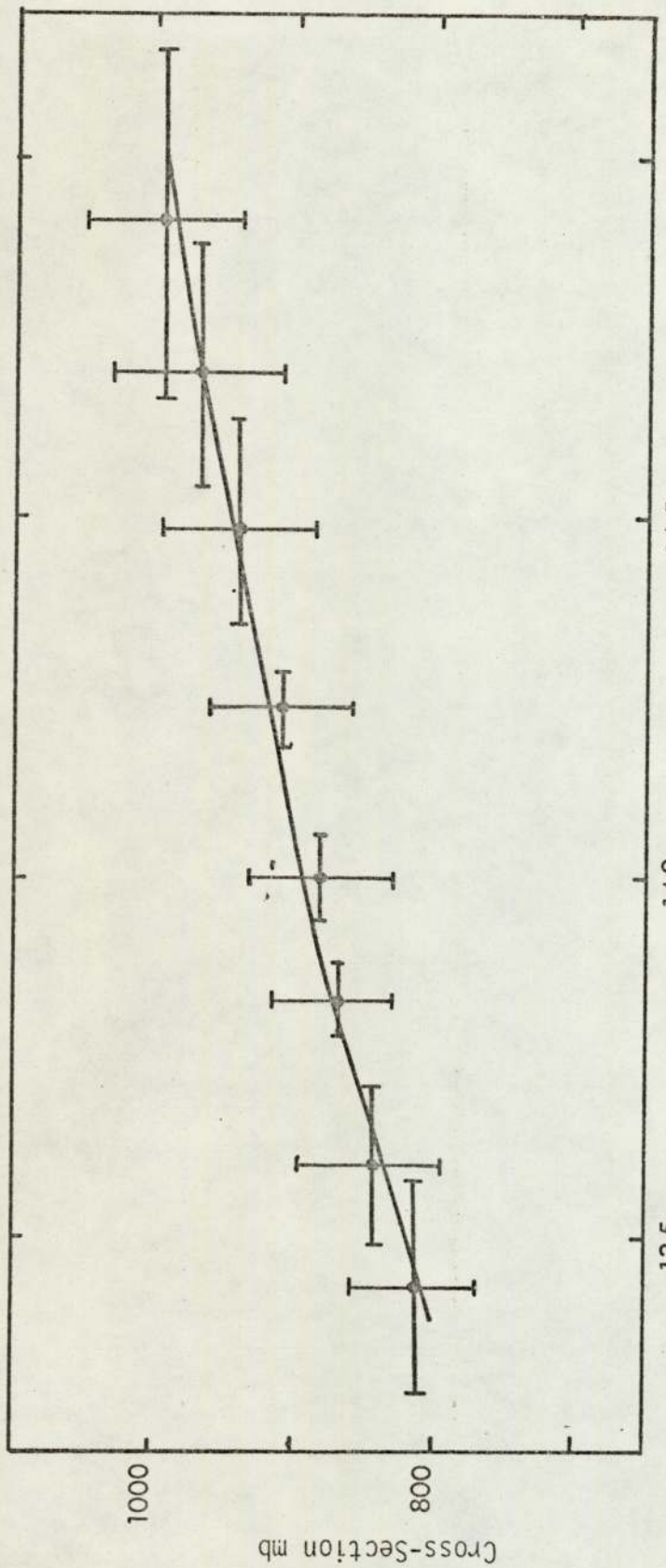

Fig. 8.12a

$^{65}Cu(n,2n)^{64}Cu$ Excitation Function

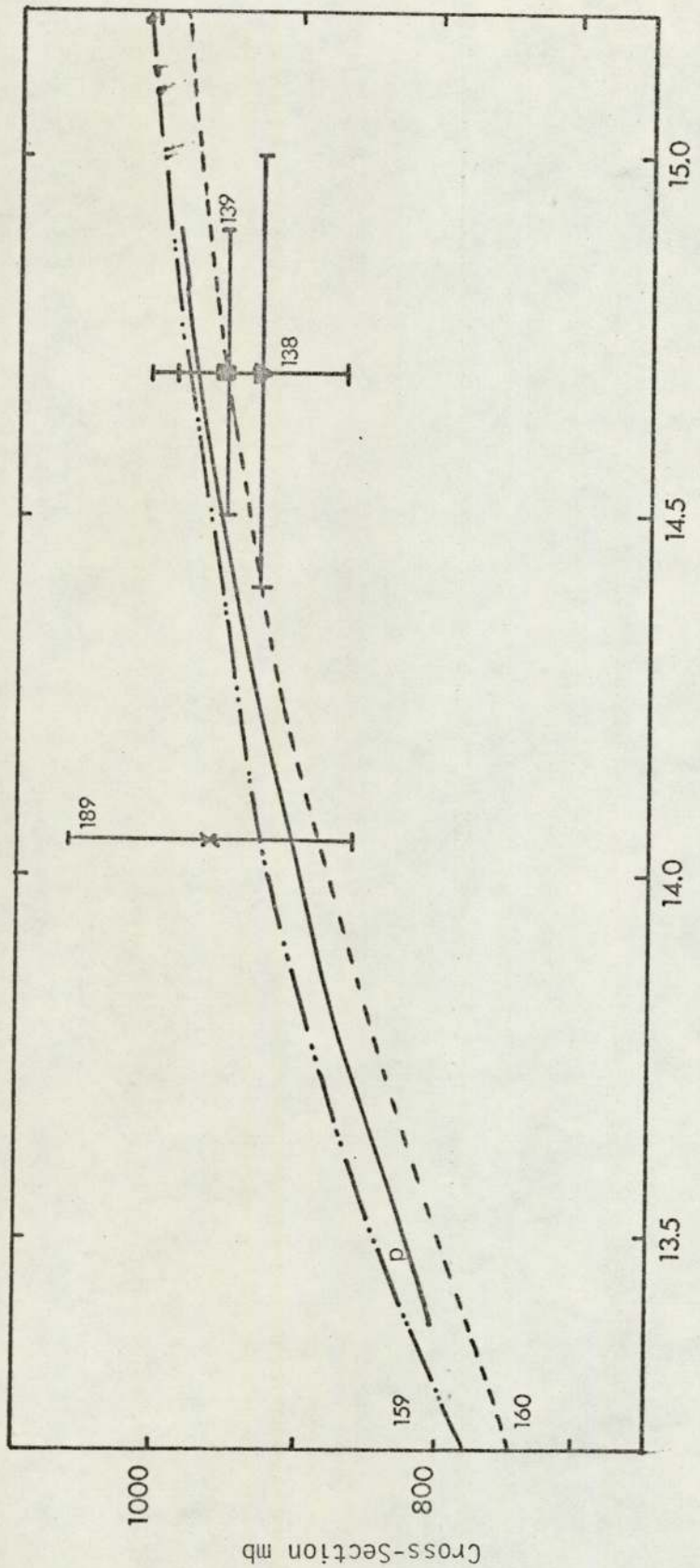

Fig. 8.12b

$^{65}Cu(n,2n)^{64}Cu$ Cross-Section Data

CONCLUSIONS

The concentric ring technique appears to be sufficiently accurate for producing good results for standard excitation functions. Therefore, it can also be used for measuring cross-section data for rare reactions, and for studying the effects of the overlapping of excitation levels. The use of the concentric ring technique will minimize the errors due to neutron flux measurement and energy estimation.

Our experimental results indicate that better information about the actual shape of the excitation function can be obtained by expanding the incident neutron energy range. Cross-section systematics should be based on a neutron energy region wider than 14-15 MeV to reduce the effect of cross-section peak position which varies by varying the mass of target nucleus, i.e. cross-sections of nuclei with a peak position within the 14-15 MeV region are underestimated. In addition to this, it will be possible to study the cross-sections for (n,xn) reactions, and learn more about the high energy ~~ring~~ tail portion of the (n,2n) excitation functions [190,191].

Accelerator neutron sources with high neutron production rate are required for obtaining advanced information about these reactions which have low cross-sections e.g. (n,t) and (n,^{3}He) and therefore improve their systematics [192-195]. Such data are important in both nuclear physics and in estimating light elements concentration build-up in future fusion reactors. The other advantage of high neutron source strength is in studying the fluctuations in neutron cross-sections as a function of energy, since samples can be placed at longer distances from the source to reduce the spread due to sample subtended angle.

REFERENCES

(1) S.M. Qaim, Proc. Int. Conf. Nuclear Cross-Sections and Technology, N.B.S. SP 425 (1975). (R.A. Schrack and C.D. Bowman, eds.)

(2) J.M. Blatt and V.C. Weisskopf, Theoretical Nuclear Physics (John Wiley & Sons, Inc., New York 1952), p.336

(3) A.S. Divatia et al., Nuclear Data for Reactors, I.A.E.A. Publications, Vol. 1

(4) J.H. Gibbons and R.L. Macklin, Phys. Rev. 114 (1959) 571

(5) A. Chatterjee, Nucl. Phys. 60 (1963) 273

(6) A. Chatterjee, Nucl. Phys. 49 (1963) 686

(7) D.G. Gardner, Nucl. Phys. 29 (1962) 383

(8) M. Bormann, Nucl. Phys. 65 (1965) 257

(9) R.K. Mohindra and S.K. Gupta, J. Phys. Soc. Jap. 39 (1975) 1147

(10) S.M. Qaim, Nucl. Phys. A185 (1972) 614

(11) E. Kondaiah, J. Phys. A: Math., Nucl. Gen., 7 (1974) 1457

(12) E. Holub and N. Cindro, J. Phys. G: Nucl. Phys. 2 (1976) 405

(13) J. Csikai and G. Peto, Phys. Lett. 20 (1966) 52

(14) T. Ericson, Ann. Phys. 23 (1963) 390

(15) W.H. Breunlich, Proc. Int. Conf. on the study of nuclear structure with neutrons (1965) p.100

(16) H.K. Vorach et al., Proc. Int. Conf. on the study of nuclear structure with neutrons (1965) p.885

(17) N. Cindro et al., Phys. Lett. 6 (1963) 205

(18) P. Strohal et al., Phys. Lett. 10 (1964) 104

(19) J. Csikai, Proc. Int. Conf. on the study of nuclear structure with neutrons (1965)

(20) J.M. Ferguson et al., Nucl. Phys. A98 (1967) 65

(21) M. Bormann and I. Riehle, Z.f. Physik 207 (1967) 64

(22) M.A. Gardner and D.G. Gardner, Nucl. Phys. A265 (1976) 77

(23) L. Colli et al, Phys. Lett. 1 (1962) 120

(24) L. Colli et al, Phys. Lett. 2 (1962) 12

(25) L. Colli et al., Nucl. Phys. 43 (1963) 529

(26) A.K.M. Siddiq et al., Indian J. Phys. 48 (1974) 318

(27) M. Bormann et al., Nuclear Data for Reactors, I.A.E.A. Publications

(28) V. Krivan and H. Munzel, J. Inorg. Nucl. Chem. 33 (1971) 1233

(29) V. Krivan and H. Munzel, J. Inorg. Nucl. Chem. 34 (1972) 2093

(30) V. Krivan and H. Munzel, J. Inorg. Nucl. Chem. 34 (1972) 2989

(31) V. Krivan and H. Munzel, J. Radioanalyt. Chem. 15 (1973) 575

(32) H.L. Rook et al., Int. Conf. Modern Trends in Activation Analysis, NBS, Washington, 1969

(33) H.P. Ule and V.P. Guinn, Proc. Int. Conf. on Peaceful Uses of Atomic Energy, I.A.E.A. Vienna, II, 111 (1964)

(34) D.C. Borg et al., Int. J. App. Radiat. Isotopes 11 (1961) 30

(35) N.A. Frigerio, Meeting on Radiological Applications of Neutron Irradiation, I.A.E.A., STI/PUB-325, Vienna, 1971

(36) S. Taczanoski, Nucl. Inst. and Meth. 104 (1972) 219

(37) L.C. Pasztor and D.E. Wood, Talanta 13 (1966) 389

(38) J. Csikai et al., Atomic Energy Review 7 (1969) 93

(39) E.L. Steele et al., Variable Energy Neutron Activation Analysis, AEC Report GA-6691, 1965

(40) O.N. Jarvis et al., Nucl. Instr. and Meth. 112 (1973) 559

(41) H. Liskein and A. Paulsen, Nuclear Data Tables 11 (1973) 569

(42) E. Magiera et al., Nucl. Phys. A246 (1975) 413

(43) H.H. Barschall, Nuclear Structure Study with Neutrons, J. Ero and J. Szucs (Eds.), Plenum Press, London, (1974),

(44) M.R. Cleland and K.H. Morganstein, Nucleonics 18 (1960) 52

(45) J.B.A. England, Techniques in Nuclear Structure Physics (I), Macmillan Press Limited, (1974).

(46) Amersham Radiation Sources for Industry and Research Catalogue (1971)

(47) J. Hoste et al., The Determination of Oxygen in Metals by 14 MeV Neutron Activation Analysis, E.U.R. 3565.e (1967)

(48) J.J. Broerse et al., Int. J. Appl. Radiation and Isotopes 22 (1971) 486

(49) D.M. Bibby et al., Nuclear Energy 11 (1970) 68

(50) J.J. Broerse, Conf. Accelerator Targets designed for the production of neutrons, E.U.R. 2641.e (1965)

(51) H. Fabian, Conf. Accelerator Targets designed for the production of neutrons, E.U.R. 2641.1 (1966)

(52) J. Pivarc, Wiss. Z. Techn. Univers. Dresden 21 (1972) 694

(53) G. Stengl et al., Nucl. Instr. and Meth. 126 (1975) 235

(54) D.M. Bibby et al., Nucl. Instr. and Meth. 94 (1971) 397

(55) D. Cossutta, Conf. Accelerator Targets designed for the production of Neutrons, E.U.R. 2641.e (1965).

(56) J. Laverlochere, Accelerator Targets designed for the production of neutrons. E.U.R. - 3895, Brussels 1968 p.202

(57) O. Reifenschweiller, Philips Res. Depts. 16 (1961) 401

(58) E. Hara, Jap. J. Appl. Phys. 7 (1968) 70

(59) J. Benveniste and J. Zenger, Information on the neutrons produced by the $^{3}H(d,n)^{4}He$ Reaction, UCRL - 4266 (1954)

(60) E.W. Saker and J.D.L.H. Wood, S.E.R.L. Tech. Report No. 61 (1958)

(61) E.M. Gunnersen and G. James, Nucl. Inst. and Meth. 8 (1960) 173

(62) S.D. Warshaw, Phys. Rev. 76 (1949) 1759

(63) N. Bohr, Mat. Fys. Medd. Dan. Vid. Selsk. 18, No. 8 (1948)

(64) J. Lindhard and M. Scharff, Mat. Fys. Medd. Dan. Vid. Selsk. 27 No. 15 (1953)

(65) L.N. Rothenberg, Phys. Rev. C1 (1970) 1226

(66) J.A. Cookson et al., Proc. Int. Conf. Nuclear Cross-Sections and Technology, N.B.S. SP425 (1975). (R.A. Schrack and C.D. Bowman, eds.)

(67) D.J. Hughes, Pile Neutron Research, Addison-Wesley Cambridge/Mass., (1953)

(68) I. Heertje, Thesis, University of Amsterdam (1963)

(69) I. Heertje et al., Physica 30 (1964) 1762

(70) E. Bruninx and J. Crombeen, Int. J. Appl. Radiat. Isotopes 20 (1969) 255

(71) R.C. Lawson et al., Radiochem. Radiological Lett. 10 (1972) 323

(72) R.C. Lawson et al., Phys. Med. Biol. 17 (1972) 771

(73) G. Oldham and K.G. Darrall, Int. J. Appl. Radiat. Isotopes 20 (1969) 255

(74) M.C. Scott, J. Nucl. Energy 35 (1971) 405

(75) De Volpi and Porges, Proc. 2nd Int. Conf. Neutron Cross-Sections and Technology, NBS Special Bulletin (1968)

(76) A.M. Atta and M.C. Scott, J. Nucl. Energy 27 (1973) 875

(77) E. Bruninx, Proc. Int. Conf. Modern Trends in Activation Analysis, NBS Publication 312 (1969)

(78) E. Bruninx, Int. J. Appl. Radiat. Isotopes 21 (1970) 657

(79) E. Bruninx, Uses of Cyclotron in Chemistry, Metallurgy and Biology, C.B. Amphett (ed.), Butterworth and Co. Ltd., London (1970)

(80) L.D. Stephens and A.R. Smith, U.S. Atomic Energy Commission Report, U.C.R.L. 8418 (1958)

(81) C.A. Feu Alvin and A.N. Das Santos, Nucl. Inst. and Meth. 105 (1972) 289

(82) W.W. Meinke and R.W. Shideler, Nucleonics 20 (3) (1962) 60

(83) F.A. Iddings, Anal. Chem. Acta. 31 (1964) 206

(84) M. Ahmad et al., Nucl. Inst. and Meth. 126 (1975) 309

(85) J.C. Robertson and K.J. Zieba, Nucl. Inst. and Meth. 45 (1966) 179

(86) P. Fieldhouse et al., Conf. Accelerator Targets Designed for the Production of Neutrons, EUR - 2641 (1966)

(87) Proc. 1965 Int. Conf. Modern Trends in Activation Analysis, College Station, Texas, April (1965)

(88) R.L. Heath, Proc. Conf. Accelerator Targets Designed for the Production of Neutrons, EUR - 2641, Brussels (1966)

(89) T. Shiokawa et al., J. Inorg. Nucl. Chem. 30 (1968) 1

(90) D. Partington et al., Analyst 95 (1970) 257

(91) B.T. Kenna and F.J. Conrad, Health Physics 12 (1966) 564

(92) K.G. Darrall and G. Oldham, Nuclear Energy (1967) 104

(93) H.F. Priest et al., Nucl. Inst. and Meth. 50 (1967) 141

(94) G. Oldham and D.M. Bibby, Nuclear Energy (1968) 167

(95) J.P. Op de Beeck, J. Radioanal. Chem. 1 (1968) 313

(96) J.P. Op de Beeck, Radiochem. Radioanal. Lett. 1 (1969) 281

(97) J. Janczyszyn and L. Loska, Radiochem. Radioanal. Lett. 3 (1970) 343

(98) T. Kishikawa, and C. Shinomiya, Radiochem. Radioanal. Lett. 7 (1971) 15

(99) J. Janczyszyn and S. Taczanowski, Radiochem. Radioanal. Lett. 9 (1972) 143

(100) D. Crumpton, Nucl. Inst. and Meth. 55 (1967) 198

(101) P. Oblozinsky and I. Ribansky, Nucl. Inst. and Meth. 7 (1971) 139

(102) S. Taczanowski, J. Radioanal. Chem. 12 (1972) 535

(103) H. Gotoh et al., Nucl. Inst. and Meth. 100 (1972) 473

(104) H. Gotoh et al., Nucl. Inst. and Meth. 116 (1974) 361

(105) E. Ricci, J. Inorg. Nucl. Chem. 27 (1965) 41

(106) H. Hollister, Nucleonics, 22 (No.6) (1964) 68

(107) S. Glasstone and M.C. Edlund, The Elements of Nuclear Reactor Technology, Van Nostrand, New Jersey (1958)

(108) M.D. Goldberg et al., USAEC Report BNL-400 (1962)

(109) D. Drake et al., Phys. Lett. 36B (1971) 557

(110) M. Valkonen and J. Kantele, Nucl. Inst. and Meth. 103 (1972) 549

(111) K. Ponnert et al., Physica Scripta 10 (1974) 35

(112) H.J. Price, "Graphical Analysis of Theoretical Neutron Flux Produced by Fast-Neutron Generators", Kaman Nuclear Corporation, Colorado Springs, Colorado (1964)

(113) S. Vass et al., Nucl. Inst. and Meth. 130 (1975) 271

(114) O.U. Anders and D.W. Briden, Anal. Chem. 3 (1964) 287

(115) J.R. Vogt and W.D. Ehman, Radiochem. Acta 4 (1965) 24

(116) V.P. Guinn and C.D. Wagner, Anal. Chem. 32 (1960) 317

(117) W.E. Mott and J.M. Orange, Anal. Chem. 37 (1965) 1338

(118) D.G. Wood et al., Conf. Anal. Chem. and Appl. Spec., Feb. (1966)

(119) S.S. Nargolwalla et al., Anal. Chem. 40 (1968) 666

(120) S.S. Nargolwalla et al., Anal. Chim. Acta, 49 (1970) 425

(121) F. Adams et al., "Instrumental and Radiochemical Activation Analysis", Monotopic Series, Butterworth, London (1971)

(122) R. Gijbels et al., Anal. Chim. Acta. 43 (1968) 183

(123) R. Gijbels et al., Proc. Int. Conf. Modern Trends in Activation Analysis, NBS Special Publication 312 (1969)

(124) R. Gijbels et al, The Industrialization of 14 MeV Neutron Activation Analysis of Oxygen in Steel, EUR-4297, Luxemburg (1969)

(125) P. Venugopala Rao and R.W. Fink, Phys. Rev. 154 (1967) 1023

(126) A.J. Cox and R.A. Jarjis, Int. J. Appl. Radiat. Isotopes 23 (1972) 301

(127) C.C. Grosjean and W. Bossert, Computing Laboratory, Ghent University, Belgium, 1965

(128) C.M. Lederer et al, Table of Isotopes, 6th Ed. (1967)

(129) Z.T. Body and T. Csikai, Atomic Energy Rev., 11 (1973) 153

(130) E.B. Paul and R.L. Clarke, Can. J. Phys. 31 (1953) 267

(131) L.A. Rayburn, Phys. Rev., 122 (1961) 168

(132) J.M. Ferguson and W.E. Thompson, Phys. Rev., 118 (1960) 228

(133) S. Yasumi, J. Phys. Soc. Japan, 12 (1957) 443

(134) L.A. Rayburn, Phys. Rev., 130 (1963) 731

(135) B. Grimeland et al., Phys. Rev. 137 (1965) B8878

(136) P. Cuzzocrea et al, Nuovo Cimento, 54B (1968) 53

(137) A. Pasquarelli, Nucl. Phys., A185 (1972) 614

(138) S.M. Qaim, Nucl. Phys., A185 (1972) 614

(139) D. Crumpton et al., J. Inorg. Nucl. Chem., 31 (1969) 1

(140) H. Kiskien, A. Paulsen, J. Nucl. Energy, A/B19(1965)73

(141) R.N. Glover and E. Weigold, Nucl. Phys. 29 (1962) 309

(142) C.S. Khurana and H.S. Hans, Proc. 4th Symp. on Low Energy Nuclear Physics, Bombay 1960

(143) F.L. Hassler and R.A. Peck, Jr., Phys. Rev. 125 (1962) 1011

(144) B. Mitra and A.M. Ghose, Nucl. Phys. 83 (1966) 157

(145) J. Kantele and D.G. Gardner, Nucl. Phys. 35 (1962) 354

(146) G.S. Mani et al, Nucl. Phys. 19 (1960) 535

(147) N. Ranakumar et al, Nucl. Phys. A122 (1968) 679

(148) H. Kaji et al, The Science Reports of the Tohoku University 58 (1975) 54

(149) G. Eder et al, Z. Physik 253 (1972) 335

(150) B.D. Kern et al, Nucl. Phys. 10 (1959) 226

(151) D. Crumpton, J. Inorg. Nucl. Chem. 31 (1969) 157

(152) J.M. Jeronymo et al, Nucl. Phys. 47 (1963) 157

(153) J.C. Robertson et al, J. Nucl. Energy 27 (1973) 531

(154) D.L. Allan, Nucl. Phys. 24 (1961) 274

(155) W. Schantle, Thesis, Vienna University, (1970)

(156) M. Bormann et al, Z. Phys. 174 (1963) 1

(157) E. Weigold and R.N. Glover, Nucl. Phys. 32 (1962) 106

(186) L. Rosen and A. Armstrong, Bull. Am. Phys. Soc. 1 (1956) 224

(187) R.S. Storey et al, Proc. Phys. Soc. A75 (1960) 526

(188) E.T. Bramlitt and R.W. Fink, Phys. Rev. 131 (1963) 2649

(189) S.G. Forbes, Phys. Rev. 88 (1952) 1309

(190) H. Liskien, Nucl. Phys., A118 (1968) 379

(191) B.P. Bayhurst et al, Phys. Rev. C12 (1975) 451

(192) S.M. Qaim et al, Proc. Int. Conf. on Chemical Nuclear Data; Measurements and Applications, Canterbury, 1971, p.12

(193) S.M. Qaim, Proc. Int. Conf. Nuclear Structure Study with Neutrons, Budapest 1972

(194) S.M. Qaim and G. Stocklin, J. Inorg. Nucl. Chem. 35 (1973) 19

(195) S.M. Qaim and G. Stocklin, Nucl. Phys. A257 (1976) 233.

ACKNOWLEDGEMENTS

I would like to thank my supervisor, Professor S.E. Hunt for his enthusiasm and guidance over the last five years, which made my research in neutron physics a memorable experience. His support over the past two years whilst I was working at Manchester University, and his valuable suggestions about the manuscript of this thesis are very much appreciated.

Among the other people I would like to acknowledge, are the department's secretary Mrs. I. Neal for her friendship and assistance, Mr. Biggs and Mr. Phull for their technical help in the nuclear physics laboratory, and the staff of the physics department's workshop for making the sample holder and target assemblies.

I would like also to thank my colleagues at Manchester University for their understanding, Mr. K. Conway for his assistance in the computer data fitting program and Miss E. Rich for the efficient typing of this thesis.

Finally, I would like to express my gratitude to my family abroad for their moral support, and my girlfriend Angela for her patience and understanding.

APPENDIX 1

```
C                    (( N E U T R E D ))
C
C
C       ( PROGRAM FOR STUDYING THE D-T NEUTRON BEAM CHARACTERISTICS )
C
    ( 0.7 MEV DEUTRONS ON A THICK TRITIATED TITANIUM TARGET OF T/TI=1.2 )
      INTEGER ELSTI, ELST, NNCL, NNN, LC, NNLL
      REAL DTCRS, DEL, EN, RN, EMAX, EMIN, EMEAN, EDMAX, EDMIN, DR, AND
      DIMENSION DTCRS(224),AND(200),ELSTI(34),ELST(34),NNCL(34),LLCL(20)
     1,NNN(34,20),EMAX(20),EMIN(20),EMEAN(20),EDMAX(20),EDMIN(20),ANISO(
     234,20),EN(34,20),TNE(20),TRN(20),DD(34),GAM(34),LLL(34,20),DEL(34)
     3,PARTNE(34,20),LC(400),NNLL(20,20),RTRN(20,20),RN(34,20),DR(24)
C
C
      READ(1,2)(DR(M),M=1,24)
    2 FORMAT(12(1X,F5.1))
C
      READ(1,3)(AND(M),M=1,200)
    3 FORMAT(6X,10(1X,F5.1))
C
      READ(1,4)(ELSTI(M),M=1,34)
    4 FORMAT(18(1X,I3))
C
      READ(1,6)(ELST(M),M=1,34)
    6 FORMAT(14(1X,I4))
C
C
      A = 3.1417/180
      I = -10
      DO 600 L = 1, 20
      B = 0.0
      C = 0.0
      IF (L - 20) 8, 7, 8
    7 I = 98
      GO TO 9
    8 I = I + 10
    9 KL = 11
      KK = 50
      KN = 1.0
      KP = 1.0
      M = 0
      ATNE = 0.0
      ATRN = 0.0
      N = 0
      DO 500 J=10,700,5
>
```

```
100 IF(J-200) 101,101,106
101 IF(J-55) 160,102,102
102 F = J/KL
103 IF(F-5) 160,104,160
104 KL = KL+2
105 GO TO 500
106 IF(J-205) 101,107,107
107 H = J/KK
108 IF(H-5) 111,109,111
109 KK = KK+10
110 GO TO 160
111 GO TO 500
160 N = N+1
    M = M+1
    IF (I-0) 25, 18, 25
 18 NNCL(N) = J
    DEL(N) = 48*ELSTI(M)/(48+3*1.2)+3*1.2*ELST(M)/(48+3*1.2)
    DD(N) = (4.00260361*(2.01410219+3.01602994)/(1.00866544*2.0141021
   19))*(3.01602994/(2.01410219+3.01602994)+(17578.5/J))
    GAM(N) = SQRT(1/DD(N))
 25 EN(N,L) = 0.001*(0.080307*J*COS(2*I*A)+0.798676*(0.599615*J+17578.
   15)+0.795126*COS(I*A)*(SQRT(0.405783*J*(0.599615*J+17578.5)*(1-0.10
   20925*J*(SIN(I*A))**2/(0.599615*J+17578.5)))))
    ANISO(N,L) = GAM(N)*(COS(I*A)+SQRT(DD(N)-(SIN(I*A))**2))**2/SQRT(D
   1D(N)-(SIN(I*A))**2)
    IF(J-200) 27,27,30
 27 DTORS(M) = DR(KN)
    KN = KN+1
    GO TO 32
 30 DTORS(M) = AND(KP)
    KP = KP+1
 32 RN(N,L) = ANISO(N,L)*DTORS(M)/DEL(N)
    PARTNE(N,L) = RN(N,L)*EN(N,L)
    TNE(L) = ATNE+PARTNE(N,L)
    ATNE = TNE(L)
    TRN(L) = ATRN+RN(N,L)
    ATRN = TRN(L)
    LLL(N,L) = I
    NNN(N,L) = J
    IF (PARTNE(N,L)-C) 50, 41, 37
 37 EMAX(L) = EN(N,L)
    IF (N-1) 40, 40, 41
 40 B = PARTNE(N,L)
 41 C = PARTNE(N,L)
 50 IF (PARTNE(N,L)-B) 52, 52, 500
 52 EMIN(L) = EN(N,L)
    B = PARTNE(N,L)
500 CONTINUE
    EMEAN(L) = TNE(L)/TRN(L)
    EDMAX(L) = EMAX(L)-EMEAN(L)
    EDMIN(L) = EMIN(L)-EMEAN(L)
    LLCL(L) = I
    M = L
    IF (M-20) 60,65,65
>
```

```
   60 LC(M) = LLCL(L)
      GO TO 600
   65 DO 570 M=20,400
      LC(M) = LC(M-19)
  570 CONTINUE
  600 CONTINUE
      DO 900 KL=1,20
      DO 850 K=1,20
      NNLL(K,KL) = LLCL(KL)
      RTRN(K,KL) = TRN(K)/TRN(KL)
  850 CONTINUE
  900 CONTINUE
C
C
      WRITE(2,605)(NNCL(N), DEL(N),N=1,34)
  605 FORMAT(1H1,///,9X,105H300KEV  DEUTERON  BEAM  ENERGY  LOSS  IN  TI
     1TANIUM  TRITIATED  TARGET  OF  TRITIUM  ATOMIC  RATIO  =  1.2,////
     2/,17H(D ENERGY IN KEV),///,5(4X,4HDEL(,I3,3H)= ,F8.3))
C
      WRITE(2,609)((NNN(N,L), LLL(N,L), ANISO(N,L),N=1,34),L=1,20)
  609 FORMAT(1H1,///,50X,20HNEUTRON   ANISOTROPY,////,35H(D ENERGY IN KE
     1V , ANGLE IN DEGREE),///,4(5X,6HANISO(,I3,1H,,I3,2H)=,F8.4))
C
      WRITE(2,612)((NNN(N,L),LLL(N,L),EN(N,L),N=1,34),L=1,20)
  612 FORMAT(1H1,///,15X,90HENERGY  OF  NEUTRONS  AS  A  FUNCTION  OF EM
     1ISSION  ANGLE  AND  INCIDENT  DEUTERON  ENERGY,////,35H(D ENERGY I
     2N KEV , ANGLE IN DEGREE),///,4(5X,3HEN(,I3,1H,,I3,2H)=,F8.4))
C
      WRITE(2,650)((NNN(N,L),LLL(N,L),EN(N,L),RN(N,L),N=1,34),L=1,20)
  650 FORMAT(1H1,///,26X,67HENERGY  DISTRIBUTION  OF  THE  NEUTRONS  AT
     1 DIFFERENT  LAB  ANGLES,////,35H(D ENERGY IN KEV , ANGLE IN DEGREE
     2),///,2(10X,1H(,I3,1H,,I3,1H),5X,6HEN =  ,F8.4,5X,6HRN =  ,F8.4),
     3//)
C
      WRITE(2,700)(LLCL(L),EMAX(L),EMIN(L),EMEAN(L),EDMAX(L),EDMIN(L),L=
     11,20)
  700 FORMAT(1H1,///,25X,70HMEAN  NEUTRON  ENERGY  AND  ENERGY  SPREAD
     1AT  DIFFERENT  LAB  ANGLES,/////,21X,11HMAX. ENERGY,5X,11HMIN. ENE
     2RGY,15X,11HMEAN ENERGY,5X,11HENERGY DIV.,5X,11HENERGY DIV.,4X,5H(M
     3EV),///,(5X,8HANGLE = ,I3,2(7X,F9.4),10X,3(7X,F9.4),//))
C
      WRITE(2,800)(LLCL(L), TRN(L), L=1,20)
  800 FORMAT(1H1,///,30X,47HFAST  NEUTRON  FLUX  AT  DIFFERENT  LAB  ANG
     1LES,////,2(20X,8HANGLE = ,I3,7X,7HFLUX = ,F8.4),//)
C
      WRITE(2,999)(((LC(M),NNLL(K,L),RTRN(K,L),K=1,20),L=1,20),M=1,400)
  999 FORMAT(1H1,///,87HANGULAR  VARIATION  OF  NEUTRON  FLUX  RELATIVE
     1 TO  THE  FLUXES  AT  REFERENCE  ANGLES,////,40X,34H( ACTUAL ANGLE
     2 ,REFERENCE ANGLE ),///,2(3X,2H( ,I3,3H ,  ,I3,6H )    ,16HRELATIVE
     3 FLUX = ,F7.3,12X),//)
C
      STOP
      END
>
```

International Journal of Applied Radiation and Isotopes, 1975, Vol. 26, pp. 57–60. Pergamon Press. Printed in Northern Ireland

A Concentric Ring Technique for the Measurement of Fast Neutron Fluxes and Energies

R. A. JARJIS and S. E. HUNT

Department of Physics, The University of Aston in Birmingham, Birmingham B47 ET, England

(*Received* 1 *May* 1974)

The limitations imposed by fixed foil, mixed powder and sandwich foil techniques for fast neutron flux measurement led the authors previously to suggest a concentric ring monitoring technique. This technique can be extended to measure neutron energies if excitation functions of the two materials are known.

The method is verified by using concentric copper monitoring rings with aluminium discs. The ratios of activities of copper and aluminium enable the neutron energy to be measured to $\pm 1{\cdot}2$ per cent.

The advantages and applications of the technique are discussed and a modified design is suggested for very short target to specimen separation.

An antimony disc with concentric copper and aluminium rings was used to measure the $^{121}Sb(n, 2n)^{120g}Sb$ excitation function, the copper and aluminium rings being used to measure both fast neutron flux and energy. It is suggested that the $^{121}Sb(n, 2n)^{120g}Sb$ reaction would be very useful as a standard for flux monitoring in the 14 MeV region since its excitation function is relatively flat between 13·5 and 15 MeV.

INTRODUCTION

Low energy particle accelerators are being used extensively in pure and applied nuclear science for the production of neutrons using the $^{3}T(d, n)^{4}He$ reaction. The fast neutrons so produced have variable energies and fluxes due to such factors as the variations in sample to target geometry, neutron scatter and absorption, non uniform loading of tritium in the target,[1] build up of deuterium and depletion of tritium in the target;[2] so it is very important to have a simple and accurate technique for the measurement of these two variable parameters at any specific point and time.

Fast neutron fluxes are usually estimated by using a single separate monitor foil, sandwich foils or the mixed powder technique, but each of these has disadvantages. The single foil cannot monitor the flux precisely at the specimen position, the sandwich technique may involve a large self absorption correction and errors introduced by the non uniform mixing of powders can be appreciable. These problems have been considered in more detail by the authors in a previous paper[3] in which a suggestion has been made for the use of a concentric ring technique. The monitor ring subtends a slightly larger angle on the target than the sample, but the increased spread in neutron energies is usually negligible; there is no "shielding effect" as in the sandwich technique, and by comparison with the mixed powders technique the monitoring ring and sample can easily be separated for subsequent counting.

In a previous communication by Cox and Jarjis[4] the use of a mixed powder sample to measure neutron energies was proposed. Use was made of the different excitation functions of the two materials for neutrons in the 14 MeV region and the ratio of activities was used to measure neutron energies to an accuracy of about .2·1 per cent. The use of the concentric ring configuration appreciably extends the

* Present address; van de Graaff Laboratory, the University, Manchester M13 9PL, England.

application of this technique. By activating two concentric rings of selected materials either alone or surrounding a disc of the sample under investigation it is possible to measure fast neutron flux and energy simultaneously.

EXPERIMENTAL PROCEDURE

Fast neutrons were produced by the D–T reaction on tritiated titanium target by its bombardment with an 0·3 MeV deuteron beam from a Van de Graaff accelerator. The target assembly was fitted with a thin flexible sample holder made of aluminium, and the specimens were subjected to neutrons of varying mean energy by altering the angular position with respect to the incident deuteron beam.[5]

The first set of experiments was on copper and aluminium which undergo the reactions ^{62}Cu(n, 2n)^{63}Cu and ^{27}Al(n, p)^{27}Mg, the products of which have half-lives of 9·8 and 9·4 min respectively. Samples were in the form of circular aluminium disc surrounded by a thin ring of copper. The samples were irradiated with different mean energy neutrons and at large and equal distance from the D–T neutron source, and the induced activities were measured for a range of mean neutron energies from 13·3 to 15 MeV.

In order to measure the ^{121}Sb(n, 2n)^{120g}Sb excitation cross section a method of measuring neutron energy and flux simultaneously was established by using a configuration of concentric rings of copper and aluminium surrounding a circular disc of pure antimony.

A 3-in. × 3-in. NaI(Tl) detector coupled to a multichannel analyser was used to measure the induced activities. The cross sections were calculated from the measurements on the 0·511 MeV annihilation radiations from ^{62}Cu and ^{120g}Sb and the 0·842 MeV gammas from ^{27}Mg.

RESULTS AND DISCUSSION

The excitation functions of ^{63}Cu(n, 2n)^{62}Cu and ^{27}Al(n, p)^{27}Mg reactions have been measured previously by a number of workers including the authors.[3] Our previous measurements indicated that the copper cross section increases approximately linearly with neutron energy with a slope of 28 per cent MeV^{-1} in the 14 MeV region, whilst the aluminium cross

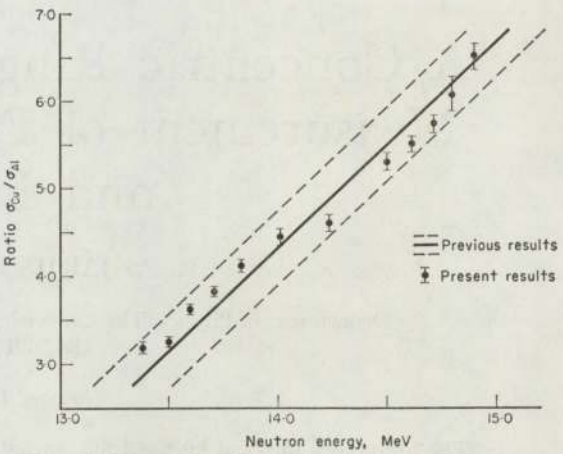

FIG. 1. The ratio of cross sections as a function of neutron energy.

section decreases with a slope of −9 per cent MeV^{-1} in this region. The ratio of these results has been plotted as a solid line in Fig. 1, the experimental uncertainties being indicated by the dotted lines. In the present work the concentric ring technique was used to establish the cross section ratios at specific energies and these are shown in the form of points in Fig. 1. The uncertainties associated with the present measurements are less due to the effective elimination of common systematic errors and they reveal a slight non linearity in the activation ratios, although there is good general agreement between the two sets of results. The accuracy of the neutron energy measurement has been improved to ±1·2 per cent by the concentric ring technique.

The neutron fluxes for the calculation of the ^{121}Sb(n, 2n)^{120g}Sb excitation curve were estimated from the activity of the copper ring, using our previously measured copper excitation curve and the recommended value of ^{63}Cu(n, 2n)^{62}Cu reaction cross section of 558 mb at 14·7 MeV proposed by BÖDY and CSIKAI,[6] this is somewhat lower than the absolute value obtained in this laboratory.[7] Neutron energies were calculated from the observed activity ratios on the copper and aluminium rings using the cross sections ratio results from Fig. 1.

The ^{121}Sb(n, 2n)^{120g}Sb cross section has been measured by few researchers,[8–12] from these only RAYBURN[8] and KANDA[9] have measured

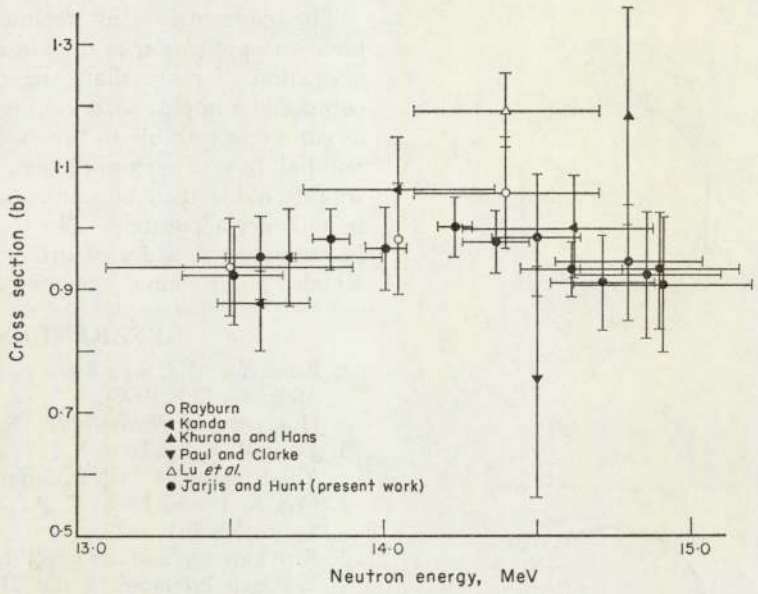

FIG. 2. $^{121}Sb(n, 2n)^{120g}Sb$ excitation function.

its variation with neutron energy. Our results are shown in Fig. 2 together with the former data and a good agreement can be noticed in the energy range which we have covered. In general the experimental uncertainties associated with the present work are less than those of previous work.

Antimony is suggested as a very suitable flux monitor for 14 MeV neutrons when used to produce activities with half lives in the 10–30 min region has the advantage of having a relatively high cross section, its radioactive product has a reasonable half life of 15·9 min and its smooth and almost flat excitation function make it suitable for many (n, p) and (n, 2n) reactions which have a similar type of excitation function.

The errors introduced by using concentric ring monitors for large target to specimen separations are small but for small target to specimen separation the increased spread in neutron energies experienced by a uniform ring becomes noticeable as shown in Fig. 3, in this case the areas A and B of the ring are exposed to wider ranges of neutron energies than the rest of the ring and the circular disc. For example if we consider a concentric sample consisting of a 3 cm diameter disc surrounded by a 1-cm thick ring, for a separation of 2 cm from the neutron source a specimen in the forward direction would be exposed to a range of neutron energies from 14·74 to 14·91 MeV, and the monitoring ring to a range from 14·60 to 14·91 MeV and at 90° the corresponding energies will be 13·67–14·56 MeV for the specimen and 13·50–14·73

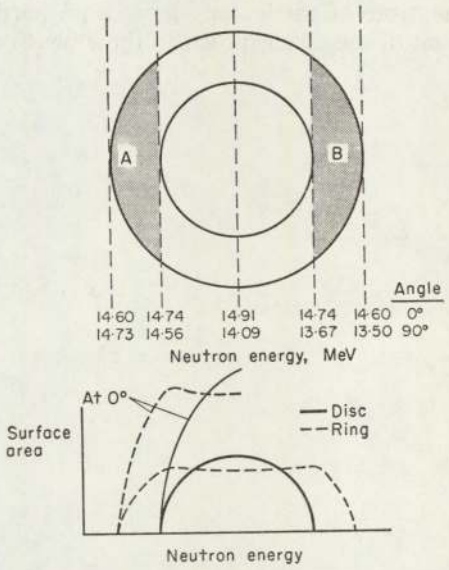

FIG. 3. The concentric ring/disc sample at a short separation from the target.

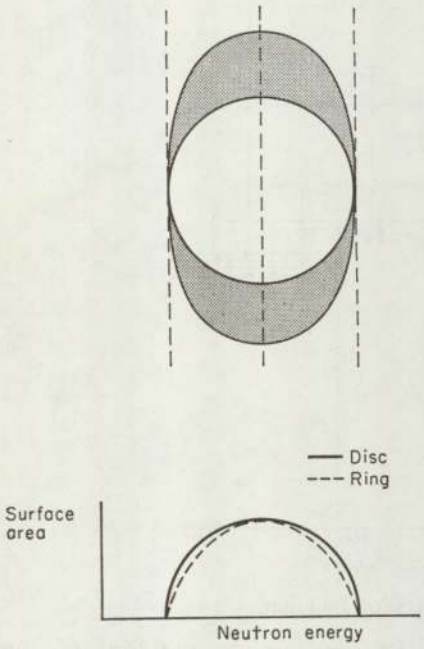

FIG. 4. The modified concentric ring.

MeV for the ring. The effect will be small for smooth excitation function and can be minimized by using a specially designed ring as shown in Fig. 4 such that the area of the ring exposed to neutrons of particular energy is proportional to that of the disc exposed to these neutrons.

The concentric ring technique could also have an application in measurements involving activation of more than one constituent in a composite sample. Monitoring rings matched as closely as possible to the excitation functions and half lives of each of the constituent elements would enable their concentrations to be determined very accurately. The technique can also be extended to wider neutron energy ranges in which "point source" geometry is used.

REFERENCES

1. ROBERTSON J. C. and ZIEBA K. J. *Nuclear Instrum. Meth.* **45,** 179 (1966).
2. HOLLISTER H. *Nucleonics* **22,** (No 6), 68 (1964).
3. JARJIS R. A. and HUNT S. E. *Proc. Int. Conf. Modern Trends Activation Analysis, Saclay, France* (1972).
4. COX A. J. and JARJIS R. A. *Int. J. appl. Radiat. Isotopes* **23,** 301 (1972).
5. BENVENISTE J. and ZENGER J. Information on the Neutrons Produced by the $^{3}H(d, n)$ ^{4}He Reaction. UCRL-4266 (1954).
6. BÖDY Z. T. and CSIKAI T. *Atomic Energy Rev.* **11,** 153 (1973).
7. CRUMPTON D. *et al. J. inorg. nucl. Chem.* **31,** 1 (1968).
8. RAYBURN L. A. *Phys. Rev.* **130,** 731 (1963).
9. KANDA Y. *J. Phys. Soc. Japan* **24,** 17 (1968).
10. KHURANA C. S. and HANS H. S. *Nucl. Phys.* **28,** 560 (1961).
11. PAUL E. B. and CLARKE R. L. *Can. J. Phys.* **31,** 267 (1953).
12. LU W. *et al. Phys. Rev.* **C1,** 350 (1970).

Journal of Radioanalytical Chemistry, Vol. 16 (1973) 611–616

AN IMPROVED NEUTRON MONITOR GEOMETRY FOR NEUTRON ACTIVATION

R. A. JARJIS, S. E. HUNT

Physics Department, University of Aston in Birmingham (England)

Introduction

A large amount of data on neutron capture cross sections and their variations with neutron energy around 14 MeV has been published during the last twenty years. The measured data are important in testing the relevant nuclear theories; and more practically in measuring neutron fluxes,[1] and in special cases neutron energies.[2] These are of great importance in the field of neutron activation analysis.

The precision of neutron activation analysis and neutron excitation function measurements depends on the accuracy of neutron flux measurements which are usually made in terms of the induced activity on standard materials, and the standards themselves can be a source of discrepancy between published data.

Errors can be introduced due to non uniform distribution of tritium in the target and the change in charged particle beam conditions which cause the neutron flux to vary in a different manner at the sample and monitor particularly if these subtend different angles to the beam.[3] In order to reduce the errors due to these factors sandwich and mixed powder methods are commonly employed. If sample and monitor are placed at different distances from the target either one behind the other or in a sandwich configuration, a correction has to be made due to the variation in flux with distance from the source[4] and this can be considerable for short sample to source distances. A correction must also be made for the flux attenuation due to absorption.

In order to reduce these errors the mixed powder technique was produced by Venugopala Rao and Fink.[5] Powders of two different materials were mixed with the powder under investigation. The powders should all have the same grain size but even so the problem of incomplete mixing and consequent difference in self absorption are difficult to eliminate. The gamma spectra for three nuclei may also be difficult to analyse. An additional improvement in the field can be made by employing a method which satisfies the conditions that sample and monitor:

(1) Are at the same distance from the neutron source but have distict boundaries between them.

(2) Are exposed to neutrons with approximately the same average energy to eliminate the errors due to the different excitation functions of monitor and sample.
(3) Can be transferred to the counting equipment so that their activites can be measured simultaneously.
(4) Have equal thickness to avoid the necessity of introducing inverse square law flux corrections.

These conditions appear to be satisfied by using a sample in the form of a disc and surrounding it by a concentric ring of the flux monitoring material.

Experimental

A Van de Graaff accelerator was used to accelerate deuterons up to an energy of 0.3 MeV. The deuteron beam was allowed to strike a tritiated titanium target, and neutrons were produced by the D — T reaction. Neutrons with different energies could be obtained by varying the angular position with respect to the deuteron beam. We have used a computer programme "NEUTRED" to provide the information concerning the neutron production by taking into account the energy loss of the deuteron beam in the target. We found that the average neutron energy varies from 13.43 MeV at 150° to 14.97 MeV at 0° with a value of 13.98 MeV at 98°. Uniform distribution of tritium throughout the target thickness was assumed.

Our sample holder was made of aluminium, and consists of a thin arc supported by three thin rigid arms at 0°, 98° and 150°; there is also a moveable arm which could be rotated through an angle of 180°, or removed if necessary, to reduce neutron scatter. This set up allows the samples to be positioned at angular interval of 5° throughout the range of 0° to 180° with respect to the incident beam. The target to specimen distance could be varied from 5 cms to 25 cms in 1 cm steps.

To count the induced gamma activities of the irradiated samples a 3" x 3" NaI(Tl) detector coupled to 400 channel RIDL multichannel analyzer were used. Crystal efficiencies were estimated from the results of Grosjean and Bossaert.[6] Each of the results obtained is based on three or more independent measurements.

Results

Excitation curve of copper standard

The excitation curve for $^{63}Cu(n, 2n)^{62}Cu$ reaction was first measured in the usual manner by counting the induced activity at each angle with respect to that at 30°. The measurements were made by counting the annihilation (0.511 MeV) gammas produced by the positron in an aluminium cover of adequate thickness. The reference cross-section value at 30° (14.8 MeV) of 558 mb[7] was used and the results are shown in Fig. 1.

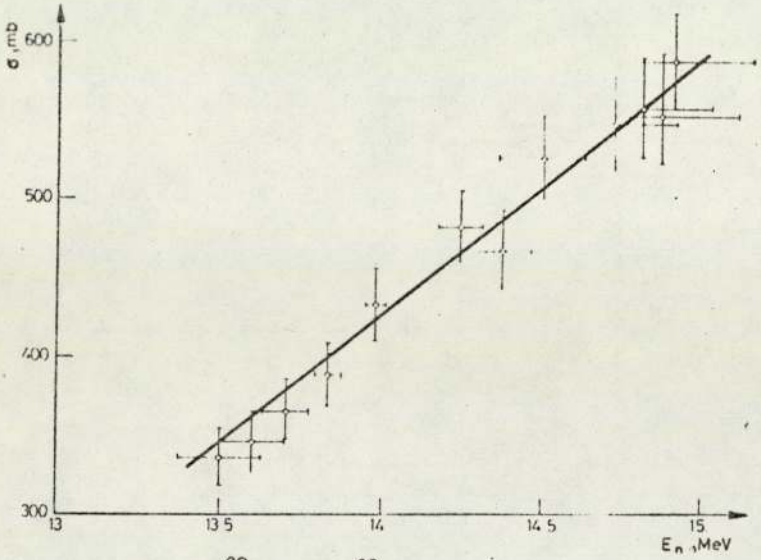

Fig. 1. $^{63}Cu(n, 2n)^{62}Cu$ excitation function

Measurement of excitation function of aluminium

^{27}Mg (T = 9. 5 m) is a beta active, it decays to various levels in ^{27}Al, a 70% of the decay leads to the 0. 842 MeV level and the rest to the 1. 015 MeV level. Measurements were made on the 0. 842 MeV γ-ray.

Samples were designed in the form of circular aluminium disc surrounded by a very thin ring of copper which was used as the monitor. The geometry was such that the additional angle subtended by the copper ring was very small and consequently the sample and monitor were exposed to neutrons of the same mean energy. These concentric samples were irradiated together, and for checking purposes a single copper sample was also exposed at the same distance from the target and at an angle of 30° to the beam direction. It was therefore exposed to neutrons of mean energy 14. 8 MeV.

The induced gamma activities in the irradiated concentric samples of aluminium and copper were counted simultaneously and a typical gammaspectrum is shown in Fig. 2.

The determination of the $^{27}Al(n, p)^{27}Mg$ excitation function was related to the measured copper excitation function Fig. 1, and the results are shown in Fig. 3. A further check was carried out by measuring the aluminium (n, p) excitation function relative to the 558 mb value of $^{63}Cu(n, 2n)^{62}Cu$ at 14. 8 MeV by using separate single aluminium and copper samples. The results showed a similar behaviour to Fig. 3, but with higher standard deviation.

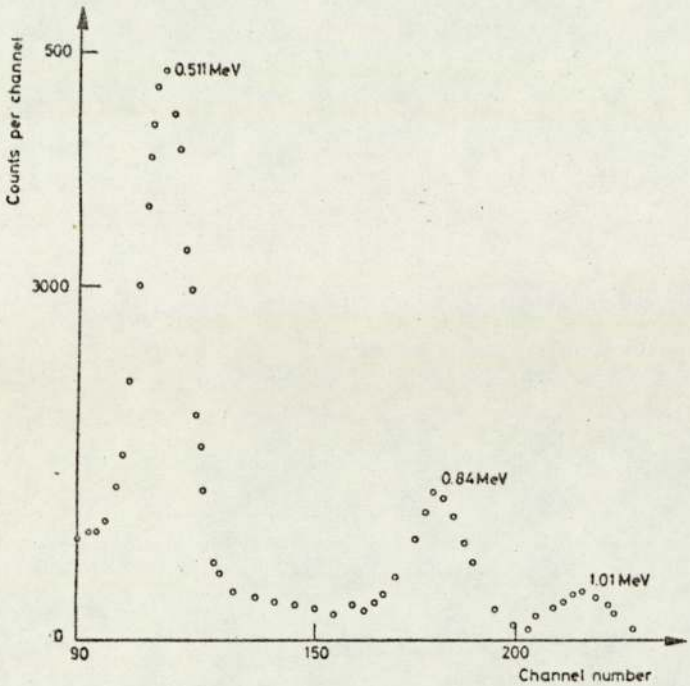

Fig. 2. Gamma-ray spectrum from the aluminium/copper sample

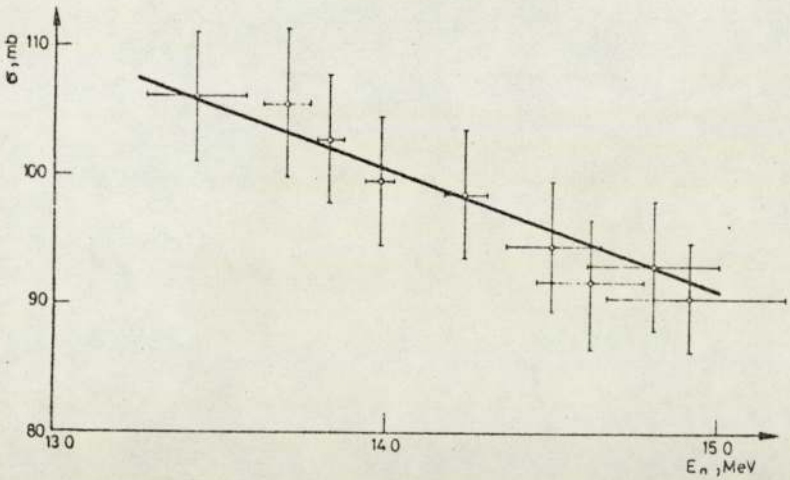

Fig. 3. $^{27}Al(n, p)^{27}Mg$ excitation function

Discussion

$^{63}Cu(n, 2n)^{62}Cu$ absolute cross-section and its variation with neutron energy have been measured by several workers.[7-16] The measured values vary from 422[8] to 469[9] mb at about 14 MeV. Between 14.7 and 14.77 MeV the published results are 577,[10] 593,[11] 507[12] and 550[13] mb, and at 14.8 MeV are 615[14] and 558[7] mb. The cross-section in the 14 MeV range increases with neutron energy and the approximate gradients of the published excitation functions vary between 25% and 26% MeV^{-1}. Our excitation function showed a slightly higher slope of 28%.

A large spread of $^{27}Al(n, p)^{27}Mg$ cross-section values at specific energies and its variation with energy can be noted from the previously published results.[17-23] Between 14 and 14.5 MeV[17-19] the cross-section values varied between 115[17] to 87[19] mb. At 14.8 MeV[20-22] the variation was between 71[20] and 97[21] mb.

Partington et al.[15] studied the variation of cross-section with neutron energy in the range 13.5–15.0 MeV and their results show a small approximate decrease in the cross-section of 3% MeV^{-1}.

Previously Cuzzocrea and Perillo[9] studied this variation in the region 13.7-14.6 MeV, their excitation function showed a larger negative slope of 12% MeV^{-1} at 14.0 MeV. Our excitation function shows a negative slope of 9% at 14.5 MeV in tne range 13.4–14.9 MeV. This value of the slope is in between the previously published results. The magnitude of the $^{27}Al(n, p)^{27}Mg$ cross-section fell from 106 millibarns to 92 millibarns in the energy range, relative to a value of 558 millibarns for the $^{63}Cu(n, 2n)^{62}Cu$ reaction at 14.8 MeV.

The smaller spread in the experimental points which was obtained using the concentric aluminium disc and copper monitoring ring indicates that random errors due to beam shift etc. were reduced.

This method of monitoring appears to have potential application in the field of fast neutron irradiation.

References

1. D. Crumpton et. al., Nucl. Instr. Methods, 92 (1971) 533.
2. A.J. Cox, R.A. Jarjis, Intern. J. Appl. Radiation Isotopes, 23 (1972) 301.
3. W.E. Mott, J.M. Orange, Proc. Intern. Conf. Modern Trends in Activation Analysis, Texas A and M University, College Station, 1965, p. 115.
4. H. F. Priest et al., Nucl. Instr. Methods, 50 (1967) 141.
5. P. Venugopala Rao, R.W. Fink, Phys. Rev., 154 (1967) 1023.
6. C.C. Grosjean, W. Bossaert, Computing Laboratory, Publication in the University Ghent, Belgium, 1965.
7. B. Grimeland et. al., Phys. Rev., 137 (1965) B8878.
8. L.A. Rayburn, Phys. Rev., 130 (1963) 731.
9. P. Cuzzocrea, E. Perillo, Nuovo Cimento, 54B (1968) 53.

10. A. Pasquarelli, Nucl. Phys., A93 (1967) 218.
11. S. M. Qain, Nucl. Phys., A185 (1972) 614.
12. J. M. Ferguson, E. Weigold, Nucl. Phys., 29 (1962) 309.
13. R. N. Glover, E. Weigold, Nucl. Phys., 29 (1962) 309.
14. D. Partington et. al., J. Inorg. Nucl. Chem., 31 (1969) 1.
15. D. Partington et. al., Analyst, 95 (1970) 257.
16. H. Liskien, A. Paulsen, J. Nucl. Energy, A/B 19 (1965) 73.
17. C. S. Kurana, H. S. Hans, Proc. 4th Symp. on Low Energy Nuclear Physics, Bombay, 1960.
18. F. L. Hassler, R. A. Reck, Jr., Phys. Rev., 167 (1968) 1091.
19. J. Kantele, D. G. Gardner, Nucl. Phys., 35 (1962) 354.
20. P. N. Tiwari, E. Kondiah, Phys. Rev., 167 (1968) 1091.
21. S. K. Mukherjjee et. al., Proc. Phys. Soc. (London), 77 (1967) 508.
22. L. Husain et. al., Phys. Rev., 1 (1970) No. 4, 1233.
23. B. Mitra, A. M. Ghose, Nucl. Phys., 83 (1966) 157.